

**UNIVERSIDADE FEDERAL DE SÃO CARLOS  
CENTRO DE CIÊNCIAS EXATAS E DE TECNOLOGIA  
PROGRAMA DE PÓS-GRADUAÇÃO EM CIÊNCIA E  
ENGENHARIA DE MATERIAIS**

ON-LINE FTIR SPECTROSCOPY SYSTEM FOR EXTRUSION-BASED  
PROCESS ANALYSIS.

LUCIVAN PEREIRA BARROS JUNIOR

São Carlos

2021



**UNIVERSIDADE FEDERAL DE SÃO CARLOS**  
**CENTRO DE CIÊNCIAS EXATAS E DE TECNOLOGIA**  
**PROGRAMA DE PÓS-GRADUAÇÃO EM CIÊNCIA E**  
**ENGENHARIA DE MATERIAIS**

ON-LINE FTIR SPECTROSCOPY SYSTEM FOR EXTRUSION-BASED  
PROCESS ANALYSIS.

LUCIVAN PEREIRA BARROS JUNIOR

Doctoral thesis conducted under *cotutelle* agreement presented to the Graduate Program in Materials Science and Engineering as a partial requirement to obtain the title of DOCTOR IN MATERIALS SCIENCE AND ENGINEERING conferred by the Federal University of Sao Carlos (UFSCar) and the title of DOCTOR IN MACROMOLECULAR SCIENCE AND ENGINEERING conferred by Case Western Reserve University (CWRU)

Advisor (UFSCar): Dr. Sebastião V. Canevarolo

Advisor (CWRU): Dr. João Maia

Funding agency: CAPES/CWRU - Code: 88887.143651/2017-00

São Carlos

2021



## **CANDIDATE'S VITAE**

Master in Materials Science and Engineering by UENF (2014)

Bachelor of Metallurgical and Materials Engineering by UENF (2012).





**UNIVERSIDADE FEDERAL DE SÃO CARLOS**  
Centro de Ciências Exatas e de Tecnologia  
Programa de Pós-Graduação em Ciência e Engenharia de Materiais

---

**Folha de Aprovação**

---

Defesa de Tese de Doutorado do candidato Lucivan Pereira Barros Junior, realizada em 11/11/2021.

**Comissão Julgadora:**

Prof. Dr. Sebastião Vicente Canevarolo Junior (UFSCar)

Prof. Dr. Leonardo Bresciani Canto (UFSCar)

Prof. Dr. Gary E. Wnek (CWRU)

Prof. Dr. Hatsuo Ishida (CWRU)

Profa. Dra. Jennifer L. W. Carter (CWRU)

Prof. Dr. João Manuel Luís Lopes Maia (CWRU)

O presente trabalho foi realizado com apoio da Coordenação de Aperfeiçoamento de Pessoal de Nível Superior - Brasil (CAPES) - Código de Financiamento 001.

O Relatório de Defesa assinado pelos membros da Comissão Julgadora encontra-se arquivado junto ao Programa de Pós-Graduação em Ciência e Engenharia de Materiais.





## ACKNOWLEDGEMENTS

During the journey to reach our goals, we are sure that great people and great friends were on our side and collaborated so that the end results were always the best.

I would like to honor all of those who contributed to the completion of this work and give them my sincere thanks.

I would like to start by thanking **God**, because He makes everything possible.

I am deeply grateful to my advisors **Professor João Maia** (CWRU) and **Professor Sebastião Canevarolo** (UFSCar), who worked together with other coordinators (UFRJ, PUC-Rio and UFRGS) in order to make the Macro/CAPES Program dual degree a reality. Professor João Maia, thank you for the opportunity you gave me. This is a gift for a lifetime and I can't express enough how grateful I am for it. Professor Sebastião Canevarolo, thank you for your friendship and the continuous dedication to my development. Thank you for listening to me when I needed to be heard and a special thanks for the great advice you've given me for both my scientific and personal life.

Thank you very much to the committee members **Professor Leonardo Canto**, **Professor Jennifer Carter**, **Professor Hatsuo Ishida** and **Professor Gary Wnek**, for considering and accepting to be part of such an important stage in my life. Thank you for the time you invested in me, for holding me to a high research standard, and for enforcing strict validations for each research result since the Research Qualifying Exam (RQE).

I owe a lot to **Theresa Claytor** and **Marcelo Cavallaro**, that helped me in many different circumstances with warmth and kindness. Special acknowledgment to the Department of Material Engineering DEMa/UFSCar, Graduate Program in Materials Sciences Engineering at UFSCar (PPGCEM), and Department of Macromolecular Sciences and Engineering at CWRU.

During my PhD I was blessed to meet fantastic people, who I am deeply grateful for. Thank you to the Macro family in Cleveland, who received me with so much kindness and warmth. Especially, the Maia group at CWRU for making me feel welcome and helping me on this journey. In particular, **Dana**, **Molin** and **Vi-**

**vek** for all the help, advice, scientific discussions, and friendship. Thank you to **Shaghayegh, Brandy** and **Saeed**. Thank you to Macro/CAPES PhD students **Irlaininha, Luix com z, Gustavo, Claudio, Ana Maria, Gabriela, Italo**, and **Lucio**. You guys will be in my mind forever. In addition, I would like to thank **Juçara, Alana, Natalia** and **Dora**. I would like to specially thank **Erika** and **Felipe** for making my PhD life more amusing and for sharing this experience with me at the highest level, for advising me, laughing with me (sometimes laughing at me) and most importantly, for never letting me go to Barrio alone.

I would like to thank my wife, **Gina**, for being so supportive while working on my dissertation. Thank you for the unconditional love and for staying with me even when I couldn't be with you in person. Thank you for spending nights reading my work, making me company, checking my English and working along with me. You made me feel encouraged and strong to keep going on. I also would like to thank my parents-in-law **Sheila** and **Sam**, and brother **Greg** for all the support and fun times.

Last but definitely not least, I would like to thank my parents **Selma** and **Lucivan** who throughout my life provided lots of love and the best environment for me to succeed in my educational and moral development. Thank you to my sisters **Rosana** and **Juliana** for your affection and the joy you bring to my life.

I would like to highlight the importance of my family giving me strength and love. While not being with you physically, and going through this journey in another country, you were always with me in my heart and mind. Thank you for sharing your positive energy so I could be here presenting this work to the world. I wouldn't be able to do this without you and this PhD dissertation is dedicated to my family and my wife.

This study was financed in part by the Coordenação de Aperfeiçoamento de Pessoal de Nível Superior - Brasil (CAPES) - Finance Code 001.

Financial agency: CAPES/CWRU - Coordenação de Aperfeiçoamento de Pessoal de Nível Superior/Case Western Reserve University for the financial support to carry out the Double Diploma Program. Process number: 88887.143651/2017-00.

The authors would also like to acknowledge to the Department of Macromolecular Science and Engineering of Case Western Reserve University, CWRU/EUA, and to the Programa de Pós-Graduação em Ciência e Engenharia de Materiais, PPGCEM/UFSCar/Brazil, both for providing their laboratorial facilities.



**RESUMO**

**SISTEMA ON-LINE DE ESPECTROSCOPIA DE INFRAVERMELHO COM  
TRANSFORMADA DE FOURIER PARA ANÁLISE DE PROCESSOS  
BASEADOS EM EXTRUSÃO.**

O processamento é uma chave fundamental para atingir as propriedades desejadas que atendam às necessidades das aplicações dos polímeros. Assim, é importante entender como o processamento contribui para as características do material durante a extrusão. Por isso, este trabalho propõe um método capaz de realizar análises do material durante o processo de extrusão: o sistema on-line espectroscópico de infravermelho por transformada de Fourier (FTIR). O sistema consiste em um dispositivo projetado para acoplar um espectrômetro de infravermelho comercial a uma extrusora de dupla rosca. As medições on-line de FTIR podem ser feitas em diferentes locais ao longo do barril da extrusora. A função matemática Pearson VII foi utilizada para melhorar o comportamento linear de misturas com diferentes composições, proposto por Beer-Lambert, em cerca de 14 % quando comparada aos métodos tradicionais. Blendas poliméricas de polipropileno (PP) e poliamida 6 (PA6) em diferentes composições em peso foram usadas para validar o sistema on-line durante a extrusão. A relação de área entre as bandas em  $1640\text{ cm}^{-1}$  ( $\nu\text{C=O}$ ) e  $1373\text{ cm}^{-1}$  ( $\sigma\text{CH}_3$ ) foram medidas on-line e mostrou-se estar de acordo com as medições feitas em off-line. Quando a blenda reativa de poliamida 6 (PA6) e polipropileno enxertado com ácido acrílico (PP-g-AA) (em misturas de 80%/20% e 30%/70% de PP-g-AA e PA6, respectivamente) foi investigada um aumento da razão da área da banda IR ( $1640/1373\text{ cm}^{-1}$ ) foi alcançado quando a agressividade da condição do processo na mistura foi aumentada devido à geração de novas interfaces entre as duas fases da blenda, mostrado por meio de microscopia eletrônica de varredura (MEV). Através de medições on-line de FTIR foi possível visualizar que o desenvolvimento da reação de mistura reativa das blendas na extrusora em diferentes condições de processo pode levar à mesma ou diferente quantidade de reação ( $1640/1373\text{ cm}^{-1}$ ) no final da extrusora, mas seguem taxas e tempos diferentes.

**Palavras-chave:** Extrusão reativa; blendas poliméricas; FTIR; análises on-line



## ABSTRACT

Polymer processing is a fundamental key to achieve the desired properties to reach the needs of polymer applications. Thus, it is important to understand how the processing can contribute to material characteristics during the extrusion, while they are being processed. That is why this work propose a method able to perform analyses of the material while it is being processed during the extrusion: the on-line Fourier transform infrared (FTIR) spectroscopic system. The system consists of a device that was designed to be able to couple a commercial infrared spectrometer to an twin-screw extruder. On-line FTIR measurements can be done in different locations along the extruder barrel. Pearson VII function was used improving the linearity of mixture composition, which is proposed by Beer-Lambert's law, by around 14% when compared to the traditional methods. Polymer blends of polypropylene (PP) and polyamide 6 (PA6) at different weight composition ratio were used to validate the on-line system during extrusion. The area ratio between the IR bands at  $1640\text{ cm}^{-1}$  ( $\nu\text{C=O}$ ) and  $1373\text{ cm}^{-1}$  ( $\sigma\text{C-H}_3$ ) were measured on-line for all the blend compositions and shown to be in good agreement with off-line measurements. When the reactive blending of polyamide 6 (PA6) and polypropylene grafted with acrylic acid (PP-g-AA) (in blends of 80%/20% and 30/70% of PP-g-AA and PA6, respectively) was investigated along the extruder length, a increase of the IR band area ratio ( $1640/1373\text{ cm}^{-1}$ ) was achieved when the process condition aggressiveness in mixing was improved due to the generation of fresh interface between the two phases, as it is shown through scanning electron microscopy (SEM). Trough on-line FTIR measurements it was possible to visualize the development of the reactive blending reaction of PP-g-AA/PA6 blends inside the extruder. For example, different process conditions lead to the same or different amount of reaction (IR area ratio  $1640/1373\text{ cm}^{-1}$ ) at the end of the extruder, but they follow different rates and times.

**Keywords:** Reactive extrusion; polymer blends; FTIR; in-processing analysis; On-line analysis





## PUBLICATIONS

Barros, L. P., Canevarolo, S. V., Klein, D., and Maia, J. On-line ATR-MIR for real-time quantification of chemistry kinetics along the barrel in extrusion-based processes. *Polymer Testing*. 2021 103:107350.

<https://doi.org/10.1016/j.polymertesting.2021.107350>

Barros, L. P., Canevarolo, S. V., Klein, D., Carter, J., and Maia, J. Compatibilization Kinetics of Nylon/Polypropylene Co-Polymer Blends in Twin-Screw Extrusion: Shear vs. Extension-Dominated Mixing. *Journal of Applied Polymer Science*. 2021 (accepted)

Barros, L. P., Canevarolo, S. V., and Maia, J. On-line assessment of cumulative compatibilization conversion of Nylon/reactive Polypropylene blends along the extruder. *Journal of Applied Polymer Science*. 2021 (submitted)

Barros, L. P., and Maia, J. Evaluation by on-line FTIR of the kinetics of PP/PA6 blend compatibilization with Pp-g-MAH during extrusion. Annual Technical Conference - ANTEC, Conference Proceedings Volume 2019-March2019 77th Annual Technical Conference of the Society of Plastics Engineers, ANTEC 2019 Detroit 18 March 2019 through 21 March 2019 Code 151545.



## CONTENTS

APPROVAL SHEET . . . . .	i
ACKNOWLEDGMENTS . . . . .	iii
RESUMO . . . . .	vii
ABSTRACT . . . . .	ix
PUBLICATIONS . . . . .	xi
CONTENTS . . . . .	xiii
LIST OF TABLES . . . . .	xvii
LIST OF FIGURES . . . . .	xix
LIST OF ACRONYMS . . . . .	xxvii
1 INTRODUCTION . . . . .	1
1.1 Motivation . . . . .	1
1.2 Objectives . . . . .	5
1.3 Unique Contributions . . . . .	7
2 LITERATURE REVIEW . . . . .	9
2.1 Polymer Extrusion Process . . . . .	9
2.1.1 Controlled process parameters . . . . .	10
2.1.2 Reactive Extrusion Process - REX . . . . .	17
2.2 FTIR Spectroscopy . . . . .	18
2.2.1 Theory of Infrared Spectrum . . . . .	19
2.3 In-process Material Characterization . . . . .	22
2.3.1 The Types of In-process Analysis . . . . .	24

2.4	In-process Analysis Tools for Reactive Extrusion . . . . .	27
2.5	Polymer Blends . . . . .	30
2.5.1	Reactive blending . . . . .	31
3	EXPERIMENTAL . . . . .	33
3.1	Probe Holder Unit, PHU . . . . .	33
3.1.1	On-line ATR-FTIR measurements . . . . .	36
3.2	Materials . . . . .	39
3.2.1	Liquid samples . . . . .	39
3.2.2	Polymer resins . . . . .	40
3.2.3	Blending reaction . . . . .	41
3.3	Twin-screw Extruder . . . . .	41
3.4	Number of scans and Signal-to-noise Ratio Dependency . . . . .	43
3.4.1	Analytical techniques: bench measurements . . . . .	43
3.5	Data Treatment with Pearson VII . . . . .	44
3.5.1	Data Pre-treatment . . . . .	44
3.5.2	Data Treatment . . . . .	44
3.5.3	IR Band Normalization . . . . .	45
3.6	Validation of Data Treatment with Pearson VII . . . . .	46
3.6.1	Spectroscopy of Binary Liquid Mixtures: acetone/water . . . . .	47
3.6.2	Spectroscopy of Binary and Ternary Liquid Mixtures: acetone/ethanol/toluene . . . . .	48
3.6.3	Comparison between method . . . . .	48
3.7	Validation of the On-line FTIR Spectroscopy system . . . . .	48
3.7.1	Composition Investigation of the non-reactive PP/PA6 Blend In-processing and Off-line . . . . .	49
3.7.2	On-line FTIR analysis of REX (PP-g-AA/PA6) measured along the Extruder Barrel . . . . .	50
3.8	Reactive Blending Investigation . . . . .	51
3.8.1	Reactive Extrusion of 80/20 (wt/wt%) of PA6/PP-g-AA and PA6/PP . . . . .	51

3.8.2	On-line ATR-FTIR Measurements . . . . .	54
3.8.3	Scanning Electron Microscopy . . . . .	56
3.8.4	Reactive Extrusion of 70/30 (wt/wt%) of PP-g-AA/PA6 and PP/PA6 . . . . .	56
3.8.5	On-line ATR-FTIR measurements . . . . .	57
3.8.6	Residence Time Distribution curves by Colorimetry . . . . .	59
3.9	Software . . . . .	60
4	RESULTS AND DISCUSSIONS . . . . .	63
4.1	Number of scans and Signal-to-noise Ratio Dependency . . . . .	63
4.2	Validation of Data Treatment with Pearson VII function . . . . .	65
4.2.1	Spectroscopy of Binary Mixture: acetone/water . . . . .	65
4.2.2	Spectroscopy of Binary and Ternary mixtures: acetone/ethanol/toluene	71
4.3	Validation of the On-line FTIR Spectroscopy system . . . . .	76
4.3.1	Composition Investigation of the non-reactive PP/PA6 Blend In-processing and Off-line . . . . .	76
4.3.2	On-line FTIR analysis of REX (PP-g-AA/PA6) measured along the Extruder Barrel . . . . .	83
4.4	Reactive Blending Investigation . . . . .	85
4.4.1	Reactive Extrusion of 80/20 (wt/wt%) of PA6/PP-g-AA and PA6/PP . . . . .	85
4.4.2	Reactive Extrusion of 70/30 (wt/wt%) of PP-g-AA/PA6 and PP/PA6 . . . . .	100
5	CONCLUSIONS . . . . .	119
6	FUTURE WORK . . . . .	123
7	BIBLIOGRAPHY . . . . .	125
	APPENDIX A: COMPONENTS OF THE ON-LINE FTIR SPECTROSCOPY SYSTEM . . . . .	145
	APPENDIX B: TOOL HOLDER COLLET CHUCK . . . . .	153

APPENDIX C: LABVIEW SOFTWARE . . . . .	155
APPENDIX D: RTD curves . . . . .	159
APPENDIX E: On-line Spectra - Deconvolution . . . . .	163
APPENDIX F: ATR-FTIR probe validation with transesterification reaction in PET/PC blend in batch mixer . . . . .	173
7.1 Introduction . . . . .	173
7.1.1 Brief Background . . . . .	173
7.2 Experimental . . . . .	173
7.2.1 Materials and Blends . . . . .	173
7.2.2 Process Conditions . . . . .	174
7.2.3 Exchange reaction: Transesterification . . . . .	174
7.3 Results and Discussion . . . . .	176
7.3.1 Benchtop Spectrometer . . . . .	176
7.3.2 Benchtop Spectrometer and ATR-FTIR Probe Comparison .	180
7.4 Conclusions . . . . .	182
APPENDIX G: IN-LINE FTIR SYSTEM . . . . .	183
APPENDIX H: DATA FRAME - EXTRUSION: EXPERIMENT 1 AND 2 . . . . .	189

## LIST OF TABLES

3.1	Materials used in this work and their main characteristics. Liquid samples, purchased from Sigma-Aldrich (SIAL) that were used to validate the data treatment proposed, and the polymer resins that were used for the on-line FTIR measurements during extrusion. . .	39
3.2	Characteristic bands of all materials used in this work and their relative mode of vibration. . . . .	43
3.3	IR band rationing used in this work. . . . .	47
3.4	Acetone/Ethanol/Toluene mixture compositions. . . . .	48
3.5	PP/PA6 wt% compositions. . . . .	49
3.6	Process conditions with the use of different screw profiles varying the distributive and dispersive mixing levels. . . . .	55
3.7	Process conditions varying the type of EME, material system, feed rate and screw speed. . . . .	58
3.8	Meaning of the coefficients of the pulse curves. . . . .	60
4.1	Characteristic bands of all materials used in this work and their relative mode of vibration. . . . .	83
7.1	PET/PC blend compositions. . . . .	174
7.2	Process conditions of PET/PC blending during batch mixing process.	174





## LIST OF FIGURES

2.1	Relationship between independent and dependent process parameters and their possible effects in the polymer melt during extrusion.	11
3.1	Infogram showing the phases 1 and 2 of the methodology used in this thesis. . . . .	34
3.2	Probe holder unit (1) and its components: collet chuck (2), collet holder part (3), measurement chamber (4), molding connector (5) and pressure dome/nut (6) for holding the ATR-FTIR probe (7) and the sampling collector (8). . . . .	35
3.3	Holding steps of the ATR-FTIR probe. In a) the collect is places in the holder, in b) ATR-FTIR probe is aligned with the collet, and in c) the pressure nut is tightened to ensure the ATR-FTIR probe is fixed in a stable way on the extruder. . . . .	36
3.4	Cross-sectional view of the PHU highlighting the measurement chamber with a) disk cavity and b) flow cavity. Material flow are transverse to the extrusion direction and is indicated by the arrows. . . .	37
3.5	Probe Holder Unit and its components: extruder connector, On/Off valve (sample collector), measurement chamber, probe holder, pressure nut and the ATR-FTIR probe. . . . .	37
3.6	On-line FTIR system with all the components attached at P/T port along the extruder barrel. . . . .	37
3.7	Operation of PHU and sampler collector. Polymer melt flow is indicated in red. . . . .	38
3.8	Scheme of blend compatibilization reaction with a) Nitrogegn electron attacking carbon pair of electrons, b) oxigegn becomes more negative, c) re-bonding of $\pi$ bond, and d) the formation of a di-block copolymer of PP and PA6. The red arrows indicate the electron movements. . . . .	42

3.9	Screw profile configurations a) KB30, b) KB90, c) EME L2 and d) EME S4 and the length of the screw that on-line FTIR measurements were done (17.75, 20.25, 30.25, 32.75 and 40.00 L/D). L/D=2 in red indicates the position and length of the mixing zone that is substituted. (T= transport, KB = kneading block, L/D = length and diameter ratio, and RT = reverse transport). . . . .	53
3.10	Extensional mixing elements (EMEs) L2 on the left and S4 on the right. . . . .	57
4.1	Resolution of acetone spectra taken at increasing number of scans.	64
4.2	Relationship between the number of scans in a FTIR measurement and the time of measurement (blue axis) and signal-to-noise (red axis). . . . .	64
4.3	Spectra of binary distilled water/acetone mixtures. Red double-headed arrows indicate the bands analyzed. . . . .	65
4.4	Absorbance (peak height) of acetone (a, b, and c) and distilled water (d) bands calculated by the traditional method, Lorentz function and Pearson VII methods. The R-Squares of the linear fitting according to the composition n shown on the plots in colors corresponding to the method used (Pearson VII = red; Lorentz = blue and; traditional method = green. . . . .	66
4.5	Range of overlapping of the bands at $1710\text{ cm}^{-1}$ and $1656\text{ cm}^{-1}$ bands calculated by the a) Lorentz function and b) Pearson VII methods. The R-Squares of the deconvoluting fitting for both, Lorentz and Pearson VII function are shown on the plots. A better R-Square is achieved by the Pearson VII function fitting. . . . .	68

4.6	Area of acetone (a, b, and c) and distilled water (d) bands calculated by the traditional method, Lorentz function and Pearson VII methods. The R-Squares of the linear fitting according to the composition $n$ shown on the plots in colors corresponding to the method used (Pearson VII = red; Lorentz = blue and; traditional method = green. . . . .	69
4.7	a) Absorbance and b) area ratios of bands of acetone at $\sim 1710$ and $\sim 1356 \text{ cm}^{-1}$ for bands calculated by the traditional method, Lorentz function and Pearson VII methods for the mixtures of 75/25 and 50/50 (vol/vol%) and pure acetone. . . . .	70
4.8	ATR-FTIR spectra for pure (a) Acetone (100A), (b) Ethanol (100E) and (c) Toluene (100T). Double-headed arrows indicate the bands at $1220, 879, 692 \text{ cm}^{-1}$ used in the analyzes. . . . .	71
4.9	ATR-FTIR spectra for binary mixture of 50/50 (vol/vol%) (a) acetone and ethanol (50A/50E/00T), (b) acetone and toluene (50A/00E/50T), and (c) ethanol and toluene (00A/50E/50T). . . . .	72
4.10	ATR-FTIR spectra for ternary mixtures in %vol Acetone, Ethanol, and Toluene. . . . .	73
4.11	Liquid mixture absorbance (right) and areas (left) calculated by the (a and b) traditional, (c and d) Lorentz and (e and f) Pearson VII methods. . . . .	75
4.12	On-line ATR-FTIR spectra . . . . .	77
4.13	Off-line ATR-FTIR spectra . . . . .	77
4.14	a) On-line and b) off-line ATR-FTIR spectra for blends off PP/PA6 at compositions 10/90, 30/70, 50/50, 70/30 and 90/10, respectively. . . . .	77
4.15	Peak area (top) and absorbance (bottom) for bands of amide I and II calculated by both traditional (left) and deconvoluting (right) methods. Results collected by On-line and Off-line ATR-FTIR mode are shown. . . . .	78
4.16	Beer-Lambert's law approximation for band of Amide I ( $1640 \text{ cm}^{-1}$ ) collected by On-line and Off-line ATR-FTIR mode. . . . .	79

4.17 Peak (a and b) area and (c and d) absorbance for peaks of Amide I and II calculated by both (a and c) traditional and (b and d) deconvoluting method with Pearson VII. Results collected by On (red plot) and Off-line (blue plots) mode are shown. . . . .	80
4.18 Peak (a and b) area and (c and d) absorbance for peaks of Amide I and II calculated by both (a and c) traditional and (b and d) deconvoluting method with Pearson VII. Results collected by On (red plot) and Off-line (blue plots) mode are shown. . . . .	81
4.19 Beer-Lambert's law approximation for band of Amide III ( $1266\text{ cm}^{-1}$ ). . . . .	84
4.20 Spectrum of blend of 40/60 (wt/wt%) PP-g-AA and PA6. The band deconvolution method is applied. Bands of amide I, amide II and at $1373\text{ cm}^{-1}$ are highlighted. . . . .	84
4.21 Peak absorbances (a and b) and areas (c and d) of Amide I ( $1640\text{ cm}^{-1}$ ) and Amide II ( $1540\text{ cm}^{-1}$ ) normalized by the band at $1373\text{ cm}^{-1}$ (PP) along the extruder barrel and at line after the die for reactive (PP-g-AA/PA6) and non-reactive (PP/PA6) blends. The screw profile used in the extrusion is shown in the plot. . . . .	86
4.22 Band area ratio ( $\text{Area}_{1640}/\text{Area}_{1373}$ ) development in the axial extruder length (L/D) for reactive and non-reactive blends processed with different screw profiles for both, non-reactive (open circles) and reactive (closed circles) blends. . . . .	88
4.23 SEM micrographs for condition S4-200-2-NR at a) 17.75, b) 20.25, C) 32.75 L/D and d) after passing through the die. In the legend all the bar scales correspond to $10\ \mu\text{m}$ . The red arrows indicate the weak adhesion at the interface between the two phases. . . . .	89
4.24 SEM micrographs for conditions a) KB30-200-2-R, b) KB90-200-2-R, c) L2-200-2-R and d) S4-200-2-R at 17.75, 20.25, 30.25 and at the die out let, respectively from the left to the right. In the legend all bar scales correspond to $10\ \mu\text{m}$ . . . . .	94
4.25 Cumulative area ratio (CAR) for conditions KB30-200-2-R, KB90-200-2-R, L2-200-2-R and S4-200-2-R at the die of the extruder. . . . .	95

4.26 Cumulative area ratio (CAR) for conditions a) KB30-200-2-R, b) KB90-200-2-R, c) L2-200-2-R and d) S4-200-2-R. . . . .	96
4.27 IR absorption band area ratio $\text{Area}_{1640}/\text{Area}_{1373}$ as a function of axial extruder length (L/D) for reactive blend PA6/PP-g-AA blends at processing conditions S4-200-2-R, S4-600-2-R, S4-200-5-R and S4-600-5-R. . . . .	98
4.28 Experimental E(t) curves (circle plots) and corresponding fitted pulse curves (solid lines) for the operating conditions S4-400-5 at 17.75, 20.25, 32.25 L/D and at the die. . . . .	101
4.29 Coefficients of the pulse function from the fitting of the experimental data for all the process conditions that were analyzed. a) Average residence time, b) delay time, c) variance, d) curve ascent time rate constant and e) curve ascent time rate constant. . . . .	102
4.30 Comparison between the E(t) fitted with pulse function of condition L2-400-5 and S4-400-5 at 17.75, 20.25, 32.25 and at the die. . . .	108
4.31 On-line chemical reaction at various process conditions along the extruder length (as L/D ). The slope of the linear fitting for the process conditions are indicated in the plot. . . . .	111
4.32 Transformation vs. mean residence time. Green dashes arrow indicates the increase of aggressiveness of the process condition. . .	114
7.1 On-line FTIR system attached to the extruder. In the picture the temperature control system, the PHU, the air cooling system and the ATR-FTIR probe is shown . . . . .	145
7.2 a) ATR-FTIR probe and b) parameters. . . . .	146
7.3 Nicolet IS 10 MID (4000 to 400 $\text{cm}^{-1}$ ) infrared spectrometer (ThermoFisher Scientific). . . . .	147
7.4 Parameters of the attenuated total reflection crystal of silicon. . . .	147
7.5 Drawings of the chamber of measurement (closed cavity option). .	147
7.6 Sample collector operation and installation, for more details see [1].	148
7.7 Probe holder unit. . . . .	149

7.8	Probe holder unit with the probe. . . . .	150
7.9	Exploded view of PHU with the probe. . . . .	151
7.10	Fibermate. . . . .	151
7.11	BT30 ER32 60mm Collet Chuck Tool Holder. Specificatitons: collet chuck accepts all ER32 collets; works on all BT 30 machines; made from alloy steel hardened to 54 - 56rc (Rockwell Hardness Scale) and; concentricity is less than 0.0001 at collet face ( <a href="https://www.maritool.com/">https://www.maritool.com/</a> ).153	
7.12	a) ER32 COLLET 12mm and b) dimensions. Specifications: total runout less than .0003 on these precise ER32 collets; made from alloy spring steel and fully hardened; all critical collet surfaces are precision ground for accurate fit; works in all ER32 collet chucks; these ER32 collets have a full 0.039 inches range of collapse while maintaining full accuracy and; this ER32 collet has a range of 0.472-0.433 inches ( <a href="https://www.maritool.com/">https://www.maritool.com/</a> ). . . . .	154
7.13	Software screen with the functions: method selection (on-line or off-line); number of spectra for analyzing; peak of reference; range of baseline correction: and save. . . . .	156
7.14	Software screen with the function of selecting of multiple IR bands.	157
7.15	Software screen with the baseline area, IR band area and IR absorbance of multiple bands. . . . .	158
7.16	Experimental E(t) curves (circle plots) and corresponding fitted pulse curves (solid lines) for the operating conditions using EME L2 at 17.75, 20.25, 32.25 L/D and at the die. . . . .	160
7.17	Experimental E(t) curves (circle plots) and corresponding fitted pulse curves (solid lines) for the operating conditions using EME S4 at 17.75, 20.25, 32.25 L/D and at the die. . . . .	161
7.18	Average on-line FTIR spectra deconvoluted by Pearson VII function at 17.75, 20.25,, 30.75 and 32.25 L/D for condition L2-100-2-R. . . .	164
7.19	Average on-line FTIR spectra deconvoluted by Pearson VII function at 17.75, 20.25,, 30.75 and 32.25 L/D for condition L2-400-2-R. . . .	165

7.20 Average on-line FTIR spectra deconvoluted by Pearson VII function at 17.75, 20.25,, 30.75 and 32.25 L/D for condition L2-100-5-R. . . .	166
7.21 Average on-line FTIR spectra deconvoluted by Pearson VII function at 17.75, 20.25,, 30.75 and 32.25 L/D for condition L2-400-5-R. . . .	167
7.22 Average on-line FTIR spectra deconvoluted by Pearson VII function at 17.75, 20.25,, 30.75 and 32.25 L/D for condition S4-100-2-R. . .	168
7.23 Average on-line FTIR spectra deconvoluted by Pearson VII function at 17.75, 20.25,, 30.75 and 32.25 L/D for condition S4-400-2-R. . .	169
7.24 Average on-line FTIR spectra deconvoluted by Pearson VII function at 17.75, 20.25,, 30.75 and 32.25 L/D for condition S4-100-5-R. . .	170
7.25 Average on-line FTIR spectra deconvoluted by Pearson VII function at 17.75, 20.25,, 30.75 and 32.25 L/D for condition S4-400-5-R. . .	171
7.26 Average on-line FTIR spectra deconvoluted by Pearson VII function at 32.25 L/D along the extruder for the non-reactive blend. . . . .	172
7.27 Transesterification reaction leads to copolymers. . . . .	175
7.28 Sequence of different copolymers as a result of the exchange reaction. . . . .	175
7.29 Spectra of pure PET and PC with and without quenching. . . . .	176
7.30 Spectra in the range on interest. . . . .	177
7.31 Spectra in the range on interest of pure PET and PC and 50/50 blends at 3 and 15 minutes mixing time. . . . .	178
7.32 Spectra in the range on interest of the 50/50 blends with and without catalyst at 3 and 15 minutes mixing time. . . . .	178
7.33 Spectra in the range on interest of the 50/50 blends with catalyst at 3 and 15 minutes mixing time. . . . .	179
7.34 Spectra of pure PET, pure PC, and all the 50/50 at 3 and 15 minutes mixing time. IR band at $1070\text{ cm}^{-1}$ relative to aromatic ester (see Figure 7.28). . . . .	179
7.35 Spectra of pure PET, pure PC, and all the 50/50 at 3 and 15 minutes mixing time collected by the ATR-FTIR probe . . . . .	180

7.36 Comparison between Spectra of pure PET and PC, and all the 50/50 at 3 and 15 minutes mixing time collected by the benchtop spectrometer (smooth spectra) and ATR-FTIR probe (noisy spectra).	181
7.37 Prototype of the In-line FTIR.	183
7.38 Components of the In-line FTIR.	184
7.39 Prototype of the water cooling system for the ATR-FTIR probe. In the figure tow hoses are depicted: water inlet and outlet.	184
7.40 Components of the probe water cooling system.	185
7.41 Assembly of the In-line FTIR system and probe water cooling system. The yellow rod simulates the ATR-FTIR probe with the cooling system installed. On the figure we can see a pressure transducer installed next to the probe for pressure measurement.	185
7.42 Digital design of the co-rotational twin-screw ex-truder ZSK 30 from Werner & Pfleiderer.	186
7.43 Assembly of whole system attached to the extruder. Direction of extrusion: right to the left.	187



**LIST OF ACRONYMS**

**UFSCar** -Universidade Federal de São Carlos

**PPGCEM** -Programa de Pós-Graduação em Ciência e Engenharia de Materiais

**ATR** Attenuated total reflection

**aR** Infrared band area ratio

**aR<sub>NREX</sub>** Infrared band area ratio of non-reactive blends

**aR<sub>REX</sub>** Infrared band area ratio of reactive blends

**CAR** Cumulative area ratio

**d<sub>p</sub>** Depth of penetration

**EME** Extensional mixing element

**EME L2** Extensional mixing element with long channel, contraction ratio 2

**EME S4** Extensional mixing element with short channel, contraction ratio 4

**F<sub>R</sub>** Feed rate

**FTIR** Fourier transform infrared

**IR** infrared

**I<sub>0</sub>** Initial intensity of pulse curve

**K** Area under the curve constant

**KB** Kneading block

**L/D** Screw length and screw diameter ratio

**MFI** Melt flow index

**MIR** Mid infrared

**MRI** Magnetic resonance imaging

**NIR** Near infrared

**PA6** Polyamide 6, Nylon 6

**PP** Polypropylene

**PP-g-AA** Polypropylene grafted with acrylic acid

**PHU** Probe holder unit

**R<sub>1</sub>** Ascent time rate constant

**R<sub>2</sub>** Descent time rate constant

**REX** Reactive extrusion

**RT** Residence time

**SEM** Scanning electron microscopy

**S<sub>S</sub>** Screw speed

**SSE** Single-screw extruder

**SME** Specific mechanical energy

**TSE** Twin-screw extruder

**t** Average or mean residence time

**t<sub>t</sub>** Total mean residence time

**t<sub>p</sub>** Partial mean residence time

**UV-Vis** Ultraviolet-visible

**X<sub>0</sub>** Delay or initial time

## 1 INTRODUCTION

### 1.1 Motivation

The extrusion process is a robust continuous manufacturing process for polymer materials. It consists of a tubular heated barrel, one (single) or more (twin or multiples) rotating screws, a motor, a hopper at the beginning from which the polymer is fed, and a die at the end for shaping the extrudate. Twin-screw extruders (TSE) are one of the most prevailing technology in the plastic industry with applications from polymer composites formulation to polymer blending [1–3]. TSEs have also been used as a continuous reactor to perform, for example, polymerization and compatibilization of polymer blends (denoted as reactive extrusion or REX) [4–6]. This is due to flexibility of TSEs in providing varying levels of mixing and a wide range of thermomechanical history in the melt. Moreover, TSEs can be modular and be used for continuous production [1, 7].

As can be seen in the literature, the variety of processing conditions in extrusion process greatly affects the reaction conversion in REX [2, 8, 9]. This can make the understanding of the REX process very challenging. Many researchers have tried to investigate the correlations between the material characteristics and processing conditions [10–12], such as, Machado et al. (2001), which discussed how varying temperature and screw profile had influenced the chemical conversion in PA6/EPM/EPM-g-MA (polyamide 6/ethylene propylene rubber/ethylene propylene rubber modified with maleicanhydride) blends by FTIR. The authors found that the increase in the temperature the grafting of maleic anhydride is accelerated by the decomposition of peroxide at higher temperatures [8]. This study is important because it proves the dependency of process parameters and chemical reaction. However, studies in reactive extrusion being analyzed during the process are still scarce because the characterization of the chemical reaction conversion inside the extruder is challenging. That is because off-line techniques require the material be sampled from the extruder and handled for laboratory characterization, further transformation (reaction) and loss of the thermomechanical history occurs. This time delay causes a lack of representability between the

sample and the material that is being processed. The possibility to increase this representability aforesaid can help to track the chemical reaction development inside the extruder improving understanding of the correlation between process condition and chemical conversion. To solve this problem, this work applies in-process measurements to investigate the material while being processed.

In-process analysis are measurements of the polymer melt characteristics performed by devices that connect the characterization instrument to the extruder. The measurement is done as the extrusion process progresses, without disrupting the flow. This increases the representability between the sample and the material that is being processed. In-process measurements provide data about the polymer melt state in real or near-real time. It can be done by in-line or on-line mode. When the characterization instrument is coupled in in-line mode, the measurement is done in the main polymer stream in the process line. Whereas, in on-line mode a representative amount of the melt is diverted from the extruder process line to the characterization instrument to perform the analysis. Short delay time and sample representability are important advantages of in-processing analysis over the off-line mode [13]. The concept of in-process investigation by using on-line mode of analysis has been successfully used previous to monitor various polymer systems and processes such as grafting of maleic anhydride into various polyolefins [14], polyolefin modification [15], and blending of liquid crystalline polymers and polypropylene [16], among others. However, these researches have investigated the reaction at the die (end) of the extruder.

However, measurement along the length of the extruder is more useful to evaluate REX. That is because at the die of the extruder all the conversion should be complete and the development of the reaction (reaction rates) can be tracked in different locations of the barrel. However, the performance of measurements along the extruder barrel is challenging because some modification of the barrel is necessary, which makes harder and costly. For example, Machado designed a device that can be inserted in between blocks in a modular extruders[15]. This device only works for specific extruders, which means that it does not work for non-modular extruders, where the barrel is not in blocks. That is why this work

proposed a device that is able to be screwed in standard 1/4" thread UNF P/T ports already available in almost all extruders and make measurement in on-line mode.

Currently, most extruders are already equipped with standards sensors (temperature and pressure transducers) able to perform in-line measurements of the melt temperature and pressure. However, the rapid development in analytical techniques, from conventional laboratory-based methods (off-line mode) to tools that can be used to analyze the material in-processing, has increased the ability to characterize more complex properties of the material during extrusion. There are vast options of characterization techniques that can be coupled into the extruder for in-process analysis. For example, rheological and optical properties can be analyzed in in-process [17, 18]. Particularly for REX, FTIR spectroscopy techniques are available for performing analysis of the development of the chemical reaction inside the extruder. The absorption of IR radiation by the material is sensitive to the changes of molecular structure, which means that the chemical reaction can be tracked by infrared spectroscopy. This can help to understand the complex relationship between process parameters and the chemical conversion of the reaction in REX inside the extruder barrel.

In fact, FTIR spectroscopy has been applied in extruders to investigate the process [13, 19–22]. However, these authors have used the technique only at the die of the extruder and in non-reactive extrusion. Most of researchers have used infrared spectroscopy in NEAR-IR wavelength region. This is because the IR radiation in near (NIR) region has higher energy and long path length, which is a result of a small extinction coefficient. However, NIR spectroscopy probes vibrational overtones and combination of fundamental vibrations, and the molecular structure information are seriously overlapped which makes it not inherently quantitative. Furthermore, it requires difficult calibration against known materials. Absorption bands in the MID-IR wavelength region (MIR) are more intense and can easily be assigned to fundamental vibrations. Thus, it is possible to have a better understanding of side reaction in case of reactive systems. Finally, it is relatively easier to implement quantitative data treatments for a wide variety of material systems and to apply method of IR peak deconvolution. This ma-

kes MIR more promising for characterization of conversion in reactive extrusion. Especially for R&D in-process analysis, where the studied material is frequently changed, MIR is preferred, since data analysis is more quantitative and accurate and no complex modifications of data treatment models is necessary when the material system is changed [23].

Attenuated total reflectance (ATR) mode, in particular, is a very common MIR technique [24]. ATR can also measure materials and samples in different phases, forms or shapes. Furthermore, there is no need for sample preparation. These factors make ATR able to be applied in on-line mode. Some authors have reported on-line measurements along the extruder, however not for REX [11, 25]. In this thesis, an ATR probe is used to do on-line measurements along the extruder in order to evaluate the development of the chemical reaction in the reactive blending of PP-g-AA/PA6 blends.

The extraction of useful information from the ATR-FTIR spectral data and conversion into physically and chemically significant findings is challenging, especially if the features (i.e., characteristic bands) overlap with one another, and when the signals contain noise. The overlapping or superposition of IR bands occurs because in multicomponents polymer systems the two components might have molecular vibration modes on similar wavelength range [26–28]. The traditional method to quantify IR bands in an IR spectrum is to draw a baseline between the on and off-set of the band of interest [29]. This is challenging when overlapped bands are present on the spectrum [30, 31]. In the literature, the method for spectral data modeling is determined by the quality and nature of the spectra set and the desired information to be extracted [27]. For example, the application of derivative and Fourier self-deconvolution (FSD) are common alternatives for compositional analyses instead of the traditional peak height data analysis approach. These data treatments eliminate baseline variation and will greatly resolve spectra bands [23, 27, 28]. However, the main limitations of these methods is that they hide possible overlapped or weak infrared bands, magnify noises, and are very operator dependent leading to artifact generation [27, 28, 30, 32, 33]. The use of mathematical functions, such as Lorentz, Gaussian and, Voigt, that describe

the IR band shape are used to deconvolute overlapped IR bands. Lorentzian function is commonly used to deconvolute IR bands. In this thesis, Pearson VII function was proposed to be used instead of Lorentz and the traditional method. The Pearson VII function was often used to describe X-ray diffraction peaks and because of the function ability to describe different tail-shapes it can be used to fit IR bands. The function was proposed to be used by Keles et al. (2014) in infrared image collected in real-time [27]. By applying Pearson VII all the curve fittings in this thesis have a R-square above 0.9, higher than the fitting with other functions that were also tested in this work such as, Lorentz, Gaussian and, Voigt functions. The comparison between Pearson VII, Lorentz and the traditional method is evaluated here.

## 1.2 Objectives

The goal of this work is to broaden the understanding of the extrusion process, especially in terms of reactive extrusion by on-line infrared spectroscopy. To achieve this goal four main objectives were envisaged, namely:

- to design and implement a device (which we call probe holder unit, PHU) to couple a commercial ATR-FTIR probe along the extruder barrel through existing pressure/temperature transducer ports available in extruder, so there is no need for barrel modifications.
  - the system ATR-FTIR probe and PHU (on-line FTIR system) work in MID-IR region of the IR spectrum and is able to analyze a relatively wide range of material systems during extrusion.
- to use Pearson VII function to deconvolute IR bands and minimize errors from the overlapping of IR bands and noises in the baseline in the MID-IR region of the IR spectrum compared to methods that are currently utilized (traditional method and Lorentzian function). The method was validated by:
  - analyzing the IR bands of acetone at 1710, 1356 and 1220  $\text{cm}^{-1}$  and distilled water at 1636  $\text{cm}^{-1}$  in different known composition (100/0, 75/25, 50/50, and 0/100) of their binary mixtures. Traditional method,

Lorentzian and Pearson VII function were applied in the binary mixture and the linearity, proposed by Beer's law, was evaluated through the R-square of the linear fitting for the compositions of the mixtures.

- analyzing the IR bands at 1220, 879, and 692  $\text{cm}^{-1}$  of acetone, ethanol and toluene, respectively, in different known compositions of their binary and ternary mixtures.
- to validate the system of ATR-FTIR probe and PHU with controlled conditions (of processing and materials) during extrusion following ASTM standard practice (D3764 and D6122) as guidelines. The validation will be achieved by:
  - comparing the proposed on-line FTIR system to two methods that measure the same property (IR band area ratio) in off-line mode.
    - \* This comparison was done by analyzing the area ratio of the IR band at 1640  $\text{cm}^{-1}$  and 1373  $\text{cm}^{-1}$  of polymer blend PP/PA6 at different compositions and at the same process conditions during extrusion. Samples were collected in order to off-line measurements.
    - \* the on-line FTIR system measurements were compared to ATR-FTIR spectroscopy and to FTIR transmission mode, both in bench.
  - the system of ATR-FTIR probe and PHU operation and accuracy is validated by analyzing reaction of the reactive blending between PP-g-AA and PA6 at different locations along the extruder during process. The validation was done at fixed process conditions and it is compared to the non-reactive blend of same composition.
- to use FTIR measurements to quantify the chemical reaction along the extruder barrel of the reactive blending of PP-g-AA and PA6, and investigate the relationship between process conditions and reaction development. This is achieved by:



- investigating the effect of different levels of shear and extensional-dominated mixing on the reactive blending of 80 % of PA6 and 20 % of PP-g-AA during extrusion by using four different mixing zones in the screw geometry, namely, kneading blocks (KB) staggered at 30°, KB staggered at 90°, extensional mixing elements (EME) with long channels of inlet and outlet contraction ratio of 2 and, EME with short channels of contraction ratio of 4.
- to investigate different levels of shear due to the variation of process parameters of screw rotation speed (100, 200, 400, and 600 rpm) and material feed rate (2 and 5 kg/h) on the reactive blending of 70% of PP-g-AA and 30 % of PA6 during extrusion during extrusion.

### 1.3 Unique Contributions

The major contributions of this research work in the field of polymer science are listed as follows:

- Designed an efficient (in terms of the ability to do on-line measurements along the extruder) tool for extrusion process investigation through mid infrared spectroscopy during process.
- Experimentally validated the accuracy of the designed system in controlled materials systems (i.e., polymer blends and reactive blending during extrusion).
- Proposed a method of infrared band quantification by using deconvolution of bands by Pearson VII [27]. The method was experimentally validated (with liquid mixtures) and compared to traditional method of IR band analysis, and deconvolution by Lorentz function, resulting in an improvement of measurement accuracy.
- Contributed to the better understanding of how process conditions of feed rate, screw speed and screw geometry influence in the residence time parameters. Increasing the screw speed the conveying of material is increased

shortening the residence time. The feed rate increases the amount of material in the screw channels, increase the pressure, leading to faster extrusion runs. The use of restrictive zones in the screw geometry increases the pressure, leading to a decrease of the residence time.

- Contributed to the better understanding of how the generation of fresh interfacial area (that is governed by the process conditions) can tremendously improve the chemical reaction along the extruder. The conclusion is that process conditions with high mixing capability lead to a higher reaction of the reactive blending of PP-g-AA and PA6. This is because the reaction between acrylic acid and the end amine group takes place on the interface between the two polymer phases. Consequently, the higher interface generated by the mixing, the higher the reaction. This was possible to achieve by comparing the FTIR analysis with SEM micrographs.

## 2 LETERATURE REVIEW

### 2.1 Polymer Extrusion Process

Extrusion process is defined as a robust continuous process that pumps material through a extruder die into a final product of uniform shape. The process is done under a controlled condition, which is achieved by a combination of process parameters that can be adjustable, such as screw speed, feed rate and, temperature [34]. The process is carried out inside an equipment called extruder. Extruders consist of a tubular heated barrel, one or more rotating screws, a motor, a hopper at the beginning from which the polymer is fed, and a die at the end for shaping the extrudate.

The process begin when the polymer, which can be in pellet or powder form, is fed through the hopper at the beginning of the process into the barrel. Inside the barrel, which can be heated in different zones individually, one or two screws rotate to transport the material along the barrel of the extruder. The barrel can be either one-piece or modular. In modular extruders the barrel can be changed to better meet the application need. The heat from the barrel and from the friction between the polymer and the extruder parts (screws and barrel wall) melt the polymer. The polymer melt is pushed through the die thanks to the pressure built inside the barrel. The pressure is increased due to the screw geometry and the amount of material inside the cavity between screw and extruder barrel wall (degree of material fill).

Particularly, twin-screw extruders (TSEs) are the most prevailing technology in the plastic industry, but single and multiple screw extruders exist as well. The application can be in polymer composite formulation and polymer blends [3, 18]. In twin-screw extruders, the two screws can rotate in the same (co-rotating) or in the opposite direction (counter-rotating). The main difference is in the application of each option. Counter-rotating extruders apply higher shear in the melt. But they operate at lower maximum screw speeds, leading to lower output.[1] Co-rotating twin-screw extruders are often fully intermeshing, which means that the screws are self-wiping. The fully intermeshing characteristic makes the material

(polymer melt) to be transferred between both screws.[6] In co-rotating extruders high screw speeds can be used, delivering high outputs. The main advantage is the good mixing of the melt due the complexity of the flow in the intermeshing region.

The screw itself can also be modular or segmented, which gives high flexibility in the screw design. The mixing, transport, pressure can be varied with the geometry of the screws. The screw design has a significant influence on the extrusion process overall. That is because the screw geometry or screw profile is build with different screw elements. Conveying or transport elements provide transport of the polymer melt along the barrel, either forward or backward. Backward or reverse element is used to increase the pressure inside the extruder. Mixing zones can be built in the screw profile by adding mixing elements. Depending on the design of the mixing elements their function can be distributive or dispersive mixing, which is related to the kind of flow that the geometry of the mixing element impart in the melt [17]. More literature related to screw geometry and the kind of flow can be found in [1, 35]. The length of a TSE is normally referred as a ratio between the length (L) and the diameter (D) of the screw, namely L/D. For example, an extruder where the screws diameter is 100 mm and length 4000 mm will have the L/D equals 40/1.

The primary goal of an extruder is to continuously transform materials aiming to enlarge the scope of use of plastics. This transformation can be in compounding and blending [7], shape, composition, morphology, and even structurally (REX). One advantage of the extrusion process is that the cost can be reduced when compared to batch processing by eliminating complex steps such as, polymerization reactions and purification of the final product. Finally, extrusion is an environmentally friendly process due to the fact that it is a solvent-free process, which has increased the interest of this process in industry [36].

### **2.1.1 Controlled process parameters**

In the extrusion process there are two factors (shown schematically in the first column of Figure 2.1) that influence the final properties of the finished material/product. The first one is the chemical and physical characteristics of the

material itself. This is related to the polymer system that will be processed, the composition and the kind of chemical bonds that will be formed between the components. In addition to the material thermal stability, which will be responsible for how much of chemical degradation will occur in the system during process. The second factor is the processing conditions, which is a combination of the process parameters [36]. The process parameters can be adjustable or part of the set up of the extrusion process (independent parameters) or a result of the independent one, which is called dependent parameters (shown schematically in the second column of Figure 2.1). The factor process condition will be the focus of this work.

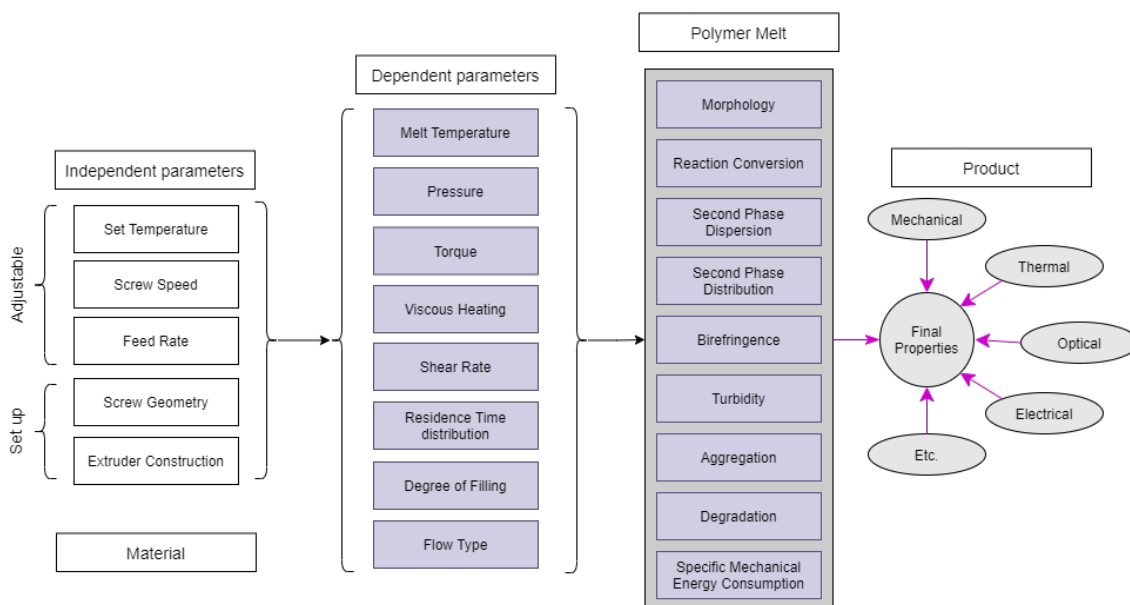


Figure 2.1: Relationship between independent and dependent process parameters and their possible effects in the polymer melt during extrusion.

The complexity of the process arises from the fact that the independent process parameters concomitantly influence the dependent process parameters, and they are associated with the behavior of the polymer melt that impact the final product properties. [37, 38]. Example of independent process parameters are the barrel temperature, screw speed, feed rate, the screw geometry and the extruder construction (single, twin, counter-rotating, co-rotating screws, and etc). They can be set and will impact the dependent ones. For example, the barrel temperature is an independent process parameter and can be set individually for each zone of the extruder. The melt temperature, on the other hand, is a result

of the viscous heating. Which is dependent on other parameters, such as, screw speed, screw geometry and barrel temperature. Another example of a dependent process variable is the pressure in the extruder. The pressure can be controlled by screw configuration, which is an independent process variable. This means that the restrictive zones (mixing zones and reverse flow zones) in the screw can considerably increase the pressure in that region or in the whole process. Similarly, shear forces during extrusion can be affected by screw configuration, screw speed and by the construction of the extruder [39, 40]. The relationship between independent and dependent process parameters is very complex and it is not part of the scope of this work. But a good discussion about it can be found in [41]. However, the main contributions of the parameters of screw geometry, screw speed, feed rate, and residence time distribution (RTD) to the process are going to be explored in the next items. That is because the focus of this work is to apply various process conditions with different screw geometries, screw speeds and feed rates and measure the residence time distribution imparted by each process conditions correlating with the chemical reaction between acrylic acid (grafted in polypropylene) and amine end group in polyamide 6, measured by FTIR spectroscopy.

### *Screw Geometry*

The screw geometry is a set of independent process parameters. The screw geometry is associated with the design of screw elements and the location along the screw they are inserted. There are screw elements with the objective of conveying the melt, mixing the material, and increase of pressure in certain location of the screw. For example, Zhang et al., (2015) found that the average diameter of nanofibers of PA6 decreased with the increase of the shear rate generated by the screw geometry due to higher deformation and higher breaking and reduced coalescence of the dispersed phase [39]. The difference in the design of the screw in trilobal (triple-flighted screw) and bilobal (double-flighted screw) also was pointed to as a factor to increase the shear by Haser et al., (2018) [42]. Sasimowski et al., (2019) used different designs of screw mixing tips (screw element at the end of the screw) in a single-screw extrusion of biocomposite of

LDPE/lignocellulosic wheat bran. The screw tips impart different kind of mixing flow (distributive and dispersive). The authors found difference in microstructure, density, water absorbance, mechanical (tensile) and thermal properties [43]. The levels of distribute and dispersive mixing provided by the screw geometry were also evaluated by Pandey et al., (2021). The morphology was improved when extensional mixing elements (EME) were use. The extensional-dominated flow imparted by the EMEs enhanced the dispersion of the second phase in immiscible polymer blends and composites, for both single and twin-screw extruders. As a consequence of the enhanced dispersion the tensile properties were optimized [44, 45]. Screw geometry has been proved to be an effective way to control morphology and rheological properties [35], glass fiber length reduction [46], fiber dispersion and wetting in composites [47], PA6 phase change [48] and mechanical behaviors [49, 50].

#### *Screw Speed and Feed Rate*

Feed rate ( $F_R$ ) and screw speed ( $S_S$ ) are the primary process parameters that can be changed to vary a wide range of dependent process parameters. Despite that the screw speed and feed rate have a coupled effect during extrusion, the starve-fed characteristic of twin-screw extruders allows them to be independent process parameters [42, 44, 51]. Consequently, these parameters can be used to control other dependent parameters. These are: residence time, shear forces, degree of fill of material inside the extruder, conveying rate, melting, back pressure, strain ranges and specific energy input [51]. These affect the polymer melt inside the extruder which, in turn, affects the final product properties. For example, Haser et al. (2018) have studied the scale-up of the extrusion process of meloxicam-copovidone amorphous solid dispersion. They varied the screw speed and feed rate to alter the degree of fill in dissimilar geometry extruders. A higher degree of fill was achieved by increasing the  $F_R$ , leading to a more efficient mixing of the polymer melt. The combination of different values of  $F_R$  and  $S_S$  were also used to control the melt residence time. In order to reduce the thermal exposure of the material, the residence time was reduced by increasing  $F_R$  and  $S_S$ . Interestingly, the parameters were varied to achieve the same SME

(specific mechanical energy) in the two extruder utilized in the study by reducing screw speed and using different temperature profiles. Differences in the opacity, purity, color (yellowness and brownness) and crystallinity of the amorphous solid dispersion, i.e., final product quality, were found [42]. Researchers have proved that the variation of screw speed can be directly proportional to the dispersion of nanofillers in composites and on the matrix crystallinity. Greater uniformity of nanofiler dispersion was found at higher screw speed in LDPE-based nanocomposites with the same filler content. On the other hand, the higher screw speed seemed to decrease the degree of crystallinity of the matrix. These coupled phenomena lead to a slight decrease of Young's modulus with the increase of screw speed [52]. Dickson and Sandquist (2020) increased the feed rate from 12 to 24 kg/h during extrusion of polypropylene/glass fiber composite. They found shorter fiber length at lower feed rate (12 kg/h) in a portion of the screw along the extruder barrel. According to the authors the fiber length tends to be more preserved when higher feed rates and lower screw speeds are used, however this effect can largely change when kneading blocks are used [46]. Screw speed has also been varied during the reactive extrusion of poly(lactic acid)/poly[(butylene succinate)-co-adipate]/epoxy chain extender (PLA/PBSA/epoxy chain extender) blends at various composition and the nanocomposites with nanoclay. The correlation between  $S_S$  and the morphology, mechanical and rheological properties were evaluated. When the screw speed is increased from 50 to 150 rpm the average diameter of the second phase particles (PBSA) is increased. They suggested that at higher screw speed the residence time is shorter than the particle breakup time [53]. This agrees with the conclusions of Bock and Deiters (2017), that the material moves faster through the extruder at higher screw speeds, leading to a decreasing residence time [37]. Mirzadeh and Kamal (2015) stated that longer particle breakup times can be related to the high viscosity of the matrix. Consequently, the short residence time at 150 rpm will not allow enough time for the particles of PBSA to break up. Narrower and shorter RTD at higher  $S_S$  were also found in studies reported by Matic et al. (2019, 2020) [38, 54]. On the nanocomposites of PLA/PBSA/epoxy chain extender/nanoclay, the degree of



intercalation of the nanoclay was found to be proportional to the screw speed. Increasing the screw speed from 50 to 150 rpm lead to thermal degradation of the PLA matrix. Consequently, this resulted in a reduction of the complex viscosity of PLA [53]. In the literature, screw speed was also associated to the filling degree. At constant feed rate the filling degree is decreased by the increase of screw speed. On the other hand, higher feed rates increase the filling degree. Consequently, higher degree of filling can be reached with high feed rates and low screw speeds [54]. According to the authors, the degree of fill is directly related to the residence time distribution. A longer length of the filled zone (degree of fill) can lead to a wider RTD. The feed rate is inversely proportional to the mean residence time because at higher  $F_R$  the material is forced to move faster at a constant  $S_S$  [38, 54]. The increase of residence time indicates that the material that is being processed is subjected to shear and temperature for a longer period of time. The longer thermal exposure can possibly lead to material degradation [38].

#### *Residence Time Distribution*

The dependent process parameter residence time (RT) is one of the most important parameters affecting the final properties of the extrudate. This is because the residence time is a measurement of how long the material remains inside the extruder being subjected to high shear and thermal exposure [55]. For reactive extrusion particularly, residence time is related to the amount of time the reactants will be in contact to react [56, 57]. For example, the time the material remains in the extruder needs to be long enough for the chemical reaction in reactive extrusion to happen [58], or for the morphological development to be completed [53]. It also has to be short enough not to cause material degradation [38] due to the thermal exposure [59]. Bernardo, Canevarolo and co-workers (2018) stated that the RTD curves are “finger-prints” of a certain processing condition [7]. That is because RTD can be an indication of flow pattern, conveying capacity, axial dispersion, and stagnation zones of an extruder. RTD curves reflect the processing conditions on the state of the extrusion process and the extruded product [60]. Polosin and Chistyakova (2018) have shown during mathematical modeling

of polymeric films extrusion that the extrudate quality index depends on the mean residence time [61].

In extruders, the residence time is a distribution of times. That is because the elements of the material entering the extruder at the same moment travel through the extruder in different paths. The polymer melt flow can be faster or slower depending on the screw movement and geometry or it can be retained in regions of the screw without transport capability (neutral) [55]. This leads to the particles to move with different velocities, resulting in a distribution of residence times (RTD) along and at the die of the extrusion [62]. Thus, this distribution of times means the longest, the shortest and the average time the material spends inside the extruder [59].

The RTD measurement is conducted through the tracer experiment. Simply, when the extruder reaches the steady-state, a tracer is injected into the extruder and its concentration is measured within the time that the material leaves the extruder [62, 63]. The tracer is a pulse of a material distinct of the processed material and it is usually injected at the hopper [64]. However, due to the modular and flexibility of twin-screw extruders, the injection can be done anywhere along the extruder as long as the injection is done with consistency. The same can be said for the measurement of the concentration of the tracer, usually at the die (total residence time), but measurements along the extruder (partial residence time) are also an important tool for investigating the development of the material along the extruder. This provides infinite possibilities when it comes to understanding the behavior of the polymer melt in different portions of the extruder barrel. The measurement can be done in off-line, at-line, on-line and in in-line mode [60].

The residence time distribution is at the heart of the understanding of the extrusion and reactive extrusion process [60]. That is because the different shapes (width, intensity, increase curve rate, decrease curve rate, area under the curve and shifting) of the RTD curves can be a report of the thermal and shear history of the polymer melt [55]. From the RTD curve the average residence time ( $\bar{t}$ ) and the variance (related to the width) can be quantified. In addition, through curve fitting (e.g., pulse function curve) information of the rate of increase and decrease of

the curve can be evaluated [9, 57]. The shape of RTD curve is dependent on the process conditions and the material being extruded. RTD curves can be affected by independent process parameters, such as screw geometry, screw speed, and feed rate. They are also affected by dependent process parameters, such as, degree of filling. There have been several investigations into the correlation between process parameters and RTD [61, 64–66]. For example, Lu et al. (2018) have used different combinations of screw speed and feed rate to keep the average or mean residence time ( $\bar{t}$ ) below of the period of time at the temperature of thermal stability of hypromellose acetate succinate (HPMCAS). This was done to avoid risk of thermodegradation [59].

Together these studies provide important insights into the correlation between the independent and dependent process parameters and the polymer melt status. This synergistic correlation will lead to variation in the quality of the final product. This corroborates the ideas of Haser and Zhang (2018), who suggested that differences in barrel and screw configurations, feed method, free volume and melt temperature can contribute to the optimization of material formulations [42].

### **2.1.2 Reactive Extrusion Process - REX**

Extruders are used to produce materials with unique properties [36]. However, according to Hopmann and Beyer (2017), it is possible to improve polymer properties even more with the use of reactive extrusion process (REX) [60]. This improvement is achieved by carrying out a controlled chemical reaction between the material components inside the extruder [36]. REX is also defined by Covas (2017) as a single operation that associates chemical reaction and extrusion melting [67]. Tzoganakis, in turn, states that REX is a process that simultaneously combines operations of shaping, processing and the modification and synthesis of polymers into a final product [68].

Most chemical reactions can be carried out in extruders. For example, polymerization reaction (coordination, condensation, free-radical, cationic and anionic), compatibilization reaction of immiscible polymer blends, *in situ* synthesis of biodegradable systems, and modification of polymer (functionalization of commodities and polymer grafting) [36, 67]. Thus, the chemical reaction can be used to im-

prove the compatibilization in polymer blends and in between fillers and matrix in composite materials by enhancing the adhesion between the material components [60]. These examples show how versatile and flexible extruders can be. In an excellent review paper on reactive extrusion, Cassagnau et al., have presented some examples of types of reactions performed by REX [69].

Twin-screw extruders (TSE) offer several advantages to perform chemical reaction inside it when compared to batch chemical reactors. As aforementioned, the lack of solvent need, while being environmentally friendly, also provides the possibility to process materials with a wide range of viscosities. Extruders are modular, which allows complex formulation to be processed. The segmented screws in twin-screw extruders also makes the extrusion a very versatile process. This provides a higher control of pressure, residence time, distributive and dispersive mixing in the polymer melt [60, 70]. In spite of that, Cassagnau (2019) and Ibañez (2020) pointed out that the high viscosity of some polymer systems can lead to a strong self heating. This, in turn can promote side reactions, e.g., thermal degradation [58, 69, 71]. However, this issue can be overcome thanks the modular design of extruders, which allows individual cooling and heating of zones targeting problematic segments of the extruder [6, 60]. Due to the relative short residence time in extruders, compare to batch processing, only quick-type reactions can be carried out in extruders [69, 71]. Nevertheless, the residence time can be improved to a certain extent to meet the application needs by modifying screw geometry, throughput and screw rotation speeds. The great mixing capabilities are considered the most important factor of the use of twin-screw extruder in REX [60, 72]. That is because extruders have the ability to continuously create new thin layers in the polymer melt, leading to a chaotic mixing. This reduces the inhomogeneity of mixtures of material [51, 68, 72]. This makes the extruder promising to run chemical reactions because the mixing of multicomponent materials is directly related to their final quality [72].

## **2.2 FTIR Spectroscopy**

Fourier transform infrared (FTIR) spectroscopy is an important tool for organic compounds analysis. That is because FTIR spectroscopy is a techni-

que than can be used to track chemical reaction in reactive extrusion process [11, 26, 27, 73, 74]. Normally, FTIR spectroscopy gives information about the molecular structure of the material and quantitative and qualitative data about chemical functional groups. FTIR spectroscopy generates an infrared (IR) spectrum that is quick and easy to run [75, 76]. The infrared spectrum is given by the interaction between the IR radiation and molecular vibrations in the material. The infrared spectrum is a plot of the transmitted radiation (after interaction with the matter) as a function of the energy of the vibration mode, which is in function of the wavelength. FTIR spectroscopy is the science that interprets this spectrum and is one of the most popular techniques for molecular structure identification. The IR spectrum is a “fingerprint” of a molecule. In addition, it is used to identify the presence or absence of chemical functional groups. Quantitative analyses of multicomponents materials can be done with this technique. FTIR spectroscopy can measure liquids, solids, and gas samples. Different types of sampling techniques are available, depending on the way the material is exposed to the IR radiation, in transmission or reflection mode [77].

### 2.2.1 Theory of Infrared Spectrum

Infrared radiation, or sometimes called as infrared light, falls between the visible light and the microwave regions of the electromagnetic spectrum, from wavelengths of  $0.78 \mu\text{m}$  to approximately 1 mm [76, 78]. In infrared spectroscopy the radiation is normally characterized by the wavenumber unit (in  $\text{cm}^{-1}$ ), the reciprocal of the wavelength. The wavenumber in turn is proportional to the energy or frequency of the wavelength [77]. The infrared radiation is divided into three energy regions: the near, mid and far infrared. From the near-infrared (NIR) region ( $13000\text{-}4000 \text{ cm}^{-1}$ ) we can observe overtones or combination of some fundamental stretching bands. The IR bands in this region are usually overlapped can occur, which made this region hard to qualitative analysis in early days. However, with the advent of the computer science development abundant information about the molecule structure can be observed in this region [79]. The far-infrared spectrum ( $400\text{-}100 \text{ cm}^{-1}$ ) is useful for analyzing molecules with heavy atoms, molecular torsion, crystal lattice vibrations and molecular skeleton vibrations [80]. For

organic chemists, mid-infrared (MIR) region is more practical in terms of usage [75]. The fundamental vibrations can be observed in mid-infrared region and the spectrum can cover basically four groups of frequency, such as, the stretching region, the triple-bond region, the double-bond region and the fingerprint region [80].

### *Infrared Radiation Absorption*

In a spectrometer, a source of IR radiation sends a polychromatic beam through the material sample, thus the sample is irradiated with a range of infrared frequencies simultaneously. The IR radiation increases the vibrational energy of the molecules in the material at the expense of the radiation energy provided by the infrared beam. This results in the absorption of infrared radiation by the sample at the same frequencies of the molecular vibrations. That is because each specific frequency is characteristic of certain chemical bonds. The intensity of the reflected or transmitted infrared radiation (that was not absorbed by the sample) is measured as a function of frequency of vibration. This provides a molecular identification. In addition, there are also vast libraries in the literature of IR spectra that help identify unknown compounds or, at least, classify them into classes of molecule structures [77, 81, 82]. The absorption of radiation by materials obeys the Beer-Lambert Law (Beer's law). According to the Beer's law, the absorbance of a chemical bond is directly proportional to the concentration of it in the molecule and the path length that the light travels [80].

### *Infrared Instrument*

The infrared instrument is called infrared spectrometer. The IR spectrometer are equipped with a source, which is a material heated by electric current, that emits black-body infrared radiation. In addition, a detector that is responsible to convert the radiation energy into a electrical signal, yielding a spectrum. In FTIR spectrometer the infrared spectrum is not measured directly, instead, an interferogram is produced by the interferometer. The interferometer is a device consisting in two perpendicularly plane mirrors, one of them is movable, and a beamsplitter positioned at 45° in relation to the mirrors. The interferogram is produced by split-

ting the IR radiation beam from the source into two parts. Each splitted part is directed to one of the mirrors. The two splitted beams parts are recombined after they have traveled different optical paths provided by the movable mirror. The interferogram is then converted into a spectrum via Fourier transformation. The radiation emerging from the source is passed through the interferometer to the sample before reaching a detector [80, 83, 84]. FTIR instruments can be run by transmitting IR radiation through the sample or by reflection, such as, attenuated total reflection (ATR) technique.

#### *Total Attenuated Reflection*

In attenuated total reflectance (ATR) spectroscopy, the sample is placed on the surface of an ATR crystal (e.g., diamond, Ge, Si, ZnSe, KRS-5). The incident IR radiation is reflected inside the ATR crystal at the interface crystal-sample. The incident IR radiation beam creates an evanescent wave (at the interface crystal-sample), which penetrates into the sample, resulting in the absorption of the IR radiation. The reflected beam energy is attenuated due the absorption and is measured by the detector. This gives rise to a reflection spectrum [85].

The depth of penetration is a measure of how far the evanescent wave extends into the sample, and is a function of the wavelength, the angle of incident IR radiation, and refractive index of the crystal and the sample. The ATR crystal must have an index of refraction higher than the sample being analyzed. Since the IR radiation beam consists of a broad range of wavelengths, the penetration depth is different for each wavelength. The higher the  $\lambda$  deeper the penetration of the radiation. Which is different from regular transmission mode, where the path length (cell thickness) is the same for every wavelength [77].

On of the main advantages of ATR spectroscopy is lack of sample preparation [98]. That is why ATR spectroscopy has found applicability in analyzing solid and liquid samples. However, a very good contact between sample and crystal surface is required for an effective measurement. This is necessary because the interaction between radiation and the material takes place on the interface sample-crystal [80].

ATR spectroscopy is a useful tool for multicomponent systems and is a promi-

sing analytical technique for in-process characterization of the chemical reactions [11, 26, 27, 73, 74].

### **2.3 In-process Material Characterization**

Grove and Wachtman (1986) rephrased the definition of materials characterization as follows: "Characterization describes those features of the composition and structure (including defects) of a material that are significant for a particular preparation, study of properties, or use, and suffice for the reproduction of the material" [86]. Indeed, characterization of materials is the basis for understanding their performance. When it comes to polymers, there are an increasing amount of studies in developing and/or modifying existing polymers, for example by blending two or more different polymers, aiming the improvement of material properties. This drives the development of material characterization sampling techniques that can be more efficient in maintaining the sample with the characteristics of the material that is being processed during test, leading to more reliable results [87].

Due to the fact that polymers are extremely thermomechanical history-dependent [13], the characterization of the polymer during the process can help to analyze the history of the polymer melt and correlate it to the quality of the final product. This type of characterization is called in-process analysis. For REX, in-process analysis can help to develop understanding of the reaction kinetics inside the extruder. These include: Where along the barrel does the reaction start and where does it end? How much of the reaction happens at the die and along the barrel? What are the main parameters that control the reaction speed and conversion? Contrary to conventional off-line characterization, in-process analysis can diminish the time delay between the material sampling and the material test. This can be decisive in the reliability of the analysis, since the polymer melt, especially for the reactive extrusion process [9], can suffer changes between testing and sampling [58].

There are three primary aims of in-process analysis: (1) scientific understanding of the process-material relationship; (2) process control and trend monitoring; and (3) real process modeling (simulation) [13, 34]. The selection of the



technique and how the measurements is decided according to the desired objectives and the technique limitations [87]. For (1) scientific understanding of the process-material relationship, for example, conducting several measurements at different locations along the extruder barrel help to understand the development of material during the whole process. For instance, Covas et al., (2002) applied capillary rheometry in on-line mode at several locations along the extruder barrel to find the starting location of the degradation and chemical reaction in reactive extrusion through the correlation between rheological response and macromolecular structure and morphology [2, 17]. Bicalho et al., (2018) used an optical device to measure the light scattering in solid particles along the extruder in on-line mode to evaluated the onset of polymer melting along the barrel [25]. Partial residence time distribution has also been investigated through optical device in on-line mode [9]. Process control and trend monitoring (2) requires continuous measurements to be done in a specific location at the extruder with variation in the process condition can be useful to control the state of the melt during extrusion to achieve proper levels of the property being analyzed. This can be achieved by controlling the process parameters in real time. Saerens et al., (2012) have used near-infrared spectroscopy for the in-line monitoring of the drug concentration [21]. While Tumuluri et al., (2008) have used Raman spectroscopy for the analysis of active pharmaceutical ingredient crystallinity in drug formulations in both, on-line and off-line mode [88]. For (3) real process modeling (simulation) measurements collected during process can be used in simulations to predict the behavior of the melt in a wider range of process conditions, the evaluation of the process parameters sensitivity and understand tendencies, enabling material and process optimization [71]. In addition, the knowledge of the polymer melt state and the flow condition inside the extruder (during process) is a precondition for process optimization. For example, an accurate understanding of the melt behavior during processing can help to develop appropriate process routines and strategies and to design new equipment elements [89].

### 2.3.1 The Types of In-process Analysis

As a conceptual framework, Callis in 1987 found it useful to classify the process analysis in off-line, at-line, on-line and, in-line. This classification is an indication of a decrease in the time delay between the material that is being processed and the material that will be tested/analyzed [90]. Off-line mode imparts the longest time delay, followed by at-line, on-line and in-line mode with no time delay. This section provides a very brief overview of the off-line and at-line methods. It then goes on to on-line and in-line modes of analysis.

Off-line mode of analysis is when the material needs to be sampled from the process line and the measurement is performed in a lab. The main advantage of this method of analysis is that the sample is tested under well defined procedures and methods, with experts available for consulting and the instruments might follow accurate maintenance schedules [90]. In addition, measurements with complex characterization techniques can only be done in off-line mode, especially when the technique requires heavily sample treatments and preparations. However, some procedures might need to be done before the sample is tested. These are: packing, unpacking, transport to another facility and sample preparation procedures. These extra steps impart a long time delay between the sample collection and sample test [13, 90]. A way to decrease the time delay is to bring the analyzer to the process room. This characterizes the mode of analysis as at-line. In at-line mode the advantage is that the analyzer stands in the same room as the extruder, thus, once the material is collected it can be analyzed in the process facility. Some sample preparation might be necessary depending on the technique of characterization. In off-line and at-line there is no connection between the process line (extruder) and the analyzer. The main characteristic of these methods is that at some point the sample needs to be handled by an operator (human), which means that they are not automatized. Another drawback pointed by Klozinski (2019) is that the amount of sample might not be representative of the material being processed when collected for off-line and at-line analysis [13, 89].

With on-line measurement the analyzer is connected to the main process

line (extruder). The sample is diverted from the extruder to the instrument for characterization. This is an attempt to minimize external factors that can disturb and change the material process characteristics, such as temperature gradient; which can cause undesired crystallization, or contact of the sample with air (in case of highly reactive materials); which can cause oxidation and contamination. Also, morphological changes can be avoided due lack of sample preparation and, time delay is decreased [58]. On-line mode can be subdivided into three categories: intermittent, continuous bypass and continuous multi-pass methods [89]. Intermittent on-line method requires that a representative amount (sample) of the polymer melt to be injected into the characterization instrument in order to do the analytical measurement [90]. This mode of analysis avoids the problem with material waste and the conditions of test can be better controlled. In continuous bypass and multi-pass methods the diverted stream flows continuously through the instrument. For the continuous bypass the material is discarded after the test. Despite of a large waste of material, a high stable flow can be achieved, which might facilitate the measurement pressure control [91]. On the other hand, when the characterization instrument is installed by the on-line continuous multi-pass method the polymer stream sampled returns to the main line of process. This can be useful to analyze the effect of the test on the final product [89]. Perhaps the most serious disadvantage of the on-line method is that some time lag may be still present between sampling and testing. This might risk the investigation of very fast reactions. However, several advantages can be pointed out. For example, the measurement being made on-process facilitates the cleaning, maintenance and adjustment operations of the sensor and the instrument while the extrusion proceeds. Also, in on-line mode it is possible to be more versatile in terms of characterization technique available and test requirements. For example, it is possible to control the temperature of the test. Especially when the measurement requires different temperatures from the operation. Also, it is easier to meet the requisite of sample shape, and use more complex techniques when compared to in-line mode [6, 18, 60]. Another crucial advantage of on-line measurements is the ease implementation of the technique along the extruder in several locations.

This is particularly important for REX and the study of reaction kinetic along the barrel [9, 13].

Lastly, in-line measurements are done directly in the process line, with no deviations of the polymer melt from the extruder like on-line methods [34, 60]. This means that the property measured in-line is able to be “seen” as the polymer is produced [92]. Of course, this implies very short or no time delay between sampling and testing, which is the main advantage of the in-line method [89]. On the other hand, the implementation of an in-line technique can often be difficult and some barrel modifications need to be done. This might narrow the range of technique that can be used in in-line mode, which is why in-line techniques are mostly applied at the die of the extruder [13]. In addition, the maintenance and adjustments in the probe or analyzer might be an issue in industry. That is because the process might have to be stopped in order to perform maintenance or replacement of parts of the in-line measurement system, leading to downtime of the extruder [92]. The volume of material that is being analyzed in in-line mode is rather controversial and not very well defined, and there is no general agreement about it in the literature [13]. Beyer et al (2017) discuss that normally a significant amount of the material is analyzed. However, depending on the technique some probes have a low signal penetration and the sample can not represent the whole material in the process [60]. This view is supported by Coates et al. (2003) who writes that a great portion of the polymer melt can be sampled. In contrast, Reshadat (1999) argues that not a large volume of the polymer melt is analyzed by probes. However, besides no time delay, another advantage is that the disturbance of the flow is minimum or null, especially when probes are flush-mounted in the extruder [13].

The decision of which method to use can be dependent on several factors such as, the material being processed, the intended property to be measured, the characterization technique and the objective of the in-process investigation (scientific understanding, process control or modeling) [87]. The this thesis on-line measurements are done. Covas (2018) pointed out some requirements and challenges of implementation of a new on-line technique in the extrusion process.

These are [67, 87]:

- the sample should be representative of the material;
- being able to acquire a large amount of data during the process in order to be statistical representative;
- being capable, as long as it is practical, to achieve short time lags between the collection of the sample and its measurement and the test result;
- using techniques that are able to assess the kinetics of the chemical reaction;
- assessing the relationship between the kinetics with processing conditions;
- being able to improve the scientific understanding correlations between the conversion of chemical reactions with morphology, material characteristics and processing conditions;
- being able to use the data to evaluate routines of process models;
- being able to use the data for process optimization and development;
- sampling and/or testing should not disturb the extruder flow;
- the extruder flow should not disturb the test.

#### **2.4 In-process Analysis Tools for Reactive Extrusion**

During the last years, researchers have been developing and testing in-process tools for material characterization during extrusion [6, 9, 17, 18]. In addition, many researchers have tried to contribute to the *in-situ* characterization aiming for shorter delay times and to avoid the loss of material characteristic due to sample collection handling [13, 93]. Canevarolo and coworkers have presented an in-line optical detection device system based on rheo-polarimetry to measure birefringence of polymer flow in real time [94]. Covas et al. have characterized morphological and viscoelastic properties of thermo-mechanically sensitive polymers with a twin-slit rheometrical die during extrusion [95]. In REX, the group have characterized the chemical degradation of polypropylene with peroxide by

on-line rheological measurements. Their results showed a relationship between the rheological properties and processing conditions [15]. Shear viscosity was *in-situ* measured by Hilliou and Teixeira during extrusion of PLA-clay nanocomposites [96]. Xi Huang et al. (2018) investigated the composition of PP/PS blends during extrusion by Raman spectroscopy as a real-time measurement tool compared to off-line infrared spectroscopy. They concluded that Raman as an in-line measurement tool showed comparative accuracy in the determination of PS content in various blend ratio composition [97]. Bicalho et al (2020) monitored in real-time the polypropylene melting process with an on-line optical device in the visible light range. Turbidity was measured to track the development of the melting process. The solid-molten interface content decreases with the melting of the polymer. This reduces the light scattering as the polymer melts along the extruder. They concluded that the melting profile is significantly changed with the increase of the screw speed and the increase of the temperature [25]. Researchers have used ultrasound in PE/PP blend to track the change in composition variation during extrusion. They observed a linear relationship between ultrasonic velocity (which is evaluated by the transit time) and the percentage of PE [13].

A wide variety of techniques can be used to track changes that occur inside the barrel during extrusion. The technique choice will depend on what information is sought out from the process and the physico-chemical nature of material that is being processed [97], in addition to the limitations imposed by the application. This means that the material needs to be detectable to the technique of analysis. For example, the components of a certain material need to be receptive to the application of magnetic field in order to the MRI (magnetic resonance imaging) to be used as a characterization technique. Another example is that the prerequisite for image analysis is having components of different colors or texture [87]. When it comes to spectroscopy techniques the radiation at different wavelengths of the electromagnetic spectrum induces different modes of vibrations in the molecule. This is useful to provide information about the structure and chemical composition of a polymer [60, 80]. However, for that to occur the molecule needs to be “infrared-active”, which means that the dipole momentum needs to

change with the vibration. The interaction of matter and radiation depends on the wavelength. For example, the interaction can promote the electron to increase the energy state by electronic transitions (UV-Vis radiation). This can be used to evaluate concentration of molecules. In the infrared region of the electromagnetic spectrum the interaction radiation/matter can be associated with the fundamental vibration of molecules (MID-IR), overtones of MID vibrations and combination of bands (NEAR-IR) [74]. Also, it can give information about crystal lattice vibration and molecular torsion (FAR-IR) [80, 98].

In this dissertation the on-line FTIR spectroscopic system for extrusion characterization during the process is presented and validated [93]. FTIR spectroscopy, particularly, can provide information about the development of the chemical reaction inside and along the extruder. This information is useful for scaling up of process and, optimization of formulations, since it is possible to add additional component once the reaction reaches a plateau. Infrared spectroscopy is a non-invasive and non-destructive technique needing none or few sample preparations [93]. The sample is irradiated by an infrared range radiation and the absorbed or reflected light is analyzed by the spectrometer. The infrared spectrum represents the intensity of the absorbed light in function of the wavenumber, which is the reciprocal of the wavelength. According to the collected spectrum, it is possible to perform quantitative and qualitative analyses determining the chemical structure and composition of the sample [80]. Infrared spectroscopy is proven to be helpful for reactive extrusion by evaluating the formation or suppression of functional groups during the chemical reaction. He et al., has implemented a NEAR IR spectroscopic in-line system to characterize the uniformity of immiscible polymer blends dispersion during extrusion. These researchers have shown that kneading blocks in a series improve the uniformity due to the strong shear reaching a plateau at the die [11]. Moghaddam et al., (2009) interfaced a laboratory extruder to an NEAR-IR spectrometer to study the melt processing behavior of TPU and TPU nanocomposites. They found that small changes in the spectra can indicate a loss of urethane bonds during extrusion, which indicates degradation of TPU [74]. The bands in NEAR-IR range of the electromagnetic spectrum show

considerable overlapping of peaks. Thus, the quantitative analyses can be more challenging. However the quantitative of NEAR-IR spectra relies in the development of calibration models (chemometrics) [67]. Reshadat et al., (1999) stated that each system requires its own calibration model, which can limit the versatility of NEAR-IR spectroscopy. The main advantage is the robustness of the optical fibers available for NEAR-IR, while for MID-IR range optical fibers are still expensive and susceptible to damage [99]. On the other hand, in the MID-IR range one can obtain direct information without treating the data with chemometrics. The data treatment in MID-IR spectra is easier and transferable to different polymers systems, which makes it promising for R&D environments [24]. For example, Covas has reported that the reaction of polystyrene grafted with maleic anhydride with alkyl amine during extrusion was monitored by MID-IR at the die. In addition, the grafting reaction of organosilanes in polyethylene has been followed in on-line MID-IR spectroscopy during the process [67]. On-line MID-IR spectroscopy was also used to evaluate the thermal degradation of polyoxymethylene (POM) during the melt extrusion [100]. In-line ATR-FTIR was used by Haberstroh et al. (2002) to evaluate the ratio of monomer and polymer during the polymerization of  $\epsilon$ -caprolactam while the extrusion process is taking place at one location of the extruder in a modified barrel. However, the authors reported that the intermeshing screw wiped material off the crystal, leading to unreliable measurements. In addition, the increasing of the viscosity, due to conversion, promoted that the material got stuck on the crystal surface, which impeded fresh material to be tested [101]. In this thesis, ATR-FTIR technique is applied on-line avoiding the high viscosity issue and it is used along the barrel at different locations, which gives the reaction information on the whole length of the extruder.

## **2.5 Polymer Blends**

A polymer blend is a mixture of polymers, in which at least two are combined to produce a new material with physical properties different from the polymers not combined, normally the expectation is to improve the final properties. Polymer blends can be classified into three categories. The first one is immiscible polymer blends: separate phases of the polymer components exist in the mate-



rial and the glass transition temperatures are observed for each phase. Second, miscible polymer blends: These blends present just one phase, consequently, just one glass transition temperature. In miscible polymer blends polymers with similar chemical structure are mixed. Third, compatible polymer blends: These are immiscible blends with strong interactions between the phases interface caused by reaction of compatibilization. Compatible polymer blends exhibit uniform physical properties [102, 103].

### **2.5.1 Reactive blending**

In practice, most of the polymers are incompatible to each other. Consequently, the problem of the incompatibility of polymer blends leads to a non-uniform and weak physical properties in the immiscible blends. The weak properties in immiscible blends are related to poor interaction between the polymer components, which leads to: phase separation due to differences in molecular structure, molecular weight and viscosity and; coarse dispersed morphology between the phases [104].

Therefore, a chemical reaction of compatibilization between the polymer phases can be carried out to improve the affinity of the components. In the compatibilization reaction a block or graft copolymers is added (compatibilization reaction) or produced (reactive blending) during the mixing. The block copolymer, which contain segments chemically identical to or having affinity with the polymer constituents locates at the interface of the polymer phases to improve their compatibility. Those additives are also called compatibilizers or interfacial modifiers, because of their tendency to reduce the interfacial tension and increase the interfacial area by promoting the dispersion of one phase (minor or second phase) in another (major phase or matrix) and to stabilize the resulting material (polymer blend). For example, the blend of polypropylene (PP) and Poly(ether sulfone) (PES) was compatibilized with PP grafted with glycidyl methacrylate (mPP). The presence of mPP in the blend of PP/PES significantly reduced the size of PES domain (second phase) to 1–3  $\mu\text{m}$ , when compared to 30–80  $\mu\text{m}$  in the same composition but without mPP, and highly improved interfacial adhesion. The authors explain the improvement of the interfacial adhesion in compatibilized polymer blends by the

fully coverage of PES domain surface [105].

In that context, an improvement in the properties and performances of the obtained polymer blends can be solved by enhancing interfacial interactions between constituents of polymer blends. In reactive blending the copolymer is produced *in situ* during mixing (extrusion process) [105].

The *in situ* compatibilization or reactive blending is achieved by reactive extrusion, where mutual compatibilization of the blend components take place. Reactive extrusion for such polymer blending application is very attractive process because it acts as a solvent-free reactor that is able to continuously process high viscous materials [106]. In reactive blending, the reaction normally takes place at the interface of the two polymer, that is why extruders are so attractive for the process because of the high levels of mixing imparted in the polymer melt during extrusion. The mixing provided by the extrusion process increases the interfacial area by breaking up the droplets, leading to more collisions between the reactants. This improve the reaction in the polymer blend [69, 107, 108].

### 3 EXPERIMENTAL

The experimental part of this thesis is divided in two phases (the outline of the structure of this chapter is shown in the diagram depicted in Figure 3.1. Phase 1 comprises the design, implementation and validation of the on-line FTIR system, and consists of four parts: the design of the probe holder unit; study of number of scan in a FTIR measurement and signal-to-noise ratio (SNR) dependency; the data treatment validation and; the validation of the on-line FTIR spectroscopy system during extrusion. In phase 2 the on-line FTIR was used to evaluate the reactive blending of polypropylene grafted with acrylic acid and polyamide 6 blends, comparing with the non-reactive blend of polypropylene and polyamide 6 also during extrusion processed at the same process conditions. Phase 2 consists of: on-line FTIR measurements (at various locations) in an extrusion run that used different screw profiles that imparts various levels of dispersive and distributive mixing in the polymer melt (by the use of mixing elements of kneading blocks and extensional mixing elements) and; on-line measurements (at various locations) in extrusion runs with variation of feed rate and screw speed. Scanning electron microscopy and residence time distribution measurement were also done in samples collected along the extruder.

#### 3.1 Probe Holder Unit, PHU

The probe holder unit (PHU) was designed to interface the ATR-FTIR probe, which is connected to the infrared spectrometer, to an twin-screw extruder along the barrel through pressure/temperature transducer ports (1/2-20 UNF thread). The ATR-FTIR probe (FlexiSpec) works in a range of temperatures from -100 C to 250 C. The attenuated total reflectance (ATR) Silicon crystal, with a transmission range between 3100-600  $cm^{-1}$ , lies on the tip of an 18 cm long cylindrical metal (Hastelloy C22) shaft of 12 mm diameter. Fiber optic cable (PIR 900/1000) is responsible to transmit and receive the IR signal between the ATR crystal and the spectrometer. Air is used to cool the ATR crystal during operation and an inner temperature controller monitors the crystal temperature. The probe is coupled into a Nicolet IS10 MID (4000 to 400  $cm^{-1}$ ) infrared FTIR spectrometer (Thermo-

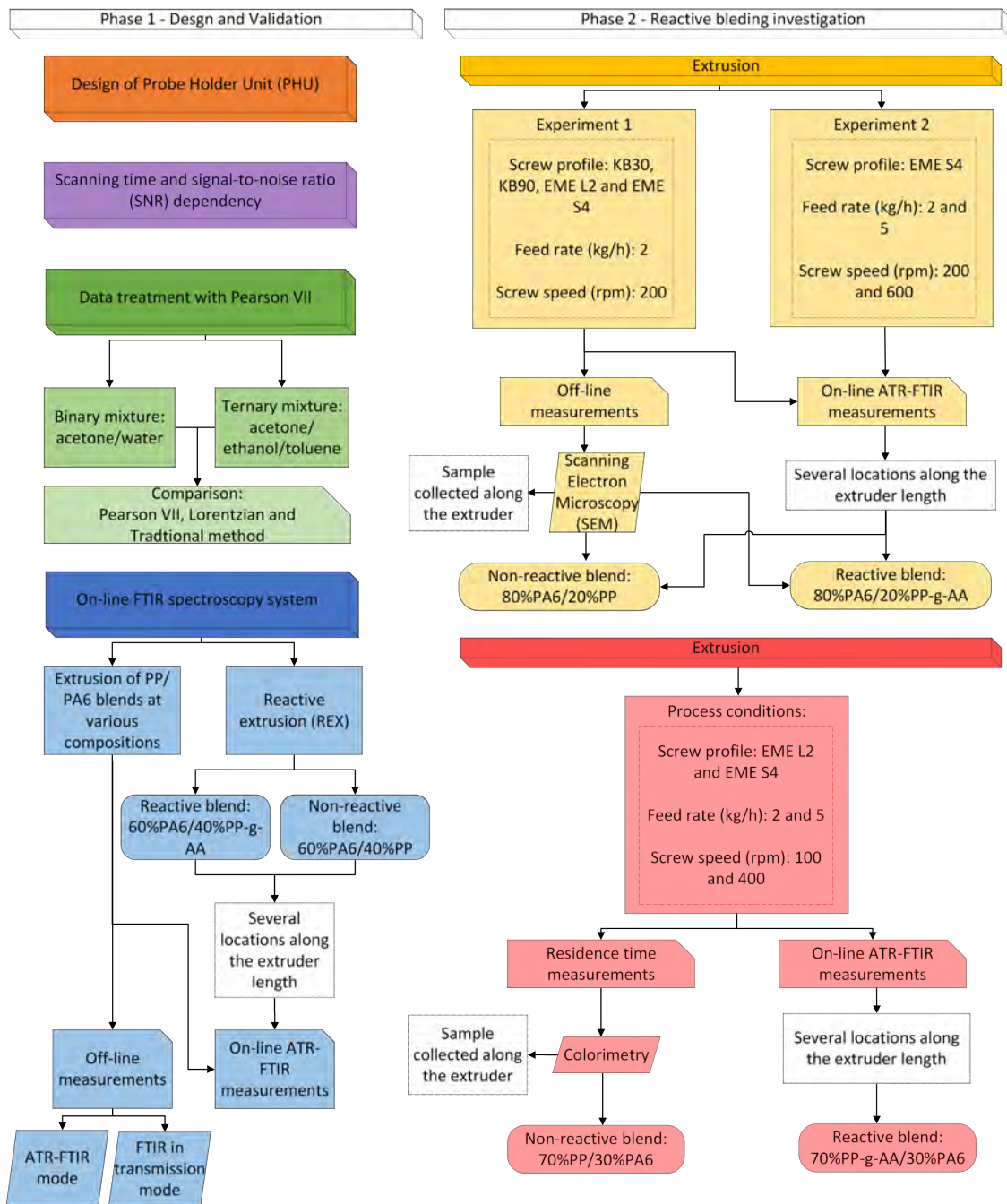


Figura 3.1: Infogram showing the phases 1 and 2 of the methodology used in this thesis.

Fisher Scientific) through the Fibermate FTIR standard coupler. Pictures of the components can be appreciated in Appendix A.

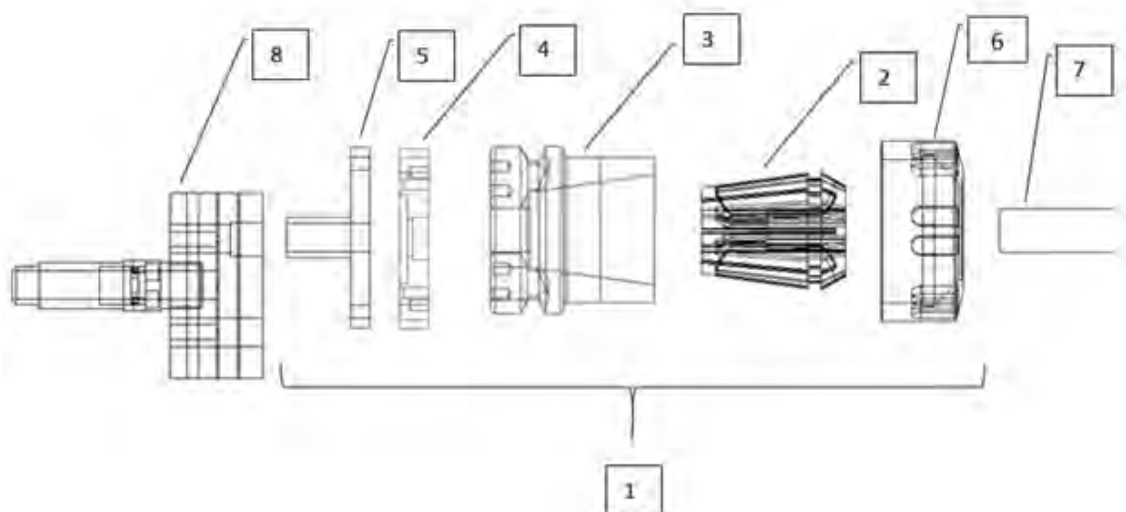


Figura 3.2: Probe holder unit (1) and its components: collet chuck (2), collet holder part (3), measurement chamber (4), molding connector (5) and pressure dome/nut (6) for holding the ATR-FTIR probe (7) and the sampling collector (8).

The PHU (Figure 3.2) consists of a collet chuck (2), collet holder part (3), measurement chamber (4), molding connector (5) and pressure dome/nut (6) for holding the ATR-FTIR probe (7) and the sampling collector, which works as an on/off valve (8). The PHU and the sample collector are suitable for diverting polymer melt from the extruder to make contact between the material and the ATR-FTIR crystal (at the tip of the ATR- to perform the FTIR measurement). The operation and effectiveness of the Sample Collector has been described previously [1]. As shown in Figure 3.3 the probe holder (1) braces the probe (7) with the collet chuck (2) in the collet holder (3) and is tightened with the pressure dome/nut (6) so that the probe (7) secure against movement is maintained. The device, PHU, was inspired in the design of tool holders for machining equipment and the dimensions and tolerance can be found in Appendix B.

The PHU permits the probe to be attached along the extruder with the ATR silicon crystal facing the measurement chamber (see Figure 3.4), where the material is diverted to and analyzed [90]. There are two types of measurement chamber available. The first consists of a closed disk cavity (Figure 4.12). The disk ca-

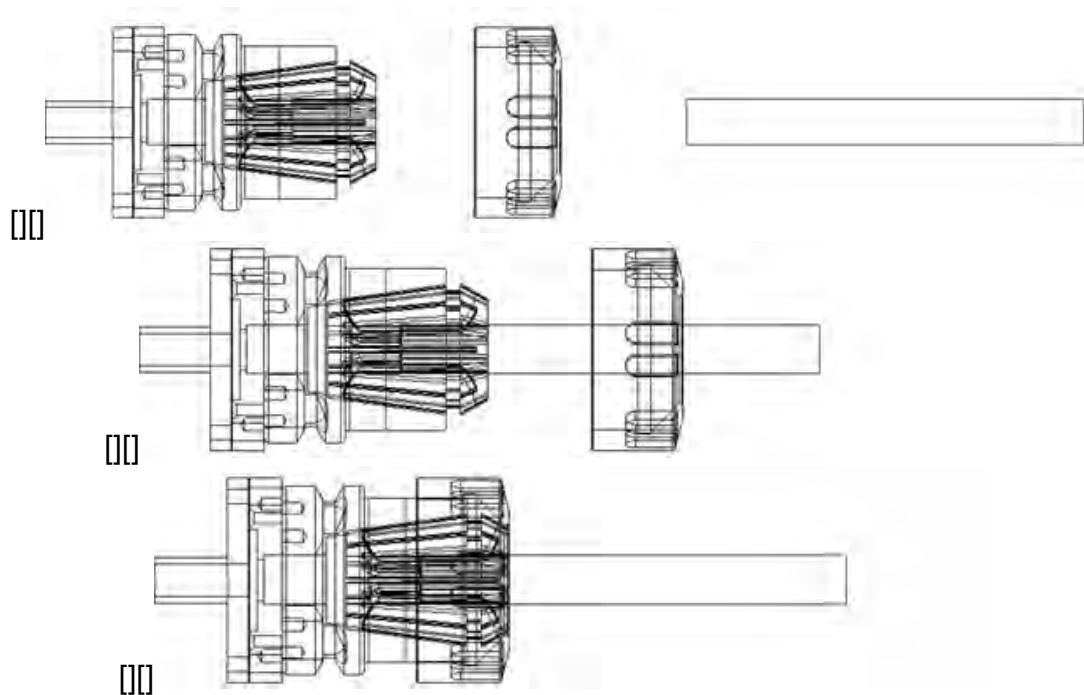


Figura 3.3: Holding steps of the ATR-FTIR probe. In a) the collect is places in the holder, in b) ATR-FTIR probe is aligned with the collet, and in c) the pressure nut is tightened to ensure the ATR-FTIR probe is fixed in a stable way on the extruder.

vity has the diameter of 25 mm and 1 mm thickness and can be used as a mold to sample of rheological measurements that can be done off-line in rheometers. This avoid posterior molding procedures in a compression molding machine. The second type of measurement chamber is an open channel where the melt flows over the ATR crystal and is discarded after the test (Figure 4.13). The PHU is heated and temperature controlled in order to allow measurements to be taken at the same temperature as inside the extruder.

### 3.1.1 On-line ATR-FTIR measurements

Figure 3.5 depicts the design of the PHU and sample collector (on/of valve) and Figure 3.6 depicts the on-line FTIR spectroscopy system attached to the extruder via the PHU at different positions (L/D) along the barrel. The operation steps for spectrum collection is illustrated in Figure 3.7.

Figure 3.7a shows the PHU and Figure 3.7b, 3.7c, 3.7d and 3.7e show the longitudinal cross-sections of PHU. The background spectrum is collected by the

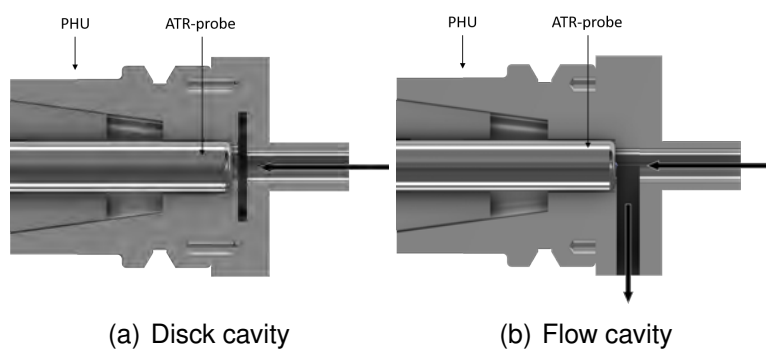


Figure 3.4: Cross-sectional view of the PHU highlighting the measurement chamber with a) disk cavity and b) flow cavity. Material flow are transverse to the extrusion direction and is indicated by the arrows.

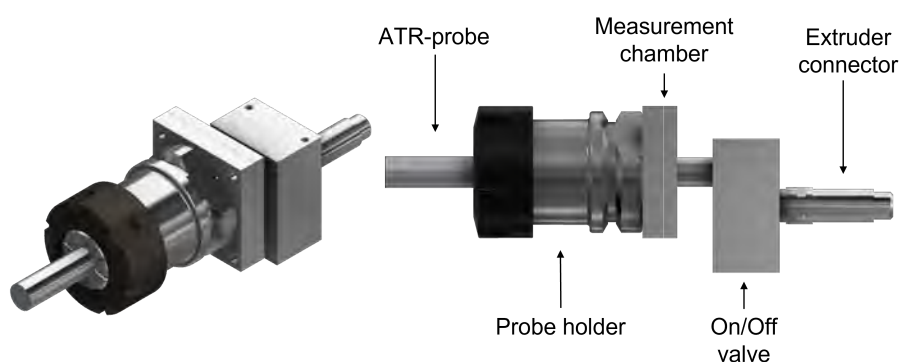


Figure 3.5: Probe Holder Unit and its components: extruder connector, On/Off valve (sample collector), measurement chamber, probe holder, pressure nut and the ATR-FTIR probe.

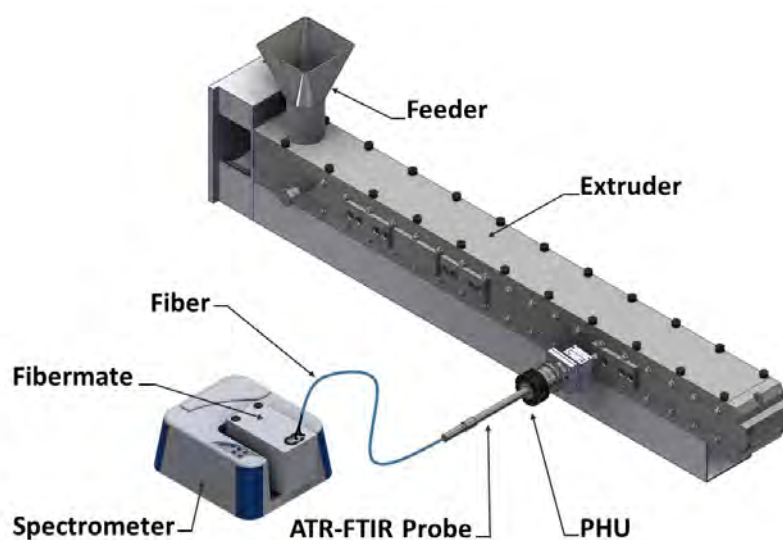


Figure 3.6: On-line FTIR system with all the components attached at P/T port along the extruder barrel.

ATR-FTIR probe while the measurement chamber is still empty (Figure 3.7a). Once the extruder is operating and it runs until steady state is achieved; the PHU is opened in the purge position (Figure 3.7b), so material that was stuck inside the connection channels can be discarded. Purge position is important since fresh material needs to be diverted to the measurement chamber; the polymer melt is then diverted by the PHU until the measurement chamber is full (a process that typically lasts less than 5 seconds depending on the process conditions) and can be seen in Figure 3.7c). The PHU is then closed (Figure 3.7d) and spectra are collected with selected resolution and number of scans. Afterward, the measurement chamber is emptied, cleaned and the procedure repeated. The step of filling the measurement chamber takes 5 seconds.

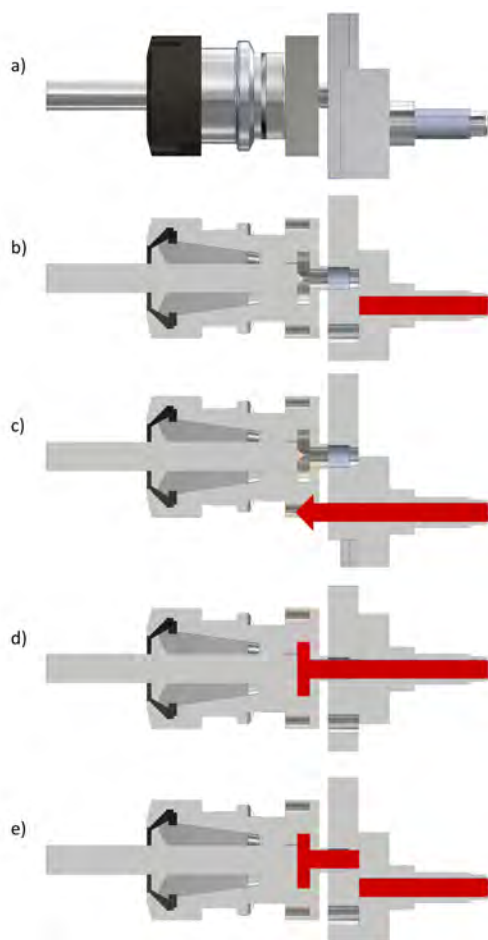


Figure 3.7: Operation of PHU and sampler collector. Polymer melt flow is indicated in red.



### 3.2 Materials

All the materials used for the subsequent parts of phase 1, namely, number of scans and signal-to-noise ratio (SNR) dependency, validation of data treatment with Pearson VII, and validation of the on-line FTIR spectroscopy system, and phase 2 are listed in Table 3.1.

Tabela 3.1: Materials used in this work and their main characteristics. Liquid samples, purchased from Sigma-Aldrich (SIAL) that were used to validate the data treatment proposed, and the polymer resins that were used for the on-line FTIR measurements during extrusion.

Material	Manufacturer	Molecular weight (g/mol)	Density (g/mL) @ 25 C	State change temperature (C)	Refraction index (no unit)
Liquid samples					
Acetone	SIAL	58.08	0.791	56*	1.359
Toluene	SIAL	94.14	0.865	110-111*	1.333
Ethanol ACS	SIAL	46.07	0.789	78*	1.360
Distilled water	SIAL	18.02	1.000	100*	1.324
Polymer resins					
PP-g-AA (Polybond 1001N)	GI Group	-	0.91	161**	-
PP	Total	-	0.91	165**	1.474
PA6 (Ultramid B27)	PolyOne	-	1.13	225**	1.530

\*Boiling point, \*\*Melting point, - = unknown

#### 3.2.1 Liquid samples

The validation of the data treatment with Pearson VII function on bench was conducted with liquid samples because liquids have the best contact to the ATR crystal, leading to the best signal-to-noise ratio [109].

Acetone, distilled water, ethanol, and toluene were selected for the validation purposes because they have IR bands that are both overlapped and isolated

when they are mixed (see Table 3.2). This makes these materials appropriate to the study of changes in the IR bands intensity and potential distortions caused by overlapping of bands.

### 3.2.2 Polymer resins

For the validation of the on-line FTIR spectroscopy system (phase 1) and reactive blending investigation in phase 2 the polymer blend of polypropylene (PP) and polyamide 6 (PA6) and polypropylene grafted with acrylic acid (PP-g-AA) and polyamide 6 were chosen. The choice for investigating these blends is based on two reasons: first, these blends, in non-reactive system, are amongst the most studied polymer blends and thus provide a good benchmark [3, 110]; and second the reaction between grafted acrylic acid on PP and the amine end group in PA6 chain has already been extensively investigated when it comes to reactive blending [4, 5, 111], who showed the effectiveness of the reaction during extrusion.

Reactive blending of PP and PA6 is also conducted by adding polypropylene grafted with maleic anhydride (PP-g-MAH) as a compatibilizer. There are two reasons why PP-g-AA was used in this thesis instead of PP-g-MAH. First, the amount of maleic anhydride grafted in PP is around 0.5-0.6 wt%, this quantity is very small when compared to around 6% of acrylic acid grafted in PP-g-AA [103, 112, 113], this makes it very difficult to track bands related to maleic anhydride by FTIR spectroscopy. Second, the reaction of maleic anhydride with amine end group forms the functional group imide, instead of amide with acrylic acid, imide group has an IR characteristic band at  $1770\text{ cm}^{-1}$ , which it was not able to be detected in the IR spectrum due to the small amount of maleic anhydride in PP-g-MAH [114].

A polypropylene grafted with acrylic acid under the trade name Polybond N 1001 supplied by SI Group (United States of America) with MFI (melt flow index) of 41.9 g/10 min was used in the reactive polymer blends studied. According to the supplier, the concentration of acrylic acid grafted on PP chains ranges from 5.5 to 6.6 %w/w. A PP purchased from Total with an MFI of 1.3 g/10 min was used to be part in the non-reactive blends studied in this work. The second polymer resin used in the blends was a PA6 under the trade name Ultramid B27 E 01.

### 3.2.3 Blending reaction

Figure 3.8 shows the mechanism of the compatibilization reaction of the reactive blend of PP-g-AA and PA6. Polypropylene is grafted with acrylic acid which reacts with the amine end groups of polyamides [115, 116]. Carbon in the carbonyl is very electropositive due to the two oxygens bonded to it. Thus, the pair of free electrons of nitrogen attacks the pair of electrons from the carbon bond in acrylic acid. This forces the pair of electrons of bond of carbonyl to surround the oxygen. This makes the oxygen more negative. However, the  $\pi$  bond is very stable and tends to be re-bonded, releasing -OH. At this moment the new bond between the carbon from acrylic acid and nitrogen from amine is formed. After the bond has formed the dehydration reaction occurs by releasing the hydrogen bonded to nitrogen. Which in turn will link to -OH in the polymer melt releasing H<sub>2</sub>O. A di-block copolymer of PP and PA6 is linked by an amide functional group. The amide has IR characteristic bands that can be used to track the reaction along the extruder barrel, such as, amide I (1640 cm<sup>-1</sup>), amide II (1540 cm<sup>-1</sup>), and amide II (1266 cm<sup>-1</sup>).

Table 3.2 contains the primary infrared characteristic bands of all materials used in this work and their relative mode of vibrations.

### 3.3 Twin-screw Extruder

A ThermoScientific TSE24MC 24-mm co-rotating intermeshing twin-screw extruder was used to process the blends. The barrel is composed of 10 independently thermo-regulated zones. The extruder is a 40:1 L/D ratio length and it is equipped with three-hole strand die with a 3 mm diameter each. The blends were fed into the extruder with a Brabender volumetric feeder. The extruder has 12 lateral and 1 top Pressure/Temperature (P/T) transducer ports along its length for on-line analyses (Figure 3.6).

The screw consists of a shaft where the screw elements can be inserted. This enables different screw profiles to be built.

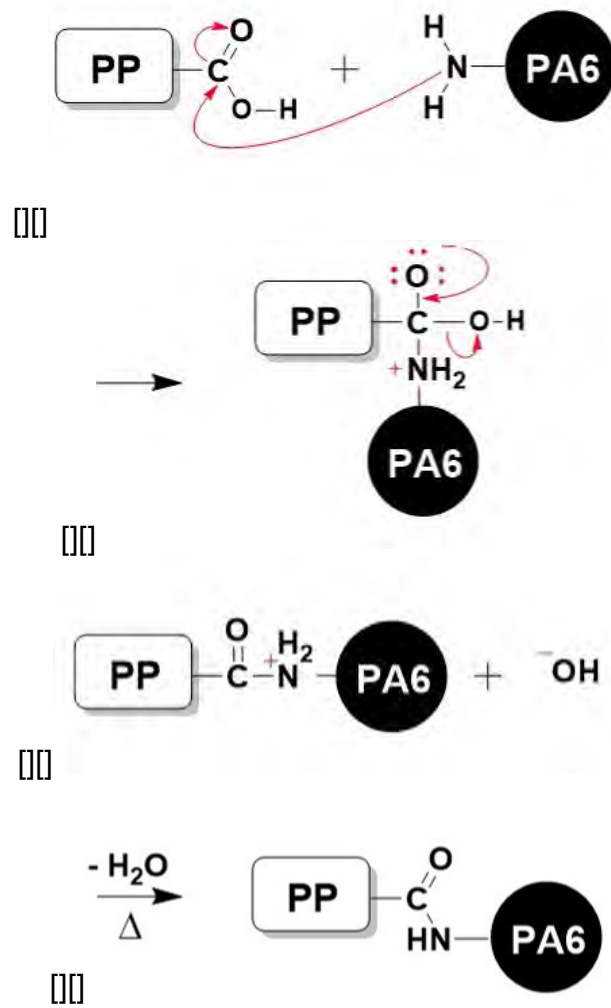


Figura 3.8: Scheme of blend compatibilization reaction with a) Nitrogegn electron attacking carbon pair of electrons, b) oxigegn becomes more negative, c) re-bonding of  $\pi$  bond, and d) the formation of a di-block copolymer of PP and PA6. The red arrows indicate the electron movements.

Tabela 3.2: Characteristic bands of all materials used in this work and their relative mode of vibration.

Wavenumber (cm <sup>-1</sup> )	Main active group vibration	Material
691	$\nu(\text{CH})$	Toluene (Data from NIST Standard Reference Database 69: NIST Chemistry WebBook)
879s	$\delta(\text{CC})$	Ethanol [117]
1200w	Amide structure	Polyamide 6 [117]
1220sr	$\nu_{17} - \nu(\text{CC})$	Acetone [33]
1266w	Amide III	Polyamide 6 [118]
1356	CH <sub>3</sub> deformation	Acetone [33]
1373s	$\delta(\text{CH}_3)_{\text{sym.}}$ , $\omega(\text{CH}_2)$ , $\delta(\text{CH})$ , $\nu(\text{CC}_b)$	Polypropylene [119]
1540vs	Amide II - $\delta(\text{CN})$ , $\nu(\text{NH})$	Polyamide 6 [117]
1636m	$\delta(\text{OH})$	distilled Water [27]
1640vs	Amide I - $\nu(\text{C=O})$	Polyamide 6 [118]
1710s	$\nu(\text{C=O})$	Acetone [33]
3066m	Overtone of Amide II	Polyamide 6 [118]
3299vs	$\delta(\text{NH})$ of the hydrogen bonded NH	Polyamide 6 [118]

Abbreviation: b = backbone, vs = very strong, s = strong, m = medium, w = weak,  $\delta$  = bending,  $\nu$  = stretching,  $\omega$  = wagging.

### 3.4 Number of scans and Signal-to-noise Ratio Dependency

The spectrum acquisition time, the data resolution and signal-to-noise levels were investigated according to the number of scans of the measurement. Pure acetone was chosen in order to avoid homogeneity issues of mixtures.

#### 3.4.1 Analytical techniques: bench measurements

The ATR-FTIR probe was submerged in a beaker containing pure acetone. Fifty IR spectra were collected at different number of scan, from 1 to 128 number of scans. Before each set of measurements the crystal was cleaned and background scanning was performed. The scan time, the intensity average and standard deviation of the absorbance at the characteristic 1710 cm<sup>-1</sup> carbonyl

band (Table 3.2) were calculated. The signal-to-noise ratio (SNR) was calculated by dividing the average (signal) of the absorbance of the IR band  $1710\text{ cm}^{-1}$  by the standard deviation (noise) [120].

### **3.5 Data Treatment with Pearson VII**

#### **3.5.1 Data Pre-treatment**

The transmission range of the silicon crystal of the ATR-FTIR probe is from  $3100$  to  $600\text{ cm}^{-1}$ . Consequently, the spectra all analysis were cropped between  $1850$  and  $1000\text{ cm}^{-1}$  because this range provides all the characteristic bands associated with the materials used in this work (Table 3.2). The cropping was done by a software developed in LabVIEW™. Details of the software and its screens can be appreciated in appendix C.

#### **3.5.2 Data Treatment**

Three data treatment methodologies were performed, the standard peak height and peak area data analysis [29], which we call of traditional method, and two methods based on the deconvolution of the peaks (IR bands). The first, the application of the function Lorentzian (which is already used for deconvolution of IR bands) [27], and the application of the function Pearson VII (which is proposed to be used for IR band deconvolution in this thesis).

##### *Traditional Analysis Method*

Baseline correction, peak area and peak height were calculated by the software developed, in house, in LabVIEW™. The software applied the traditional method of IR band analysis described by Parker (1971) in his book entitled as *Applications of Infrared Spectroscopy in Biochemistry, Biology, and Medicine* [29]. The height was calculated from the peak absorbance to the baseline and the area was done by integrating the band considering the baseline correction.

##### *Peak Deconvolution Method*

The data treatment of peak deconvolution is used here to take into consideration the overlapping of IR characteristic bands. The overlapping of IR bands convolute information and can not be accounted for using traditional peak height and area calculation. Specially in complex heterogeneous mixtures, where over-

lapped peaks provide useful insight into mixture amount or reaction [27, 28]. By deconvoluting the peaks in the region of interest the overlapped peaks are separated, making it possible to gain insight into physical mechanism from the peak deconvolution.

Before the deconvolution of the bands a second order derivative in the cropped spectral range was found useful to identify peaks present in the range of interest. Especially in regions where it is known that bands are overlapped. However, caution was taken because noises will be magnified with this technique, and they can be mistaken for a real component [27].

Analytical functions can be used to describe the line-shape of a FTIR spectrum in order to fit the curves. Lorentz is normally used for infrared spectrum data fitting [30, 31]. But this would be in a perfect scenario. In a real world infrared analyses, the spectrum can have many features that might affect the shape of the bands. These features can include but are not limited to hydrogen bonding and structure distortion. Furthermore, as it is known ATR-FTIR absorption (depth of penetration) is wavelength dependent [121], which can also cause shape distortion. All of these factors can contribute to asymmetry in some extent, even if IR spectra is not too susceptible to it. Thus, Lorentz shape would not always fit these bands. Therefore, we have considered to use Pearson VII profile of peak curve fitting.

In this thesis, analytical function Lorentz and Pearson VII was used to describe the line-shape of the FTIR spectra in order to fit the curves [27]. The IR bands were deconvoluted by a routine created in Origin version 2019b (OriginLab Corporation, Northampton, MA, USA).

### **3.5.3 IR Band Normalization**

ATR-FTIR is often used as a fingerprint technique for identification of functional groups present in the sample. However, for multiple reasons, accurate quantitative analyses are tricky to make by attenuated total reflectance (ATR) sampling mode. One of the reasons is the difficulty to obtain good reproducibility of the contact between the sample and the crystal. Another reason, easier to overcome, is to assure that the crystal has always the same dimensions (length

and thickness). And finally, the absorptivities increase proportionally with wavelength. For all the reasons presented, band normalization is used successfully for quantitative analyses [109]. In this technique, peak height or peak area must be normalized by reference band [73, 122].

### *Liquid Samples*

For the liquid samples, quantitative precision may be greater in ATR than by transmission sampling mode. This is because the contact between sample and crystal has no difficulty and there are no interference fringes presented in ATR [109, 123]. In this work, the absorbance and area for the bands in the liquid samples were used without any band rationing.

### *Polymer Blends*

The physical meaning of band normalization is the composition ratio between the two IR bands of each polymer, in the case of this work, polyamide 6 and polypropylene [30]. The ratio or relationship between the two polymer component IR bands is proportional to the composition of the two polymers in the blend.

In this work, all peak (height and area) value of PA6 ( $1640\text{ cm}^{-1}$ , Amide I -  $\nu(\text{C}=\text{O})$ ;  $1540\text{ cm}^{-1}$ , Amide II -  $\delta(\text{CN})$ ,  $\nu(\text{NH})$ ; and  $1266\text{ cm}^{-1}$ , Amide III [117]) were normalized by the reference IR band at  $1373\text{ cm}^{-1}$  (symmetric bending vibration mode of the  $\text{C}-\text{H}_3$  functional group) because it does not participate in the reaction. This vibrational mode belongs to the polypropylene structure, therefore, it can be used to normalize any characteristic bands of polyamide 6, especially the strong bands at  $1640$  and  $1540\text{ cm}^{-1}$ . These last two bands and the band at  $1266\text{ cm}^{-1}$  are vibration modes of amide functional groups. Amide is the product of the reaction between the terminal group of  $\text{N}-\text{H}_2$  (amine) present in the PA6 chain ends with the carboxyl of the grafted acrylic acid, at the PP chain as aforementioned (see Figure 3.8).

## **3.6 Validation of Data Treatment with Pearson VII**

This section of the dissertation shows the validation of the proposed data treatment of deconvoluting the IR spectra by the mathematical function Pearson VII. This validation was done by collecting IR spectra with the ATR-FTIR probe by



Tabela 3.3: IR band rationing used in this work.

<i>aR</i>	
$aR_{1640}$	$1640\text{cm}^{-1}/1373\text{cm}^{-1}$
$aR_{1540}$	$1540\text{cm}^{-1}/1373\text{cm}^{-1}$
$aR_{1266}$	$1266\text{cm}^{-1}/1373\text{cm}^{-1}$

submerging it in liquid mixtures (acetone, distilled water, ethanol, and toluene) in bench.

One of the biggest source of high signal-to-noise ratio in ATR spectroscopy is the contact between the ATR crystal and the sample, which can easily be affected by the kind of sample tested [29]. This is since infrared radiation absorption occurs in the interface between the crystal and the sample [80]. Liquids have the best crystal/sample interface contact [109]. Consequently, liquids samples were selected for validation purposes.

The proposed data treatment was compared by the traditional method of IR band quantification and by the deconvolution with Lorentz function (which is used for IR band deconvolution) [27].

### 3.6.1 Spectroscopy of Binary Liquid Mixtures: acetone/water

Binary mixtures of acetone and distilled water were prepared by varying composition (100 vol%/0 vol%, 75 vol%/25 vol%, 50 vol%/50 vol% and 0 vol%/100 vol% of acetone and distilled water, respectively) at a fixed total volume (6 ml) for easier mixture preparation in bench. The concentration and vibrational frequency shifts were investigated by the ATR-FTIR probe. This system was chosen mainly because the distilled water and acetone infrared spectra contain both bands that are very distinct and slighted overlapped (see Table 3.2).

#### *Analytical techniques: bench measurement*

Fifty IR spectra were collected with a wavelength resolution of  $4\text{ cm}^{-1}$  and 32 scans for each measurement at each composition. The absorbance of bands at  $1710$ ,  $1636$ ,  $1360$  and  $1220\text{ cm}^{-1}$  wavelength (Table 3.2) were calculated by deconvoluting these bands by Pearson VII, Lorentz and by the traditional method.

### 3.6.2 Spectroscopy of Binary and Ternary Liquid Mixtures: acetone/ethanol/toluene

A design of experiments to conduct linear trend of the composition of binary and ternary Acetone/Toluene/Ethanol mixtures with various compositions (table 3.4) were prepared. This DoE was selected because the mixture components do not react and thus results should follow simple rule of mixture linearity.

*Analytical techniques: bench measurement*

Fifteen spectra were collected at  $4\text{ cm}^{-1}$  and with 5 scans. The characteristic bands at  $1219$ ,  $879$  and  $691\text{ cm}^{-1}$  (Table 3.2) were analyzed for each mixture composition.

Tabela 3.4: Acetone/Ethanol/Toluene mixture compositions.

Mixture name	Acetone (%)	Ethanol (%)	Toluene (%)
100A	100	0	0
100E	0	100	0
100T	0	0	100
50A/50E/00T	50	50	0
50A/00E/50T	50	0	50
00A/50E/50T	0	50	50
50A/25E/25T	50	25	25
25A/50E/25T	25	50	25
25A/25E/50T	25	25	50
33A/33E/33T	33	33	33

### 3.6.3 Comparison between method

For the validation of the proposed data treatment with Pearson VII the three analytical methods were applied and results were compared by R-square of the fitting of the curves. Data dispersion, linearity and trends were analyzed. All the curve fittings with Pearson VII have a R-square above 0.9 in this work.

### 3.7 Validation of the On-line FTIR Spectroscopy system

In this section, the ATR-FTIR probe was interfaced with the extruder through PHU to validate the On-line FTIR spectroscopy measurements with known poly-

meric mixtures.

The usefulness of IR spectroscopy to analyze molecular features, including molecular structure, is a particular value when it comes to polymer blend composition investigation [13]. In this extrusion runs, the polymer blend PP/PA6 was employed in order to assess the sensitivity of the on-line FTIR system. First (item 3.7.1), a series of non-reactive PP/PA6 polymer blends were used to investigate the accuracy of the on-line FTIR system in measuring blend composition. The on-line measurements were compared to off-line measurements done by ATR-FTIR and transmission infrared. Second (item 3.7.2), two polymer blends in non-reactive and in reactive systems were compared to evaluate the application of the On-line FTIR system in reactive extrusion.

### 3.7.1 Composition Investigation of the non-reactive PP/PA6 Blend In-processing and Off-line

Immiscible PP/PA6 polymer blends were prepared by mechanical blending of weighed amounts of pellets at the required wt.% ratio (Table 3.5) in 5 kg batches before extrusion. The blends were dried overnight at 90C under vacuum to remove humidity.

Tabela 3.5: PP/PA6 wt% compositions.

Polypropylene	Polyamide 6
90	10
70	30
50	50
30	70
10	90

#### *Extrusion*

The PP/PA6 blends were extruded twice at 230 C, at a feeding rate of 2 kg/h and screw rotation speed of 100 rpm, for better dispersion. Samples were collected after the second extrusion for off-line analysis.

*Analytical technique: on-line ATR-FTIR measurements*

The On-line FTIR system was attached to the extruder via the PHU at position 32.75 L/D along the extruder barrel. On-line measurements were done by following the sequence of operation presented in item 3.1.1. For statistical purposes 12 spectra were collected with a resolution of  $4\text{ cm}^{-1}$  and 5 scans for each blend composition (Table 3.5).

*Analytical technique: off-line ATR-FTIR measurements*

Samples collected during extrusion underwent off-line ATR-FTIR spectroscopy measurement in a Cary 630 FTIR Spectrometer manufactured by Agilent. A single bounce diamond ATR crystal with a transmission range from  $5100\text{--}600\text{ cm}^{-1}$  was used as the ATR accessory. Twenty spectra were collected in different location of different samples collected during extrusion with  $4\text{ cm}^{-1}$  of resolution and 16 scans.

*Analytical technique: off-line Transmission FTIR measurements*

0.04 to 0.05 mm films were prepared by hot-pressing the samples at 230 C for 6 minutes, releasing the pressure built up every other 2 minutes. FTIR transmission analyses, using Smart Transmission accessory, were done in the same IR spectrometer used in the on-line FTIR System. Ten spectra were collected with a resolution of  $4\text{ cm}^{-1}$  and 5 scans for each blend composition film. The transmittance (%T) spectra were converted to absorbance [80] spectra for purpose of comparison.

### **3.7.2 On-line FTIR analysis of REX (PP-g-AA/PA6) measured along the Extruder Barrel**

*Reactive Extrusion*

Blends of 40/60 (wt/wt%) PP and PA6 in non-reactive (PP) and reactive (PP-g-AA) conditions were extruded at 230 C, screw speed of 100 rpm and feed rate of 2 kg/h. On-line ATR-FTIR measurements were taken at positions 20.25, 30.25, 32.75 and 40 L/D and at-line mode of measurement were done at the die. Measurement of non-reactive blend were compared to model predictions from item 3.7.1.

### *Analytical technique: on-line ATR-FTIR measurements*

The polymer melt was diverted by the PHU to the ATR crystal. 16 spectra were collected for statistical purposes. Each spectrum was collected with an accumulation of 10 scans and resolution of  $4\text{ cm}^{-1}$ . The time of acquisition for each spectrum is 11 seconds. The balance between time and number of scans is a compromise of accuracy and speed, which will be discussed below. The area of IR bands at  $1640$  and  $1540\text{ cm}^{-1}$  were evaluated and normalized by the PP band at  $1370\text{ cm}^{-1}$ . An increase of area ratios ( $1640$  and  $1540\text{ cm}^{-1}$ ) are expected along the extruder barrel only for the reactive blend, whereas the area ratio for the non-reactive one is expected to be constant for all locations of the on-line measurements.

## **3.8 Reactive Blending Investigation**

### **3.8.1 Reactive Extrusion of 80/20 (wt/wt%) of PA6/PP-g-AA and PA6/PP**

Two series of blends were prepared, one reactive and its non-reactive counterpart. The non-reactive blend was a matrix of polyamide 6 in 80 wt.% with the dispersed phase consisting of 20 wt.% of polypropylene (80PA6/20PP), whereas in the reactive system the polypropylene was substituted by a polypropylene grafted with acrylic acid (80PA6/20PP-g-AA). In this experiment, the two polymers at the given blend ratio were hand tumbled in a bag in 5 kg batches. Before processing the materials were dried under vacuum at  $90^\circ\text{C}$  overnight. The blends were processed and the chemical reaction kinetic between acrylic acid and amine terminal group in the PA6 chain (Figure 3.8) was investigated by FTIR spectroscopy during the extrusion process in on-line mode. As said in item 3.2.3, the IR characteristic band of amide I ( $1640\text{ cm}^{-1}$ ) normalized by the IR band at  $1373\text{ cm}^{-1}$  is used to track the reaction along the extruder barrel.

Two sets of experiments were carried out into the same twin-screw extruder presented in item 3.3. First, different screw configuration is used during extrusion applying various levels of dispersive and distributive mixing. Second, process parameters of feed rate and screw speed are varied during extrusion. A variation of the area ratio of  $1640\text{ cm}^{-1}$  and  $1373\text{ cm}^{-1}$  is expected for the reactive

blends along the extruder length with different screw configuration and process parameters applied during extruder. The area ratio for the non-reactive blends are expected to remain constant along the extruder barrel.

#### *Experiment 1: Screw Configuration*

For the first series of experiment, the two polymer blends of 80% of PA6 and 20% of PP and 80% of PA6 and 20% of PP-g-AA were processed with the barrel set temperature at 230C at all zones of the extruder, except for the feed zone, which was 210C. The screw speed was set at 200 rpm and a feed rate at 2 kg/h. Four screw configurations were tested in order to evaluate the difference of distribute and dispersive mixing degree of the screws on the reaction. The screw profiles are identical, except for the (2 L/D length) mixing zone at 18.25 L/D, shown in Figure 3.9.

Figure 3.9 shows four screw profiles used in this set of experiment. Before the individual, different, mixing zones at 18.25 L/D, the screw profile contains an 8 ½ L/D conveying or transport (T) zone, followed by a zone of 4 ¼ L/D length comprised of 17 kneading blocks reversely staggered at 30°. Then a zone of 5 L/D conveying elements, followed by two kneading blocks (KB) staggered at 90°.

After the mixing zone at 18.25 L/D the profile contains one kneading block and a left-handed conveying element, as well as a second mixing zone consisting of thirteen kneading disks staggered at 90° followed by a left-handed conveying element. The left-handed conveying zone is placed after the mixing zone to ensure that the portion of screw is full of material and to build the necessary pressure in order to withdraw material by the P/T ports.

The four different mixing zone (Figure 3.9) contain either eight kneading blocks (KB) staggered at 30° (Figure 3.9a) or eight kneading disks staggered at 90° (Figure 3.9b), respectively. For the third (Figure 3.9c) and fourth (Figure 3.9d) screw configurations, the 2 L/D length mixing zone was replaced by extensional mixing elements (EME) of 2:1 (L2) and 4:1 (S4) contraction ratios, respectively. The short and aggressive EME S4 imposes a 4.2x strain rate at the centerline and a 5x linear strain by comparison with the longer and milder EME L2. This first set of experiments aims to analyze how the mixing can modify the chemical reac-

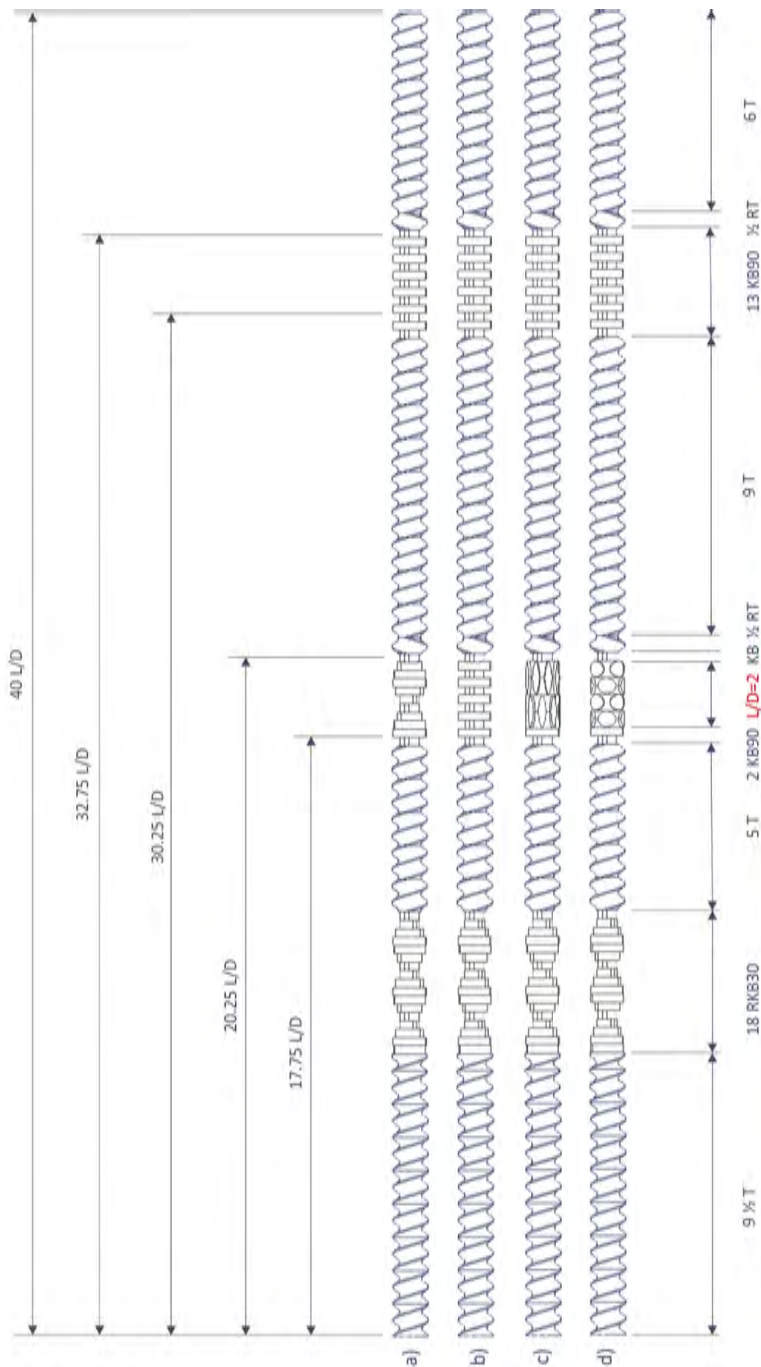


Figura 3.9: Screw profile configurations a) KB30, b) KB90, c) EME L2 and d) EME S4 and the length of the screw that on-line FTIR measurements were done (17.75, 20.25, 30.25, 32.75 and 40.00 L/D). L/D=2 in red indicates the position and length of the mixing zone that is substituted. (T= transport, KB = kneading block, L/D = length and diameter ratio, and RT = reverse transport).

tion behavior of the polymer blends by varying the mixing power in the sense of distributive and dispersive mixing degree of the mixing zone within the screw profile. The aggressiveness of the mixing zone in the screw configuration increases from the first screw profile (KB30), being the least aggressive, to the fourth profile (EME S4), the most aggressive one [1, 35, 41, 48, 50].

#### *Experiment 2: Process Condition Variation*

In the second set of experiments, the blends were processed at feed rates and screw speeds listed in Table 3.6, while the extrusion temperature was kept constant at 230°C. Only (Figure 3.9d) EME S4 was selected due to it having the most aggressive converging-diverging channels when compared to the other screws, which makes it able to generate the most interface [44, 45, 48, 49].

The notation for the various processing conditions is made of 4 elements of information (Table 3.6). The first element specifies the screw profile, KB30, KB90, L2 and S4 for EME-L2 and EME-S4, respectively. The second element refers to the screw rotation speed, 200 or 600 rpm, the third one is associated to the feed rate of 2 or 5 kg/h, and the last represents the non-reactive (NR) and the reactive (R) polymer blend system used. For example, the condition S4-200-5-NR was performed using the fourth screw configuration with EME S4 as the mixing zone, at screw speed of 200 rpm, feed rate at 5 kg/h and extruding the non-reactive blend.

### **3.8.2 On-line ATR-FTIR Measurements**

Infrared spectra were collected along the extruder barrel by using the on-line FTIR spectroscopic system developed in our laboratories [93] and described in item 3.1.1.

#### *Experiment 1: Screw Configuration*

In the first series of experiments to quantify the chemical reaction, the measurements were done in the on-line mode, taken at various locations along the screw profile: 17.75 L/D, 20.25 L/D (these two flanking the mixing zone), 32.75 L/D, and finally after the die, but measured in at-line mode.



Tabela 3.6: Process conditions with the use of different screw profiles varying the distributive and dispersive mixing levels.

Condition	System	Screw configuration	Temperature (C)	Screw speed (RPM)	Feed Rate (kg/h)
Experiment 1: Screw Configuration					
KB30-200-2-NR	PA6/PP	KB30	230	200	2
KB90-200-2-NR		KB90	230	200	2
L2-200-2-NR		EME L2	230	200	2
S4-200-2-NR		EME S4	230	200	2
KB30-200-2-R	PA6/PP-g-AA	KB30	230	200	2
KB90-200-2-R		KB90	230	200	2
L2-200-2-R		EME L2	230	200	2
S4-200-2-R		EME S4	230	200	2
Experiment 2: Process Condition Variation					
S4-600-2-R	PA6/PP-g-AA	EME S4	230	600	2
S4-200-5-R		EME S4	230	200	5
S4-600-5-R		EME S4	230	600	5

### *Experiment 2: Process Condition Variation*

In the second set of experiments, the ATR-FTIR measurements were performed in on-line mode at 17.75, 20.25, 30.25 and 40.00 L/D, using only reactive PA6/PP-g-AA blends. As indicated in Figure 3.9, the location along the barrel enables an overview of the development of the reaction along the whole length of the extruder in both sets of experiments.

Approximately 20 ATR-FTIR spectra for each blend at each port location (L/D) were collected with  $4\text{ cm}^{-1}$  of resolution and 5 scans for both sets of experiments. Before performing the measurements, the extrusion run for 15 min in order to reach the steady-state regime. The data frame is provided in Appendix H.

### 3.8.3 Scanning Electron Microscopy

During extrusion, samples were collected at each port, for the first series of experiment, and quenched in cold water in order to decrease the temperature of the sample, thus avoid further reactions and modification of the morphology of the samples. Scanning electron microscopy (SEM) on a JEOL JSM-6510LV was performed on fracture surface of the specimens broken at cryogenic temperature (liquid nitrogen), at a voltage of 15 kV, under high vacuum, and the fracture surfaces of the samples sputter coated with palladium.

#### *Quantitative Analysis of Particle Size*

The second phase particle areas were manually measured from SEM by Image J software and particle size distribution curves were built. 400 particles were measured per sample. The cumulative area ratios (CAR) proposed by Novais et al. (2012) were calculated in each SEM micrographs with the methodology demonstrated by Chen et al. [44, 45] and Emin [124] by the following equation

$$F_{[i,j]} = \frac{\sum_{i=j} A_{[i,j]}}{\sum_n A_n} \quad (3.1)$$

where  $A_{[i,j]}$  represents the area of the second phase particle that has been ranked from the smallest to the  $j^{th}$  particle, and  $A_n$  represents the total particle area. These values were plotted against particle area  $A_i$ . In this way, the particle size distribution of the measured particles is accounted for in the statistical analysis [125, 126].

### 3.8.4 Reactive Extrusion of 70/30 (wt/wt%) of PP-g-AA/PA6 and PP/PA6

Two blends were prepared in a non-reactive and a reactive system. The polymers were hand-tumbled in a bag in 5 kg batches in the concentration of 70% of the major phases (PP or PP-g-AA) and 30% of PA6. Before extrusion the blends were dried under vacuum at 90C overnight. All polymers were used in pellet form.

The experiments were carried out into the same twin-screw extruder presented in item 3.3.

### *Process Parameters*

Table 3.7 shows the process conditions with varying screw profile, feed rate and screw rotation speed used in this work. The process conditions identification is made up the same as previous in section 4.4. The first element specifies the screw profile, L2 and S4 to extensional mixing elements EME-L2 and EME-S4, respectively. The second element refers to the screw rotation speed, 100 or 400 rpm. The third element is associated to the feed rates of 2 or 5 kg/h, and the last element of information represents the non-reactive (NR) and the reactive (R) polymer blend system used. For example, the condition L2-400-2-R was performed using the extensional mixing element EME-L2 as the mixing zone, at speed of 400 rpm, feed rate at 5 kg/h and extruding the reactive blend.

This experiment uses two screw profiles depicted in Figure 3.9. These are: the third (Figure 3.9c) and the fourth (Figure 3.9d) screw configurations, where the 2 L/D length mixing zone is comprised by extensional mixing elements (EME) of 2:1 (L2) and 4:1 (S4) contraction ratios, respectively. EMEs were used due to the high dispersive ability of mixing [1, 35, 49]. Figure 3.10 show in details both EME's.

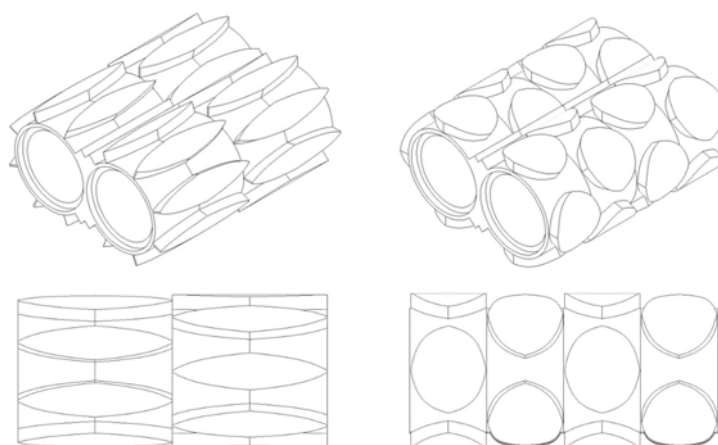


Figura 3.10: Extensional mixing elements (EMEs) L2 on the left and S4 on the right.

### **3.8.5 On-line ATR-FTIR measurements**

Once the extrusion run reached the steady state (defined as the stable average torque reaching and extrusion over approximately 15 minute of processing),

Tabela 3.7: Process conditions varying the type of EME, material system, feed rate and screw speed.

Condition	System	Screw configuration	Temperature (C)	Feed Rate (kg/h)	Screw speed (RPM)
L2-100-2-NR	PP/PA6	EME L2	240	2	100
L2-400-2-NR					400
L2-100-5-NR		EME S4		5	100
L2-400-5-NR					400
S4-100-2-NR		5		2	100
S4-400-2-NR					400
S4-100-5-NR					100
S4-400-5-NR					400
L2-100-2-R	PP- g- AA/PA6	EME L2	240	2	100
L2-400-2-R					400
L2-100-5-R		EME S4		5	100
L2-400-5-R					400
S4-100-2-R		5		2	100
S4-400-2-R					400
S4-100-5-R					100
S4-400-5-R					400

on-line ATR-FTIR measurements were done at  $L/D = 17.75, 20.25, 30.2$  and  $32.75$  (please see Figure 3.9), where  $L$  is the axial length and  $D$  is the diameter of the screw.

The resolution of the analysis were set at  $4 \text{ cm}^{-1}$  with an accumulation of five scans. The acquisition time for each spectrum is approximately 7 seconds. For each location in the extruder barrel, a total of 20 to 25 spectra were collected during the extrusion runs for the calculation of average and errors.

### 3.8.6 Residence Time Distribution curves by Colorimetry

#### *Experimental RTD Curves*

Determination of blend residence time distribution (RTD) curves was conducted by the tracer experiment [62]. A tracer (pulse) of red dyed polyethylene pellets of approximately 0.3 g was added to the melt stream during extrusion for all the process conditions (Table 3.7). Samples were collected at locations 17.75 L/D, 20.25 L/D, 32.75 L/D and at 40 L/D (die) continuously at fixed time intervals of 10 s. The intensity of color red ( $a^*$ ) in each sample was measured based on CIE  $L^*a^*b^*$ -System by a portable spectrophotometer BYK-Gardner Additives Instruments Spectro-guide 45/0 gloss. CIELAB is a color space in which values of  $L^*$ ,  $a^*$  and  $b^*$  are part of a Cartesian coordinate system. The distances in the space approximately represent the color differences. Values of  $L^*$  represent the lightness; values of  $a^*$  represent the red/green intensities; and values of  $b^*$  represent the intensities of yellow/blue [127]. The residence time distribution function  $E(t)$  was applied in the recorded experimental data ( $a^*$ ) and plotted against time.

#### *Theoretical RTD Curves*

The pulse function was applied to fit the  $E(t)$  curves obtained from the experimental data. The shape of pulse function curves is very similar to the curve of the variation of tracer (pulse) concentration with time in the extrusion process of polymers. Consequently, this function can be used as theoretical RTD curve fitting for the experimental data [57, 128]. The pulse function can be described this way:

$$I(t) = I_0 + K \left[ 1 - e^{-\frac{(t-t_i)}{R_1}} \right]^p * e^{-\frac{(t-t_i)}{R_2}} \quad (3.2)$$

$I_0$  is the initial intensity or base line value, which is normally attributed to 0.  $K$  is a constant relative to the curve area,  $t_i$  ( $X_0$ ) is the delay/initial time value,  $p$  is a power exponent and  $R_1$  and  $R_2$  are the curve ascent and descent time rate constant respectively. Table 3.8 shows the parameters that can be obtained from the curve fitting and how they are related to the shape of the curve.

Tabela 3.8: Meaning of the coefficients of the pulse curves.

	Coefficient	Effect on shape
$I_0$	Initial intensity	The intensity of the tracer concentration, forming the baseline, usually taken as zero (0).
$X_0$	Delay time	The delay or initial time, when the intensity of the tracer starts to increase.
$K$	Area constant	Constant related to the area under the curve.
$R_1$	Curve ascent time rate constant	The higher the $R_1$ , the higher the ascent time of the curve, the longer the curve takes to reach the maximum. This means that the material comes out of the extruder slower.
$R_2$	Curve descent time rate constant	The higher the $R_2$ , the higher the descent time of the curve, the longer the curve takes to decrease. This means the material remains in the extruder longer.
$p$	power exponent	It affects the ascent part of the curve, the higher the $p$ , the wider the pulse curve distribution

### 3.9 Software

#### *3D Computer-aided Design software*

To design the parts and assemblies of the On-line FTIR spectroscopic system two 3D CAD software were used: SolidWorks (Dassault Systèmes SolidWorks Corporation) and Inventor®(Autodesk).

#### *LabVIEW™(National Instruments)*

Baseline correction, peak area and peak height were calculated by the software developed in LabVIEW™, a platform for data acquisition, real-time measurements, screen presentation and data archiving [7].

*Origin®*

The IR bands were deconvoluted by a routine created in Origin version 2019b (OriginLab Corporation, Northampton, MA, USA). Analytical function Pearson VII was used to describe the line-shape of the FTIR spectra in order to fit the curves.

*ImageJ*

Open source software for image processing and analysis in Java.

*OMNIC™*

Commercial software of the spectrometer for data collection and visualization.





## 4 RESULTS AND DISCUSSIONS

### 4.1 Number of scans and Signal-to-noise Ratio Dependency

Figure 4.1 shows the acetone spectra taken at different numbers of scans. As expected, the higher the number of scans the smoother the spectra is. That is because the number of scans co-added in a FTIR measurement is associated to the achievement of an acceptable signal-to-noise ratio [28].

For a FTIR measurement, the infrared spectrometers scan the sample through its range of IR radiation. In a measurement, one can set different number of scans (normally from 1 to 1000). Subsequently, the absorbance at each wavenumber is averaged by the number of scans used in the measurement (1, 2, or 1000 scans) to yield an IR spectrum. The average is close to the absorbance expected by a measurement made at only one scan. The difference is that a FTIR measurement using a number of scan equals 1 will lead to an IR spectrum with lower signal-to-noise ratio (SNR) than a IR spectrum collected in a measurement at a number of scan equals 10, for example. Noises in the baseline can also be diminished using a high number of scans.

In this analysis fifty measurements were done for various number of scans. The fifty spectra collected in a measurement with the number of scan set at 1 were averaged (signal) and the standard deviation (noise) was calculated. The signal (average) of the IR band at  $1710\text{ cm}^{-1}$  was divided by the standard deviation to calculate the signal-to-noise ratio [28, 129]. The same procedure was done for the measurements with number of scan set at 2, 4, 8, 16, 32, 64, and 128. Figure 4.2 shows SNR at  $1710\text{ cm}^{-1}$ . The higher SNR means less deviation from the average, thus, smoother and less noisy data, higher quality the spectrum. On the other hand, the higher the number of scans the longer the measurement takes, i.e., to increase the spectra resolution one has to increase the measuring time. For reactive processes measurement time is a parameter that needs to be minimized. That is because during the measurement some reaction can keep taking place, leading to errors in the results [130].

A desired balance between time of analysis and SNR of the spectra needs to

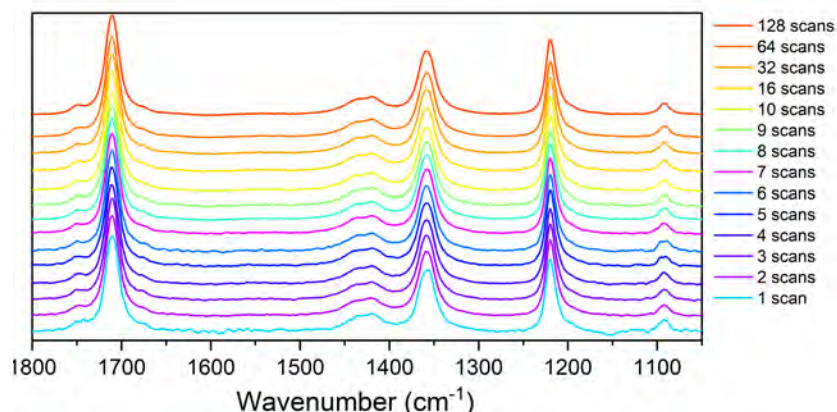


Figura 4.1: Resolution of acetone spectra taken at increasing number of scans.

be agreed before the number of scans is chosen. This agreement is dependent on the functional groups that are being investigated, their band intensities (for example, high intense bands are less affected by noise in the spectra due to their high absorptivity) and on the interaction with other functional group bands. In this thesis, the number of scans was fixed at 5, for reactive systems, to maintain consistency. This takes a measurement time of approximately 6 seconds. This is because the studied reaction is an interface reaction, that is, it only occurs at the interface between the two polymers, therefore, as during the online measurement no interface is being generated due to lack of mixing, the resolution was prioritized instead of time [131].

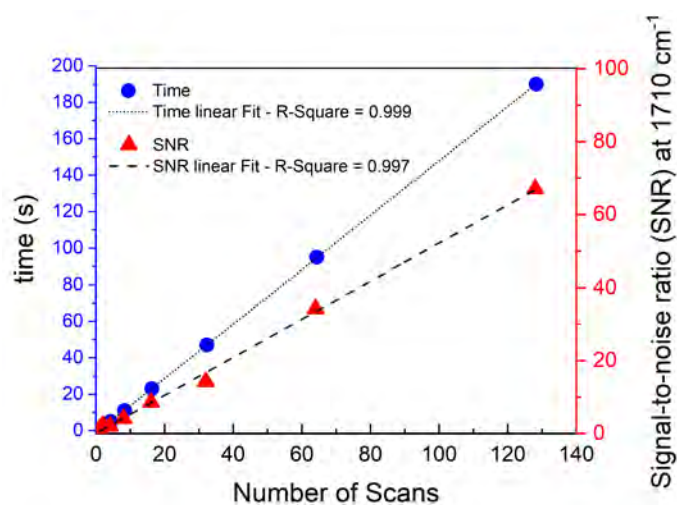


Figura 4.2: Relationship between the number of scans in a FTIR measurement and the time of measurement (blue axis) and signal-to-noise (red axis).

## 4.2 Validation of Data Treatment with Pearson VII function

### 4.2.1 Spectroscopy of Binary Mixture: acetone/water

An average of twenty spectra of the acetone/distilled water mixture for each composition studied are presented in Figure 4.3.

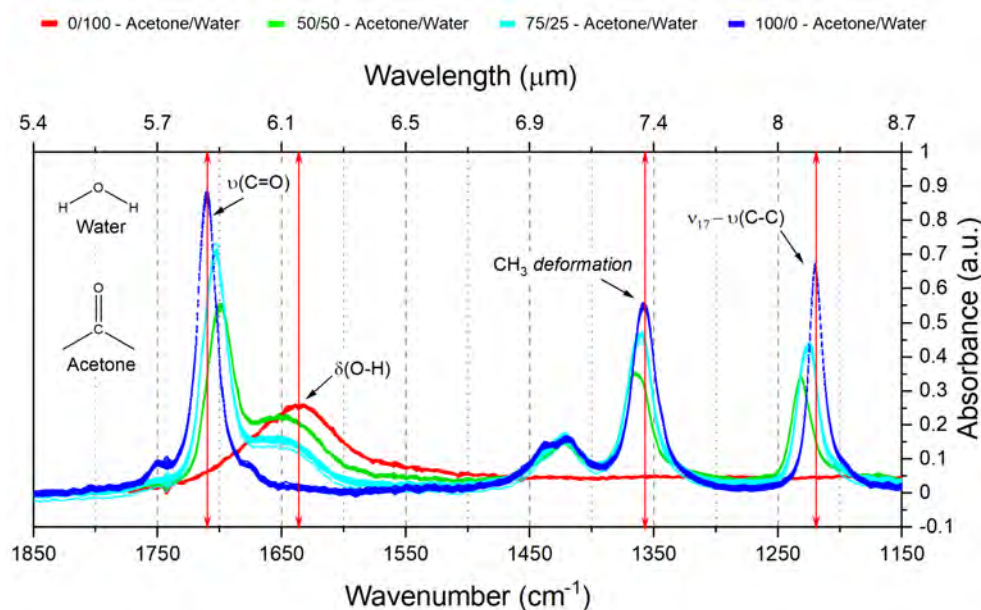


Figure 4.3: Spectra of binary distilled water/acetone mixtures. Red double-headed arrows indicate the bands analyzed.

The plots shown in Figure 4.4(a), 4.4(b) and, 4.4(c), related to the bands of acetone ( $\sim 1710$ ,  $1365$  and  $1220 \text{ cm}^{-1}$ ), are the ratio between the absorbance of the mixture ( $A_i$ ) of the pure acetone ( $A_{100}$ ). Figure 4.4(a) show that  $A_i/A_{100}$  of bands at  $1710 \text{ cm}^{-1}$  measured, from the spectra collected by the ATR-FTIR probe in bench, by the three methods, namely, traditional method, deconvoluting method by Lorentz function and the deconvoluting method by Pearson VII function, increase linearly with the amount of acetone content (composition of the mixtures), as expected, and are independent of the method used to calculate them. This applies particularly to the  $A_i/A_{100}$  of the bands at  $1360$  and  $1220 \text{ cm}^{-1}$  (Figures 4.4(b) and 4.4(c)), since they do not overlap with any band of the distilled water infrared spectrum [132]. When the band at  $1710 \text{ cm}^{-1}$  is calculated by the traditional method in Figure 4.4(a), one can see a deviation of the linearity of the composition proposed by Beer's law. However, when the deconvolution methods

(Pearson VII and Lorentz) are applied, one can see the linear behavior present in the plots. The R-Square of the linear fit for both, Pearson VII and Lorentz, are the same, 0.999, which means that both methods are efficiently equivalent for the band at  $1710\text{ cm}^{-1}$ . The high absorptivity coefficient (or extinction coefficient, which is a measurement of how strongly a chemical species absorbs light at a given wavelength) associated to carbonyl stretching  $\nu(\text{C}=\text{O})$  ( $1710\text{ cm}^{-1}$ ), compared to the band at  $1656\text{ cm}^{-1}$  of distilled water, can explain its independence of the method used (Pearson VII or Lorentz).

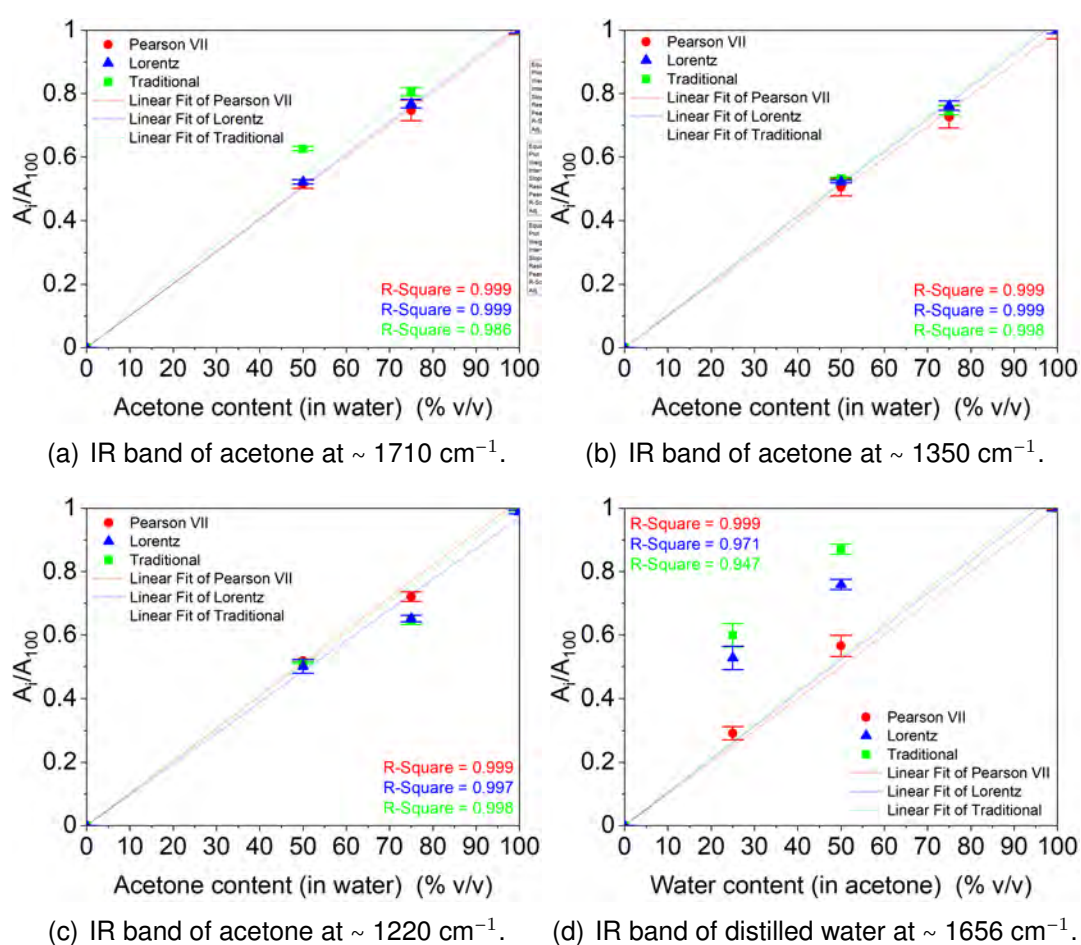


Figure 4.4: Absorbance (peak height) of acetone (a, b, and c) and distilled water (d) bands calculated by the traditional method, Lorentz function and Pearson VII methods. The R-Squares of the linear fitting according to the composition  $n$  shown on the plots in colors corresponding to the method used (Pearson VII = red; Lorentz = blue and; traditional method = green).

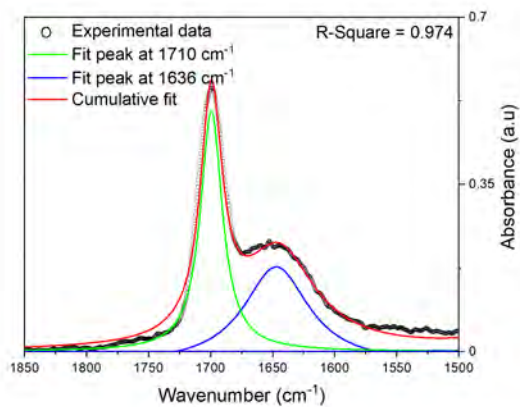
The  $A_i/A_{100}$  of the band at  $1636\text{ cm}^{-1}$  (distilled water), on the other hand, is markedly affected by this overlapping due to its lower absorptivity coefficient

when compared to  $\nu(\text{C}=\text{O})$ , compromising the determination of its absorbance [27]. Consequently, the distilled water band does not show a linear trend with the increase of the distilled water content when it is calculated by the traditional method, as is shown in Figure 4.4(d). Applying the convolution method with Lorentz function the R-Square of the linear fitting is improved when compared to the traditional method (see Figure 4.4(d)). However, when the function Pearson VII is applied, the bands can be differentiated from one another and the expected linear increase is restored (R-Square = 0.999). The difference between the both deconvolution methods, Pearson VII and Lorentz, is because Pearson VII function has the ability to "see" the tail of the IR band, leading to better fitting.

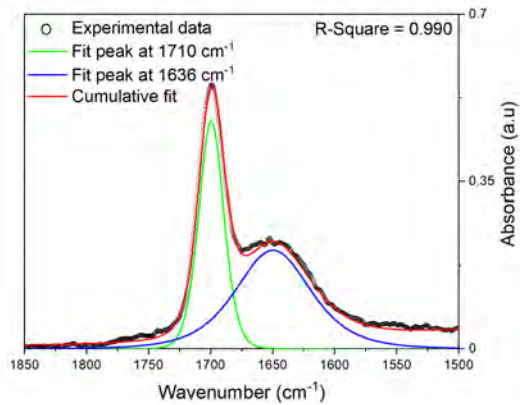
Figure 4.5 shows the deconvolution fitting applied by Lorentz and Pearson VII function for the mixture of 50/50 (vol/vol%) of acetone and distilled water. Pearson VII function leads to a higher R-Square of the deconvolution fitting, which are shown on the plots (4.5(a) and 4.5(b)).

The band areas ( $\text{Area}_i/\text{Area}_{100}$ ) associated to acetone molecular structure follow the same trend of the absorbances (Figures 4.6(a) and 4.6(b)). However, a slight improvement in the R-square (see Figure 4.6) of the linear fit was achieved by the use of the deconvolution approach. In contrast, the  $\text{Area}_i/\text{Area}_{100}$  of the band relative to distilled water molecular structure shows a more problematic trend. Linearity for  $\text{Area}_i/\text{Area}_{100}$  is only achieved when the deconvolution method is applied as well.

Focusing on the distilled water band at  $1636\text{ cm}^{-1}$ , the trend of its peak height ( $A_i/A_{100}$ ) and area ( $\text{Area}_i/\text{Area}_{100}$ ) calculated by the deconvolution method of Pearson VII shows a very good linear fit, which is expected. Surprisingly, differences were found in peak height ( $A_i/A_{100}$ ) and area ( $\text{Area}_i/\text{Area}_{100}$ ) calculated by the traditional method and by the deconvolution method of Lorentz. The  $A_i/A_{100}$  is somehow above the expected absorbance, whereas  $\text{Area}_i/\text{Area}_{100}$  are below the expected areas, when calculated by the traditional method. The application of Lorentz function leads to an improvement of the linearity (see R-Square on the plot of Figure 4.4 and 4.6). However, good R-Square ( $\sim 0.999$ ) is only achieved by Pearson VII function fitting due to the better ability of Pearson VII in consider the



(a) Lorentz function.



(b) Pearson VII function.

Figure 4.5: Range of overlapping of the bands at  $1710 \text{ cm}^{-1}$  and  $1656 \text{ cm}^{-1}$  bands calculated by the a) Lorentz function and b) Pearson VII methods. The R-Squares of the deconvoluting fitting for both, Lorentz and Pearson VII function are shown on the plots. A better R-Square is achieved by the Pearson VII function fitting.



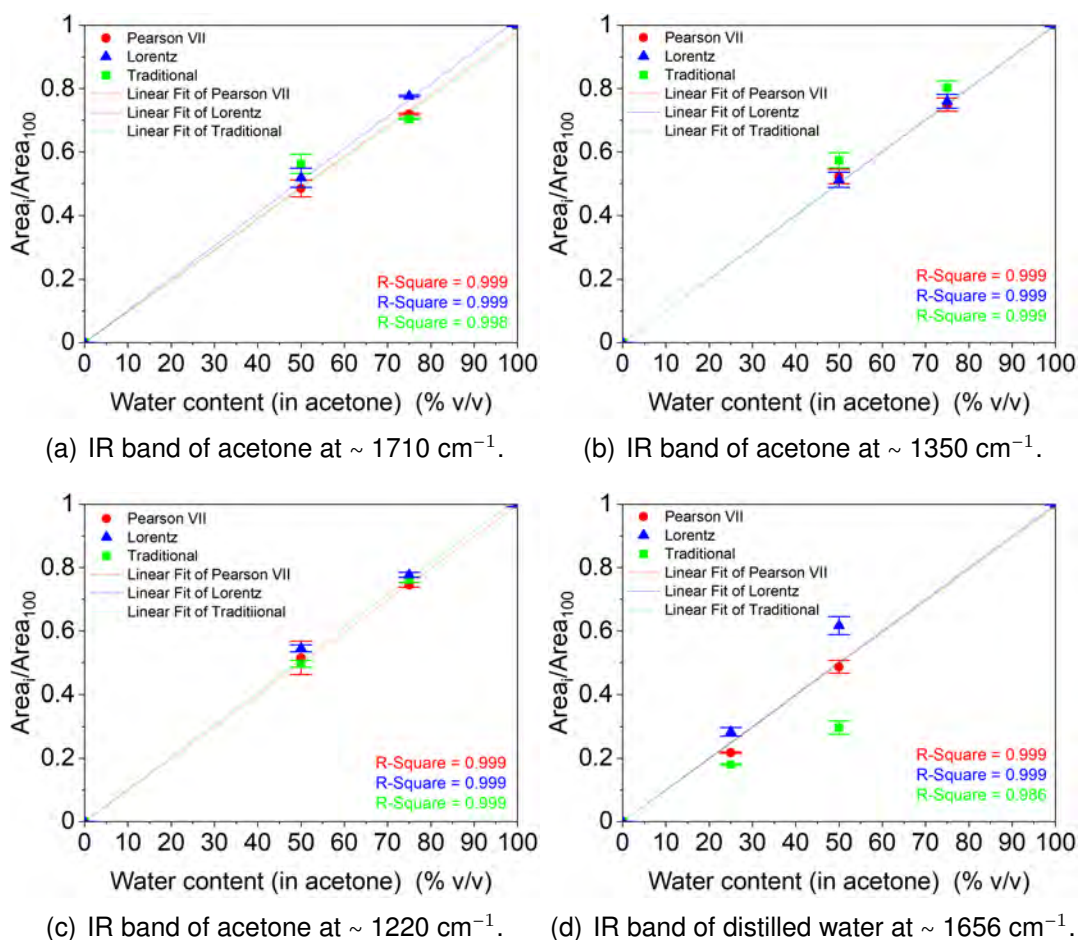
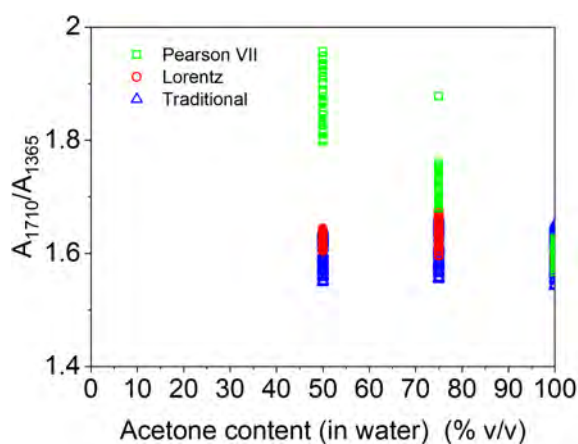


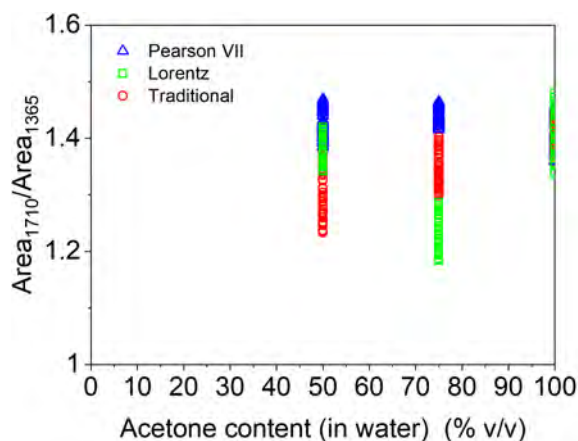
Figure 4.6: Area of acetone (a, b, and c) and distilled water (d) bands calculated by the traditional method, Lorentz function and Pearson VII methods. The R-Squares of the linear fitting according to the composition  $n$  shown on the plots in colors corresponding to the method used (Pearson VII = red; Lorentz = blue and; traditional method = green).

tails of the IR band. Taken together, these results suggest that the traditional method is prone to errors in calculation of absorbance and band area, especially for peak area, where the overlapping of bands is not considered.

Figure 4.7(a) and 4.7(b) show the absorbance and area ratio (normalization) between the bands of acetone at  $\sim 1710$  and  $\sim 1365\text{ cm}^{-1}$  for the three methods used in this work. The relation (ratio) between IR band of the same material should be kept constant, even when the concentration of that specie is change, which is the case of the mixtures. The plots show that both, absorbance and area ratio, are not constant for all the compositions (75/25 and 50/50 - vol/vol%). On the other hand the deconvolution methods, both Lorentz and Pearson VII, the expected trend is achieve. This show that interference of the overlapping of the band of



(a) Absorbance ratios of bands of acetone at  $\sim 1710$  and  $\sim 1356$   $\text{cm}^{-1}$ .



(b) Area ratios of bands of acetone at  $\sim 1710$  and  $\sim 1356$   $\text{cm}^{-1}$ .

Figure 4.7: a) Absorbance and b) area ratios of bands of acetone at  $\sim 1710$  and  $\sim 1356$   $\text{cm}^{-1}$  for bands calculated by the traditional method, Lorentz function and Pearson VII methods for the mixtures of 75/25 and 50/50 (vol/vol%) and pure acetone.

acetone  $\sim 1710$  and the band of distilled water at  $\sim 1656$   $\text{cm}^{-1}$  can affect the behavior of the IR spectra.

Variation in the environment around water molecule gives rise to considerable line broadening with vibration shifts. Most of this shifting in vibrational frequencies can be related to hydrogen bonding [118]. As a matter of fact, hydrogen bonds in acetone-water mixture are observed on the carbonyl stretch band of acetone at  $1710$   $\text{cm}^{-1}$  [110], causing its redshifting. The blueshifting (shown in Figure 4.3) of  $1360$  and  $1220$   $\text{cm}^{-1}$  bands can be associated to the weakening of carbonyl stretch band due to hydrogen bond with water molecule [27]. In summary,



these results show that the ATR-FTIR probe is sensitive to composition changes in binary liquid mixtures and to vibration frequency shifting.

#### 4.2.2 Spectroscopy of Binary and Ternary mixtures: acetone/ethanol/toluene

Figure 4.8 depicts the infrared spectra collected by the ATR-FTIR probe for pure acetone (100A), ethanol (100E) and toluene (100T). Figure 4.9 depicts the infrared spectra collected by the ATR-FTIR probe for binary mixture of 50/50 (vol/vol%) of acetone, ethanol and toluene and Figure 4.10 shows the infrared spectra for their ternary mixtures.

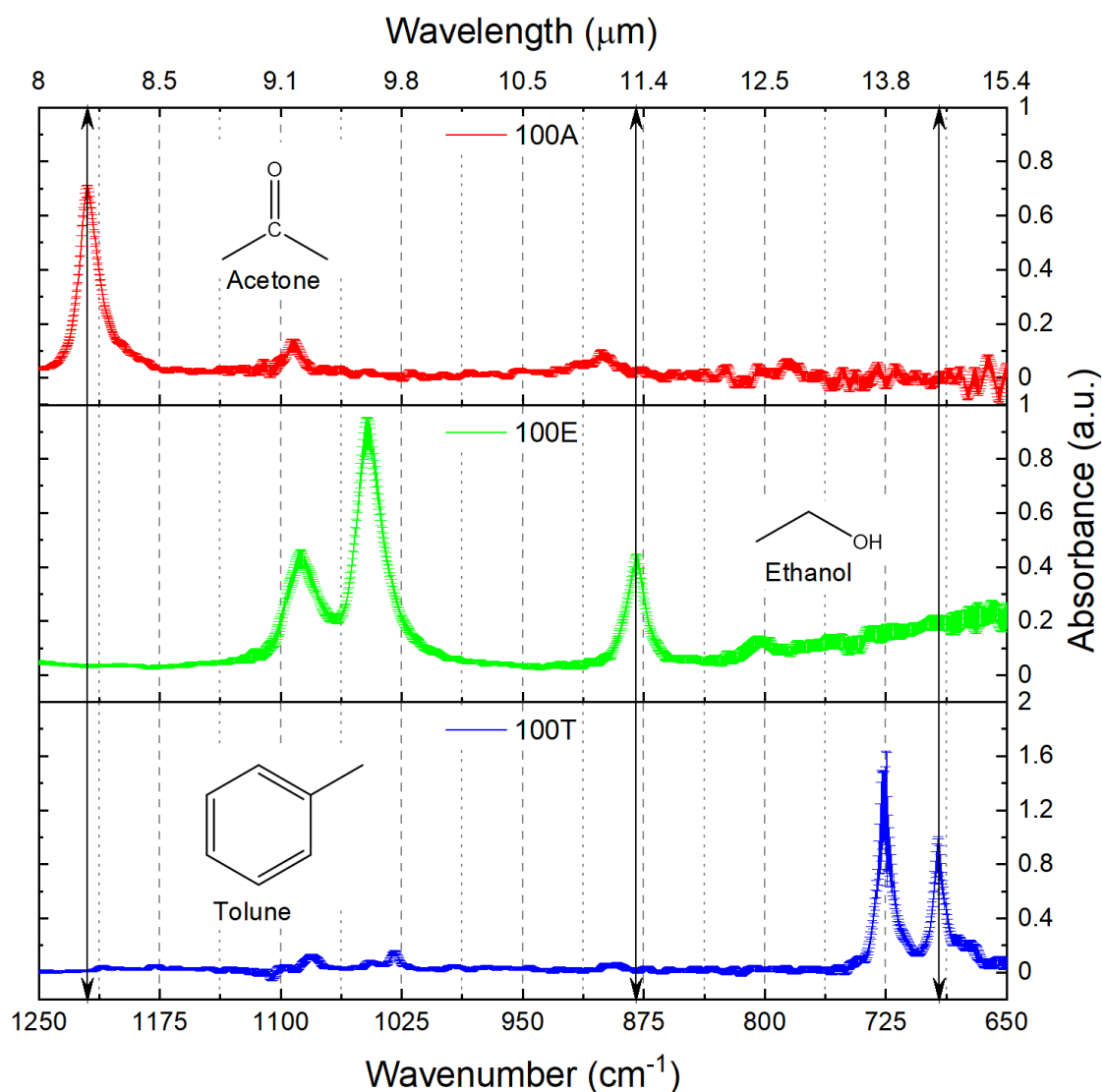


Figure 4.8: ATR-FTIR spectra for pure (a) Acetone (100A), (b) Ethanol (100E) and (c) Toluene (100T). Double-headed arrows indicate the bands at  $1220$ ,  $879$ ,  $692$   $\text{cm}^{-1}$  used in the analyzes.

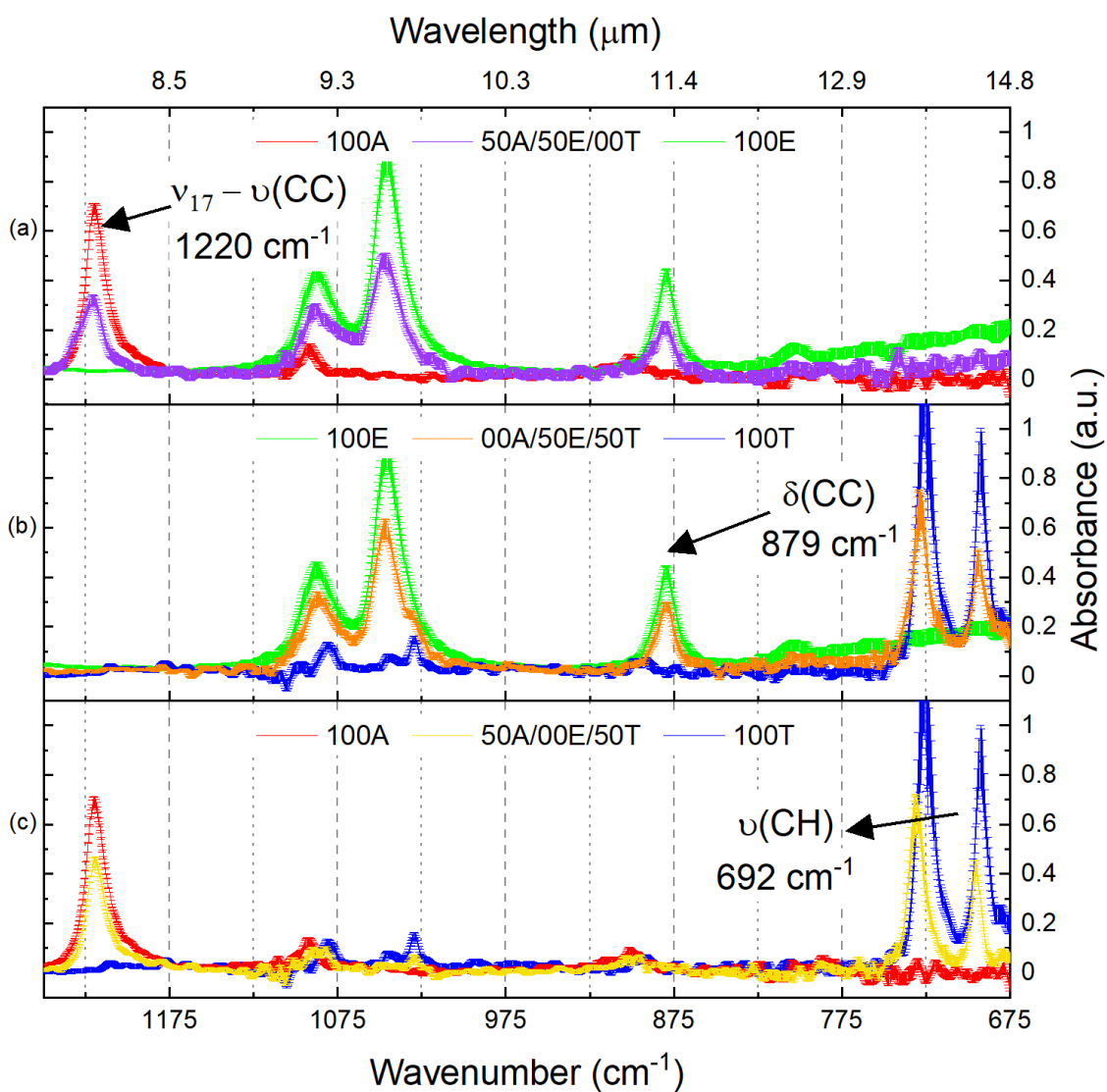


Figure 4.9: ATR-FTIR spectra for binary mixture of 50/50 (vol/vol%) (a) acetone and ethanol (50A/50E/00T), (b) acetone and toluene (50A/00E/50T), and (c) ethanol and toluene (00A/50E/50T).

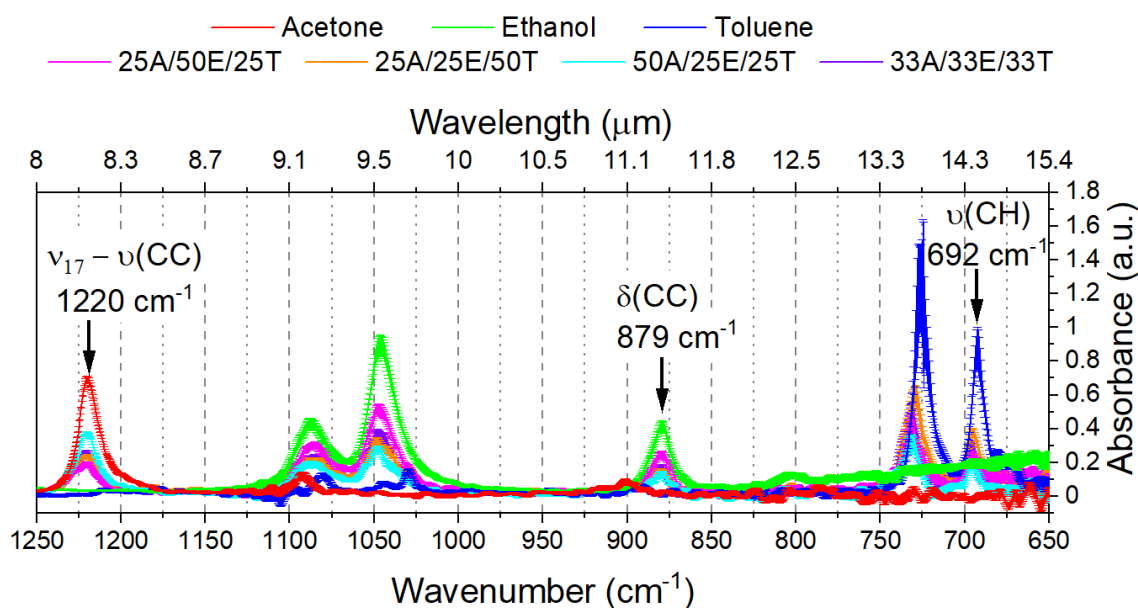


Figura 4.10: ATR-FTIR spectra for ternary mixtures in %vol Acetone, Ethanol, and Toluene.

In order to build the ternary phase diagrams that are shown in Figure 4.11 the absorbances and areas of bands at  $1220$ ,  $879$  and  $692\text{ cm}^{-1}$ , assigned to acetone, ethanol and toluene, respectively, were considered to be 100% for the pure liquids (100A, 100E and 100T). The absorbances and areas of these bands for the mixtures were then calculated and are shown in percentage of concentration of acetone, ethanol and toluene for all binary and ternary mixtures.

Due to the fact that the analyzed bands do not overlap with each other in the infrared spectra of the mixtures, no detectable difference in the absorbance (Figures 4.11(a), 4.11(c) and 4.11(e)) can be seen when they are calculated by three methods (traditional, Lorentz and Pearson VII), unlike in the case of band areas. Differences in the area value with the use of the methods can be seen in Figures 4.11(b), 4.11(d) and 4.11(f). The areas calculated by the traditional method are shifted in the ternary plot for almost all the compositions, but the 25A/50E/25T and 50A/50E/00T sample. When the deconvolution of the bands, both Lorentz and Pearson VII, are done this shifting is diminished (Figure 4.11(d) and 4.11(f)), but the results are more dispersed. A probable explanation for the observed shifting and dispersion data in Figure 4.11 is the possibility of noise in

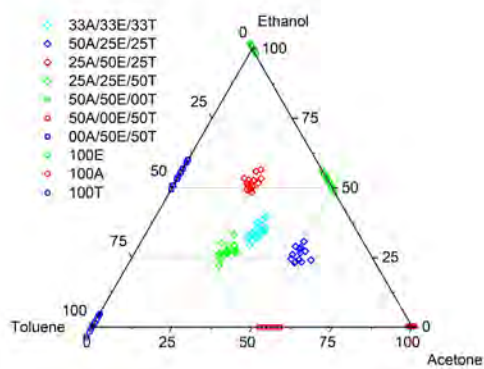
the spectra baseline that can be seen in Figures 4.8, 4.9 and 4.10.

As can be seen in Figures 4.8, 4.9 and 4.10, baselines of the spectra have noises, especially in the range between  $750\text{-}650\text{ cm}^{-1}$ , which is close to the limit of the range of transmission of silicon ATR crystal. These noises are considered in the calculation of the area, leading to incongruous results. In contrast, the peak height is less affected by a noisy baseline. The function Lorentz took long time to iterate in the software used (Origin™). A total of 400 iterations is applied by the software. However, not all the spectra collected (total of 15) had the iterations converged for the fitting, that is why there is less data point for the ternary plot for Lorentz function (around 6). This might also have to do with the noisy baseline, being an issue for the application of Lorentz function for the deconvolution of bands, which it does not happen for Pearson VII function. That is because Pearson VII, as aforementioned, has a better ability to consider the tails of the IR bands. The noisy baseline make it difficult to apply Lorentz function in all the spectra collected.

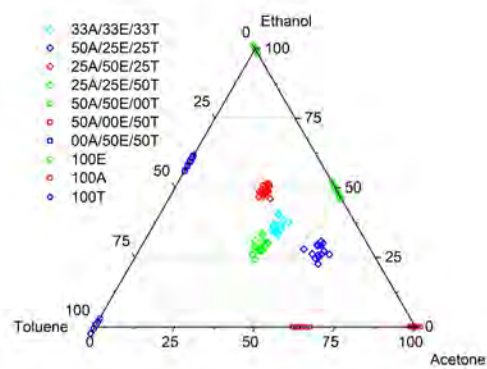
The present results are significant in at least two major respects. First, one needs to consider taking a close look at the spectrum before choosing between absorbance and area for their infrared analyses. Noisy baseline, broad bands, red and blueshifting can be determinant for this choice [29]. Second, the use of band deconvolution can help avoid those misleading results and get correct information from an infrared spectrum, specially if the IR bands are overlapped or the baseline is noisy.

Figure 4.9 and 4.10 also show that there has been a blueshifting of toluene band at  $691\text{ cm}^{-1}$  with the decrease in toluene quantity in the mixtures. This happens either in binary (Figure 4.9) or ternary mixtures (Figure 4.10) and is independent of whether it is with acetone, ethanol or both. The reason for this is out of the scope of this work but it may be related with the non-polar characteristic of toluene. Acetone and ethanol are polar solvents, which can cause frequency shifting in toluene.

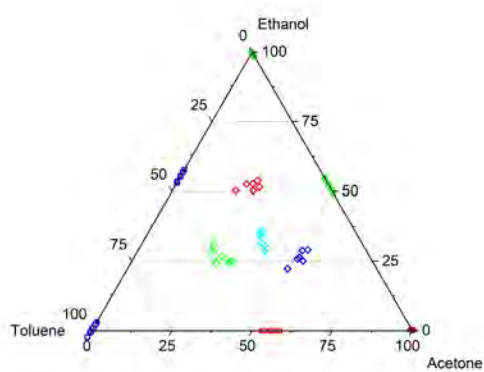
The findings from these experiment make two contributions to the validation of the proposed data treatment by using Pearson VII function to deconvolute IR



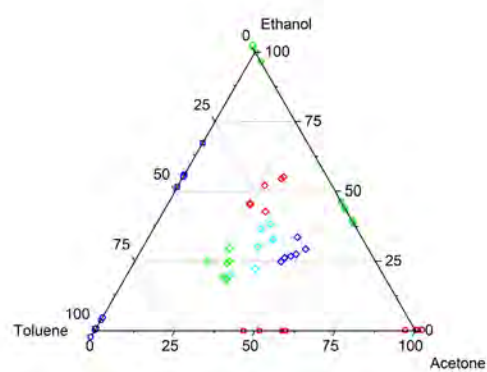
(a) Absorbance - Traditional method



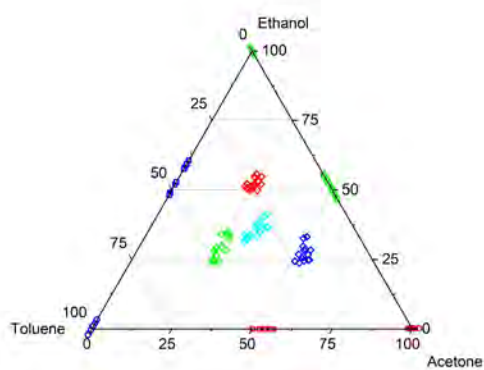
(b) Area - Traditional method



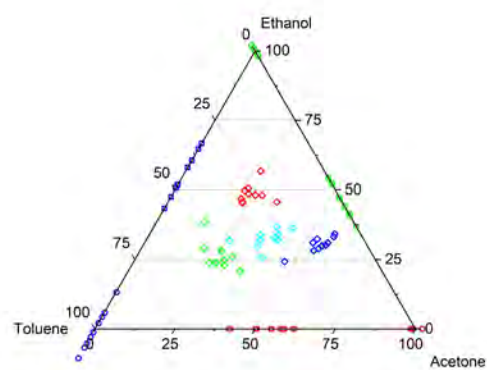
(c) Absorbance - Lorentz function



(d) Area - Lorentz function



(e) Absorbance - Pearson VII function



(f) Area - Pearson VII function

Figura 4.11: Liquid mixture absorbance (right) and areas (left) calculated by the (a and b) traditional, (c and d) Lorentz and (e and f) Pearson VII methods.

bands. First, area and absorbance of the band can be used for qualitative and quantitative infrared spectrum. Second, the deconvolution method reduces errors introduced in the spectrum by signal, baseline and overlapping issues. Secondary contributions of this experiment can be highlighted such as, the ATR-FTIR probe was successful in measuring both intensity changes with composition and frequency shifting of bands due to molecular interactions in bench.

### **4.3 Validation of the On-line FTIR Spectroscopy system**

#### **4.3.1 Composition Investigation of the non-reactive PP/PA6 Blend In-processing and Off-line**

Figure 4.14 shows the average of 12 spectra of the polymer blends at different composition collected with both, on-line ATR-FTIR system and off-line ATR-FTIR methods.

An increase of peak ratio, for absorbance and area, of amide I and II by  $1373\text{ cm}^{-1}$  with PA6 is seen in data treated with both the traditional and deconvolution methods. However, from Figure 4.15, it is clear that the linear relationships were significantly better for the data treated with the deconvolution method, with linear trends with a zero intercept clearly visible on both plots (Amide I and II). Absorbance peak ratios yielded better fits than area peak ratio. As mentioned before, the calculation of band area, regardless the method, takes into account the baseline, noises, and distortion imparted by peak shifting and overlapping. This same trend is present in the curves treated by the traditional method in Figure 4.15(a) and 4.15(d). Monsoor (2001) also has found greater precision for FTIR measurement of carboxyl group in ester samples when the peak height ratio was used relative to the peak area [133]. These results provide further support for the hypothesis that distortions on the band and having a noisy baseline in a IR spectrum may not affect the absorbance of the band at the same extent as it affects the area.

We may consider that the relationship between concentration and absorbance in attenuated total reflection sampling mode is not as simple as directly applying

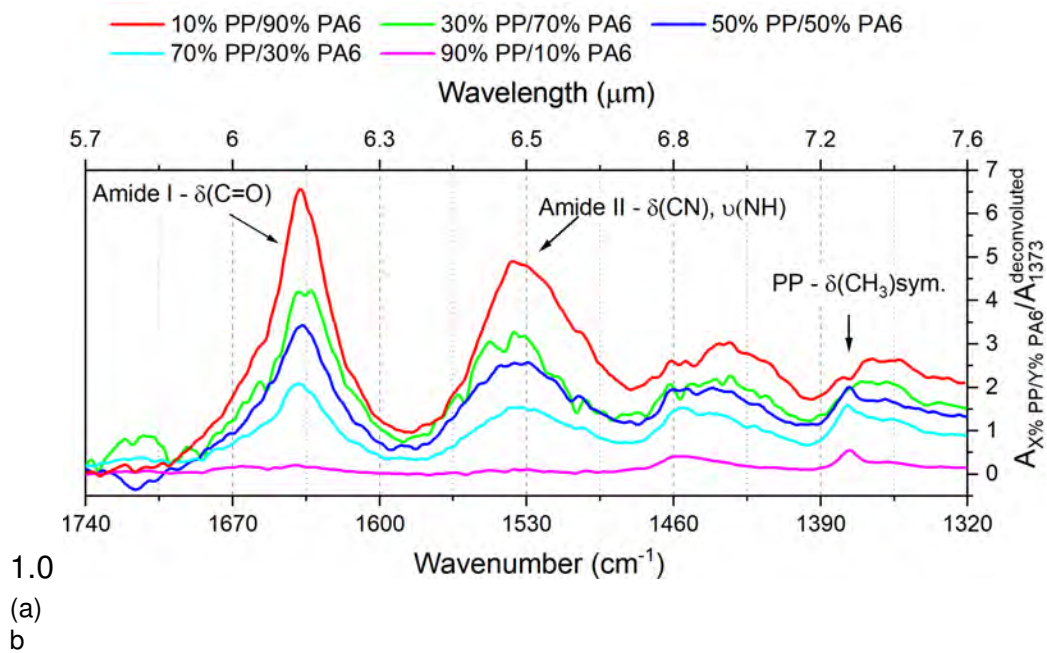


Figure 4.12: On-line ATR-FTIR spectra

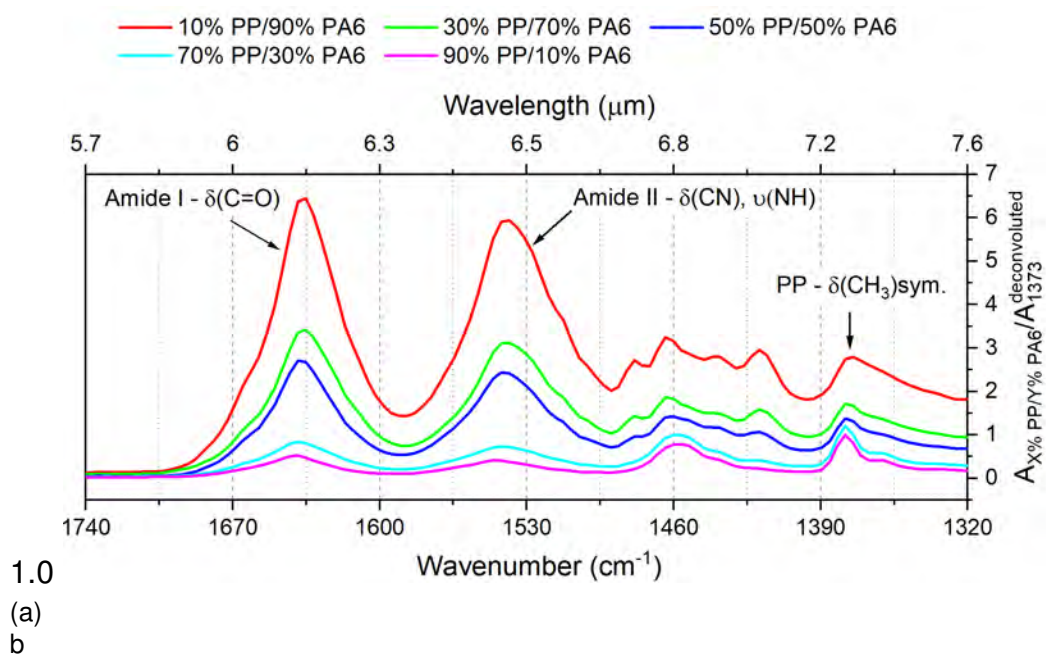
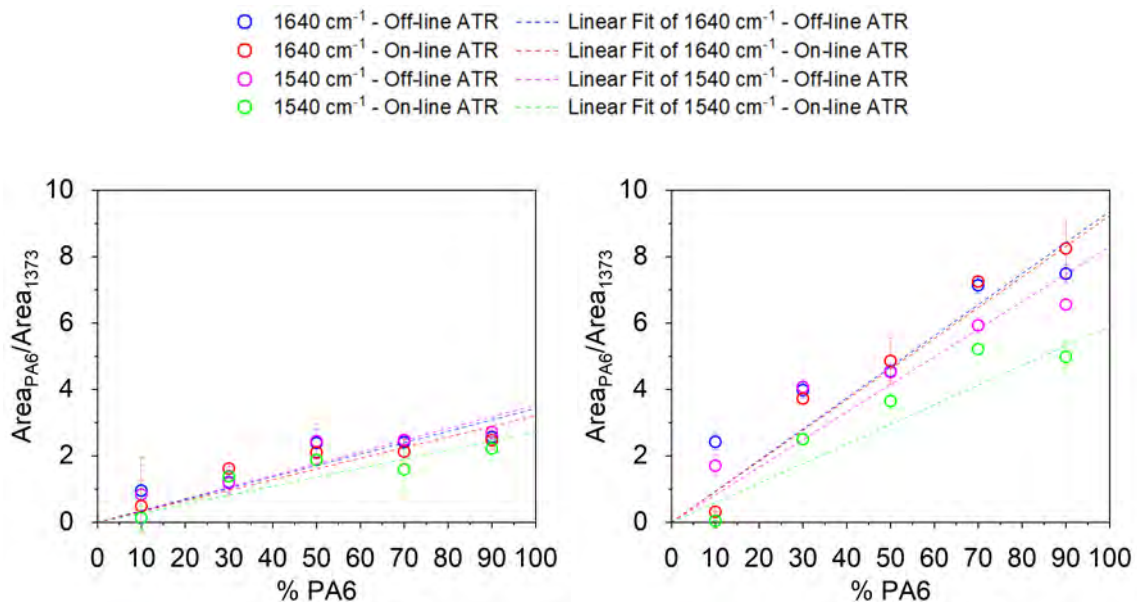


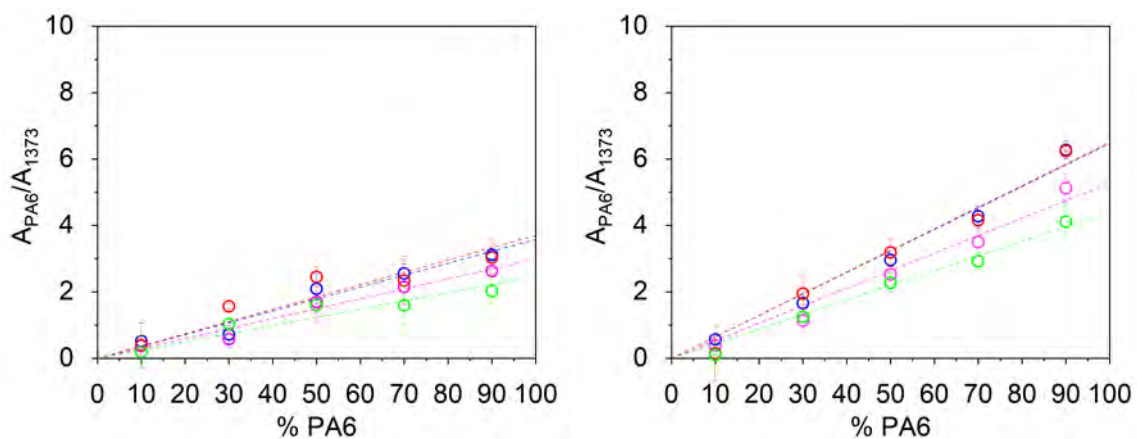
Figure 4.13: Off-line ATR-FTIR spectra

Figure 4.14: a) On-line and b) off-line ATR-FTIR spectra for blends off PP/PA6 at compositions 10/90, 30/70, 50/50, 70/30 and 90/10, respectively.





(a) Peak area calculated by the traditional method (b) Peak area calculated by the deconvoluting method



(c) Absorbance calculated by the traditional method (d) Absorbance calculated by the deconvoluting method

Figure 4.15: Peak area (top) and absorbance (bottom) for bands of amide I and II calculated by both traditional (left) and deconvoluting (right) methods. Results collected by On-line and Off-line ATR-FTIR mode are shown.



the Beer-Lambert law [109], since the path length of the light in ATR is not the thickness of the sample as it is in transmission mode. That notwithstanding, many ATR spectroscopy users use the very well known depth of penetration ( $d_p$ ) as an approximation for the path length ( $l$ ) in transmission measurements [123, 134–136]. For these reasons in this work, and for approximation purposes only,  $d_p$  was used as an estimation of the path length of the evanescent wave through the sample. Applying the Beer-Lambert's law as a function of  $\epsilon$ , which can be a constant [135], we can approximate the absorbance at  $1640\text{ cm}^{-1}$  for each polymer blend. Figure 4.16 compares the experimental data with the approximation theoretically calculated by the Beer-Lambert's law, showing that they are in good agreement.

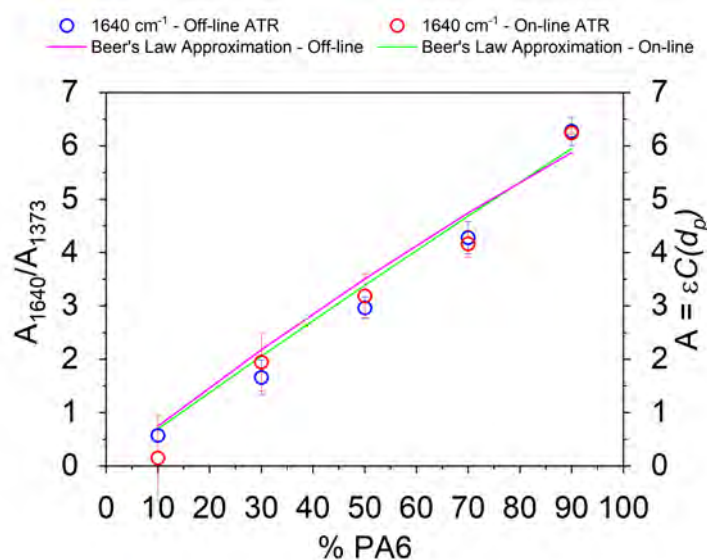
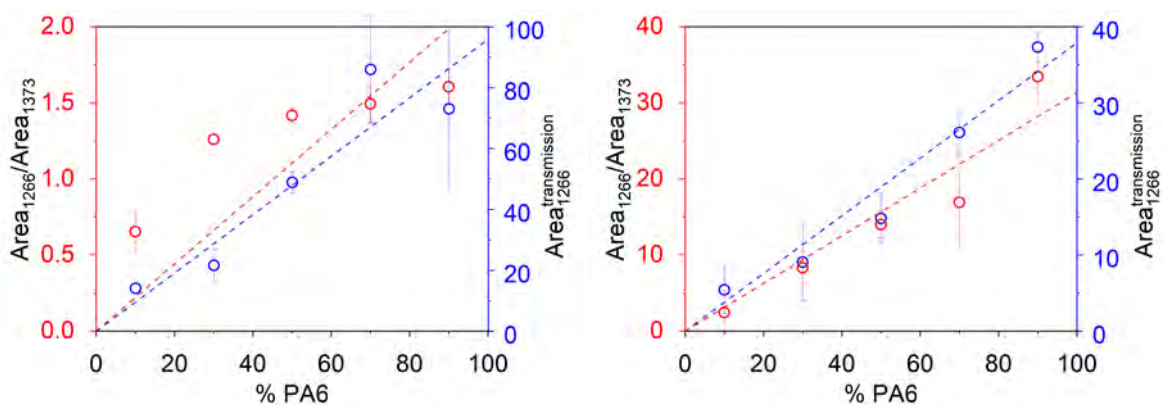


Figura 4.16: Beer-Lambert's law approximation for band of Amide I ( $1640\text{ cm}^{-1}$ ) collected by On-line and Off-line ATR-FTIR mode.

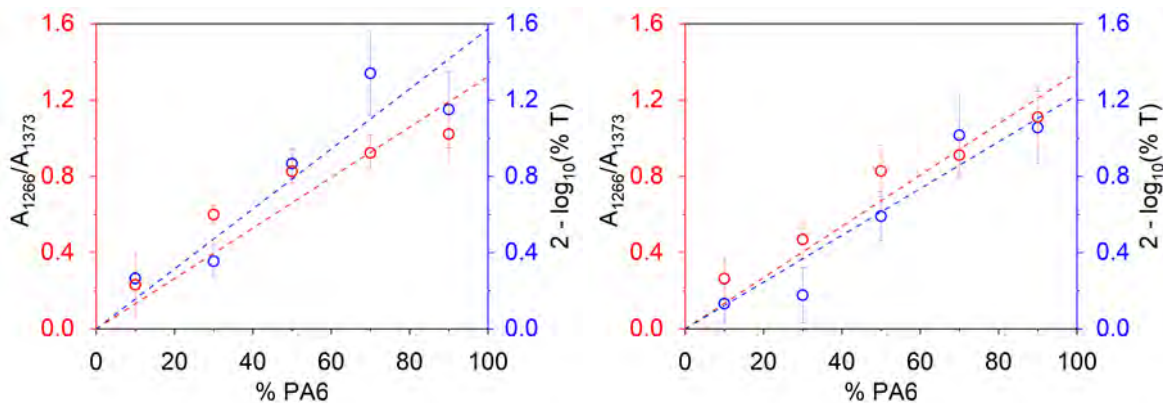
For further validation of the system, infrared spectroscopy in transmission sampling mode was used as a base of comparison. The amide III absorbance (peak height) and area of the band at  $1266\text{ cm}^{-1}$  [117] was again calculated by both the traditional and deconvolution methods, the results being shown in Figure 4.18.

Figure 4.18 shows the peak area calculated by the traditional (Figure 4.18(a)) and by the deconvolution (Figure 4.18(b)) methods. The most striking result to

○ 1266  $\text{cm}^{-1}$  - Off-line transmission      - - - Linear Fit of 1266  $\text{cm}^{-1}$  - Off-line transmission  
○ 1266  $\text{cm}^{-1}$  - On-line ATR                      - - - Linear Fit of 1266  $\text{cm}^{-1}$  - On-line ATR



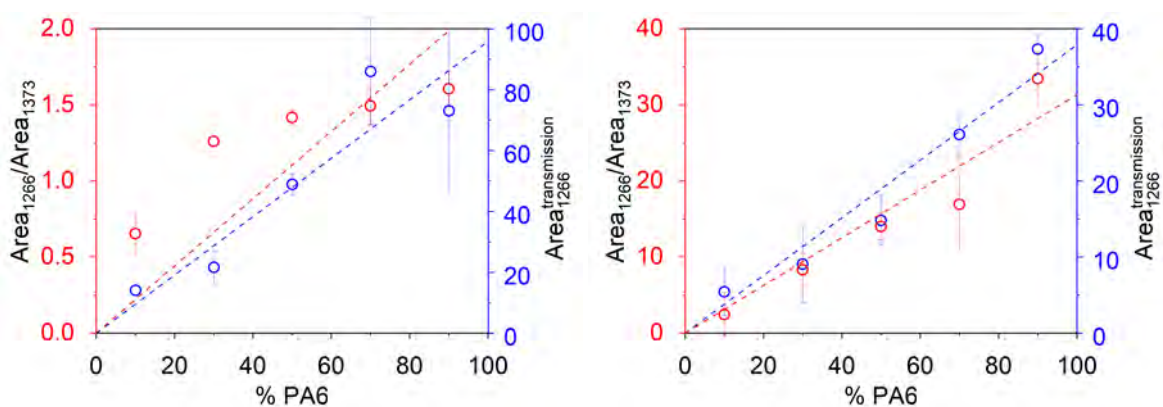
(a) Peak area calculated by the traditional method (b) Peak area calculated by the deconvoluting method



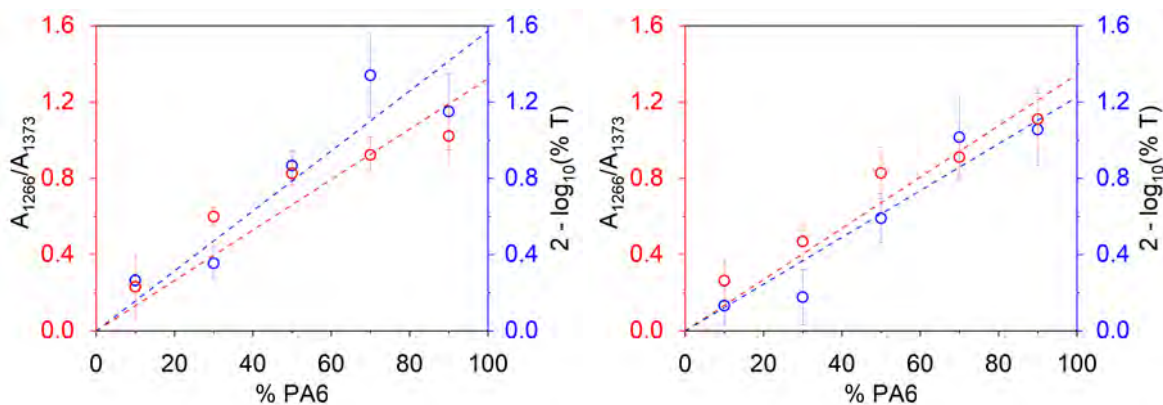
(c) Absorbance calculated by the traditional method (d) Absorbance calculated by the deconvoluting method

Figure 4.17: Peak (a and b) area and (c and d) absorbance for peaks of Amide I and II calculated by both (a and c) traditional and (b and d) deconvoluting method with Pearson VII. Results collected by On (red plot) and Off-line (blue plots) mode are shown.

○ 1266  $\text{cm}^{-1}$  - Off-line transmission      - - - Linear Fit of 1266  $\text{cm}^{-1}$  - Off-line transmission  
○ 1266  $\text{cm}^{-1}$  - On-line ATR                      - - - Linear Fit of 1266  $\text{cm}^{-1}$  - On-line ATR



(a) Peak area calculated by the traditional method (b) Peak area calculated by the deconvoluting method



(c) Absorbance calculated by the traditional method (d) Absorbance calculated by the deconvoluting method

Figure 4.18: Peak (a and b) area and (c and d) absorbance for peaks of Amide I and II calculated by both (a and c) traditional and (b and d) deconvoluting method with Pearson VII. Results collected by On (red plot) and Off-line (blue plots) mode are shown.

emerge from these plots is that the peak area calculated by the traditional method is very sensitive to the mode of analysis, on-line ATR or off-line transmission. In addition, the areas measured in off-line transmission show large errors bars. The most likely cause of this discrepancy is that the band amide III is less intense when compared to amide I and amide II, which makes it harder to distinguish from other neighboring bands by the traditional method. However, this is overcome when the deconvolution method is applied. Normally, the envelope of a band is a sum of interference of many other neighboring bands. This can cause distortion of the band and the baseline and greatly contributes to errors in the peak area calculation using the traditional method. Again, the effect is much less evident in the absorbance of the band (Figures 4.18(c) and 4.18(d)). In the current study, comparing absorbance with peak area has shown that the former is less prone to be affected from external sources of errors in the spectra than the latter. Figure 4.18 clearly illustrates this observation. The application of the deconvolution method in the peak height calculation improve the linear fit. These results are consistent with data previously shown in Figure 4.11.

Table 4.1 shows the adjusted R-square calculated in OriginLab and its percent (%) improvement. When the deconvolution method is applied one can achieve an improvement of the R-square up to 18% compared to the traditional method.

This observation supports the hypothesis that analyzing infrared spectral data of superimposed bands is more accurate when done by applying the deconvoluted peak height method, as is the case here. This is mainly due to the fact that the deconvolution method has a positive impact on the IR bands that are overlapping one another, not having much improvement in isolated bands or in bands with a good baseline. In these latter cases, the application of the traditional method would lead to faster results with little to no loss in the accuracy. For complex mixtures, like polymer blends, calibration for quantitative analysis with ATR infrared spectroscopy must be based on transmission measurements [136]. From the absorbance, which is acquired from the transmittance spectra, a calibration curve for the absorptivity ( $\epsilon$ ) can be built using the Beer-Lambert law. Chen et al. (1998) have based the calibration for quantitative ATR analysis on transmission measu-

Tabela 4.1: Characteristic bands of all materials used in this work and their relative mode of vibration.

ATR-FTIR sampling mode	Traditional method		Deconvoluting method		Improvement (%)	
	Absorbance	Area	Absorbance	Area	Absorbance	Area
1640 cm <sup>-1</sup> Amide I - $\nu(\text{C}=\text{O})$						
Off-line	0.95	0.85	0.99	0.95	3.7	12.2
On-line	0.8	0.84	0.99	0.96	11.5	14.9
1540 cm <sup>-1</sup> Amide II - $\delta(\text{CN}), \nu(\text{NH})$						
Off-line	0.96	0.87	0.99	0.94	2.8	7.7
On-line	0.89	0.76	0.99	0.89	11.2	17.4
1266 cm <sup>-1</sup> Amide III - $\nu(\text{CN}), \delta(\text{CNH})$ in-place, $\nu(\text{CH}_3\text{-C})$						
Transmission	0.84	0.85	0.98	0.98	16.3	16.0
On-line	0.91	0.81	0.97	0.96	6.0	18.2

rements in polymer blends [136]. In this paper, the absorptivity calculated by Beer-Lambert's law using the off-line transmission sampling mode data was used to build an approximation of the on-line ATR mode. What can be clearly seen in the plots in Figure 4.19 is the small variability, within the experimental error, of the three sets of data, namely, on-line ATR, off-line transmission and Beer-Lambert's law calibration curve.

According to this data, it is possible to infer that the proposed on-line FTIR system was successful in the analysis of polymer blends in various composition and in-processing. The on-line system showed to have a good accuracy when compared to off-line modes of analyses, either attenuated total reflection or transmission modes.

#### 4.3.2 On-line FTIR analysis of REX (PP-g-AA/PA6) measured along the Extruder Barrel

Figure 4.20 represent the data treatment of IR band deconvolution using Pearson VII for the polymer blend of PP-g-AA/PA6. The method (Pearson VII) was applied for all blend spectra and the area and absorbance of amide I, amide II

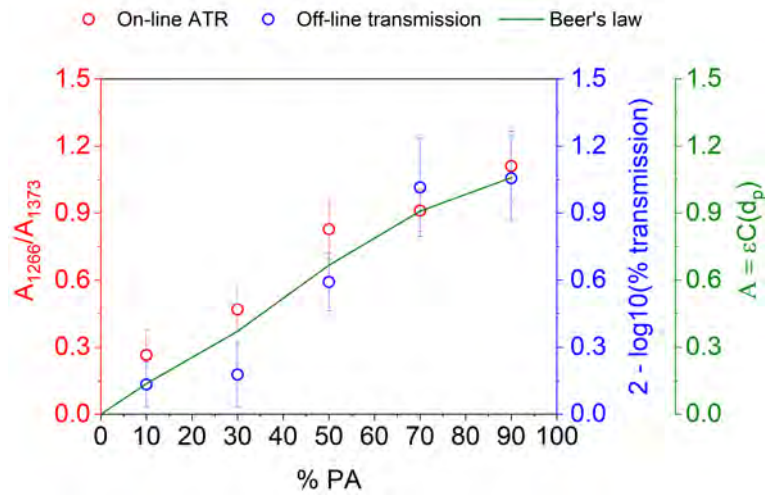


Figure 4.19: Beer-Lambert's law approximation for band of Amide III ( $1266 \text{ cm}^{-1}$ ).

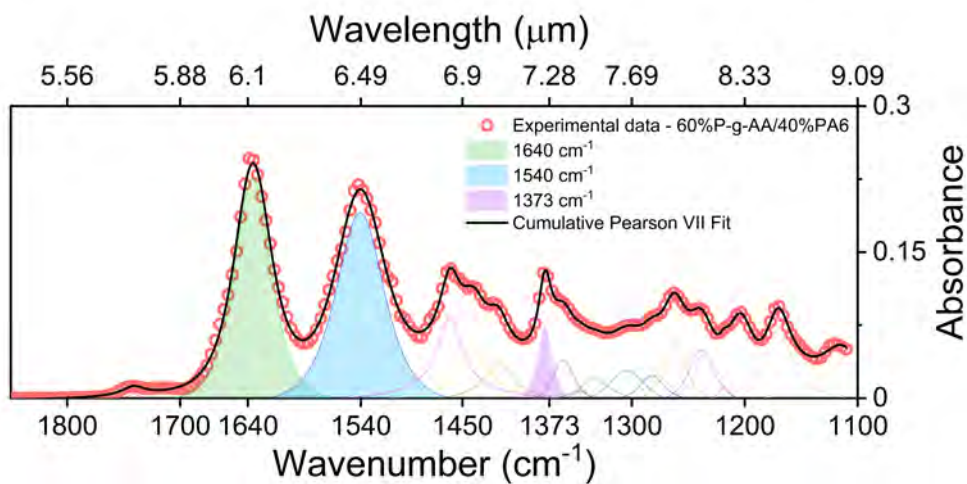


Figure 4.20: Spectrum of blend of 40/60 (wt/wt%) PP-g-AA and PA6. The band deconvolution method is applied. Bands of amide I, amide II and at  $1373 \text{ cm}^{-1}$  are highlighted.

and the band at  $1373\text{ cm}^{-1}$  (PP) were calculated.

Figure 4.21 presents the results obtained from the on-line FTIR analysis, measured at various ports, along the extruder barrel. Amide I ( $1640\text{ cm}^{-1}$ ) and Amide II ( $1540\text{ cm}^{-1}$ ) peak absorbances and areas normalized by the PP band at  $1373\text{ cm}^{-1}$  of the reactive (PP-g-AA/PA6) and non-reactive (PP/PA6) blends were used to quantify the evolution kinetics of the reaction in the extruder.

The on-line ATR-FTIR measurements show that the peak absorbance and area for both Amide I and II are the same for the reactive and non-reactive blend in the first location of  $L/D = 20.25$ . From  $L/D = 30.25$  onwards, the peak absorbance and area of the reactive blend increases, whereas for the non-reactive blend remains constant. This increase is due to the reaction between the acrylic acid of the PP grafted copolymer and the amine end group present at the end of PA6 chain. This compatibilization reaction produces a PP grafted Amide diblock copolymer, which acts as compatibilizer for the PP/PA6 blend [4, 5, 12], increasing the content of amide groups, which is quantified on-line by both FTIR bands. From the curves, it is possible to infer that the reaction takes place mainly between  $20 < L/D < 30$ , which corresponds to the first mixing zone of the screw used for this extrusion run and also where most of the melting occurs. It can also be seen that there is a significant difference in the standard deviation of the results of the reactive and non-reactive blends, it being up to 44% higher for the latter. The reason could be due to the more homogeneous blend morphology induced by the presence of the newly formed PP/PA6 compatibilizer, which reduces the interface tension between the two phases (PP and PA6) thus resulting in a finer morphology in the reactive compatibilized blend. FTIR measurements are sensitive to the homogeneity of the material, imparting greater data variability (error bars) for the non-reactive blend morphology.

#### **4.4 Reactive Blending Investigation**

##### **4.4.1 Reactive Extrusion of 80/20 (wt/wt%) of PA6/PP-g-AA and PA6/PP**

In this section, the influence of process conditions on IR characteristic absorption bands during REX (reactive blending) of the blend of 80% of PA6 and 20% of PP-g-AA, for the reactive blend, and 80% of PA6 and 20% of PP for the non-



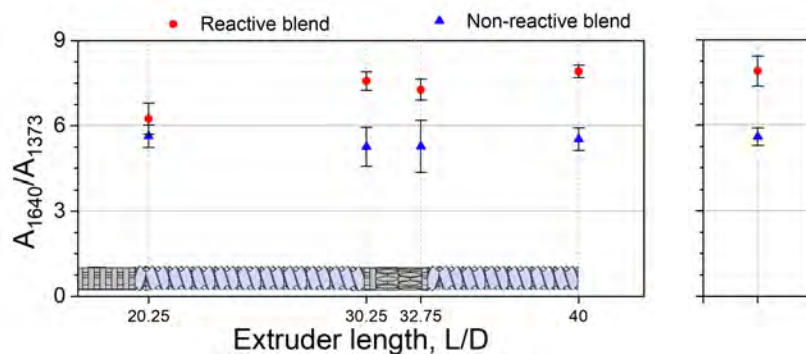
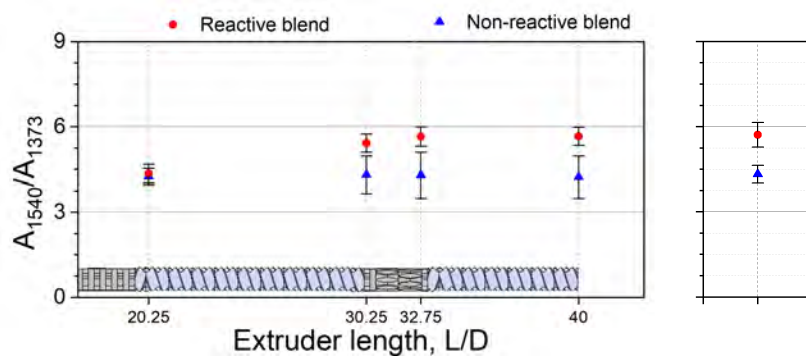
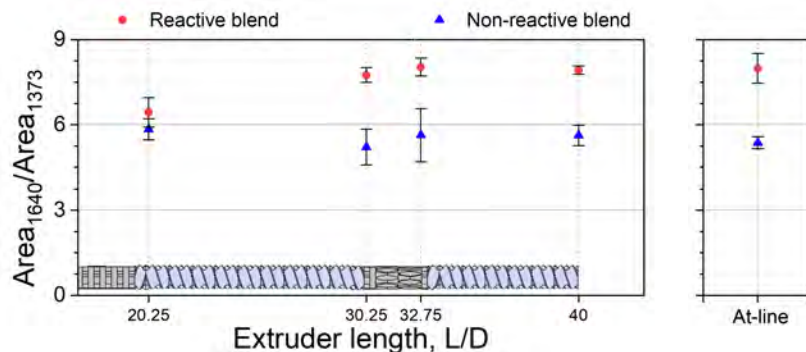
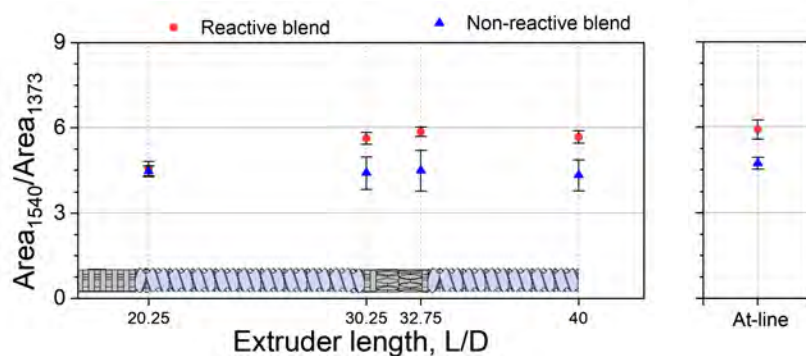
(a) Absorbance of Amide I normalized by  $1373\text{ cm}^{-1}$ (b) Absorbance of Amide II normalized by  $1373\text{ cm}^{-1}$ (c) Area of Amide I normalized by  $1373\text{ cm}^{-1}$ (d) Area of Amide II normalized by  $1373\text{ cm}^{-1}$ 

Figure 4.21: Peak absorbances (a and b) and areas (c and d) of Amide I ( $1640\text{ cm}^{-1}$ ) and Amide II ( $1540\text{ cm}^{-1}$ ) normalized by the band at  $1373\text{ cm}^{-1}$  (PP) along the extruder barrel and at line after the die for reactive (PP-g-AA/PA6) and non-reactive (PP/PA6) blends. The screw profile used in the extrusion is shown in the plot.



reactive blend. This composition was chosen in order to have all the AA grafted with PP used in the reaction with amine end group in PA6. First, experiment 1 (shown in the infogram in Figure 3.1) was performed using different mixing zones in the screw profile (configuration). The expected results of this experiment is the increase of interfacial area by breaking up the droplets of the second phase due to the aggressiveness of mixing of the different screw profile utilized. The experiment 2 (also shown in the infogram in Figure 3.1) was performed varying the parameters of processing of feed rate and screw speed. In this experiment the effect of the variation of shear (due to higher screw speed), location of melting (due to variation of feed rate) and degree of filling were responsible to increase the area ratio of the FTIR results.

All the process parameters for each process condition are gathered for easier comparison on the Table 3.6.

#### *Experiment 1: Screw Configuration*

In the first set of experiments, the development of the reaction has been studied at different mixing degree of the screw profile. The screw profile has been changed by replacing the mixing zone from a very mild (KB30) to a very aggressive (EME S4), and intermediate aggressiveness (KB90 and EME L2) screw blocks. The aggressiveness is relative to the dispersive mixing provided by the elements [1, 35, 48]. All other processing parameters have been kept constant, especially the set temperature which always remained 230C for all zones in the extruder.

The area ratio of bands of Amide I ( $1640\text{ cm}^{-1}$ ) and PP ( $1373\text{ cm}^{-1}$ ) were used to determine the amount of reaction between acrylic acid and the terminal amine group at PA6 chain. From the previous experiment (see Figure 4.21), one can see that the area ratios present a larger difference between reactive and non-reactive blends when compared to absorbance ratio, which might be related to the order of magnitude of the areas under the curve being higher than the absorbance. Thus, because of that the area ratio will be used from now on instead absorbance ratios. The bands at  $1640\text{ cm}^{-1}$ , is relative to  $\nu(\text{C}=\text{H})$  of PA6 and at  $1373\text{ cm}^{-1}$  due to  $\delta(\text{CH}_3)_{\text{sym.}}$ ,  $\omega(\text{CH}_2)$ ,  $(\text{CH})$ ,  $\nu(\text{CC}_b)$  in PP chain. These bands were chosen

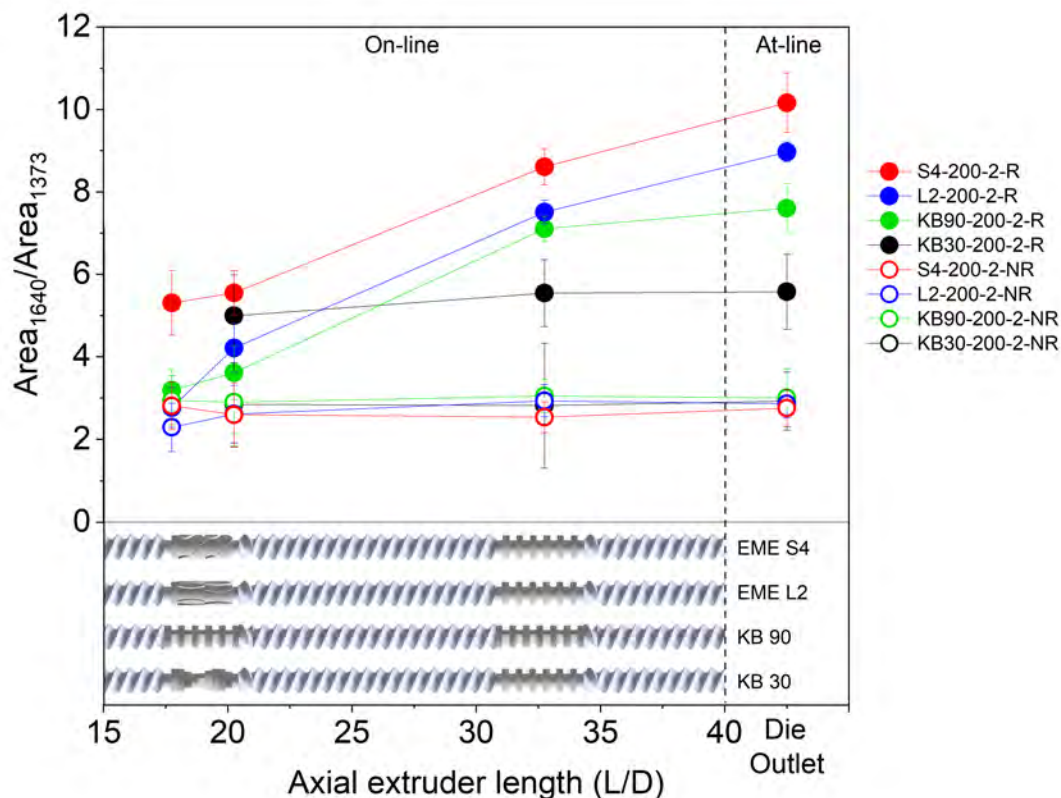


Figure 4.22: Band area ratio ( $\text{Area}_{1640}/\text{Area}_{1373}$ ) development in the axial extruder length (L/D) for reactive and non-reactive blends processed with different screw profiles for both, non-reactive (open circles) and reactive (closed circles) blends.

because they are relatively strong and do not overlap with any other very intense band in the IR spectrum of the blend [118, 137]. The reaction between the -OH of the acrylic acid and -N-H (amine group) termination in the PA6 chain yields to a di-block copolymer with amide functional group  $\text{RC}(=\text{O})\text{NRR}$ , where R, R', and R represent PP, PA6 chains or hydrogen atoms [5, 12, 111].

Figure 4.22 shows the band area ratio ( $\text{Area}_{1640}/\text{Area}_{1373}$ ) as a function of the axial length (L/D) of the extruder for all the screw profiles used in this work. The graph shows  $\text{Area}_{1640}/\text{Area}_{1373}$  calculated from the FTIR spectra collected with the on-line FTIR system at the L/D positions 17.75, 20.25, 30.25. At-line measurements were made after the die outlet for all the screw profiles. For the KB30 screw profile (Figure 3.8a) the measurements were made only after the mixing zone at 20.25, 30.25 and after at the die; position 17.75 L/D does not allow mea-

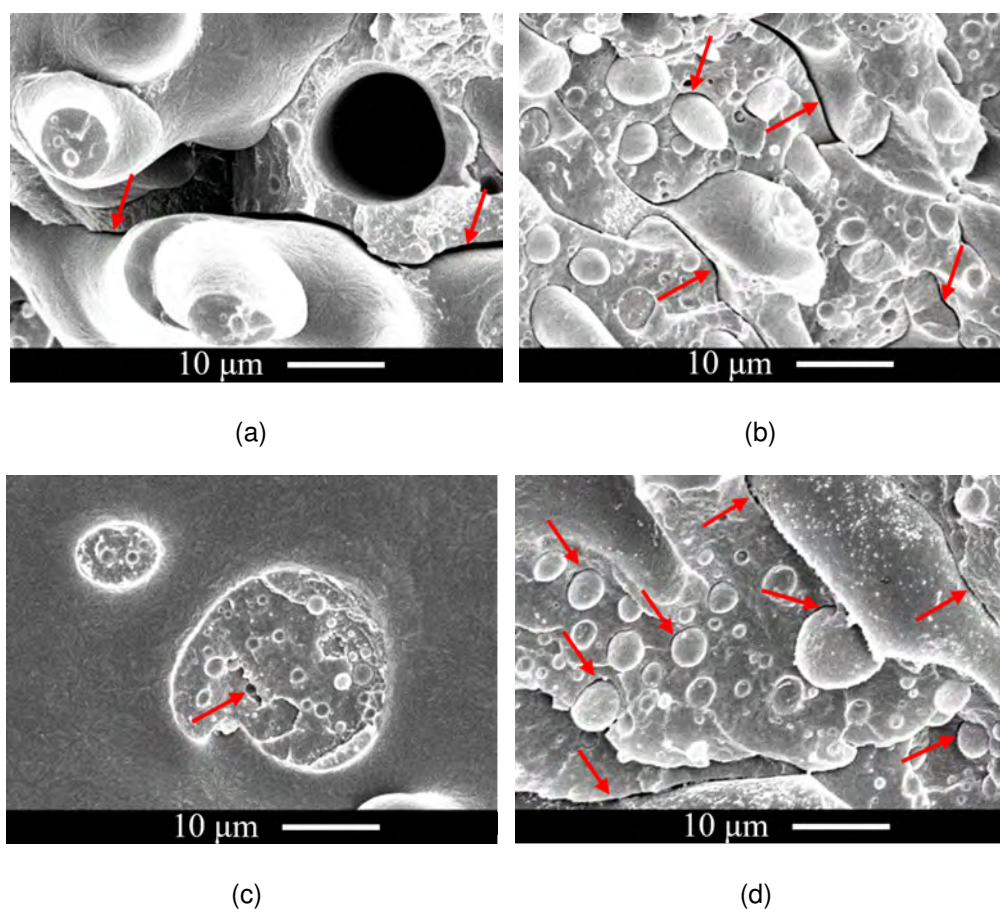


Figure 4.23: SEM micrographs for condition S4-200-2-NR at a) 17.75, b) 20.25, C) 32.75 L/D and d) after passing through the die. In the legend all the bar scales correspond to 10  $\mu\text{m}$ . The red arrows indicate the weak adhesion at the interface between the two phases.

surement because the mixing zone with kneading blocks staggered at 30 does not build enough pressure in the screw in order to withdraw polymer melt, preventing the on-line measurement.

It can be seen from the curves in Figure 4.22 that  $\text{Area}_{1640}/\text{Area}_{1373}$  ratios of the non-reactive blend (open circles) do not change along the axial length, regardless of the screw profile used. This outcome was anticipated because no reaction was expected to happen in the non-reactive blend. This means that the amount of amide functional group in the blend does not alter along the whole screw length during extrusion, independently of the aggressiveness of the mixing element used.

Figure 4.23 shows the development of the morphology along the extruder bar-

rel for condition S4-200-2-NR, chosen because it is the most aggressive amongst the non-reactive blend conditions; consequently, it is expected to have a higher impact on the morphology of the blend. From the micrographs it is possible to see that the morphology is modified through the screw. Figure 4.23a shows the blend morphology before the extensional mixing element (EME S4). By this SEM micrograph at 17.75 L/D we can see that the morphology is coarse and very heterogeneous. The average particle area is  $112.8 \mu\text{m}^2$  with a standard deviation of 72.2. This average was calculated from 300 particles of the second phase (PA6) in the polymer blend shown in SEM (Figure 4.23). Large particles that are poorly dispersed can be seen in the matrix. At 20.25 L/D, when the material has already passed through the mixing zone, the morphology is finer (Figure 4.23b) presenting smaller particles. The average particles area has decreased immensely to  $13.3 \mu\text{m}^2 \pm 1.4$ . This indicates that the particles were broken up into smaller ones because of the extensional flow introduced by the mixing zone [1, 35, 48, 50]. As shown in Figure 4.23, at 20.25 the distribution of particles is better than at 17.75 L/D. Figure 3c shows the blend at 32.75 L/D. The morphology at 32.75 L/D depicts large particles of PP with inclusions of PA6 [137]. The coarse morphology in Figure 4.23c is the result of particle coalescence during the conveying of the blend through the screw and by the shear-dominated flow imparted by kneading blocks staggered at 90 (see Figure 3.8). Yielding to an average particle area of  $336.4 \mu\text{m}^2 \pm 92.5$ . This coalescence is only possible because of the weak interaction between the two phases, which means the phase separation is favorable due to the lack of the di-block copolymer stabilizing the interface of the blend. As a result of this circumstance, the particle size increases [107]. This happens because the evolution of the morphology during the process involves a competing process between droplets stretching, break up and coalescence [138]. The last morphology depicted in Figure 4.23d shows a finer structure with an average particle area of  $12.1 \mu\text{m}^2 \pm 3.9$ , which can be caused by the increase of pressure and shear at the die outlet. The finer morphology is a result of a high pressure and elongation stresses built at the die that can break the particles up. From Figure 4.23 it is clearly observable that there is poor adhesion at the interface between layers

and particles (indicated by red arrows), which confirms the incompatibility of the two phases. Here, can be seen by the SEM micrographs, the blend of PA6 and PP in the proportion of 80 and 20%, respectively, forms a complex morphology. The morphology can have some continuous structure aspect in some locations of the sample. This structure makes the particle size distribution investigation more difficult for non-reactive blends.

Although the morphology alters during extrusion throughout the extruder length, the band area ratio does not change for the non-reactive blend. As obvious as it may be, it is important to state that these results indicate that the band area ratios appeared to be unaffected by the morphology created by the screw profile, since some authors have claimed that attenuated total reflection infrared spectroscopy can indirectly evaluate the state of the homogeneity of mixtures [139]. Yoshida and co-authors have stated that mixture of epoxy resin and the hardener efficiency can be detected by ATR-FTIR when they varied the time of mixing [139]. This is due to the fact that, specifically for ATR technique, one of the mixture phases can occupy the majority of the surface area of the ATR crystal than the other phase during one measurement. When several measurements are made, this inconsistency can affect result accuracy, which can lead to high error bars due to the broad range of results. In the present work the morphology does not affect the band area ratio. This is because the relationship between the particle size in the blend (no larger than  $20 \mu\text{m}$ , see Figures 4.23 and 4.24) and the operational measuring surface area ( $7.10 \text{ mm}^2$ ) of the ATR crystal is very large. Consequently, the heterogeneity of the size of the particles cannot be detected by the FTIR measurements. This demonstrates that any increase and/or decrease in the band area ratios in the reactive blend system will not depend on the morphology itself, but on the conversion of the compatibilization reaction. It also highlights the importance of the continuous creation of fresh interface in order for the reaction conversion to keep proceeding.

In what concerns the reactive blends, the band area ratios have a significant difference along the extruder length, shown at condition KB30-200-2-R, KB90-200-2-R, L2-200-2-R and S4-200-2-R (Figure 4.22). This reflects the increase of

the amount of amide functional groups by the reaction in the blend, which affects the band area ratio intensity. The amount of the reaction which here is translated by the band area ratio, increases along the extruder length, regardless of the screw profile. In addition, there was a significant difference between the four conditions or screw profiles. The most interesting aspect of this graph is that the area ratios are higher when the aggressiveness of the condition is increased. Condition S4-200-2-R has the highest band area ratio throughout all of the axial lengths, followed by L2-200-2-R, KB90-200-2-R and KB30-200-2-R. Interestingly, the difference of chemical reaction (translated by the area ratio) at the first location of on-line measured can be a indication of the higher pressure in the screw equipped with EME S4 (red curve in Figure 4.22).

Chemical reactions of immiscible blends compatibilization normally happen at the interface of the two polymer phases. The interactions between the two reagents (-OH and -NH) are directly related to the amount of reaction during the process. The distributive and dispersive mixing degree imparted by the screw profile can vary significantly the morphology of the second phase (droplets) in a polymer blend. Therefore, the interfacial area between the phases also varies. Conditions S4-200-2-R and L2-200-2-R rely upon extensional mixing elements (EMEs), whereas KB90-200-2-R and KB30-200-2-R have only kneading elements. Extensional-dominated flows are known to be more effective in droplet breakup compared to shear-dominated flow, which means better dispersive mixing is expected [48]. The interfacial area in extensional flow scales exponentially with strain, while it does so linearly in shear flows. Breaking droplets up is more prone to happen when stress is being applied in the flow rather than deformation [50]. This makes the conditions S4-200-2-R and L2-200-2-R more effective in droplet breakup, creating a finer morphology and increasing the interfacial area. Thus, leading to a higher amount of chemical reaction. On the other hand, as shown in the literature, kneading blocks can only achieve dispersive mixing to a relatively low extent. This is because the flow provided by the kneading blocks are mainly shear-dominated, which leads to an efficiently distributive mixing in the melt, but not a high dispersed morphology [48, 50]. The higher amount of the

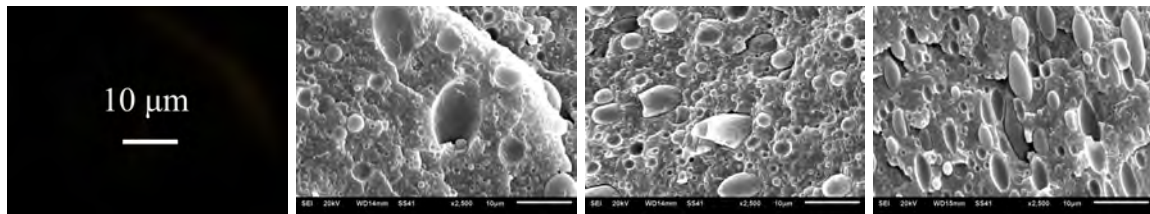
reaction in condition KB90-200-2-R compared to the condition KB30-200-2-R is due to the fact that a larger staggering angle between the kneading blocks causes a reduction of the conveying action of the polymer melt. Consequently, the mixing performance is improved. The particular reason for this circumstance is the generation of more leakage streams and the increase of the residence time [140].

Structurally, the differences in the design of EME L2 and EME S4 used in the condition L2-200-2-R and S4-200-2-R, respectively, are not only in the contraction ratio but the length of the converging-diverging channels. When shortening the length of the channel the number of extension cycles increases. Both higher contraction ratio and shorter channel length, increase the strain rates, which in turn increases the aggressiveness of the profile. Furthermore, higher contraction ratios increase the pressure drop. According to Manas et al., the mixing index increases with pressure drop [141]. This provides a more dispersive mixing character for the screw profile with higher contraction ratios. For all of these reasons, EME S4 is more aggressive than EME L2, leading to better dispersive mixing, while creating more interface area between the two polymer phases. This can increase the possibilities of reagent interaction, enhancing the chemical reaction for S4-200-2-R compared to L2-200-2-R.

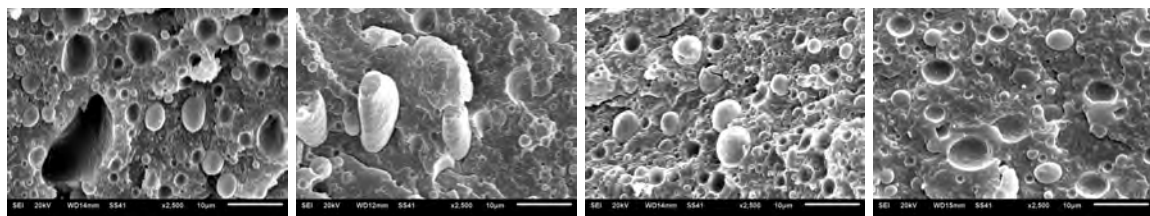
Figure 4.24 shows the SEM micrographs of all the reactive PA6/PP-g-AA blends for conditions KB30-200-2-R, KB90-200-2-R, L2-200-2-R and S4-200-2-R at different locations along the screw. Each image is shown as a representative sample collected for each condition at L/D locations 17.75, 20.25, 30.25 and at the die, from left to right. In general, the distribution and dispersion of the PP phase was improved from the least aggressive (KB30-200-2-R) to the most aggressive condition (S4-200-2-R). The improvement of the morphology, i.e., size reduction [2, 16, 110], is related to the dispersive mixing imparted by the screw profile. S4-200-2-R condition morphology was the finest over all the other conditions, followed by L2-200-2-R, KB90-200-2-R and KB30-200-2-R.

Publications that concentrate on particle size distribution investigation frequently adopt the concept of cumulative cross section particle area, or simply

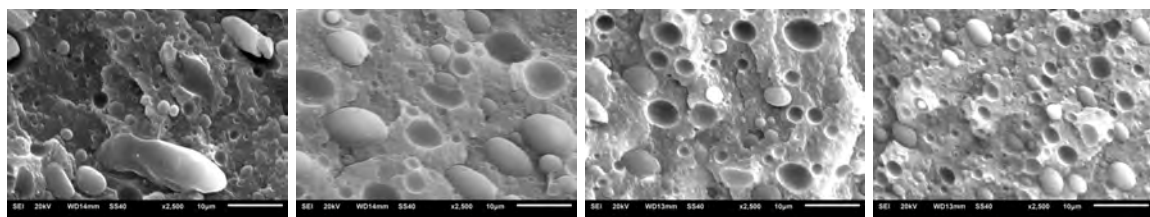




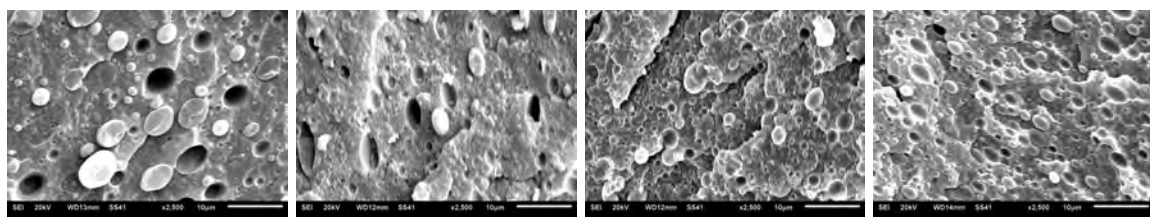
(a) KB30-200-2-R



(b) KB90-200-2-R



(c) L2-200-2-R



(d) S4-200-2-R

Figura 4.24: SEM micrographs for conditions a) KB30-200-2-R, b) KB90-200-2-R, c) L2-200-2-R and d) S4-200-2-R at 17.75, 20.25, 30.25 and at the die out let, respectively from the left to the right. In the legend all bar scales correspond to 10  $\mu\text{m}$ .



Cumulative Ratio Distribution (CAR) in order to apply statistical analysis [45, 48–50, 124]. We used the same methodology applied by Chen (2020) to calculate the CAR of the blends, processed in the four different conditions, through the SEM micrographs [48]. Figure 4.25 depicts the CAR at the die for the 4 screw profiles. The CAR plots for each screw configuration at all the locations along the extruder are depicted in Figure 4.26.

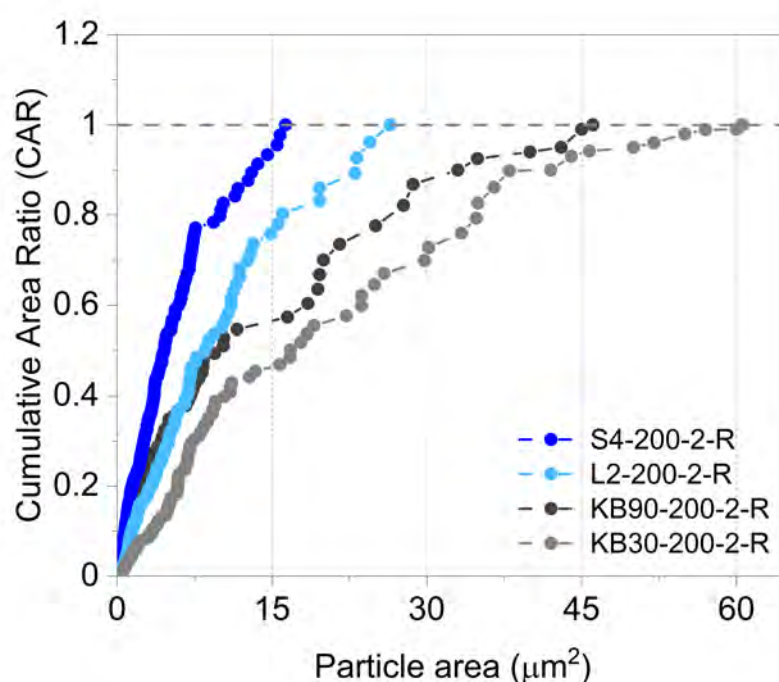


Figura 4.25: Cumulative area ratio (CAR) for conditions KB30-200-2-R, KB90-200-2-R, L2-200-2-R and S4-200-2-R at the die of the extruder.

The curves in Figure 4.26 show that the distribution of the particles vary according to the condition and location along the extruder barrel. Not surprisingly, the screws with higher dispersive mixing power have the finest morphology and a higher chemical reaction. This is a consequence of the screw greater efficiency in generating a fresh interfacial area, allowing more interactions between the reagents (-NH group in PA6 chain ends and the acrylic acid group AA in the PP graft copolymer). The graph in Figure 4.25 shows that there has been a marked rise in the CAR curve with the increase of aggressiveness of the processing condition. This means a better dispersion of PP in the PA6 matrix in conditions S4-200-2-

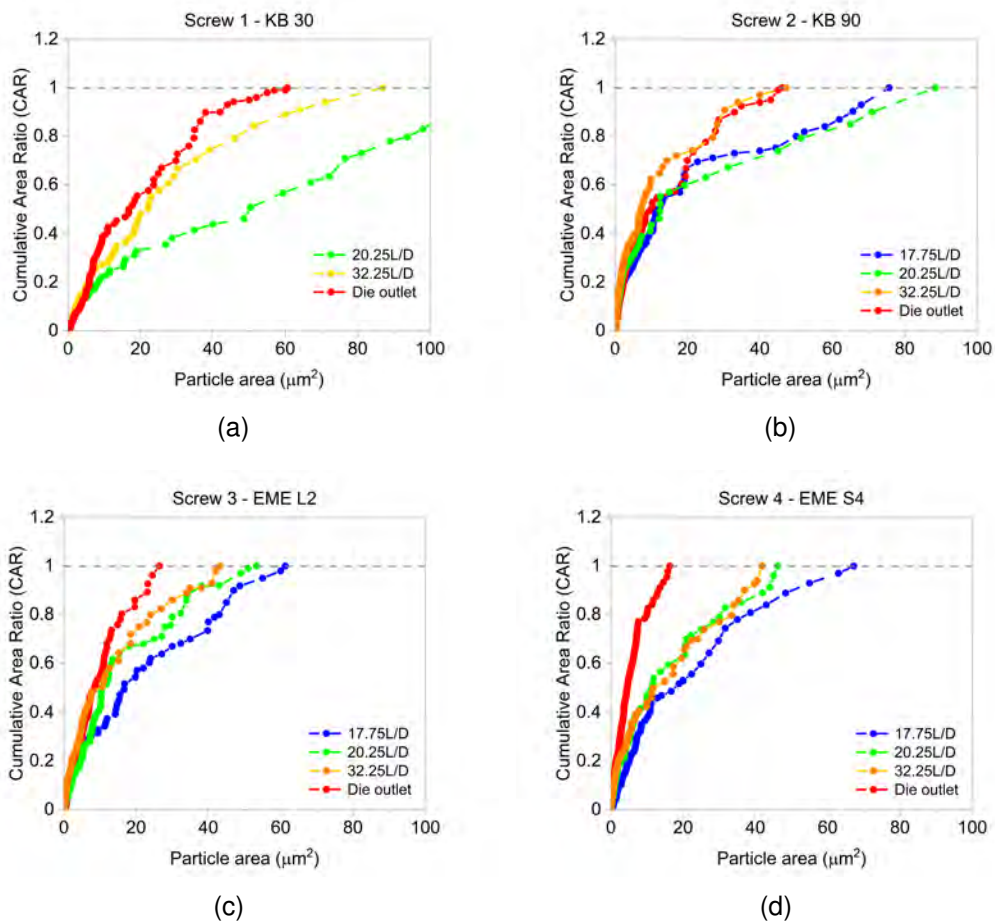


Figura 4.26: Cumulative area ratio (CAR) for conditions a) KB30-200-2-R, b) KB90-200-2-R, c) L2-200-2-R and d) S4-200-2-R.

R, followed by L2-200-2-R, KB90-200-2-R and KB30-200-2-R, by increasing the interfacial area between the two phases.

The great insight that can get from the on-line FTIR measurements is the development of the reaction along the barrel. Knowing the level of the reaction at different location along the extruder is important for extrusion process due to the fact that downstream material feeding is a common practice, specially for addition of composite fillers and dye. These composite fillers and dye need, depending on the material, to be added in a matrix that is completed reacted. On-line FTIR provides the ability to confirm where along the barrel the polymer melt has completed the reaction in REX. On the other extreme, reactive fillers in nanocomposites need to be added into the polymer melt while the reaction has still not finished [142]. For example, in the reactive extrusion of poly (lactic acid)/amidated graphene oxide (PLA/AGO) nanocomposites, the polymerization of PLA needs to be completed along the extruder in order to add AGO [143]. In the work by Zheng et al. (2019), the author performed the polymerization of PLA to produce PLA during extrusion, then in a second extrusion run they added AGO (amidated graphene oxide). The investigation of the polymerization of PLA along the barrel would be useful to know at which location along the extruder the polymerization would be completed and then, AGO can be added at that location without the necessity for a second extrusion run.

#### *Experiment 2: Feed Rate and Screw Speed Effect on IR Absorption Band*

Figure 4.27 compares the band area ratio ( $\text{Area}_{1640}/\text{Area}_{1373}$ ) development along the axial length of the extruder when the process parameters are changed. Feed rate, or flow rate, and the screw rotation speed were varied according to Table 3.2 using the screw profile #4 (see Figure 3.9). The feed rate and screw speed were varied in order to investigate their effect on the reaction. The first thing that can be seen from the curves are that all the conditions have an increase on the area ratio along the length of the extruder. This indicates that the reaction between acrylic acid and the amine end group is being carried out during the process. Additionally, the reaction development profile along the barrel increases at different rates depending on the process parameters used in the conditions. In

Figure 4.27 it seems that the plot is divided into two groups of curves, depending on throughput. Clearly, increasing throughput from 2 kg/h to 5 kg/h increases the area ratio, i.e., the extent of the reaction, significantly. This is due to the fact that when there is a higher feed rate the melting of the material occurs earlier [140], which leads to the anticipation of the onset of the compatibilization reaction [144]. Similarly, increasing the screw speed, i.e., the shear and extension rates, leads to a higher area ratio in both groups of curves.

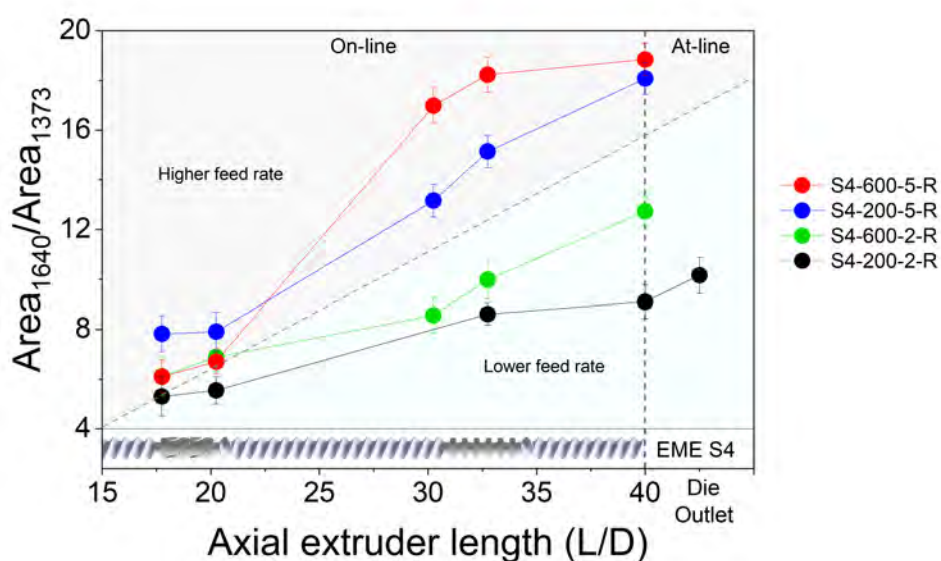


Figura 4.27: IR absorption band area ratio  $\text{Area}_{1640}/\text{Area}_{1373}$  as a function of axial extruder length (L/D) for reactive blend PA6/PP-g-AA blends at processing conditions S4-200-2-R, S4-600-2-R, S4-200-5-R and S4-600-5-R.

In addition to the chemical reaction of compatibilization (AA grafted in PP and PA6), the reactive extrusion of the blend of 80%PA6/20%PP-g-AA involves several physical processes. These physical processes include a complex conveying of material, melting of both polymer phases, self-assembly of ungrafted and grafted AA and migration of the newly formed block copolymer with grafted PA6 chains onto a PP chain PP-g-PA6 to the PP/PA6 interface [137]. All these physical processes can be varied during extrusion and they are dependent on the process condition (type and content of reactive groups, temperature, shear level and type) and the residence time imparted by each condition [66].

In terms of mixing, the same screw profile was used for all the conditions in this second set of experiments. However, the aggressiveness in terms of mixing power is not only relative to the screw configuration, it is also dependent to the process parameters used, i.e., screw speed and feed rate [145, 146]. The feed rate and screw speed together can be associated with the amount of material that is filling the screw channels. Twin-screw extruders work in starve-fed mode, as opposed to single-screw ones, which means that the screw channel is never completely full of polymer melt. Starve-fed extrusion is preferred over flood fed extrusion for many reasons. For example, starve-fed extrusion has a relative lower pressure along the screw, which can lead to an improved mixing action. Another benefit of starve-fed extrusion particularly important for reactive extrusion is that the screw speed can be varied at a constant throughput. This results in a great degree of control of the extruding process [147]. It is known that a higher feed rate results in a higher throughput and increase in die pressure, which fills up the screw channels. On the other hand, at a higher screw speed the fraction filled is decreased. This is because at a higher screw speed more slip is evident, meaning more back leakage is observed. Feed rate and screw speed work in the opposite direction when it comes to the degree of fill in the screw channels [148]. For that reason, the ratio between the feed rate and screw speed ( $F_R/S_S$ ) is normally used, and it can indicate the degree of fill [146]. The  $F_R/S_S$  is significantly affected by increasing the feed rate and screw speed, being directly proportional to the feed rate. On the other hand, as the screw speed increased from 200 to 600 rpm,  $F_R/S_S$  was decreased. The reduction of  $F_R/S_S$  is correlated with the lower pressure in the material. These findings agree with literature [148].

The degree of filling can affect the amount of the reaction, in some extent, because it can be associated with the mixing power of the process condition. Higher degree of fill ( $F_R/S_S$ ) can increase the melt pool formed before any flow restrictive zones (i.e., before extensional, kneading and left-handed elements) increasing the local melt pressure, which makes the material to be more compacted at these specific locations inside the extruder than with lower  $F_R/S_S$ . With lower  $F_R/S_S$  and less compacted material, the axial dispersion in the extruder is improved, le-

ading to enhanced interactions between the two polymer phases. This illustrates the increase of the reaction at a higher screw speed in both groups of curves in Figure 4.27. The increase of the screw speed lowers the  $F_R/S_S$ , and the increase of feed rate increases the  $F_R/S_S$  creating two groups of curves. This is the sum of two effects simultaneously. First, the earlier melting is caused by higher feed rates that divide the graph in two groups (higher and lower feed rate); then, the back leakage caused by more slips with higher screw speed, increasing the axial dispersion. In addition, having two groups of curves confirms what Yeh et al. have stated in their works that changes in the feed rate is more effective than in the screw speed [145, 146].

#### 4.4.2 Reactive Extrusion of 70/30 (wt/wt%) of PP-g-AA/PA6 and PP/PA6

In this section, the influence of process conditions on IR characteristic absorption bands during REX (reactive blending) of the blend of 70% of PP-g-AA and 30% of PA6, for the reactive blend, and 70% of PP and 30% of PA6 for the non-reactive blend and correlated with residence time at the locations of on-line FTIR measurements. First, the RTD (total and partials) was measured in all location along the extruder barrel at various process conditions. The expectation is that the use of different process conditions (feed rate, screw speed and screw configuration) have a great impact in the time that the polymer melt travels the extruder length. Then, on-line FTIR measurements were performed for both, reactive and non-reactive blends at the same process conditions. The area ratio (1640/1373  $\text{cm}^{-1}$ ) of the non-reactive blend was used as a reference for the reactive blend one. The expectation is that the area ratios (1640/1373  $\text{cm}^{-1}$ ) along the extruder vary with the process condition, achieve distinct values at different times.

##### *Total and Partial RTD Curves Along the Extruder*

In this section, we analyze the total and partial average residence times at different process conditions. The shape of the residence time distribution (RTD) curves was also analyzed. A red dyed PE pellet was used as an inert tracer in the tracer experiment. We compared the total RTD (recorded at the die of the extruder) to the partial RTD's recorded along the extruder at different locations

(L/D). Similarly, Covas et al. (2004) in their paper about on-line monitoring of RTD write that the knowledge of the residence time at various locations along the extruder barrel is required in order to control or monitor the kinetics of reaction in REX [128]. According to our experimental setup the feed rate was varied from 2 kg/h to 5 kg/h and the screw speed from 100 to 400 rpm for two different screw profiles (the specific parameters for each experimental run are shown in Table 3.7).

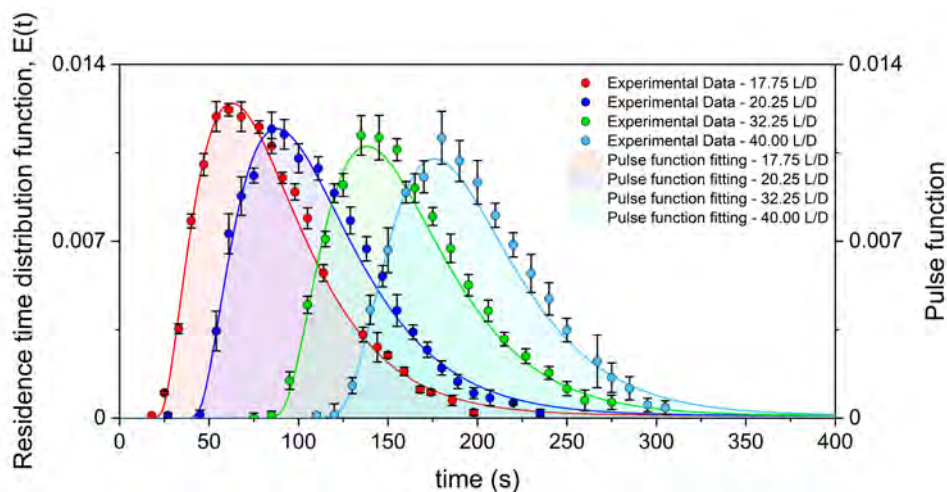


Figure 4.28: Experimental  $E(t)$  curves (circle plots) and corresponding fitted pulse curves (solid lines) for the operating conditions S4-400-5 at 17.75, 20.25, 32.25 L/D and at the die.

Figure 4.28 depicts  $E(t)$  function obtained from the experimental data and the theoretical curve fitting (pulse function) for each location of on-line analysis (L/D). In Figure 4.28 we show only one (S4-400-2) of the eight process conditions (3.7) used in this work. All the other conditions can be appreciated in Appendix D. As shown in Figure 4.28, the pulse function curve fits the experimental data ( $E(t)$  curves) well. Through the curve fitting with the pulse function the average residence times  $\bar{t}$  and variance ( $\sigma^2$ ) can be calculated and the parameters of  $X_0$ ,  $R_1$  and  $R_2$  can be acquired and plotted in function of L/D (Figure 4.29). This was done for all the process conditions. All the RTD coefficients appear to have a linear increase along the extruder length, though the slope of the linearity changes for the different process conditions. This agrees with the literature [128].

From the fitting curves the average residence times ( $\bar{t}$ ) were calculated by the



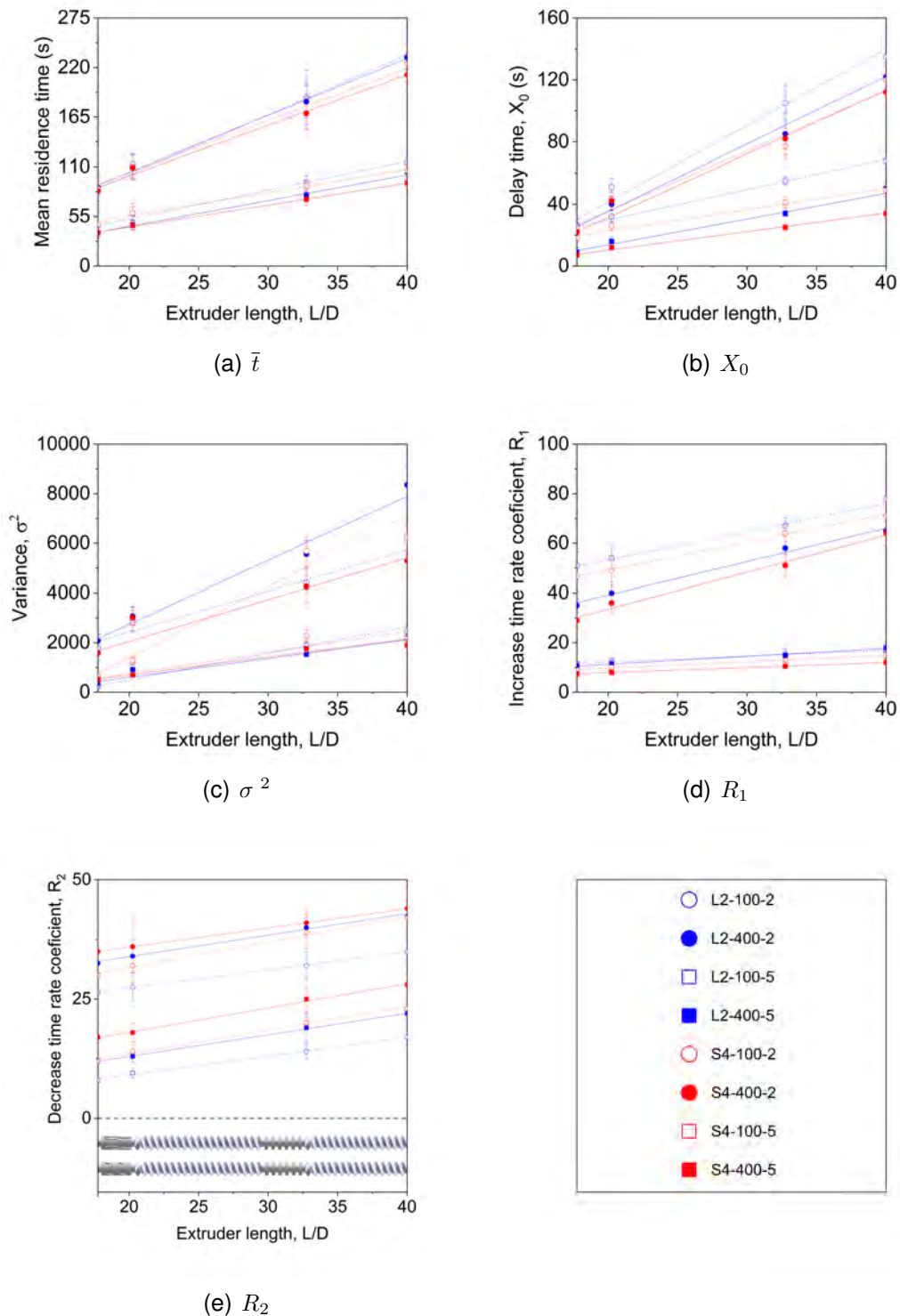


Figure 4.29: Coefficients of the pulse function from the fitting of the experimental data for all the process conditions that were analyzed. a) Average residence time, b) delay time, c) variance, d) curve ascent time rate constant and e) curve descent time rate constant.



same methodology used previously by other authors [57, 128, 149], and it is given by:

$$\bar{t} = \frac{\int_0^{\infty} tcdt}{\int_0^{\infty} cdt} = \frac{\sum_0^{\infty} t\Delta a^* \Delta t}{\sum_0^{\infty} \Delta a^* \Delta t} \quad (4.1)$$

and the variance,  $\sigma^2$ , is given by

$$\sigma^2 = \int_0^{\infty} (t - \bar{t})^2 E(t) dt = \sum_0^{\infty} (t - \bar{t})^2 E(t) \Delta t \quad (4.2)$$

$\Delta a^*$  is the intensity of red color in the CIELAB scale, which is taken as equivalent to the concentration ( $c$ ) of the tracer and  $E(t)$  is the residence time distribution function.

The total average residence times ( $\bar{t}_t$ ), which means  $\bar{t}$  recorded from the hopper to the die, vary between 87 and 231 seconds and agree with those reported in literature for extruders with the same L/D [65]. Figure 4.29(a) also shows the partial average residence times ( $\bar{t}$ ) at 17.75, 20.25 and 32.75 L/D, which vary between 36 s and 90 s, 44 s and 113 s, and 68 s and 177 s, respectively. The delay times ( $X_0$ ) (Figure 4.29(b)) are the times where the first particle or element of the material leaves the extruder, in our case, the first particle of red-dyed PE. In other words, the instant at which the material reaches the location of measurement [128]. Delay times and average residence times should have the same trend of behavior, but average residence time should be longer than delay times (see Figure 4.29(a) and 4.29(b)). This wide variation in  $\bar{t}_t$  and in  $X_0$  is related to a variation of the process parameters in the process conditions, which is also wide (see Table 3.7). As stated by Pinto and Tadmor (1970) RTD is dependent on the process conditions used within the extrusion run. They have shown by computational numerical solution that even the curvature of screw flights, i.e., screw profile, has a significant influence on RTD [149].

Our results indicate that an increase of feed rate ( $F_R$ ) leads to a decrease in the  $\bar{t}_t$  regardless of the screw speed ( $S_S$ ) and screw profile (EME L2 or EME S4) used. At 100 rpm, increasing the feed rate from 2 kg/h to 5 kg/h  $\bar{t}_t$  is decreased up to 49% and at 400 rpm,  $\bar{t}_t$  can be decreased up to 61% when  $F_R$  goes from 2 to

5 kg/h. A similar correlation between shorter residence times at higher feed rates has been stated by Shirazian et al. for continuous twin screw wet granulation [65]. Also, this correlation is reported in the study by Puaux et al [150]. As expected, this relationship does not seem to be dependent on the location where  $\bar{t}$  was recorded. The partial average residence times ( $\bar{t}_t$ ) are also observed to have decreased in all the locations along the screw, namely, 17.75, 20.25, 32.75 L/D. Similar to  $\bar{t}_t$ , at higher  $S_S$  this decrease is larger for  $\bar{t}$  as well. At 100 rpm the decrease in all the locations varies from 46-50%, whereas at 400 rpm it varies from 55-58% when  $F_R$  is increased. Similarly,  $X_0$  is decreased when  $F_R$  is increased. Figure 4.29(b) shows that  $X_0$  are shifted to shorter times when  $F_R$  is increased. The shift is larger downstream the extruder barrel, up to 78 seconds earlier at 5 than 2 kg/h, at the die. The reason for that is that at higher feed rates the throughput forces are increased while the back mixing is decreased. Another reason why  $\bar{t}$  and  $X_0$  have decreased with higher feed rates is that a relatively larger amount of material is present in the screw channels, increasing the pressure. All these reasons lead to a faster extrusion run and narrow RTD [65], decreasing the average residence times (total and partials) at high  $F_R$ .

Now looking at the effects of the screw speed ( $S_S$ ) on the  $\bar{t}_t$ , we see that increasing  $S_S$  from 100 to 400 rpm  $\bar{t}_t$  is decreased. This finding has also been reported by Baron et al. (2010) [56] and has been predicted by other authors [128, 149]. As expected, the decrease of  $\bar{t}$  with the increasing  $S_S$  happens in all the locations along the extruder for the partial average residence times ( $\bar{t}_t$ ) as well. Likewise,  $X_0$  is decreased with the increase of  $S_S$ . Delay times ( $X_0$ ) are shifted up to 21 seconds earlier when the  $S_S$  is increased from 100 to 400 rpm. Interestingly, the correlation between  $S_S$  and times ( $\bar{t}_t$ ,  $\bar{t}$  and  $X_0$ ) seems to be also dependent on the  $F_R$ . Increasing the screw speed from 100 rpm to 400 rpm  $\bar{t}_t$  and  $\bar{t}$  are decreased up to 23% at 5kg/h, whereas at 2 kg/h the decrease is only around 2-5% depending on the L/D. In the same way,  $X_0$  decreases up to 61% at 5kg/h and it only decreases around 21% at 2 kg/h, when  $S_S$  is changed from 100 to 400 rpm depending on the L/D. This suggests that the  $\bar{t}_t$ ,  $\bar{t}_p$  and  $X_0$  are dependent on the degree of fill. As we could see from the results in the previous section the degree

of fill in turn is a synergistic relationship between  $S_S$  and  $F_R$  [148]. The higher the  $F_R$  the higher the pressure drop is. Pressure drop is defined as the pressure at the entrance of a restrictive zone, such as a mixing zone, minus the pressure at the exit of this specific zone of the screw. This happens regardless the  $S_S$ . The higher the pressure drop the higher the amount of material in the screw channels (degree of fill). By contrast, at faster screw rotation speeds more back leakage is observed due to more slip of material. This decreases the pressure drop at the entrance of the mixing zone, thus contributing to diminishing the degree of fill [148], slightly increasing the axial mixing [150]. However, the effect on  $S_S$  in the pressure drop is also dependent on the  $F_R$ . Jinescu and Sporea have made a screening in the variation of  $S_S$  at small, medium and higher  $F_R$ . They concluded that the degree of fill changes more with the variation of the screw speed at higher feed rates. For that, the effect of the  $S_S$  is more pronounced at 5 kg/h than at 2 kg/h [148]. In addition, according to Covas et al. (2004) the average residence time seems to be less dependent on the screw speed variation [128]. Our results show that the screw speed variation impacts more significantly the delay times ( $X_0$ ) than the average residence times (Figure 4.29(a) and 4.29(b)). Delay times ( $X_0$ ) are shifted up to 21 seconds earlier when the  $S_S$  is increased from 100 to 400 rpm.

Many authors use Variance (4.29(c)) as an indirect indication of the axial dispersion. This is the dispersion of material along the length of the extruder barrel [151]. This also indicates the flow uniformity [152]. However, the symmetry of the RTD curve needs to be considered as well. When the experimental data is fitted by the pulse function  $R_1$  and  $R_2$  can be acquired.  $R_1$  (the curve ascent time rate constant) is related to the time of ascension of the RTD curve. This means how long it takes to reach the maximum. Whereas  $R_2$  (the curve descent time rate constant) is related to the rate that RTD curve decreases after the maximum in order to reach zero, meaning that the concentration of the pulse is zero and all the tracer was gone. See table 3.8. Nevertheless,  $R_1$  and  $R_2$  are both related to the symmetry of the RTD curve. In terms of the extrusion process,  $R_1$  can be described as how fast the material is pumped out of the extruder. While  $R_2$  is re-

lated to how long the material remains inside it, correlating to the ‘tail’ of the RTD curve [151]. The Higher the  $R_1$  the longer the time it takes to reach the maximum of the RTD curve, leading to a lower slope of the curve. The higher the  $R_2$  means the longer the time it takes to reach zero after the maximum. This leads to less steep curves and higher axial dispersion (longer ‘tails’).

Figure 4.29(d) shows that  $R_1$  is higher for “slower” process conditions, i.e., longer  $\bar{t}$  and delay times (Figure 4.29(a) and 4.29(b)).  $R_1$  decreases when  $F_R$  is increased from 2 to 5 kg/h.  $R_1$  also decreases when  $S_S$  is increased from 100 to 400 rpm. This indicates the material is leaving the extruder in a faster rate at higher  $F_R$  and  $S_S$ . A likely explanation is that the times ( $\bar{t}$  and delay time) are shorter at 5 kg/h and at 400 rpm. Despite that, the effect of  $S_S$  in  $R_1$  seems to be stronger at 2 kg/h than at 5 kg/h. At 2 kg/h  $R_1$  is decreased by 38% when the  $S_S$  is increased from 100 to 400 rpm. While at 5kg/h this decrease is around 19% depending on the process condition. The possible explanation for this is that at 5 kg/h the extrusion run is fast enough, due to the high pressure drop, which makes the effect of  $S_S$  not to be very evident at 5 kg/h as it is at 2 kg/h [153].

As aforementioned,  $R_2$  is related to the “tail” of the curve. This is an indication of axial dispersion before the mixing or restrictive zones.  $R_2$  decreases when the  $F_R$  is increased. When the  $F_R$  is changed from 2 to 5 kg/h  $R_2$  is decreased up to 69%, depending on the process condition. This might mean that the axial dispersion is lower at higher feed rates. As stated before, at higher feed rates the pressure drop is raised which increases the material resistance to flow. This not only leads to more material in the screw channels (degree of fill), but it also leads the material to be more compressed before and in the restrictive zones, consequently, diminishing the axial dispersion. Shorter “tails” are seen at lower  $R_2$  [151]. On the other hand, increasing the  $S_S$  from 100 to 400 rpm  $R_2$  appears to be increased. The observed correlation between  $S_S$  and  $R_2$  might be explained because of the higher slip of material at higher  $S_S$  [149], leading to higher values of  $R_2$ , i.e., longer “tails”.

As shown in Figure 4.29(a) and 4.29(b), the use of EME S4 leads to shorter times in the extrusion run, especially for the delay time ( $X_0$ ).  $R_1$  is also diminished

(Figure 4.29(d)) in the screw profile equipped with EME S4 than with EME L2. As discussed earlier, lower values of  $R_1$  are related to faster rates of material being pumped out of the extruder. These behaviors are relative to the high pressure drop at the entrance of the mixing zone in the EME S4 when compared to EME L2. This is caused by the higher contraction ratio in the converging-diverging channels of the extensional mixing elements S4. This behavior lends support to previous findings in the literature [50, 141]. The higher pressure imparted by EME S4 yields to faster extrusion runs, decreasing the times ( $\bar{t}$  and  $X_0$ ) and making the material to be pumped out of the extruder at higher rates. In contrast,  $R_2$  is increased when EME S4 is used. This result is somewhat counter-intuitive, since EME S4 provides higher pressure drop, which would yield to lower values of  $R_2$ . The reason for this is not clear but it may have something to do with the higher intensity of the RTD curves when EME S4 is used in the screw profile. According to recent study, the intensity of the RTD curve is related to the concentration of the tracer [152]. From the curves in Figure 4.30 we can see that the RTD curves with screw profile equipped with EME S4 show significantly higher intensity than those with EME L2 in all locations along the extruder at 400 rpm and at 5kg/h. Even though the best attempts to keep the same concentration of the tracer were done by weighing the PE pellets in a high-resolution scale, it can be noticed in Figure 4.30 that the area under the curve is not necessarily constant. Similar results have been reported in the literature. According to Covas et al. (2004) this can be associated to the methodology used. The measuring methodology might not see all the tracer particles. This can happen for in-process and off-line methods of RTD curves acquisition. Particularly, in off-line measurements because it can involve manual sample collection, leading to lower data resolution. In addition, this has to do with the inherent characteristic of co-rotating twin-extruders in working with flow channels mostly independent of each other [6, 128].

Taken together, these results suggest that there is an association between the variation of process parameters and the distribution of residence time in the extruder. Not only at the die, but also along the barrel. The fitting of the experimental data with the pulse function was useful to better understand the behavior of the

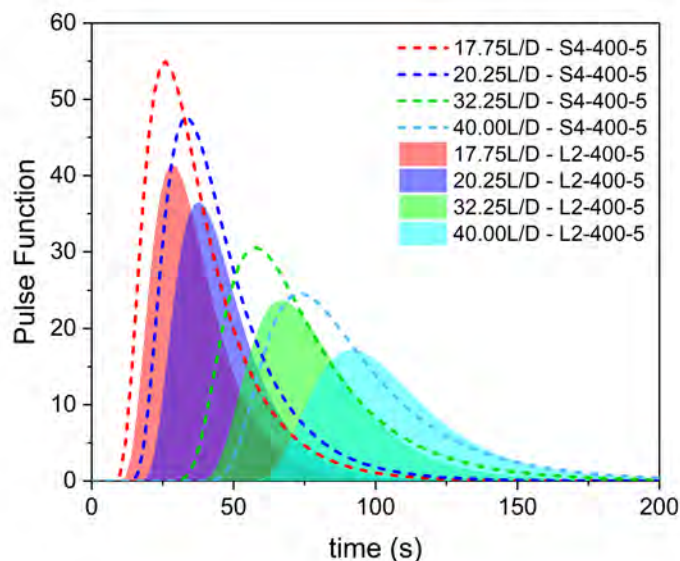


Figura 4.30: Comparison between the  $E(t)$  fitted with pulse function of condition L2-400-5 and S4-400-5 at 17.75, 20.25, 32.25 and at the die.

curves with the process conditions studied.

#### *Chemical Transformation*

In order to investigate the amount of reaction, we have proposed the use of the concept of chemical transformation. The term transformation can be broadly used in chemical science to mean a change in material composition, in its state, or its organization. Also, it can mean material movement or rearrangement caused by temperature, diffusion or flow variation [154]. Throughout this section of the dissertation, the term transformation will refer to how much the reaction was obtained by the reactive blends compared to the non-reactive ones during extrusion. This comparison is made when the blends are being processed under the same methodology and the same process conditions.

Thus, the transformation here will be defined as the difference between the area ratio of the absorption bands of the reactive blend ( $aR_{REX}$ ) and of the non-reactive ( $aR_{NREX}$ ) and equals

$$\Delta aR = aR_{REX} - aR_{NREX} \quad (4.3)$$

The transformation tells how much the area ratio increases or decreases du-

ring the process having the non-reactive blend as a reference (or baseline). The non-reactive blend can be used as a baseline because its area ratio ( $aR_{NREX}$ ) should be kept constant along the extruder barrel due to the lack of reaction during the process. Consequently, the composition ratio of the components will be unaltered, as we can see in the previous section in Figure 4.22. This way, the  $aR_{NREX}$  can be used as a reference (baseline) to evaluate the changes of  $aR_{REX}$  in the reactive blend spectra. More precisely, the changes in the relationship between characteristic bands of polyamide 6 and polypropylene due to the chemical reaction. As mentioned before, the band at  $1373\text{ cm}^{-1}$  is referred to the functional group  $C - H_3$  that does not participate in the reaction. Therefore, the area of this band is expected, within the experimental error, to be the same for both the non-reactive and the reactive blend. Knowing that, the relationship between this band and bands relative to polyamide 6 should not change, unless the composition of the blend changes. A change in the composition of the blend is expected only in the reactive blend due to chemical reaction. IR bands relative to amide functional group are expected to be more intense with the chemical reaction development, in the reactive blend. As previously stated, the difference between  $aR_{REX}$  and  $aR_{NREX}$  means how much of chemical reaction (transformation) was acquired for the reactive blend in relation to the non-reactive blend in the same process conditions.

The transformation can be either positive or negative. This is because the amide group can be formed from the chemical reaction between amine end group and acrylic acid yielding a positive transformation (see Figure 3.8). On the other hand, the amide functional group can suffer chemical degradation from the extrusion process, this would be characterized as a negative transformation [4, 5].

If the chemical reaction proceeds continuously along the extruder barrel,  $\Delta aR$  is cumulative. This means, whether the  $\Delta aR$  is positive or negative, it needs to be considered in the whole length of the screw and not only at the location (L/D) that is measured. For example,  $\Delta aR_N$  measured at a determined L/D along the extruder is the transformation calculated in that port  $\Delta aR_{L/DN}$  summed up to the  $\Delta aR_{N-1}$  calculated in the previous port (L/D) like in the scheme below:

$$\begin{aligned}
 \Delta aR_1 &= \Delta aR_{L/D1} \\
 &\Downarrow \\
 \Delta aR_2 &= \Delta aR_{L/D2} + \Delta aR_1 \\
 &\Downarrow \\
 \Delta aR_3 &= \Delta aR_{L/D3} + \Delta aR_2 \\
 &\Downarrow \\
 &\dots \\
 &\Downarrow \\
 \Delta aR_N &= \Delta aR_{L/DN} + \Delta aR_{N-1}
 \end{aligned}$$

#### *Amount of Reaction and Phase Interfacial Area Dependency*

Figure 4.31 provides the results obtained from the on-line ATR-FTIR measurements at different positions along the extruder. The curves show the variation of transformation ( $\Delta aR$ ) with L/D when the process conditions are varied. Figure 4.31 is quite revealing in several ways. First, there is a clear trend of increasing of  $\Delta aR$  downstream the extruder length. Second, there is a significant difference in the behavior of  $\Delta aR$  between the process conditions. These facts confirm that the reaction is taking place continuously along the extruder. Additionally, this behavior is dependent on the process parameters, yielding different rates of chemical reaction. Closer inspection of the Figure 4.31 shows that  $\Delta aR$  is different from zero at the first location (17.75 L/D) of measurement. 17.75 L/D corresponds to 42.6 cm, which is approximately 44% of the total length of the extruder (96 cm). The observed transformation that is different from zero at 17.75 L/D can be attributed to the reaction happening along this length range of the extruder, i.e., before the first point of measurement. Due to practical constraints, no researchers have been able to investigate one hundred percent of the extruder barrel length, from the hopper to the die. This reveals to be one of the most common drawbacks associated with the investigation of extrusion process, especially REX [128]. To the best of our knowledge, this inevitably has been a limitation for many earlier studies. However, the data shows that despite that most of the reaction will be happening after this point (17.75 L/D). This is where we will be focusing the discussion of the results.



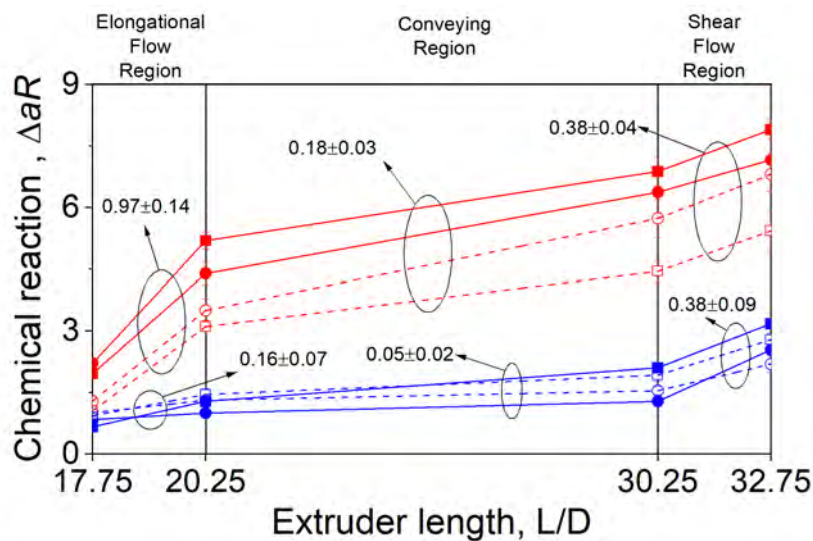


Figure 4.31: On-line chemical reaction at various process conditions along the extruder length (as  $L/D$ ). The slope of the linear fitting for the process conditions are indicated in the plot.

Considering that the reaction happens continuously along the extruder barrel, we can divide the curves in Figure 4.31 in three regions. The regions are: elongational flow region, conveying flow region, and shear flow region. The elongational flow region is comprised of extensional mixing elements EME S4 or EME L2. The conveying flow region encompasses the region between 20.25 and 30.75  $L/D$ , made exclusively by conveying elements. Lastly, the shear flow region consists of kneading block elements staggered at 90 degrees. See Figure 3.9. From the Figure 4.31 the length of each region can be seen. Both the elongational and the shear flow regions are 2.5  $L/D$  in total length, while the conveying flow region is 10  $L/D$ .

Figure 4.31 depicts the experimental data of  $\Delta aR$  and the linear fitting for each region mentioned before. The reason for applying a linear fitting is to evaluate the difference in the slope of the variation of  $\Delta aR$  against the position and the length of the extruder in which the material traveled. Given the continuous increments of  $\Delta aR$ , the slopes of the linear fitting curves are the rates of  $\Delta aR$  change along  $L/D$ . As known, the set-up of the experiments in this study used two screw profiles. The first one equipped with EME L2 and the second with EME S4. In the elongational flow region (Figure 4.31), the average of the slopes for the curves of the conditions

with EME S4 is  $0.97 \pm 0.14$ , whereas with EME L2 is only  $0.16 \pm 0.11$ . This means that  $\Delta aR$  increases at a rate approximately five times higher in EME S4 than EME L2. From Figure 4.31 we can see that the screw profile seems to separate the curves into two groups. The first group with lower values of  $\Delta aR$  belongs to the screw profile equipped with EME L2. While the second group with higher values of  $\Delta aR$  is associated to the screw profile equipped with EME S4. The most likely reason for the differences between  $\Delta aR$  and the slope of the linear fitting curves (Figure 4.31) in both screw profiles is associated to changes in the blend's morphology. Extensional mixing elements have been proved to be highly efficient in droplet breakups [1, 35, 44, 45, 49]. Both EME S4 and L2 impart extensional flow to the polymer melt in the extrusion process. This is due to the hyperbolic converging-diverging (C-D) channels designed in a series which force the melt to go into a converging-diverging flow as well. The hyperbolic contraction converges the melt at the entrance and diverges it at the exit of the channel, causing the melt to stretch. This can impose uniform extension rate on the fluid [155]. However, due to the higher contraction ratio in the C-D channel of EME S4 the aggressiveness in droplet breakup is higher than in EME L2, as can be seen in the SEM micrography in Figures 4.24(c) and 4.24(d). Another reason why EME S4 is more efficient is the length and number of C-D channels. Both EME S4 and EME L2 is a 2 L/D in total length, which is 4.8 cm. EME S4 has short channels (this is what 'S' stands for), and each channel is 0.5 L/D, i.e., 1.2 cm in length. By contrast, EME L2 is designed with long channels ('L' stands for long) measuring 1 L/D (2.4 cm) in length. This means that EME S4 has four C-D channels in a series against only two in EME L2. This can be clearly seen in Figure 2. Having more channels in a series means that the polymer melt is undergoing higher number of converging-diverging stretches. The higher contraction ratio and number of channels in EME S4 also contribute to increasing the pressure in the melt during extrusion. This helps the droplet to breakup to be more efficient in EME S4. All these factors yield to a finer blend's morphology when EME S4 is used instead EME L2. The effect of different design of EMEs in the material morphology has been extensively investigated in previous work [44, 45, 48, 49, 156] and discussed

in section 4.4.

A finer morphology means that the particles of the second phase are smaller and therefore, the total interfacial area is larger. Macosko et al. (2005) stated that for a polymer blend to be compatibilized the phase interfaces need to be covered with the copolymer formed from the compatibilization reaction [157]. This means that the interface between the phases serves as a substrate for the reaction shown in Figure 3.8 to take place. This statement is in accordance with He et al. (2021), who has recently published that immiscible polymer blend compatibilization is accomplished through the formation of graft or block polymers at the interface of phases [158]. The fresh interface created by the EME S4 and L2 increases the contact between reactants allowing the reaction to take place. This is more effective in EME S4, since it generates more interfaces. This makes the process conditions with screw profile equipped with EME S4 to obtain higher  $\Delta aR$ . Consequently, curves with higher slopes (higher rate) in Figure 4.31 for EME S4. This suggests that a large reaction is happening when the material is passing through the EME, simultaneously with the creation of the fresh interface. Macosko et al. (2005) confirms that the reaction is extremely accelerated by the creation of fresh interface during mixing [157]. This finding is consistent with that Zhao et al. (2019) who concluded that the transesterification reaction between PC/PBT blends occurs at the phase interface. They were able to establish a correlation between the degree of transesterification and the morphology of the phases [159].

Besides the screw profile there are two more factors that can make  $\Delta aR$  to increase along the extruder barrel. These are: feed rate ( $F_R$ ) and screw rotation speed ( $S_S$ ). In Figure 4.31 the curves relative to the screw profile with EME L2 (blue curves) show few differences in the transformation with the variation of  $F_R$  and  $S_S$ . The curves for the conditions L2-100-2-R, L2-400-2-R, L2-100-5-R and L2-400-5-R are overlapped to each other and even when the error bars show some statistical differences, the increase of  $\Delta aR$  is negligible. The red curves relative to EME S4 show more differences in  $\Delta aR$ . Especially between the curves with different  $S_S$ . Conditions S4-400-2-R and S4-400-5-R have higher chemical

reaction than conditions at 100 rpm (S4-100-2-R and S4-100-5-R). Despite that, these differences do not seem to be very significant. These results are likely to be related to the different times that the polymer melt arrive at the location of on-line FTIR measurement. As said in section 4.4.2, the variation of  $F_R$  and  $S_S$  change significantly RTD curve parameters. In other words, polymer melt arrives at the same location in different times ( $X_0$ ) and they remain inside the extruder for different lengths of time ( $\bar{t}$ ) as well. This is extremely important for REX because of the dependency on local residence times and temperatures along the extruder with the chemical reaction [128].

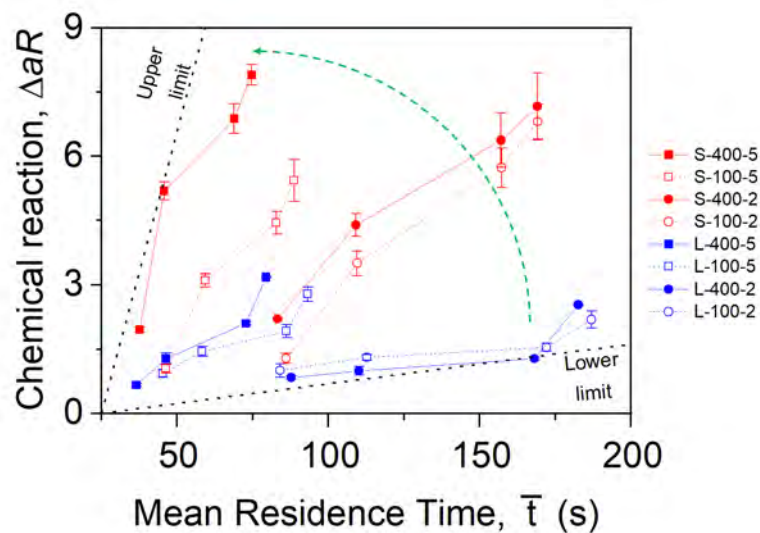


Figure 4.32: Transformation vs. mean residence time. Green dashes arrow indicates the increase of aggressiveness of the process condition.

When the time available for the reactants to react, i.e., the mean residence time ( $\bar{t}$ ), is take into consideration  $F_R$  and  $S_S$  effect is more noticeable. This is highlighted in Figure 4.32. There are several important considerations that can be made from Figure 4.32.

First, the difference between curves related to EME S4 (red) and EME L2 (blue) largely stands out on the graph. The reasons for higher  $\Delta aR$  in EME S4 was explained prior. The second important behavior of the curves is regarding  $F_R$ . As can be seen in Figure 4.32, process conditions at 5 kg/h (L2-100-5, L2-400-5, S4-100-5 and S4-400-5) have a relatively higher  $\Delta aR$  when compared to conditions with same parameters but at 2 kg/h (L2-100-2, L2-400-2, S4-100-

2 and S4-400-2). However, the most striking result observed from Figure 4.32 is that conditions at 5kg/h achieved higher  $\Delta aR$  at shorter times. As extensively discussed in section 4.4.2, the main contribution of  $F_R$  is the rising of the pressure. The increase of pressure affects the degree of fill. This means the more material is present inside the screw channels due to the higher  $F_R$ . This might increase the collision probability. Another contribution of higher  $F_R$  is the shifting of the melting of the material to an upstream position due to a high degree of filling. The melting starts at the location where the screw is fully filled [146]. Consequently, the material starts to melt at an earlier position (L/D) at 5 kg/h than at 2 kg/h. The compatibilization reaction showed in Figure 3.8 occurs in the molten state [144]. This means that the reaction beginning is anticipating at higher  $F_R$ . This leads to higher  $\Delta aR$  in conditions at 5 kg/h. For example, conditions L2-100-2, L2-400-2, L2-100-5 and L2-400-5 have the same chemical reaction at the die of the extruder when we look at Figure 4.31. However, Figure 4.32 shows that conditions L2-100-5 and L2-400-5 were able to achieve the same amount of chemical reaction but at residence times about 50% shorter. All these reasons seem to have a positive contribution on the reaction, even though there is a shorter residence time at 5 kg/h. This same effect is expected to happen with the variation of screw rotation speed ( $S_S$ ). Figure 4.31 shows that the curves tend to have higher values of  $\Delta aR$  when  $S_S$  is increased from 100 to 400 rpm. Additionally, shorter residence times at higher  $S_S$  can also be seen. The main reason for that is that increasing  $S_S$  leads to higher thermomechanical polymer stress and shear [140]. This contributes to the increase of shear heat (or viscous heating), which increases the local temperature and can increase the mobility of the polymer chains [159]. This can favor the reaction by improving the collision between the reactants [8, 14, 128, 160].

The conveying flow region shown in Figure 4.31 have the lowest average of slope of the linear fitting curve among the regions. This outcome is expected due to the minimal mixing power of the conveying elements. However, some reaction is observed in this region due to the large length of 10 L/D. In addition to the material being exposed to high temperature and some friction between the material and the extruder wall [140]). Surprisingly enough, the curves that belong to EME

S4 (red) in this region have a higher slope than the curves of EME L2. A possible explanation for this is that at the exit of the EMEs at 20.25 L/D the morphology is different for EME S4 and L2. As explained before, EME S4 generates more interface between phases. This interface might still have some contribution for the reaction in the following conveying zone, even in a small extent. However, the most striking result to emerge from Figure 4.31 is in the shear flow region. In this region all curves have the same average of fitting linear slopes. This indicates the  $\Delta aR$  is increased at the same rate when they pass through the KB90 zone, regardless the previous shearing history used. This is explained since the polymer melt is passing through the same mixing zone of kneading block elements staggered at 90 degrees (Figure 3.9), which is imparting the same amount of melt shear in all cases [9, 44, 48]. We can suppose that all or most of the increase in  $\Delta aR$  in the second mixing zone is due to dispersive mixing contribution that kneading blocks can impart in the melt, which happens between the end of the blocks with the extruder wall.

Figure 4.32 shows that there has been a gradual increase in the transformation when the aggressiveness of the conditions is increased. This is shown by the increase of the steepness of the curves following an angular increase indicated by the green dashed arrow in the plot. In order to discuss that, the term “goodness of mixing” will kindly be borrowed from Pinto and Tadmor (1970). The term was used for the first time in 1970 to quantify the aggressiveness of a giving extruder at a giving process condition. This quantification was in terms of the extrudate mixing according to the strain that was imposed to the melt. They considered the length and height channel ratio (L/H) the most important parameter affecting the “goodness of mixing”, which is related to the geometry design of the screw [149]. Obviously, the authors have used a much simpler model that has approximated the flights of the screw to rectangular channels, which differs from the complex geometries considered in the present study. However, steeper curves were observed for conditions S4-400-5-R, S4-100-5-R, S4-400-2-R and S4-100-2-R than for the same conditions using EME L2. This indicated that in our study the geometry was also the most important factor affecting the mixing, therefore, the the

amount of reaction. This has to do with the ability of generate fresh interface. This leads to higher “goodness of mixing” for the screw using EME S4 as the mixing geometry. The reasons for that were presented before. Following the discussion of the trend in Figure 4.32,  $F_R$  seems to be the second factor increasing the “goodness of mixing” due the higher pressures and increasing the amount of material in the screw channels. Lastly, the  $S_S$  due to higher stresses in the melt. For example, there are conditions on the two extremes of the plot. S4-400-5-R with higher values of  $\Delta aR$  in the upper limit of the plot and, the conditions L2-100-2-R and L2-400-2-R that share the lower limit. Condition with intermediate “goodness of mixing” rely in between these two extremes. These findings show that the amount of the chemical reaction is more affected by the parameters of the process conditions, i.e., the ability to produce fresh new interfaces to the compatibilization reaction to happens, than by the time that the reactants remain inside the extruder in order to react. This yields higher reaction rates translated by the transformation even at shorter times.

Finally, the analysis previously discussed may be very useful. Knowing the “goodness of mixing” of a giving operating condition can provide the fundamentals to foretell the expected amount of chemical reaction during the extruder process. This can be used as a tool for understanding extrusion-based processes.





## 5 CONCLUSIONS

The main goal of the current study was to improve the understanding of the extrusion and reactive extrusion process, for reactive blending, through infrared spectroscopy. This research extends our knowledge of how the process parameters can influence the development of chemical reaction along the extruder in REX. For the conclusion, this dissertation can be divide into two kinds of contributions: technological and fundamental conclusions.

- The technological conclusions of this dissertation are:

This project was undertaken to design the On-line Fourier Transform Infrared Spectroscopy System and validate the system in controlled conditions of materials and processes. The system was successfully validated in the investigation of various PP/PA6 polymer blend compositions during extrusion and to detect reaction in reactive blending extrusion of PP-g-AA/PA6 blend. In addition, the On-line FTIR system proved to be precise when compared to off-line infrared measurements, in both, ATR-FTIR and transmission FTIR.

The on-line FTIR system was prototyped to be of ease of coupling to the TSE while avoiding major modifications to the barrel. It was also able to quantitatively analyze the kinetics of chemical reactions along the extruder barrel, by measuring the IR band area ratio between 1640 and 1373  $\text{cm}^{-1}$  with a no disruption of the melt flow.

The present study also proposed and successfully validated a methodology of infrared band quantification. The validation was performed in bench and, it showed to be accurate in analysis of binary and ternary liquid mixtures of acetone, distilled water, ethanol and toluene. The methodology of band deconvolution by Pearson VII function effectively minimized the effect of band distortion and shifting caused by overlapping of IR bands, when compared to traditional method and the deconvolution method using Lorentz function. In addition, the method also helped to decrease the interference of noises in the baseline of IR spectra in the final results of band area. The linearity of

the composition, proposed by Beer's law, of acetone/distilled water mixtures was improved in 14 % with the application of Pearson VII when compared to the traditional method and Lorentz function. Results of absorbance and area of IR bands at 1220, 879, and 692  $\text{cm}^{-1}$  of acetone, ethanol and toluene, respectively, in different known compositions of their binary and ternary mixtures were also improved by the use of Pearson VII.

- The fundamental conclusion of this dissertation is:

The infrared band area ratios (chemical reaction) of PP/PA6 and PP-g-AA/PA6 blend's morphology depended on the processing conditions, i.e., the elements forming the screw profile at the main mixing zone, feed rate and screw speed. Feed rate and screw speed ratio define the degree of fill of the extruder screw channel, mainly before restrictive melt flowing zones. Feed rate had a higher effect on the amount of the compatibilization chemical reaction between acrylic acid (PPg-AA) and amine end group (PA6) than screw speed. The main reason for that can be the anticipation of the melting upstream at high feed rates, which leads the chemical reaction to start earlier in the extruder barrel.

This study has introduced the concept of chemical transformation. The chemical transformation is the difference of chemical reaction in a reactive blend using the non-reactive blend in the same composition as a baseline. The study has also shown the correlation between the RTD coefficients and the process parameters variation. The experiments confirmed that increasing feed rate and screw speed, the delay time and average residence time are decreased, leading to faster extrusion runs for blends of PP/PA6 and PP-g-AA/PA6. Pressure drop and degree of filling are the most important reason for this effect. The study correlated the variation of times of extrusion with the transformation from the chemical reaction.

One of the more significant findings to emerge from this study is that in REX, when done at a fixed temperature, the most important parameter controlling the compatibilization reaction between Pp-g-AA and PA6 is the formation

of new and fresh interfacial area. That is because this is an interfacial reaction. This means that the two immiscible components are able to meet and the compatibilization reaction can take place at the interface. In general, it seems that the amount of chemical reaction between acrylic acid (PP-g-AA) and amine end group (PA6) is more stress-dependent than time-dependent. The results indicated that the amount of chemical reaction was higher for process conditions that were more aggressive in terms of mixing, regardless of the time. An increase of the extensional character in the flow imparted by the screw elements (extensional mixing elements, EME) resulted in a smaller particle size and, consequently, in higher chemical reaction amount when compared to shear dominant flows imparted by the kneading blocks.

Thus, all processing parameters like feeding rate, screw speed, screw elements and profile, residence time, etc., should be chosen in order to increase the probability of creating new and fresh interfaces between the components for interfacial reaction, which is the case of the blending reaction between PP-g-AA and PA6.



## 6 FUTURE WORK

This work provides the following insights for future research:

- A number of possible future studies using the same experimental set up are apparent. In order to broaden the understanding of reactive extrusion the on-line FTIR system can be applied to a wide variety of polymer systems, including polymer composites.
- The natural progression of this work is to apply the ATR-FTIR probe in in-line mode. The prototype was already designed, but not manufactured, and can be appreciated in appendix G. The use of FT-MIR (MID region of IR spectrum) has been vigorously challenged in recent years by a number of writers, especially when high viscous polymer systems are used, leading to a stationary layer over the ATR crystal.
- Another suggestion for future work is the development of a software that is able to treat the spectral data during the process, since the data acquisition is collected in real-time. A software for treat the data was developed in LabVIEW™ to quantify IR bands and the code can be appreciated in appendix C.



## 7 BIBLIOGRAPHY

- [1] Carson, S.O., Covas, J.A., Maia, J.M.. A new extensional mixing element for improved dispersive mixing in twin-screw extrusion, part 1: Design and computational validation. *Advances in Polymer Technology* 2015;36:455–465. doi:10.1002/adv.21627.
- [2] Covas, J.A., Carneiro, O.S., Maia, J.M., Filipe, S.A., Machado, A.V.. Evolution of chemistry, morphology and rheology of various polymer systems along a twin-screw extruder. *The Canadian Journal of Chemical Engineering* 2002;80:1065–1074.
- [3] Filipe, S., Cidade, M.T., Wilhelm, M., Maia, J.M.. Evolution of the morphological and rheological properties along the extruder length for compatibilized blends of a commercial liquid-crystalline polymer and polypropylene. *Journal of Applied Polymer Science* 2006;99:347–359. doi:10.1002/app.22393.
- [4] Pinheiro, L.A., Hu, G.H., Pessan, L.A., Canevarolo, S.V.. In-line measurements of the morphological parameters of pp/pa6 blends during extrusion in the transient mode. vol. 48. 2008, p. 806–814. doi:10.1002/pen.21009.
- [5] Pinheiro, L.A., Bitencourt, C.S., Pessan, L.A., Canevarolo, S.V.. Morphological parameters of pp/pa6 blend measured in-line during extrusion. *Macromolecular Symposia* 2006;245-246:347–354. doi:10.1002/masy.200651348.
- [6] Covas, J.A., Maia, J.M., Machado, A.V., Costa, P.. On-line rotational rheometry for extrusion and compounding operations. *Journal of Non-Newtonian Fluid Mechanics* 2008;148:88–96. doi:10.1016/j.jnnfm.2007.04.009.
- [7] Bernardo, F.O., Silva, J.M., Canevarolo, S.V.. Dispersed particle size characterization by in-line turbidimetry during polymer extrusion. *Polymer Testing* 2018;70. doi:10.1016/j.polymeresting.2018.08.005.
- [8] Machado, A.V., Covas, J.A., Duin, M.V.. Monitoring polyolefin modifica-

- tion along the axis of a twin screw extruder. i. effect of peroxide concentration. *Journal of Applied Polymer Science* 2001;81:58–68. doi:10.1002/app.1413.
- [9] Covas, J., Carneiro, O., Costa, P., Machado, A., Maia, J.. Online monitoring techniques for studying evolution of physical, rheological and chemical effects along the extruder. *Plastics, Rubber and Composites* 2004;33:55–61. URL: <http://www.tandfonline.com/doi/abs/10.1179/146580104225018300>. doi:10.1179/146580104225018300.
- [10] Machado, A.V., Covas, A.. Monitoring the evolution of the properties of pa-6/epm-g-ma blends in a twin-screw extruder. *Polymer Engineering Science* 2002;42:2032–2041.
- [11] He, Z., Zhang, F., Lei, Y., Lin, Z., Wang, M., Jin, G.. In-line characterization of dispersion uniformity evolution during a twin-screw blending extrusion based on near-infrared spectroscopy. *Polymer Engineering and Science* 2020;doi:10.1002/pen.25453.
- [12] Pinheiro, L.A., Bittencourt, C.S., Canevarolo, S.V.. Real time assessment of the compatibilization of polypropylene/polyamide 6 blends during extrusion. *Polymer Engineering Science* 2009;50:826–834. doi:10.1002/pen.21594.
- [13] Coates, P.D., Barnes, S.E., Sibley, M.G., Brown, E.C., Edwards, H.G., Scowen, I.J.. In-process vibrational spectroscopy and ultrasound measurements in polymer melt extrusion. *Polymer* 2003;44:5937–5949. doi:10.1016/S0032-3861(03)00544-5.
- [14] Machado, A.V., Covas, J.A., Duin, M.V.. Chemical and morphological evolution of pa-6/epm/epm-g-ma blends in a twin screw extruder. *Journal of Polymer Science Part a-Polymer Chemistry* 1999;37:1311–1320. doi:10.1002/(sici)1099-0518(19990501)37:9<1311::aid-pola11>3.0.co;2-y.
- [15] Machado, A.V., Maia, J.M., Canevarolo, S.V., Covas, J.A.. Evolution of peroxide-induced thermomechanical degradation of polypropylene along the extruder. *Journal of Applied Polymer Science* 2004;91:2711–



2720. doi:10.1002/app.13476.
- [16] Filipe, S., Cidade, M.T., Wilhelm, M., Maia, J.M.. Evolution of morphological and rheological properties along the extruder length for blends of a commercial liquid crystalline polymer and polypropylene. *Polymer* 2004;45:2367–2380. doi:10.1016/j.polymer.2003.12.080.
- [17] Maia, J.M., Carneiro, O.S., Machado, A.V., Covas, J.A.. On-line rheometry for twin-screw extrusion (along the extruder) and its applications. *Applied Rheology* 2002;12:18–24. doi:10.1515/arh-2002-0002.
- [18] Covas, J.A., Nóbrega, J.M., Maia, J.M.. Rheological measurements along an extruder with an on-line capillary rheometer. *Polymer Testing* 2000;19:165–176. doi:10.1016/S0142-9418(98)00086-5.
- [19] Rohe, T., Becker, W., Krey, A., Nägele, H., Kölle, S., Eisenreich, N.. In-line monitoring of polymer extrusion processes by nir spectroscopy. *Journal of Near Infrared Spectroscopy* 1998;6:325–333.
- [20] Fischer, D., Sahre, K., Abdelrhim, M., Voit, B., Sadhu, V.B., Pionteck, J., et al. Process monitoring of polymers by in-line atr-ir, nir and raman spectroscopy and ultrasonic measurements. *Comptes Rendus Chimie* 2006;9:1419–1424. doi:10.1016/j.crci.2006.06.006.
- [21] Saerens, L., Dierickx, L., Quinten, T., Adriaensens, P., Carleer, R., Vervaet, C., et al. In-line nir spectroscopy for the understanding of polymer-drug interaction during pharmaceutical hot-melt extrusion. *European Journal of Pharmaceutics and Biopharmaceutics* 2012;81:230–237. URL: <http://dx.doi.org/10.1016/j.ejpb.2012.01.001>. doi:10.1016/j.ejpb.2012.01.001.
- [22] Porep, J.U., Kammerer, D.R., Carle, R.. On-line application of near infrared (nir) spectroscopy in food production. *Trends in Food Science and Technology* 2015;46:211–230. URL: <http://dx.doi.org/10.1016/j.tifs.2015.10.002>. doi:10.1016/j.tifs.2015.10.002.
- [23] Reed, W.F.. *Monitoring Polymerization Reactions : From Fundamentals to Applications*. Wiley; 2013. ISBN 9780470917381.

- [24] Marziano, I., Sharp, D.C., Dunn, P.J., Hailey, P.A.. On-line mid-ir spectroscopy as a real-time approach in monitoring hydrogenation reactions. *Organic Process Research and Development* 2000;4:357–361. doi:10.1021/op000030m.
- [25] Bicalho, L.A., Covas, J.A., Canevarolo, S.V.. Online optical monitoring of polymer melting in a twin-screw extruder. *Polymer Engineering and Science* 2020;60:2163–2175. doi:10.1002/pen.25460.
- [26] Asemani, M., Rabbani, A.R.. Detailed ftir spectroscopy characterization of crude oil extracted asphaltenes: Curve resolve of overlapping bands. *Journal of Petroleum Science and Engineering* 2020;185. doi:10.1016/j.petrol.2019.106618.
- [27] Keles, H., Naylor, A., Clegg, F., Sammon, C.. The application of non-linear curve fitting routines to the analysis of mid-infrared images obtained from single polymeric microparticles. *Analyst* 2014;139:2355–2369. doi:10.1039/c3an01879b.
- [28] Manohar, N., Jayaramudu, J., Suchismita, S., Rajkumar, K., Reddy, A.B., Sadiku, E.R., et al. A unique application of the second order derivative of ftir–atr spectra for compositional analyses of natural rubber and polychloroprene rubber and their blends. *Polymer Testing* 2017;62:447–453. URL: <http://dx.doi.org/10.1016/j.polymertesting.2017.07.030>. doi:10.1016/j.polymertesting.2017.07.030.
- [29] Parker, F.S.. *Applications of Infrared Spectroscopy in Biochemistry, Biology, and Medicine*. Springer US; 1971. doi:10.1007/978-1-4684-1872-9.
- [30] Tooke, P., Espen, P.V., Nobels, J., Limbourg, J., Janssens, K., Van, P.. *Fourier self-deconvolution in ir spectroscopy*. 1986.
- [31] Zhang, H.C., hao Kang, B., Chen, L.S., Lu, X.. Enhancing toughness of poly (lactic acid)/thermoplastic polyurethane blends via increasing interface compatibility by polyurethane elastomer prepolymer and its toughening mechanism. *Polymer Testing* 2020;87. doi:10.1016/j.polymertesting.2020.106521.

- [32] Nahar, S., Tajmir-Riahi, H.A., Carpentier, R.. A quantitative analysis of protein secondary structure of photosystem ii particles and light-harvesting complex of chloroplast thylakoid membranes by ft-ir spectroscopy. 1994.
- [33] Max, J.J., Chapados, C.. Infrared spectroscopy of acetone-water liquid mixtures. i. factor analysis. *Journal of Chemical Physics* 2003;119:5632–5643. doi:10.1063/1.1600438.
- [34] Saerens, L., Vervaet, C., Remon, J.P., Beer, T.D.. Process monitoring and visualization solutions for hot-melt extrusion: A review. *Journal of Pharmacy and Pharmacology* 2014;66:180–203. doi:10.1111/jphp.12123.
- [35] Carson, S.O., Maia, J.M., Covas, J.A.. A new extensional mixing element for improved dispersive mixing in twin-screw extrusion, part 2: Experimental validation for immiscible polymer blends. 2016. doi:10.1002/adv.21653.
- [36] Formela, K., Hejna, A., Haponiuk, J., Tercjak, A.. *In situ processing of biocomposites via reactive extrusion*. Elsevier Ltd.; 2017. ISBN 9780081007938. URL: <http://linkinghub.elsevier.com/retrieve/pii/B9780081007938000089>. doi:10.1016/B978-0-08-100793-8.00008-9.
- [37] Bock, J.E., Deiters, P.. Laboratory-scale extrusion: Open the black box of extrusion processing for improved product development. *Cereal Foods World* 2017;62:151–155. doi:10.1094/CFW-62-4-0151.
- [38] Matić, J., Alva, C., Witschnigg, A., Eder, S., Reusch, K., Paudel, A., et al. Towards predicting the product quality in hot-melt extrusion: Small scale extrusion. *International Journal of Pharmaceutics: X* 2020;2. doi:10.1016/j.ijpx.2020.100062; feed rate em RTD.
- [39] Zhang, P., Xu, D., Xiao, R.. Morphology development and size control of pa6 nanofibers from pa6/cab polymer blends. *Journal of Applied Polymer Science* 2015;132. doi:10.1002/app.42184.
- [40] Kim, B.J., White, J.L.. Thermal/peroxide induced degradation and maleation of polypropylene by reactive extrusion. *International Polymer Processing* 1995;X:213–220. URL: [www.hanser-elibrary.com](http://www.hanser-elibrary.com).
- [41] Kolter, K., Karl, M., Gryczke, A.. *Introduction to Solid Dispersions*. 2012.

ISBN 9783000394157.

- [42] Haser, A., Haight, B., Berghaus, A., Machado, A., Martin, C., Zhang, F.. Scale-up and in-line monitoring during continuous melt extrusion of an amorphous solid dispersion. *AAPS PharmSciTech* 2018;19:2818–2827. doi:10.1208/s12249-018-1162-5.
- [43] Sasimowski, E., Majewski, L., Grochowicz, M.. Influence of the design solutions of extruder screw mixing tip on selected properties of wheat bran-polyethylene biocomposite. *Polymers* 2019;11. doi:10.3390/polym11122120.
- [44] Pandey, V., Chen, H., Ma, J., Maia, J.M.. Extension-dominated improved dispersive mixing in single-screw extrusion. part 2: Comparative analysis with twin-screw extruder. *Journal of Applied Polymer Science* 2021;138. doi:10.1002/app.49765.
- [45] Maia, J., Chen, H., Pandey, V., Carson, S.. Enhanced dispersive mixing in twin-screw extrusion via extension-dominated staticmixing elements of varying contraction ratio. *International Polymer Processing* 2020;.
- [46] Dickson, A., Teuber, L., Gaugler, M., Sandquist, D.. Effect of processing conditions on wood and glass fiber length attrition during twin screw composite compounding. *Journal of Applied Polymer Science* 2020;137. doi:10.1002/app.48551.
- [47] Irfan, M.S., Umer, R., Rao, S.. Optimization of compounding parameters for extrusion to enhance mechanical performance of kenaf-polypropylene composites. *Fibers and Polymers* 2021;22:1378–1387. doi:10.1007/s12221-021-0676-8.
- [48] Chen, K., Cui, Y., Wang, S., Xue, P., Yang, Q., Jia, M.. Characterization of plasticizing process of single screw extruder with grooved melting zone. *Journal of Polymer Research* 2020;27. URL: <https://doi.org/10.1007/s10965-020-2041-9>. doi:10.1007/s10965-020-2041-9/Published.
- [49] Danda, C., Pandey, V., Schneider, T., Norman, R., Maia, J.M.. Enhanced dispersion and mechanical behavior of polypropylene composites com-

- pounded using extension-dominated extrusion. *International Polymer Processing* 2020;XXV:1–21.
- [50] Danda, C., Amurin, L.G., Munoz, P.A.R., Nagaoka, D.A., Schneider, T., Troxell, B., et al. Integrated computational and experimental design of design of ductile, abrasion resistant thermoplastic polyurethane/graphene oxide nanocomposites. *ACS Applied Nano Materials* 2020;3:9694–9705.
- [51] Tadmor, Z., Gogos, C.G.. *Principles of polymer Processing*. 2006.
- [52] Zhu, J., Abeykoon, C., Karim, N.. Investigation into the effects of fillers in polymer processing. *International Journal of Lightweight Materials and Manufacture* 2021;4:370–382. doi:10.1016/j.ijlmm.2021.04.003.
- [53] Mirzadeh, A., Ghasemi, H., Mahrous, F., Kamal, M.R.. Reactive extrusion effects on rheological and mechanical properties of poly(lactic acid)/poly[(butylene succinate)-co-adipate]/epoxy chain extender blends and clay nanocomposites. 2015. doi:10.1002/app.42889.
- [54] Matic, J., Witschnigg, A., Zagler, M., Eder, S., Khinast, J.. A novel in silico scale-up approach for hot melt extrusion processes. *Chemical Engineering Science* 2019;204:257–269. doi:10.1016/j.ces.2019.04.016.
- [55] da R. Mandarino, B., da Silva, A.L.N., Michel, R.C.. A new in-line optical system for monitoring residence time during polymer processing along a twin-screw extruder. *Macromolecular Symposia* 2020;394. doi:10.1002/masy.202000065.
- [56] Baron, R., Vauchel, P., Kaas, R., Arhaliass, A., Legrand, J.. Dynamical modelling of a reactive extrusion process: Focus on residence time distribution in a fully intermeshing co-rotating twin-screw extruder and application to an alginate extraction process. *Chemical Engineering Science* 2010;65:3313–3321. doi:10.1016/j.ces.2010.02.019.
- [57] Canevarolo, S.V., Melo, T.J.A., Covas, J.A., Carneiro, O.S.. Direct method for deconvoluting two residence time distribution curves. *International Polymer Processing* 2001;XVI:334–340. URL: [www.hanser-elibrary.com](http://www.hanser-elibrary.com).
- [58] Cassagnau, P., Bounor-Legaré, V., Vergnes, B.. Experimental and mo-

- deling aspects of the reactive extrusion process. *Mechanics and Industry* 2019;20. URL: <https://doi.org/10.1051/meca/2019052>. doi:10.1051/meca/2019052.
- [59] Lu, J., Obara, S., Ioannidis, N., Suwardie, J., Gogos, C., Kikuchi, S.. Understanding the processing window of hypromellose acetate succinate for hot-melt extrusion, part i: Polymer characterization and hot-melt extrusion. *Advances in Polymer Technology* 2018;37:154–166. doi:10.1002/adv.21652.
- [60] Beyer, G., Hopmann, C.. *Reactive extrusion : principles and applications*. 2017. ISBN 9783527340989.
- [61] Polosin, A.N., Chistyakova, T.B.. *Mathematical modeling for resource and energy saving control of extruders in multi-assortment productions of polymeric films*. vol. 1015. Institute of Physics Publishing; 2018,doi:10.1088/1742-6596/1015/3/032104.
- [62] Danckwerts, P.V.. *Continuous flow systems. distribution of residence times*. *Chemical Engineering Science Genie Chimique* 1958;2:1–18.
- [63] Rodrigues, A.E.. *Residence time distribution (rtd) revisited*. *Chemical Engineering Science* 2021;230. doi:10.1016/j.ces.2020.116188.
- [64] Chen, J.Y., Tseng, C.C., Huang, M.S.. *Quality indexes design for online monitoring polymer injection molding*. *Advances in Polymer Technology* 2019;2019. doi:10.1155/2019/3720127.
- [65] Shirazian, S., Zeglinski, J., Darwish, S., Kuhs, M., Albadarin, A.B., Croker, D.M., et al. *Continuous twin screw wet granulation: The combined effect of process parameters on residence time, particle size, and granule morphology*. *Journal of Drug Delivery Science and Technology* 2018;48:319–327. doi:10.1016/j.jddst.2018.09.016.
- [66] Verma, T., Subbiah, J.. *Use of residence time versus screw speed in the response surface model for microbial inactivation during single-screw extrusion of low-moisture food*. *Food Control* 2020;115. doi:10.1016/j.foodcont.2020.107293.

- [67] Covas, J.A.. In-process measurements for reactive extrusion monitoring and control. 2018.
- [68] Tzoganakis, C.. Reactive extrusion of polymers: A review. *Advances in polymer Technology* 1989;9:321–330.
- [69] Cassagnau, P., Bounor-Legaré, V., Fenouillot, F.. Reactive processing of thermoplastic polymers: A review of the fundamental aspects. *International Polymer Processing* 2007;XXII. URL: [www.hanser-elibrary.com](http://www.hanser-elibrary.com).
- [70] Matić, J., Alva, C., Eder, S., Reusch, K., Paudel, A., Khinast, J.. Towards predicting the product quality in hot-melt extrusion: Pilot plant scale extrusion. *International Journal of Pharmaceutics*: X 2021;3. doi:10.1016/j.ijpx.2021.100084.
- [71] Ibañez, R., Casteran, F., Argerich, C., Ghnatios, C., Hascoet, N., Ammar, A., et al. On the data-driven modeling of reactive extrusion. *Fluids* 2020;5. doi:10.3390/fluids5020094.
- [72] Nakayama, Y., Kajiwara, T., Masaki, T.. Strain mode of general flow: Characterization and implications for flow pattern structures. *AIChE Journal* 2016;62:2563–2569. doi:10.1002/aic.15228.
- [73] Brittain, H.G.. Mid-infrared spectroscopy of pharmaceutical solids. *Profiles of Drug Substances, Excipients and Related Methodology* 2018;:1–38 URL: <http://dx.doi.org/10.1016/bs.podrm.2017.12.002>. doi:10.1016/bs.podrm.2017.12.002.
- [74] Moghaddam, L., Martin, D.J., Halley, P.J., Fredericks, P.M.. Vibrational spectroscopic studies of laboratory scale polymer melt processing: Application to a thermoplastic polyurethane nanocomposite. *Vibrational Spectroscopy* 2009;51:86–92. doi:10.1016/j.vibspec.2008.10.015.
- [75] Spectroscopy, I.. Infrared spectroscopy : Theory. *Journal of Molecular Spectroscopy* 2002;214:155–164. URL: <http://onlinelibrary.wiley.com/doi/10.1002/0470027320.s0103/full>. doi:10.1006/jmsp.2002.8570.
- [76] Ghosh, S.N.. *Ir spectroscopy*. 2001.
- [77] Colthup, N.B.. *Infrared spectroscopy*. American Cyanamid Company

2001;

- [78] Zhang, P.. Transducers and valves. 2010. doi:10.1016/b978-1-4377-7807-6.10004-x.
- [79] Lin, H., Ying, Y.. Theory and application of near infrared spectroscopy in assessment of fruit quality: A review. *Sensing and Instrumentation for Food Quality and Safety* 2009;3:130–141. doi:10.1007/s11694-009-9079-z.
- [80] Stuart, B.H.. *Infrared Spectroscopy: Fundamentals and Applications*; vol. 8. 2004. ISBN 9780470011140. URL: <http://doi.wiley.com/10.1002/0470011149>. doi:10.1002/0470011149.
- [81] Kristo, M.J.. Nuclear forensics. 2012. doi:10.1016/B978-0-12-384873-4.00021-9.
- [82] Quirk, R.P., Pickel, D.L.. Controlled end-group functionalization (including telechelics). 2012. doi:10.1016/B978-0-444-53349-4.00168-0.
- [83] Shaw, R.A., Mantsch, H.H.. *Near-ir spectrometers*. 1999.
- [84] Ready, F.J.. Principles used in measurement. 1997. doi:<https://doi.org/10.1016/B978-0-12-583961-7.X5000-5>.
- [85] Hauchecorne, B., Lenaerts, S.. Unravelling the mysteries of gas phase photocatalytic reaction pathways by studying the catalyst surface: A literature review of different fourier transform infrared spectroscopic reaction cells used in the field. 2013. doi:10.1016/j.jphotochemrev.2012.09.003.
- [86] Groves, D., Wachtman, J.B., Washington, D.C., Piscataway, N.J.. *Materials characterization-vital and often successful, yet still a critical problem*. 1986.
- [87] Bowler, A.L., Bakalis, S., Watson, N.J.. A review of in-line and on-line measurement techniques to monitor industrial mixing processes. *Chemical Engineering Research and Design* 2020;153:463–495. doi:10.1016/j.cherd.2019.10.045.
- [88] Tumuluri, V.S., Kemper, M.S., Lewis, I.R., Prodduturi, S., Majumdar, S., Avery, B.A., et al. Off-line and on-line measurements of drug-loaded hot-melt extruded films using raman spectroscopy. *International Journal of*



- Pharmaceutics 2008;357:77–84. doi:10.1016/j.ijpharm.2008.01.036.
- [89] Klozinski, A., Barczewski, M.. Comparison of off-line, on-line and in-line measuring techniques used for determining the rheological characteristics of polyethylene composites with calcium carbonate. *Polimery/Polymers* 2019;64:83–92. doi:10.14314/polimery.2019.2.1.
- [90] Callis, J.B., Lllman, D.L., Kowalski, B.R.. *Process Analytical*; vol. 59. 1987. doi:10.1021/ac00136a001.
- [91] Mould, S., Barbas, J., MacHado, A.V., Nóbrega, J.M., Covas, J.A.. Measuring the rheological properties of polymer melts with on-line rotational rheometry. *Polymer Testing* 2011;30:602–610. URL: <http://dx.doi.org/10.1016/j.polymertesting.2011.05.002>. doi:10.1016/j.polymertesting.2011.05.002.
- [92] Reshadat, R., Desa, S., Joseph, S., Mehra, M., Stoev, N., Balke, S.T.. In-line near-infrared monitoring of polymer processing. part i: Process/monitor interface development. *APPLIED SPECTROSCOPY* 1999;53.
- [93] Barros, L.P., Canevarolo, S.V., Klein, D., Maia, J.. On-line atmir for real-time quantification of chemistry kinetics along the barrel in extrusion-based processes. *Polymer Testing* 2021;103:107350. URL: <https://doi.org/10.1016/j.polymertesting.2021.107350>. doi:10.1016/j.polymertesting.2021.107350.
- [94] Soares, K., Santos, A.M.D.C., Canevarolo, S.V.. In-line rheo-polarimetry: A method to measure in real time the flow birefringence during polymer extrusion. *Polymer Testing* 2011;30:848–855. doi:10.1016/j.polymertesting.2011.08.007.
- [95] Teixeira, P.F., Ferrás, L.L., Hilliou, L., Covas, J.A.. A new double-slit rheometrical die for in-process characterization and extrusion of thermo-mechanically sensitive polymer systems. *Polymer Testing* 2018;66:137–145. doi:10.1016/j.polymertesting.2018.01.013.
- [96] Teixeira, P.F., Covas, J.A., Hilliou, L.. In-process assessment of clay

- dispersion in pla during melt compounding: Effects of screw speed and filler content. *Polymer Degradation and Stability* 2020;177. doi:10.1016/j.polymdegradstab.2020.109190.
- [97] Huang, X., Lei, Y., Wang, M., Jin, G.. In-line monitoring of component content of polypropylene/polystyrene blends during melt extrusion using raman spectroscopy. *Journal of Raman Spectroscopy* 2018;49:513–519. doi:10.1002/jrs.5309.
- [98] Stuart, B.. *Infrared spectroscopy*. 2015. URL: <http://doi.wiley.com/10.1002/0471238961.0914061810151405.a01.pub3>. doi:10.1002/0471238961.0914061810151405.a01.pub3.
- [99] Melling, P.J., Thomson, M., Chalmers, J.M., Editors, P.R.G.. *Fiber-optic probes for mid-infrared spectrometry fiber-optic probes for mid-infrared spectrometry*. *Handbook of Vibrational Spectroscopy* John 2002;doi:10.1002/0470027320.s2703.
- [100] Rajan, V.V., Wäber, R., Wieser, J.. Online monitoring of the thermal degradation of pom during melt extrusion. *Journal of Applied Polymer Science* 2010;115:2394–2401. doi:10.1002/app.31209.
- [101] Haberstroh, E., Jakisch, L., Henßge, E., Schwarz, P.. *Real-time monitoring of reactive extrusion processes by means of in-line infrared spectroscopy and infrared temperature measurement*. 2002.
- [102] Qin, Y.. *Applications of advanced technologies in the development of functional medical textile materials*. 2016. doi:10.1016/b978-0-08-100618-4.00005-4.
- [103] Shashidhara, G.M., Biswas, D., Pai, B.S., Kadiyala, A.K., Ferroze, G.S.W., Ganesh, M.. Effect of pp-g-mah compatibilizer content in polypropylene/nylon-6 blends. *Polymer Bulletin* 2009;63:147–157. doi:10.1007/s00289-009-0074-7.
- [104] Niaounakis, M.. *Blending*. 2015. URL: <https://linkinghub.elsevier.com/retrieve/pii/B9780323266987000039>. doi:10.1016/B978-0-323-26698-7.00003-9.

- [105] Tomić, N.Z., Marinković, A.D.. Compatibilization of polymer blends by the addition of graft copolymers. 2019. doi:10.1016/B978-0-12-816006-0.00004-9.
- [106] Mekonnen, T.H., Misra, M., Mohanty, A.K.. Processing, performance, and applications of plant and animal protein-based blends and their biocomposites. 2015. doi:10.1016/B978-1-78242-373-7.00017-2.
- [107] Litmanovich, A.D., Plate, N.A., Kudryavtsev, Y.V., Topchiev, A.V.. Reactions in polymer blends: interchain effects and theoretical problems. *Progress in Polymer Science* 2002;27:915–970. URL: [www.elsevier.com/locate/ppolysci](http://www.elsevier.com/locate/ppolysci).
- [108] Zhou, X., Zhang, P., Jiang, X., Rao, G.. Influence of maleic anhydride grafted polypropylene on the miscibility of polypropylene/polyamide-6 blends using atr-ftir mapping. *Vibrational Spectroscopy* 2009;49:17–21. doi:10.1016/j.vibspec.2008.04.004.
- [109] Wilks, P.A., Hirschfeld, T.. Internal reflection spectroscopy. *Applied Spectroscopy Reviews* 1967;1:99–130. doi:10.1080/05704926708547582.
- [110] Cho, S., Hong, J.S., Lee, S.J., Ahn, K.H., Covas, J.A., Maia, J.M.. Morphology and rheology of polypropylene/polystyrene/clay nanocomposites in batch and continuous melt mixing processes. *Macromolecular Materials and Engineering* 2011;296:341–348. doi:10.1002/mame.201000194.
- [111] Lu, M., Keskkula, H., Paul, D.R.. Acrylic acid containing copolymers as reactive compatibilizers for toughening nylon 6. *Polymer Engineering and Science* 1994;34.
- [112] Xu, W., Liang, G., Zhai, H., Tang, S., Hang, G., Pan, W.P.. Preparation and crystallization behaviour of pp/pp-g-mah/org-mmt nanocomposite. *European Polymer Journal* 2003;39:1467–1474. doi:10.1016/S0014-3057(03)00015-6.
- [113] Lee, H.G., Sung, Y.T., Lee, Y.K., Kim, W.N., Yoon, H.G., Lee, H.S.. Effects of pp-g-mah on the mechanical, morphological and rheological properties of polypropylene and poly(acrylonitrile-butadiene-styrene) blends.

2009.

- [114] Sathe, S.N., Devi, S., Rao, G.S.S., Rao, K.V.. Relationship between morphology and mechanical properties of binary and compatibilized ternary blends of polypropylene and nylon 6. *Journal of Applied Polymer Science* 1996;61:97–107. URL: [http://linkinghub.elsevier.com/retrieve/pii/0014305790901765%5Cnhttp://doi.wiley.com/10.1002/\(SICI\)1097-4628\(19960705\)61:1%3C97::AID-APP11%3E3.0.CO;2-X](http://linkinghub.elsevier.com/retrieve/pii/0014305790901765%5Cnhttp://doi.wiley.com/10.1002/(SICI)1097-4628(19960705)61:1%3C97::AID-APP11%3E3.0.CO;2-X). doi:10.1002/(SICI)1097-4628(19960705)61:1<97::AID-APP11>3.0.CO;2-X.
- [115] Kitayama, N., Keskkula, H., Paul, D.R.. Reactive compatibilization of nylon 6/styrene-acrylonitrile copolymer blends. part 1. phase inversion behavior. *Polymer* 2000;41:8041–8052. URL: [www.elsevier.nl/locate/polymer](http://www.elsevier.nl/locate/polymer).
- [116] Roeder, J., Oliveira, R.V.B., Gonçalves, M.C., Soldi, V., Pires, A.T.N.. Polypropylene/polyamide-6 blends: Influence of compatibilizing agent on interface domains. *Polymer Testing* 2002;21:815–821. doi:10.1016/S0142-9418(02)00016-8.
- [117] Plyler, E.K.. Infrared spectra of methanol, ethanol and n-propanol. *Journal of Research of the National Bureau of Standards* 1952;4.
- [118] Iwamoto, R., Murase, H.. Infrared spectroscopic study of the interactions of nylon-6 with water. 2003.
- [119] Andreassen, E.. *Polypropylene: an A-Z reference*. Springer Netherlands; 1999. ISBN 978-94-010-5899-5. URL: <http://link.springer.com/10.1007/978-94-011-4421-6>. doi:10.1007/978-94-011-4421-6.
- [120] Blitz, J.P., Klarup, D.G.. *Signal-to-noise ratio, signal processing, and spectral w information in the instrumental analysis laboratory*. 2002.
- [121] Chan, K.L.A., Kazarian, S.G.. *New opportunities in micro-and macro-attenuated total re ection infrared spectroscopic imaging: Spatial resolution and sampling versatility*. 2003.
- [122] Rytwo, G., Zakai, R., Wicklein, B.. The use of atr-ftir spectroscopy for quantification of adsorbed compounds. *Journal of Spectroscopy*

- 2015;2015. doi:10.1155/2015/727595.
- [123] Qiu, K., Song, X., Lai, Y., Wu, L., Tang, G., Min, S.. Comparison of atr/transmittance ftir combined with beer's law and pls to determine fipronil in matrine formulation. *Analytical Methods* 2013;5:4790–4797. doi:10.1039/c3ay40406d.
- [124] Emin, M.A., Schuchmann, H.P.. Droplet breakup and coalescence in a twin-screw extrusion processing of starch based matrix. *Journal of Food Engineering* 2013;116:118–129. doi:10.1016/j.jfoodeng.2012.12.010.
- [125] Novais, R.M., Covas, J.A., Paiva, M.C.. The effect of flow type and chemical functionalization on the dispersion of carbon nanofiber agglomerates in polypropylene. *Composites Part A: Applied Science and Manufacturing* 2012;43:833–841. doi:10.1016/j.compositesa.2012.01.017.
- [126] Jamali, S., Paiva, M.C., Covas, J.A.. Dispersion and re-agglomeration phenomena during melt mixing of polypropylene with multi-wall carbon nanotubes. *Polymer Testing* 2013;32:701–707. doi:10.1016/j.polymertesting.2013.03.005.
- [127] Woods, J.W.. Image perception and sensing. 2012. doi:10.1016/b978-0-12-381420-3.00006-0.
- [128] Carneiro, O.S., Covas, J.A., Ferreira, J.A., Cerqueira, M.F.. On-line monitoring of the residence time distribution along a kneading block of a twin-screw extruder. *Polymer Testing* 2004;23:925–937. doi:10.1016/j.polymertesting.2004.05.001.
- [129] Wake, N., Vincent, J., Robb, F.. Chapter 2 - medical imaging technologies and imaging considerations for 3d printed anatomic models. In: Wake, N., editor. *3D Printing for the Radiologist*. Elsevier. ISBN 978-0-323-77573-1; 2022, p. 11–29. URL: <https://www.sciencedirect.com/science/article/pii/B9780323775731000051>. doi:<https://doi.org/10.1016/B978-0-323-77573-1.00005-1>.
- [130] Jeon, H.K., Kim, J.K.. Effect of reaction rate'on morphological change of reactive blends. *Macromolecules* 2000;33:8200–8210. doi:10.1021/

ma000842i.

- [131] Schulze, J.S., Cernohous, J.J., Hirao, A., Lodge, T.P., Macosko, C.W.. Reaction kinetics of end-functionalized chains at a polystyrene/poly(methyl methacrylate) interface. *Macromolecules* 2000;33:1191–1198. doi:10.1021/ma9911344.
- [132] Bouteiller, Y., Perchard, J.P.. The vibrational spectrum of (h<sub>2</sub>o)<sub>2</sub>: Comparison between anharmonic ab initio calculations and neon matrix infrared data between 9000 and 90 cm<sup>-1</sup>. *Chemical Physics* 2004;305:1–12. doi:10.1016/j.chemphys.2004.06.028.
- [133] Monsoor, M.A., Kalapathy, U., Proctor, A.. Improved method for determination of pectin degree of esterification by diffuse reflectance fourier transform infrared spectroscopy. *Journal of Agricultural and Food Chemistry* 2001;49:2756–2760. doi:10.1021/jf0009448.
- [134] Corujo, M.P., Sklepari, M., Ang, D.L., Millichip, M., Reason, A., Goodchild, S.C., et al. Infrared absorbance spectroscopy of aqueous proteins: Comparison of transmission and atr data collection and analysis for secondary structure fitting. *Chirality* 2018;30:957–965. doi:10.1002/chir.23002.
- [135] Averett, L.A., Griffiths, P.R., Nishikida, K.. Effective path length in attenuated total reflection spectroscopy. *Analytical Chemistry* 2008;80:3045–3049. doi:10.1021/ac7025892.
- [136] Chen, J., Gardella, J.A.. Quantitative atr ft-ir analysis of surface segregation of polymer blends of polystyrene/poly(dimethylsiloxane)-copolymer. 1998.
- [137] Ohlsson, B., Hassander, H., Tornell, B.. Effect of the mixing procedure on the morphology and properties of compatibilized polypropylene/polyamide blends. *Polymer* 1998;39:4715–4721.
- [138] Sui, G., Jing, M., Zhao, J., Wang, K., Zhang, Q., Fu, Q.. A comparison study of high shear force and compatibilizer on the phase morphologies and properties of polypropylene/polylactide (pp/pla) blends. *Polymer* 2018;154:119–127. doi:10.1016/j.polymer.2018.09.005.

- [139] Yoshida, S.. Quantitative evaluation of an epoxy resin dispersion by infrared spectroscopy. *Polymer Journal* 2014;46:430–434. URL: <http://dx.doi.org/10.1038/pj.2014.15>. doi:10.1038/pj.2014.15.
- [140] Kohlgruber, K.. Co-rotating twin-screw extruder : fundamentals, technology, and applications. Hanser; 2007. ISBN 9783446413726.
- [141] Manas-Zloczower, I.. Mixing and compounding of polymers: theory and practice. 2009.
- [142] Li, S., He, G., Liao, X., Park, C.B., Yang, Q., Li, G.. Introduction of a lon-chain branching structure by ultraviolet-induced reactive extrusion to improve cell morphology and processing properties of polylactide foam. Royal Society of Chemistry 2017;7.
- [143] Zheng, L., Geng, Z., Zhen, W.. Preparation, characterization, and reaction kinetics of poly (lactic acid)/amidated graphene oxide nanocomposites based on reactive extrusion process. *Journal of Polymer Research* 2019;26. doi:10.1007/s10965-019-1722-8.
- [144] hua Hu, G., Lambla, M.. 6 fundamentals of reactive extrusion : An overview. 2006.
- [145] Yeh, A.I., Jaw, Y.M.. Effects of feed rate and screw speed on operating characteristics and extrudate properties during single-screw extrusion cooking of rice flour. *Cereal Chemistry* 1999;76:236–242. doi:10.1094/CCHEM.1999.76.2.236.
- [146] Yeh, A.I., Hwang, S.J., Guo, J.J.. Effects of screw speed and feed rate on residence time distribution and axial mixing of wheat flour in a twin-screw extruder. 1992.
- [147] Wilczyński, K., Lewandowski, A., Wilczyński, K.J.. Experimental study for starve-fed single screw extrusion of thermoplastics. *Polymer Engineering and Science* 2012;52:1258–1270. doi:10.1002/pen.23076.
- [148] Jinescu, V., Sporea, N.. Twin screw extruders optimization. *Material PLastiche* 2009;46. URL: <https://www.researchgate.net/publication/286502978>.

- [149] Pinto, G., Tadmor, Z.. Mixing and residence time distribution in melt screw extruders. *Polymer Engineering and Science* 1970;10.
- [150] Puaux, J.P., Bozga, G., Ainsler, A.. Residence time distribution in a corotating twin-screw extruder. 2000.
- [151] Chuang, G.C.C., Yeh, A.I.. Effect of screw profile on residence time distribution and starch gelatinization of rice flour during single screw extrusion cooking. *Journal of Food Engineering* 2004;63:21–31. doi:10.1016/S0260-8774(03)00278-4.
- [152] Wang, J., Yang, J., Sundén, B., Wang, Q.. Assessment of flow pattern and temperature profiles by residence time distribution in typical structured packed beds. *Numerical Heat Transfer; Part A: Applications* 2020;77:559–578. doi:10.1080/10407782.2020.1713694.
- [153] Dalbhat, C.G., Mishra, H.N.. Effects of extrusion process conditions on system parameters; physicochemical properties and cooking characteristics of extruded fortified rice kernels. *Journal of Cereal Science* 2019;89. doi:10.1016/j.jcs.2019.05.016.
- [154] Breslow, R., Tirrel, M.K., Barton, J.K., Barteau, M.A.. *Beyond the Molecular Frontier*. National Academies Press; 2003. doi:10.17226/10633.
- [155] Cogswell, F.N.. *Converging flow and stretching flow: A compilation \**. 1978.
- [156] Mangadlao, J.D., Huang, R., Foster, E.L., Pangilinan, K.D., Danda, C., Advincula, A., et al. Graphene oxide – poly ( ethylene glycol ) methyl ether methacrylate nanocomposite hydrogels. *Macromolecular Chemistry and Physics* 2016;:101–107.
- [157] Macosko, C.W., Jeon, H.K., Hoyer, T.R.. Reactions at polymer-polymer interfaces for blend compatibilization. vol. 30. 2005, p. 939–947. doi:10.1016/j.progpolymsci.2005.06.003.
- [158] He, M., Wang, J., Wang, Z., Mo, J., Zhang, J., Zhen Fan, X., et al. Effects of side chains in compatibilizers on interfacial adhesion of immiscible plla/abs blends. *Materials Chemistry and Physics* 2021;262. doi:10.1016/j.matchemphys.2021.124219.



- [159] Zhao, T., Ai, J., Wang, P., Tong, W., Ding, C., Cen, Y., et al. Research of the influence factors on transesterification reaction degree in pc/pbt blends. *Advanced Industrial and Engineering Polymer Research* 2019;2:203–208. doi:10.1016/j.aiepr.2019.09.005.
- [160] da Silva, D.F., Araújo, E.M., de Melo, T.J.A.. Development of polyamide 6/compound by recycled rubber blends using graphitized polyethylene or polypropylene with maleic anhydride as compatibilizer agent. *Journal of Aerospace Technology and Management* 2013;5:231–240. doi:10.5028/jatm.v5i2.164.
- [161] Devaux, J., Godard, P., Mercier, J.P., Polymgres, H., Touillaux, R., Dereppe, J.M.. Bisphenol-a polycarbonate-poly( butylene terephthalate) transesterification. 11. structure analysis of the reaction products by ir and lh and 13c nmr. *Journal of Polymer Science: Polymer Physics* 1982;20:1881–1894.
- [162] Montaudo, G., Puglisi, C., Samperi, F.. Mechanism of exchange in pbt/pc and pet/pc blends. composition of the copolymer formed in the melt mixing process. *Macromolecules* 1998;31:650–661. URL: <https://pubs.acs.org/sharingguidelines>.



## APPENDIX A: COMPONENTS OF THE ON-LINE FTIR SPECTROSCOPY SYSTEM




Figura 7.1: On-line FTIR system attached to the extruder. In the picture the temperature control system, the PHU, the air cooling system and the ATR-FTIR probe is shown



(a) ATR-FTIR probe.

Common Parameters of HT-ATR-Probes for High Temperatures <i>FlexiSpec</i> ®	
Total Length	2m (opt. up to 5m)*
Shaft Length	300 mm (opt.: 300-700 mm)*
Shaft Diameter	12mm
Shaft Material	Hastelloy C22
Length of Legs	500mm (opt.: 300mm to 500mm)
Protective Tube Material	Liquid Tight SS-Conduit, KOPEX-Tube
Minimal Bending Radius	130mm
Input / Output Connectors	Long SMA (opt.: any other type)
Cooling Air Flow Parameters	Excess pressure 0.5Bar, Flow 2300l/h
Inner temperature control	Inside the shaft to control ATR tip temperature



(b) ATR-FTIR probe parameters.

Figura 7.2: a) ATR-FTIR probe and b) parameters.



Figura 7.3: Nicolet IS 10 MID (4000 to 400  $\text{cm}^{-1}$ ) infrared spectrometer (ThermoFisher Scientific).

Specification of IR-Fiber HT-ATR-Probes for High Temperatures <i>FlexiSpec</i>			
Probe type	Diamond ATR	Silicon	Cubic Zirconium ATR
Transmission range	5.2-17 $\mu\text{m}$ (600-1900 $\text{cm}^{-1}$ ) + 3.2-4.5 $\mu\text{m}$ (2300-3100 $\text{cm}^{-1}$ )	5.2-17 $\mu\text{m}$ (600-3100 $\text{cm}^{-1}$ )	1.1 - 6.5 $\mu\text{m}$ (1550-6650 $\text{cm}^{-1}$ )
Fiber type	PIR-900/1000 Silver Halide	PIR-900/1000 Silver Halide	Chalcogenide glass (As-S)
Temperature range	-100°C / + 250°C	-100°C / + 250°C	-100°C / + 200°C
Pressure (max)	200Bar	100Bar	100Bar

Figura 7.4: Parameters of the attenuated total reflection crystal of silicon.

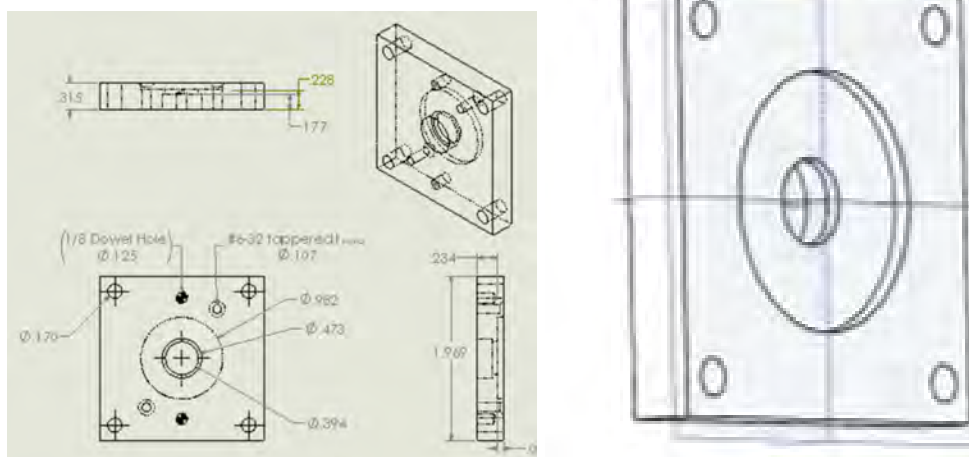


Figura 7.5: Drawings of the chamber of measurement (closed cavity option).

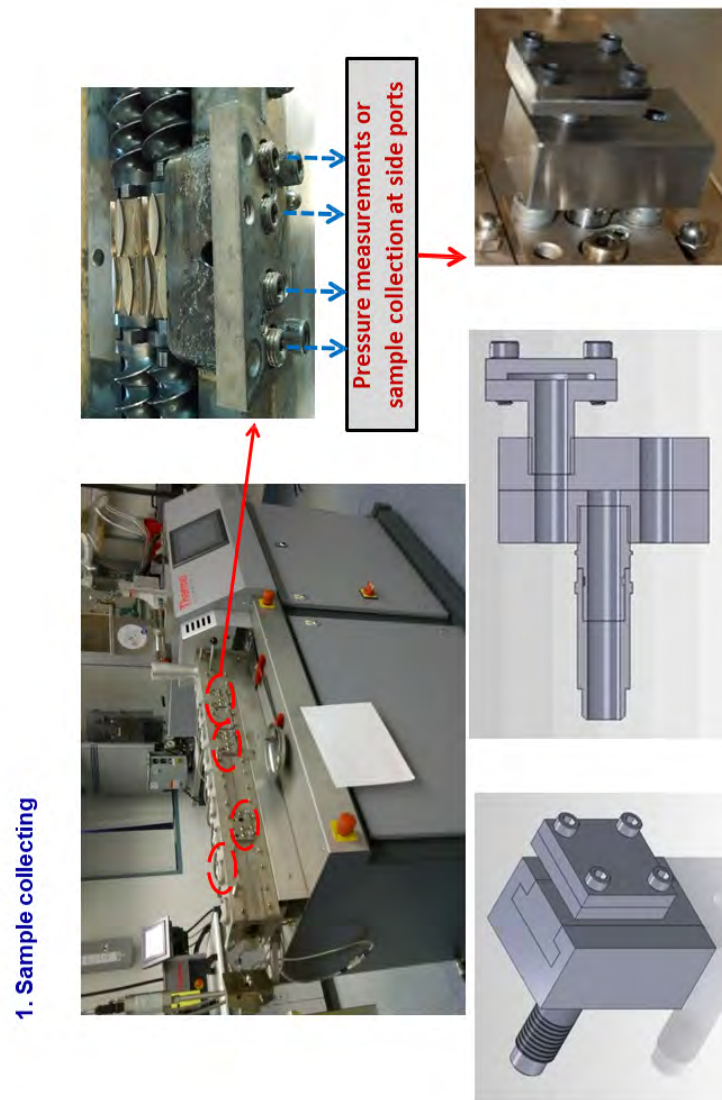


Figura 7.6: Sample collector operation and installation, for more details see [1].

2. IR Probe Holder with the probe



Figura 7.7: Probe holder unit.

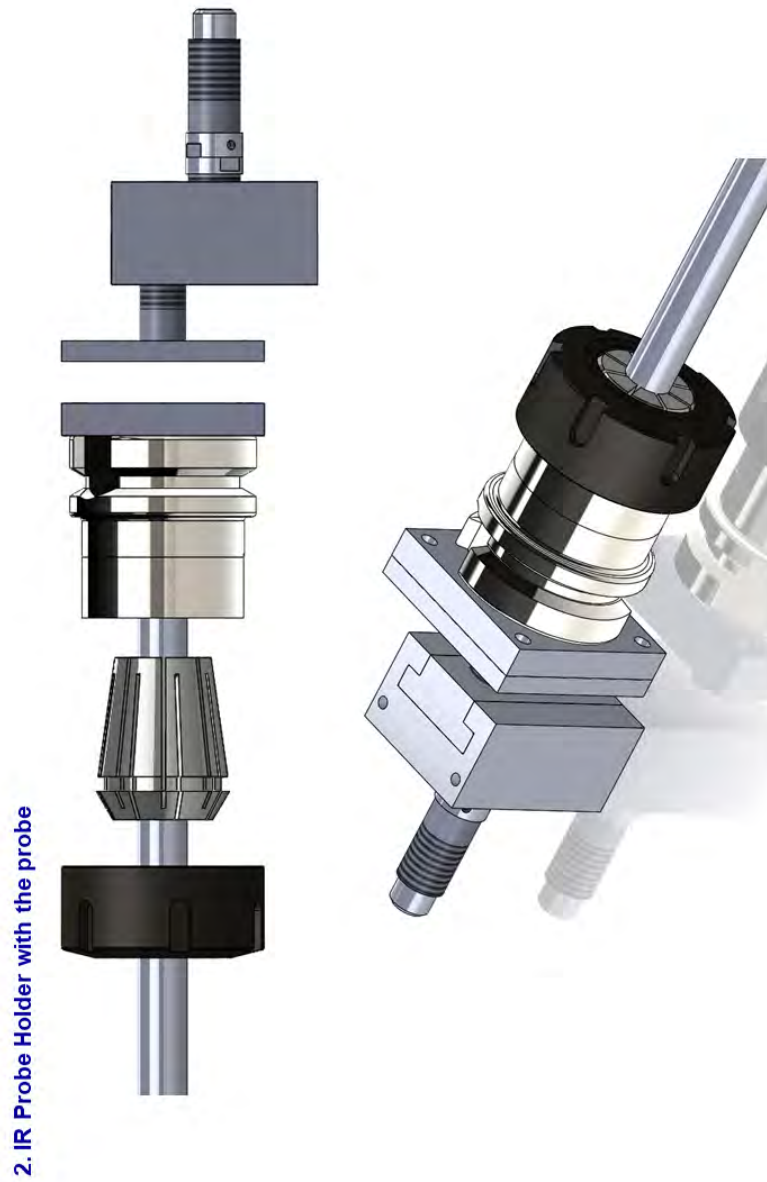


Figura 7.8: Probe holder unit with the probe.





Figura 7.9: Exploded view of PHU with the probe.

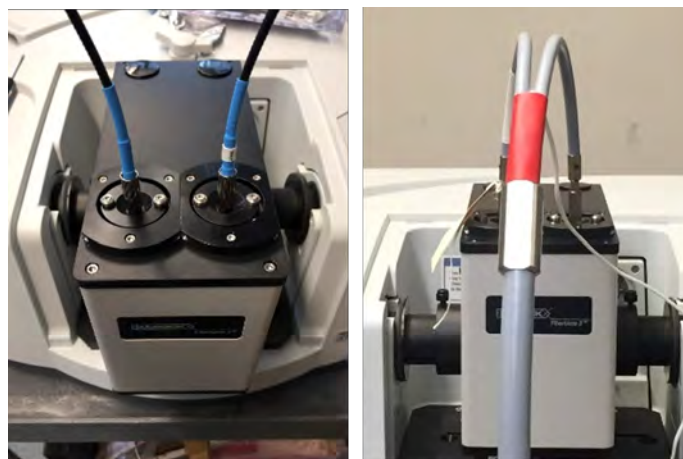


Figura 7.10: Fibermate.



## APPENDIX B: TOOL HOLDER COLLET CHUCK

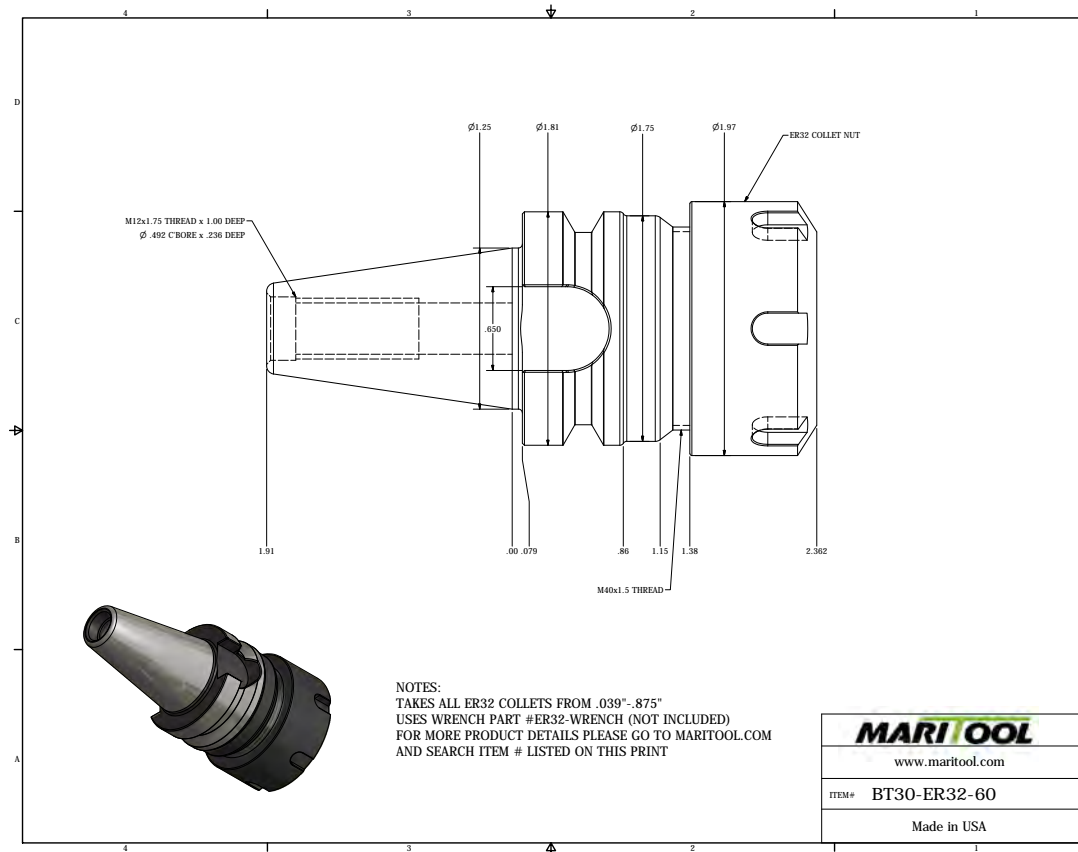
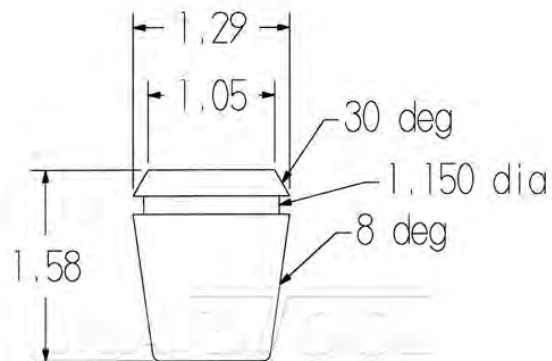


Figura 7.11: BT30 ER32 60mm Collet Chuck Tool Holder. Specifications: collet chuck accepts all ER32 collets; works on all BT 30 machines; made from alloy steel hardened to 54 - 56rc (Rockwell Hardness Scale) and; concentricity is less than 0.0001 at collet face (<https://www.maritool.com/>).



(a) ER32 COLLET 12mm.



MariTool Inc.  
ER32 Collet Detail  
Dimensions Are Approximate

(b) Dimensions.

Figura 7.12: a) ER32 COLLET 12mm and b) dimensions. Specifications: total runout less than .0003 on these precise ER32 collets; made from alloy spring steel and fully hardened; all critical collet surfaces are precision ground for accurate fit; works in all ER32 collet chucks; these ER32 collets have a full 0.039 inches range of collapse while maintaining full accuracy and; this ER32 collet has a range of 0.472-0.433 inches (<https://www.maritool.com/>).

## **APPENDIX C: LABVIEW SOFTWARE**

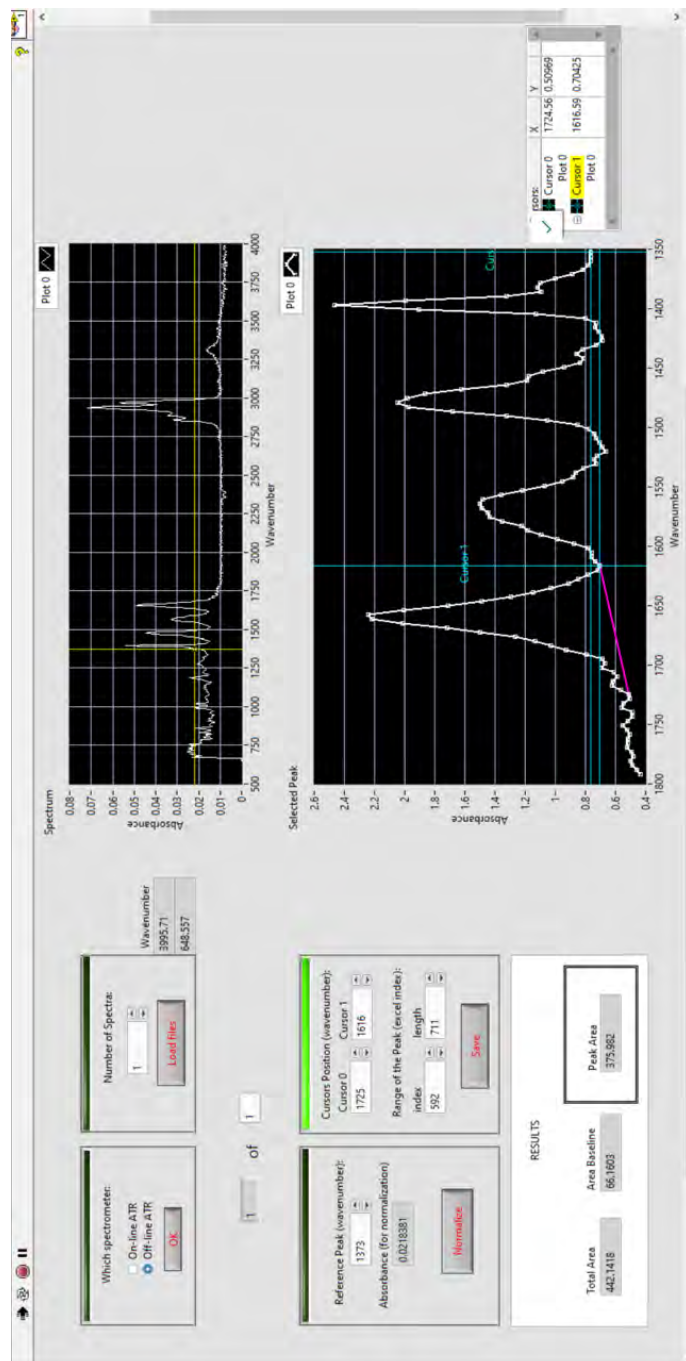


Figura 7.13: Software screen with the functions: method selection (on-line or off-line); number of spectra for analyzing; peak of reference; range of baseline correction: and save.

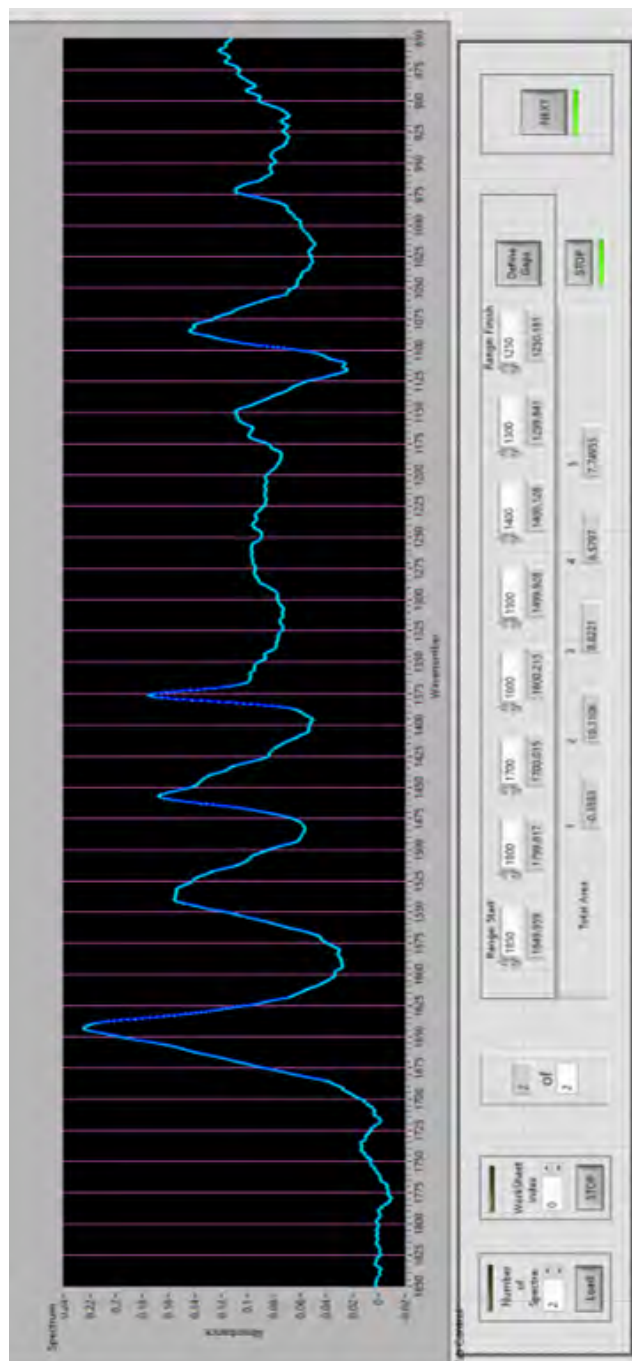


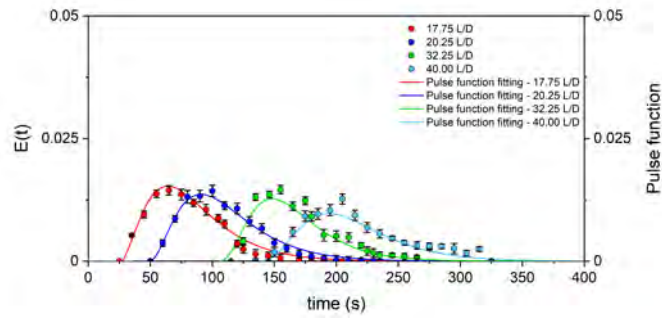
Figura 7.14: Software screen with the function of selecting of multiple IR bands.

	PEAK 1	PEAK 2	PEAK 3	PEAK 4	PEAK 5
Wavenumber	1748.23	1640.71	1530.79	1458.95	1376.98
	1 3	2 3	3 3	4 3	5 3
Area BL	-0.1215	0.8894	2.6760	2.3636	2.3600
	1 2	2 2	3 2	4 2	5 2
Absorbance	0.012584	0.204112	0.123419	0.129619	0.133712
	1 4	2 4	3 4	4 4	5 4
Peak Area	-0.236727	9.42121	6.14607	6.21609	5.38957

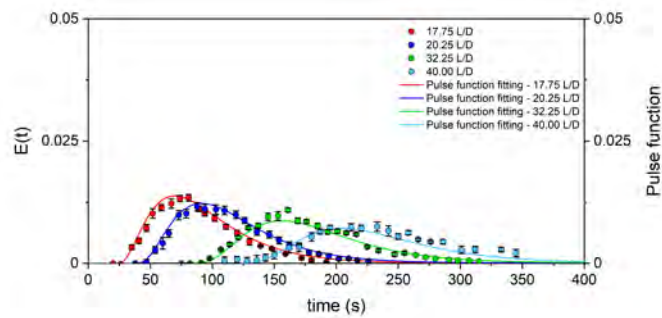
Figura 7.15: Software screen with the baseline area, IR band area and IR absorbance of multiple bands.



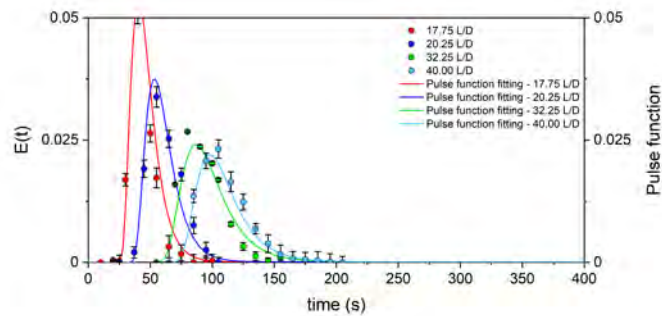
**APPENDIX D: RTD curves**



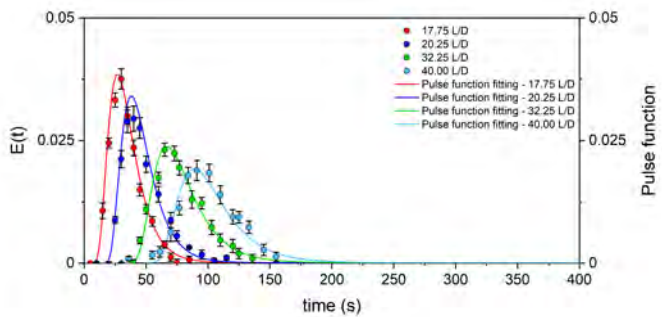
(a) L2-100-2-NR.



(b) L2-400-2-NR.

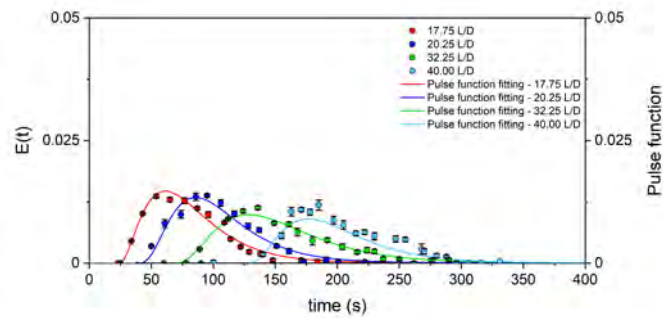


(c) L2-100-5-NR.

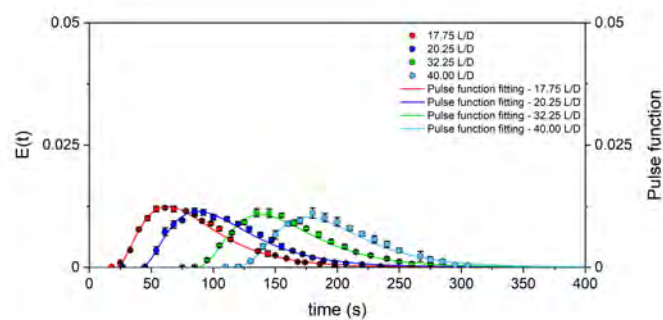


(d) L2-400-5-NR.

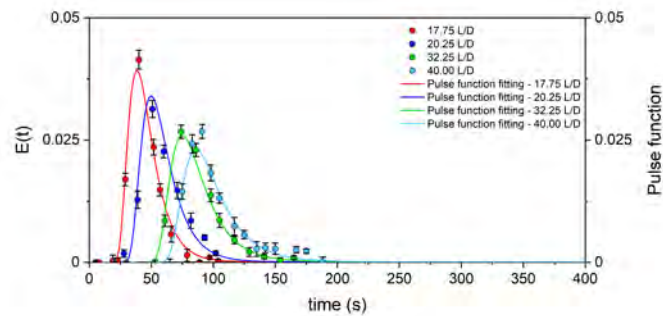
Figura 7.16: Experimental  $E(t)$  curves (circle plots) and corresponding fitted pulse curves (solid lines) for the operating conditions using EME L2 at 17.75, 20.25, 32.25 L/D and at the die.



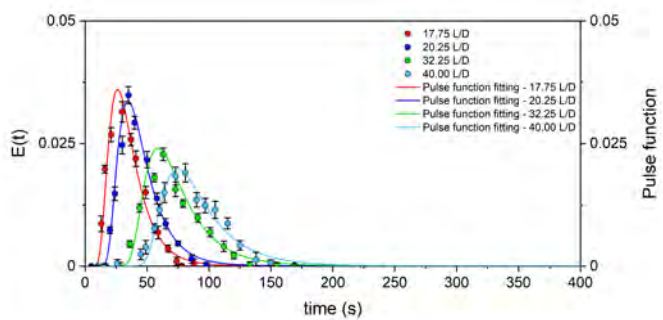
(a) S4-100-2-NR.



(b) S4-400-2-NR.



(c) S4-100-5-NR.

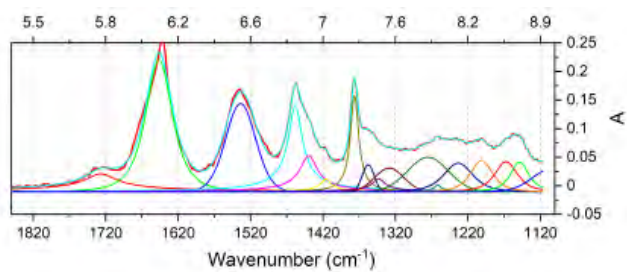


(d) S4-400-5-NR.

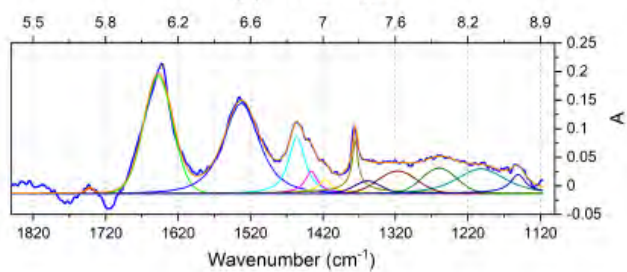
Figura 7.17: Experimental  $E(t)$  curves (circle plots) and corresponding fitted pulse curves (solid lines) for the operating conditions using EME S4 at 17.75, 20.25, 32.25 L/D and at the die.



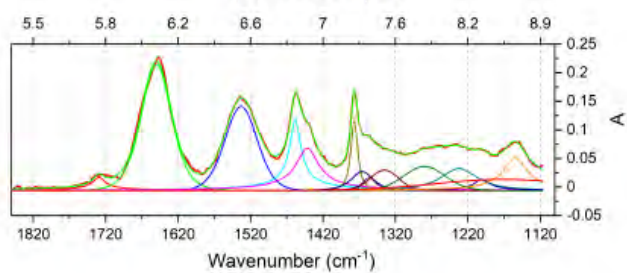
**APPENDIX E: On-line Spectra - Deconvolution**



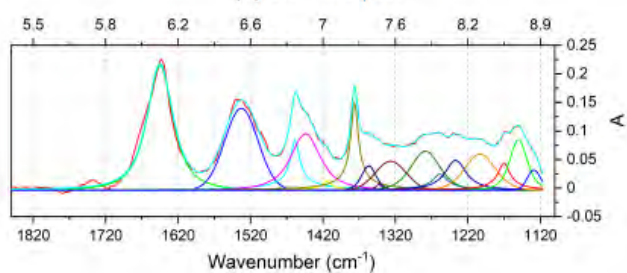
(a) 17.75 L/D.



(b) 20.25 L/D.

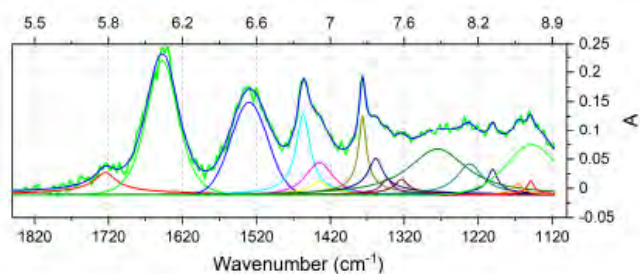


(c) 30.75 L/D.

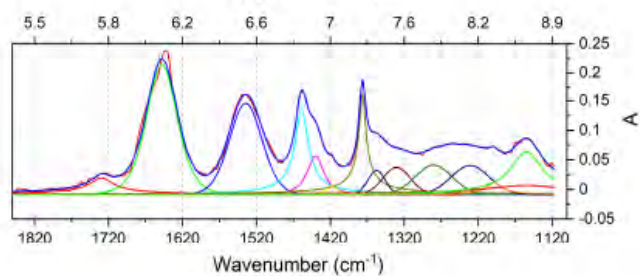


(d) 32.25 L/D.

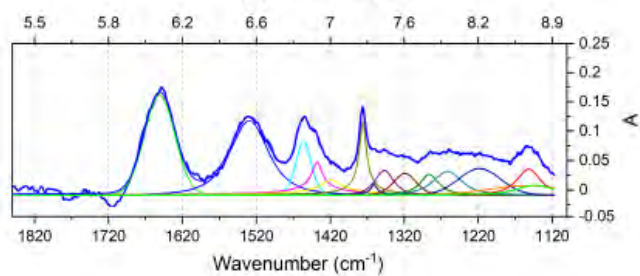
Figure 7.18: Average on-line FTIR spectra deconvoluted by Pearson VII function at 17.75, 20.25, 30.75 and 32.25 L/D for condition L2-100-2-R.



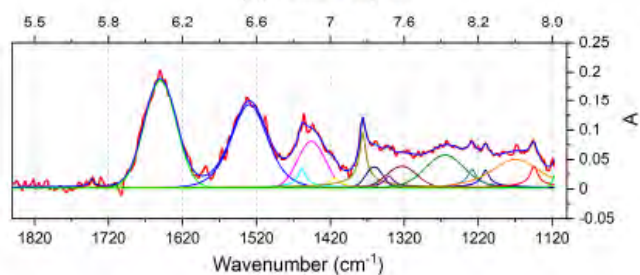
(a) 17.75 L/D.



(b) 20.25 L/D.



(c) 30.75 L/D.



(d) 32.25 L/D.

Figure 7.19: Average on-line FTIR spectra deconvoluted by Pearson VII function at 17.75, 20.25, 30.75 and 32.25 L/D for condition L2-400-2-R.

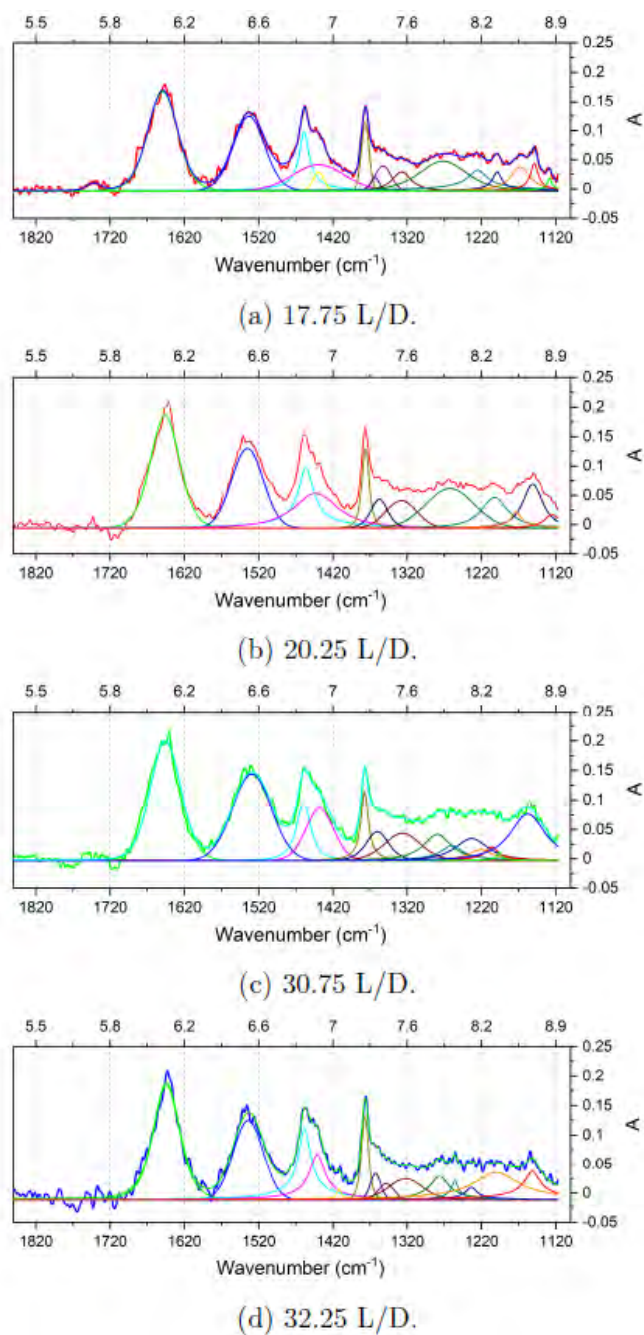
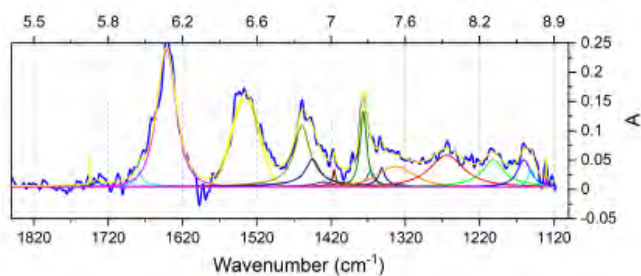
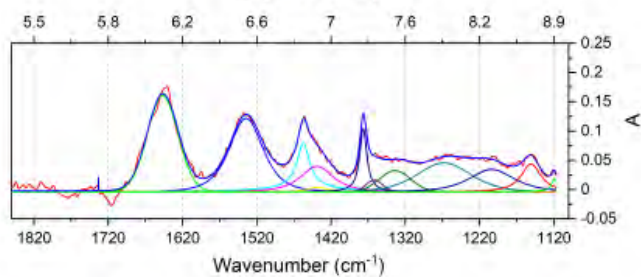


Figura 7.20: Average on-line FTIR spectra deconvoluted by Pearson VII function at 17.75, 20.25, 30.75 and 32.25 L/D for condition L2-100-5-R.

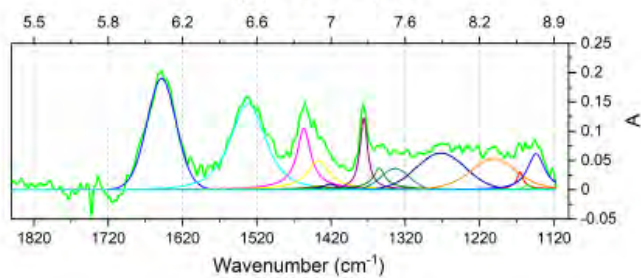




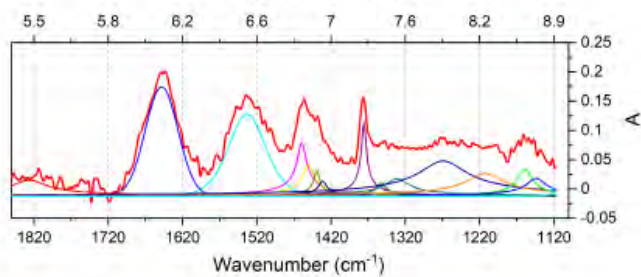
(a) 17.75 L/D.



(b) 20.25 L/D.



(c) 30.75 L/D.



(d) 32.25 L/D.

Figure 7.21: Average on-line FTIR spectra deconvoluted by Pearson VII function at 17.75, 20.25, 30.75 and 32.25 L/D for condition L2-400-5-R.

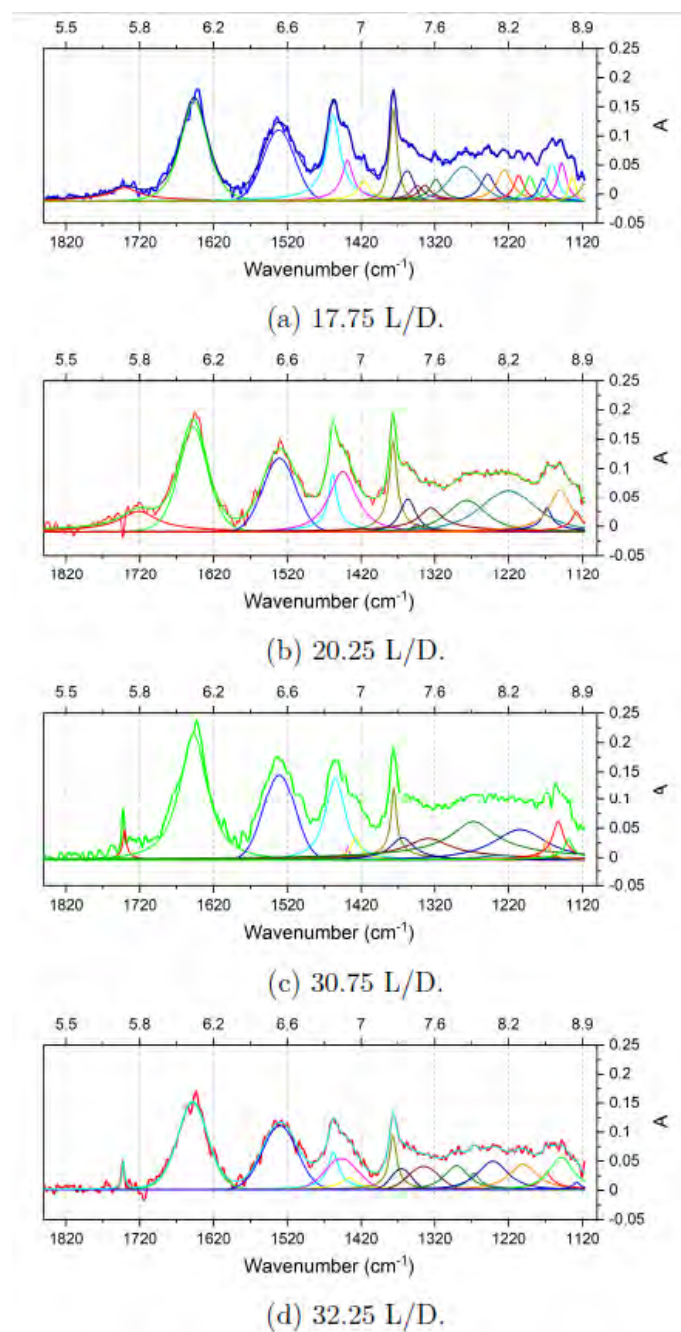


Figure 7.22: Average on-line FTIR spectra deconvoluted by Pearson VII function at 17.75, 20.25, 30.75 and 32.25 L/D for condition S4-100-2-R.

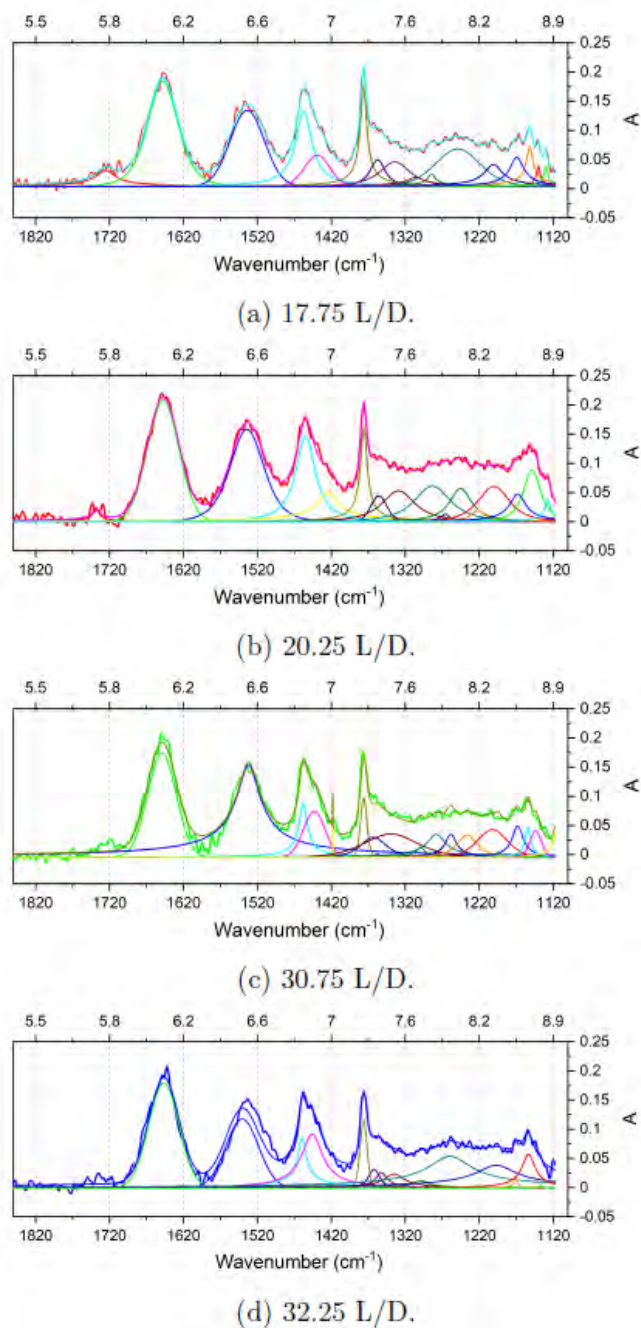


Figura 7.23: Average on-line FTIR spectra deconvoluted by Pearson VII function at 17.75, 20.25, 30.75 and 32.25 L/D for condition S4-400-2-R.

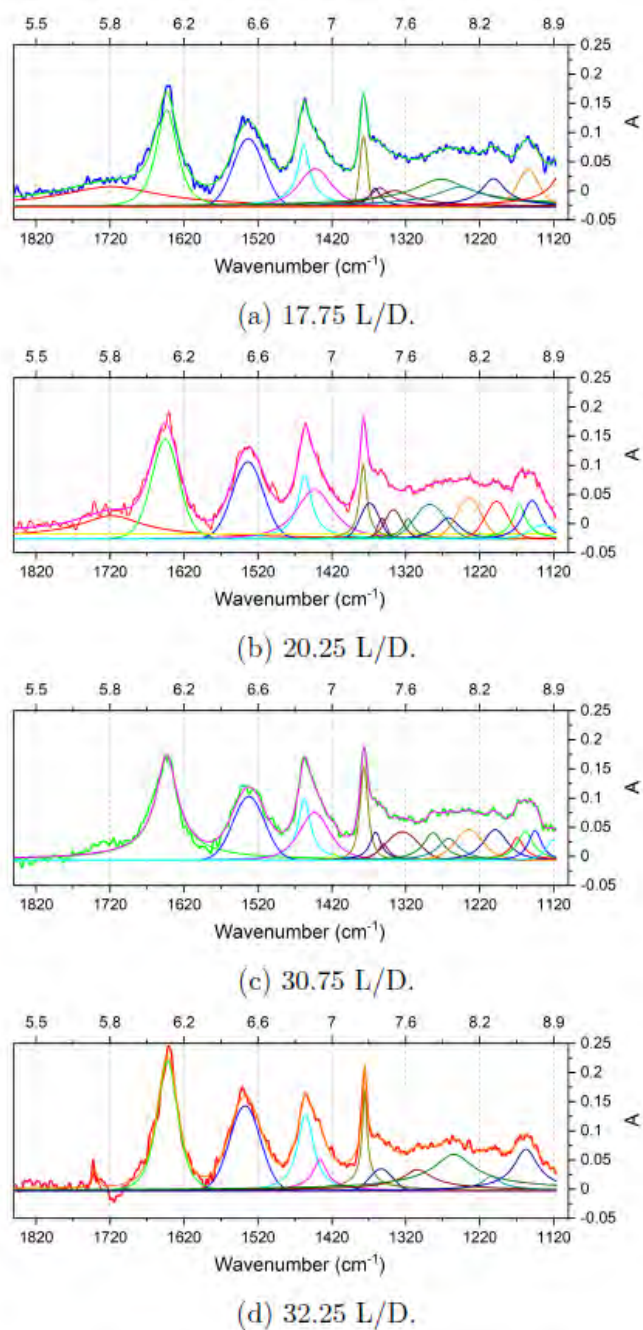
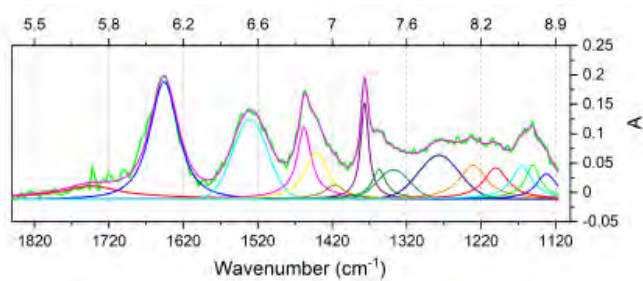
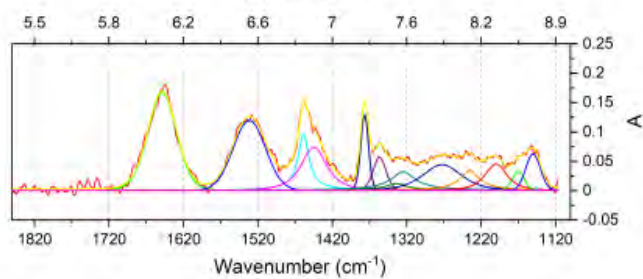


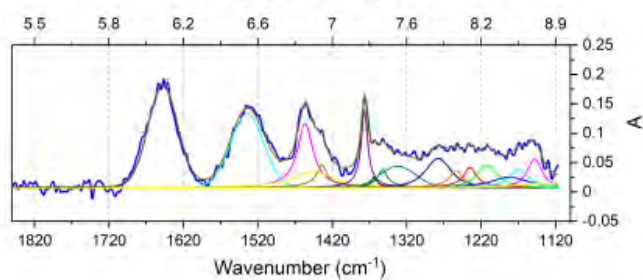
Figure 7.24: Average on-line FTIR spectra deconvoluted by Pearson VII function at 17.75, 20.25, 30.75 and 32.25 L/D for condition S4-100-5-R.



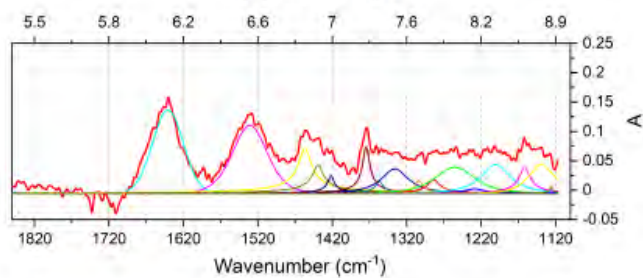
(a) 17.75 L/D.



(b) 20.25 L/D.



(c) 30.75 L/D.



(d) 32.25 L/D.

Figure 7.25: Average on-line FTIR spectra deconvoluted by Pearson VII function at 17.75, 20.25, 30.75 and 32.25 L/D for condition S4-400-5-R.



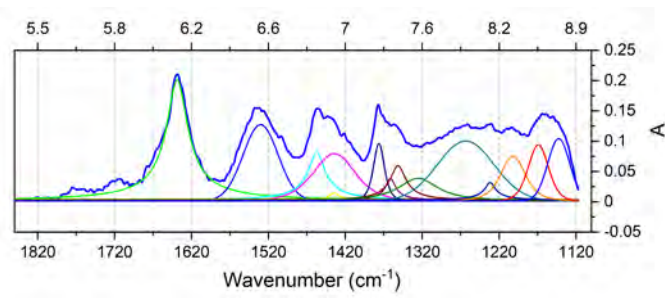


Figura 7.26: Average on-line FTIR spectra deconvoluted by Pearson VII function at 32.25 L/D along the extruder for the non-reactive blend.

## **APPENDIX F: ATR-FTIR probe validation with transesterification reaction in PET/PC blend in batch mixer**

### **7.1 Introduction**

This appendix deals with a validation on the ATR-FTIR probe in off-line mode. The motive that this experiment is in an appendix is because the contact crystal/sample was very poor, leading to very noisy spectra.

#### **7.1.1 Brief Background**

The exchange reaction of esterification takes place in the molten state between mixtures of polycarbonate (PC) and polybutylene terephthalate (PBTP) or polyethylene terephthalate (PET) mixtures [161].

The exchange reaction has two different mechanisms. The first is a direct exchange reaction between functional groups located inside the polymer chains (inner-inner). The second mechanism is by attack of reactive chain ends functional groups (outer) on inner groups (outer-inner) [162]. The mechanism can be determined by the composition of the PET/PC blends.

The esterification reaction can be end-group-activated or catalyst-activated (below 300 C). However, the exchange reaction can also be thermal activated exchange (i.e., without catalysts) and thermal decomposition can occur above 300 C.

### **7.2 Experimental**

The exchange reaction between polyethylene terephthalate (PET) and polycarbonate (PC) was carried out in a batch mixer at different mixing times and with and without the presence of catalyst.

#### **7.2.1 Materials and Blends**

A polyethylene terephthalate (PET) manufactured by DAH Americas LLC and a polycarbonate (PC) under the commercial name of Makrolon®2658 by Covestro. A metal catalyst was used. Table 7.1 shows the blend composition used in this study.

Tabela 7.1: PET/PC blend compositions.

PET (%)	PC (%)	Catalyst (% additional)
50	50	0
50	50	0.1

### 7.2.2 Process Conditions

The reaction (Figure 7.27) was carried out in a HAAKE <sup>texttrademark</sup> Rheomix batch mixer. Two different mixing times were used (see table 7.2). After each mixing time, the batch mixer was opened and the ATR-FTIR probe was inserted into the molten polymer for spectra collection. Subsequently, samples were collected and with and without quenching for analysis in a benchtop spectrometer.

Tabela 7.2: Process conditions of PET/PC blending during batch mixing process.

Time (min)	Rotation speed (RPM)	Temperature (/degree C)
3	100	275
15	100	275

### 7.2.3 Exchange reaction: Transesterification

#### *IR bands*

The IR bands related to carbonyl group in PET and PC were evaluated. Carbonyl in PC vibrates in a frequency around  $1770/80 \text{ cm}^{-1}$ , while carbonyl in PET vibrates in the range of  $17215/20 \text{ cm}^{-1}$ . Two ranges of the IR spectrum were evaluated: range 1, from  $1770/80 \text{ cm}^{-1}$  and, range 2 around  $1715/20 \text{ cm}^{-1}$ . During the exchange reaction different sequences of copolymer can be formed (see Figure 7.28). The two top sequences shown in Figure 7.28 have the carbonate functional group, while the two bottom have the terephthalic structure linking PC and PET. The intensity of range 1 and range 2 IR associated to the sequence of the copolymer formed during reaction [161].



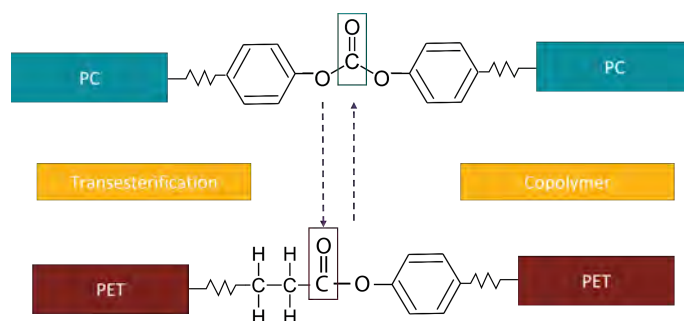


Figura 7.27: Transesterification reaction leads to copolymers.

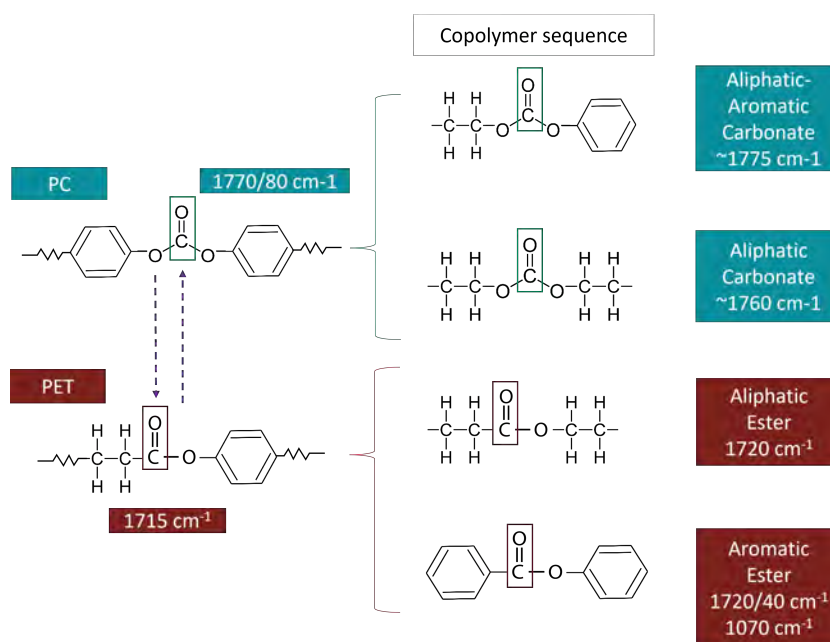


Figura 7.28: Sequence of different copolymers as a result of the exchange reaction.

## 7.3 Results and Discussion

### 7.3.1 Benchtop Spectrometer

#### *Quenching effect*

Figure 7.29 shows the spectra of pure PET and pure PC collect by the benchtop spectrometer. The samples were collected with and without quenching. As can be seen in Figure 7.29 the quenching does not have a strong effect on IR spectra, so only the quenched sampled will be considered in this study.

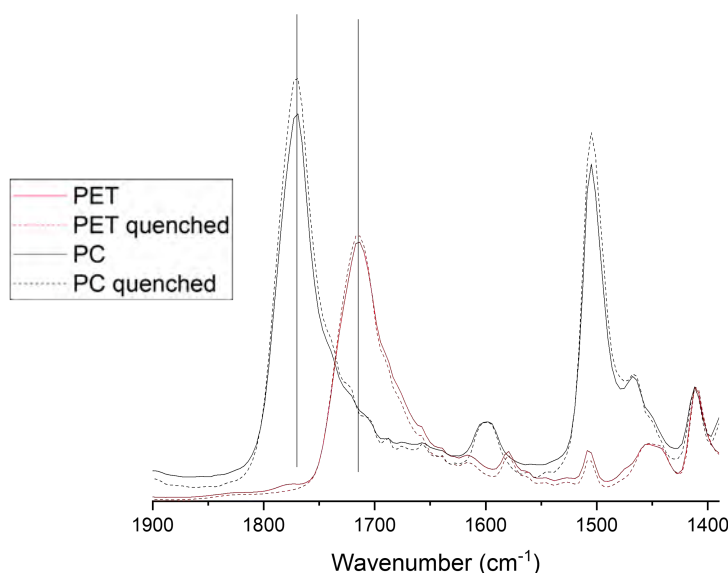


Figura 7.29: Spectra of pure PET and PC with and without quenching.

#### *Time and Catalyst Effect*

Figure 7.30 shows the IR spectra collected with the benchtop spectrometer. In the PC spectrum we can see the IR band at  $1770\text{ cm}^{-1}$  (range 1) relative to carbonyl stretching in the carbonate structure, whereas in the PET spectrum (red), the IR band at  $1715\text{ cm}^{-1}$  (range 2) is shown.

Figure 7.31 depicts the pure PET and PC and the blends of 50/50 without catalyst at different times. We can see by the spectra that the band in the range 2 for the blends are slightly blueshifted in comparison with pure PET. In range 1 we can see the effect of time in the intensity of the IR band. Higher times (15 minutes) increase the intensity of the band. This can possibly be explained by the incre-

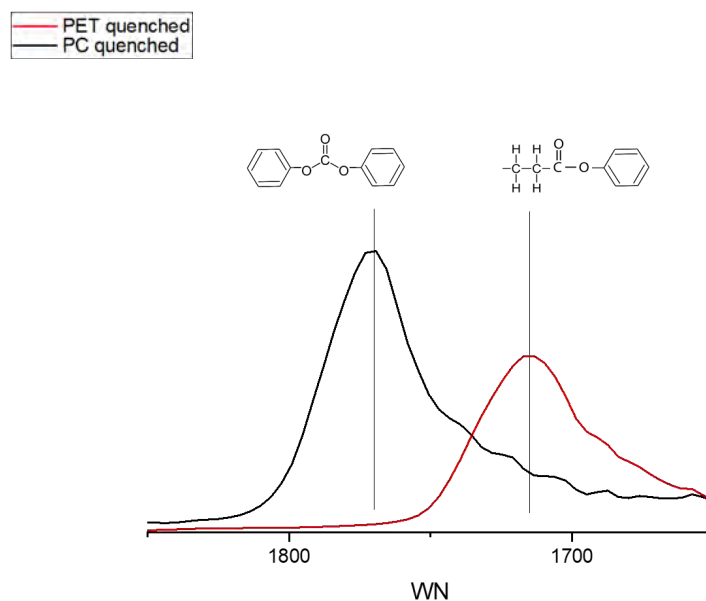


Figura 7.30: Spectra in the range on interest.

ase of the copolymers related to PC, namely, aliphatic-aromatic carbonate and aliphatic carbonate.

Figure 7.32 depicts the blends of 50/50 with and without catalyst at different times. The addition of the catalyst in the blend seems to have no effect when the time of mixing is 3 minutes. On the other hand, at 15 minute mixing time the blueshifting is more pronounced and there is a marked decrease in the intensity of the band in range 1. The blueshifting in range 2, showed in detail in 7.33, can be associated to an increase the content of aromatic ester (see Figure 7.28). The carbonyl in aromatic ester vibrates at  $1720/40 \text{ cm}^{-1}$ , which can make the band of PET at  $1715 \text{ cm}^{-1}$  to blueshift. This makes the band in range 1 to decrease its intensity and the band at range 2 to be increased. This can be explained that the exchange reaction is happening in favor to PET copolymer formation. This can also explain why the band at range 2 ( $1715 \text{ cm}^{-1}$ ) of the blends does not vary its intensity compared to the pure PET. The shoulder at  $1070 \text{ cm}^{-1}$  showed in Figure 7.34 can confirm the formation of aromatic ester in the blend. The IR band at  $1070 \text{ cm}^{-1}$  appears only in the blend of 50/50 with catalyst at 15 minute mixing time. Which means that the presence of the catalyst at 15 minutes was effective in the exchange reaction.

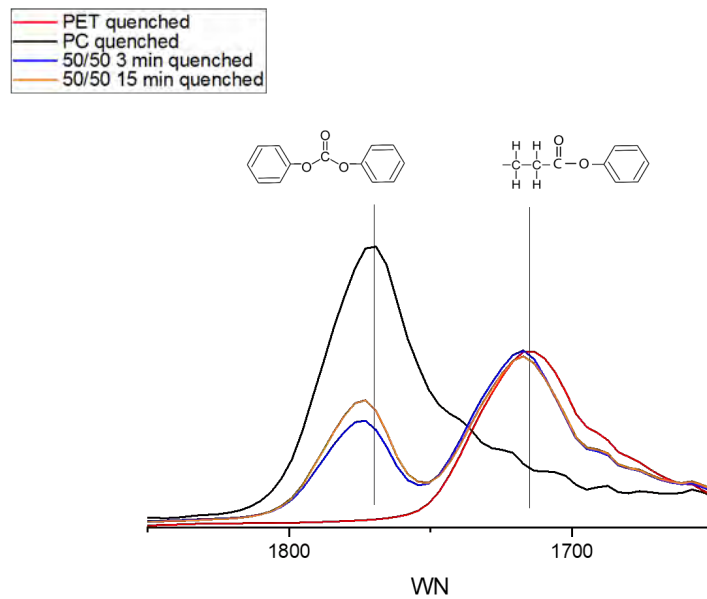


Figura 7.31: Spectra in the range on interest of pure PET and PC and 50/50 blends at 3 and 15 minutes mixing time.

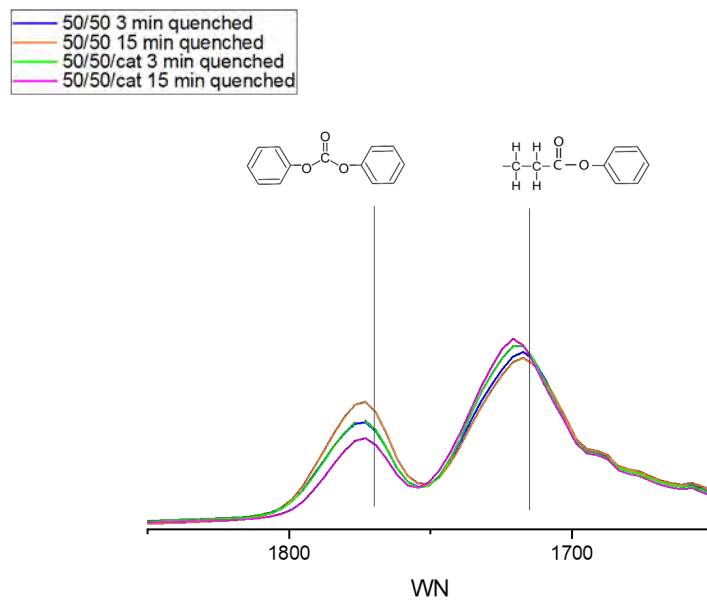


Figura 7.32: Spectra in the range on interest of the 50/50 blends with and without catalyst at 3 and 15 minutes mixing time.

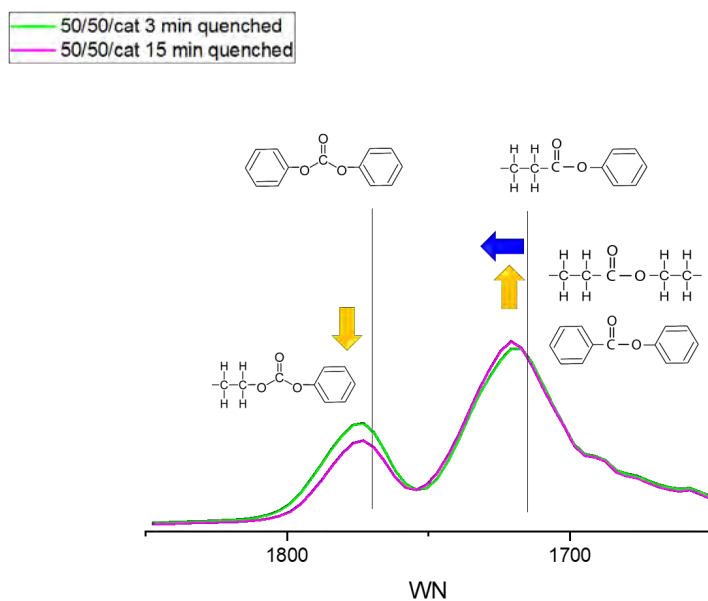


Figura 7.33: Spectra in the range on interest of the 50/50 blends with catalyst at 3 and 15 minutes mixing time.

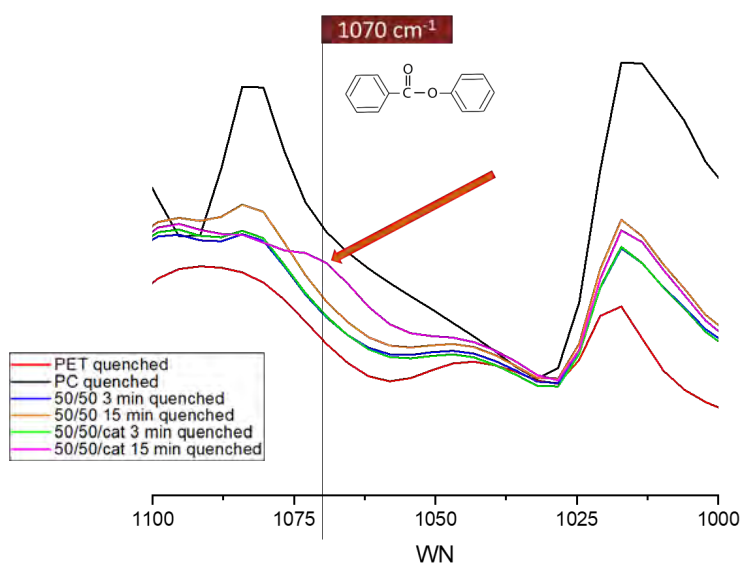


Figura 7.34: Spectra of pure PET, pure PC, and all the 50/50 at 3 and 15 minutes mixing time. IR band at  $1070 \text{ cm}^{-1}$  relative to aromatic ester (see Figure 7.28).

### 7.3.2 Benchtop Spectrometer and ATR-FTIR Probe Comparison

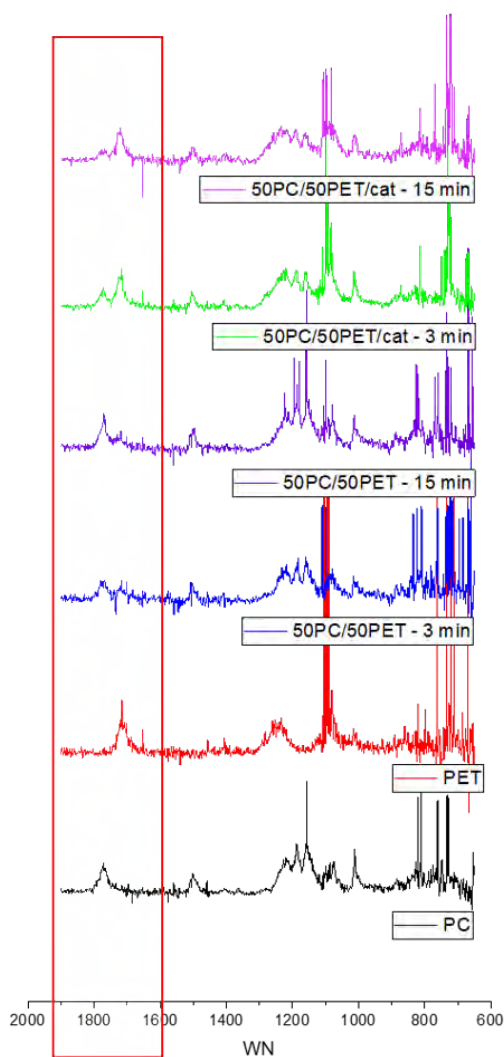
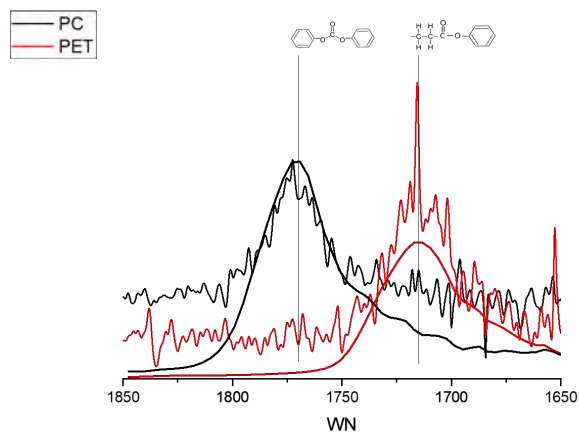
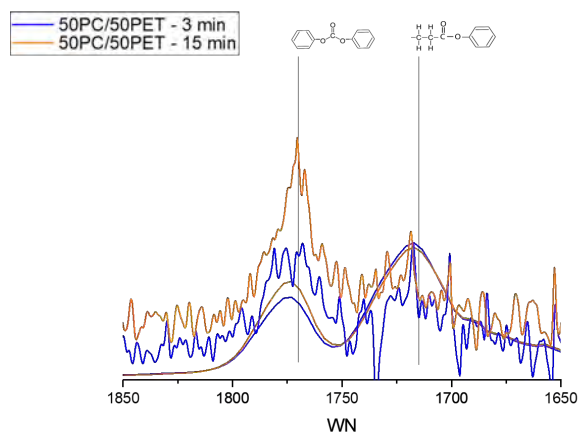


Figure 7.35: Spectra of pure PET, pure PC, and all the 50/50 at 3 and 15 minutes mixing time collected by the ATR-FTIR probe

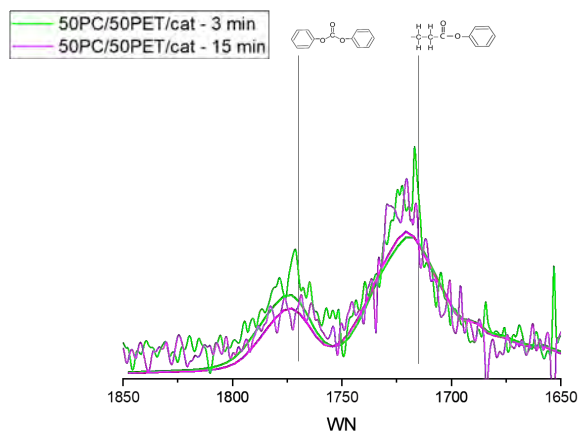
Figure 7.35 shows the spectra for pure PC and PET and all the 50/50 blends with and without catalyst. In the figure we can see the highlighted range of interest. The plots show very noisy spectra. This noise was associated to bad contact between sample and crystal. The probe was inserted in the batch mixer chamber with no pressure, this caused a bad contact, leading to noisy spectra.



(a) Pure PET and PC.



(b) 50/50 blends of PET and PC without catalyst.



(c) 50/50 blends of PET and PC with catalyst.

Figura 7.36: Comparison between Spectra of pure PET and PC, and all the 50/50 at 3 and 15 minutes mixing time collected by the benchtop spectrometer (smooth spectra) and ATR-FTIR probe (noisy spectra).

Figure 7.36 show the comparison between the spectra collected by the ATR-FTIR probe and by the benchtop spectrometer. We can see that the spectra collect by the ATR-FTIR probe are very noisy and they do not superimpose exactly on the spectra collected by the benchtop spectrometer. Despite of that we can see that the spectra collecte by the ATR-FTIR probe follow the same trend that was acquired by the spectra collected by the benchtop spectrometer. This means that all the changes in the blend due to the exchange reaction see in the benchtop spectrometer (in better conditions of analysis) were also seen by using the ATR-FTIR probe.

#### **7.4 Conclusions**

These experiments added to this appendix proposed to evaluate the sensibility of the ATR-FTIR probe in evaluate chemical reaction in bench, not during extrusion. This experiment was done in order to validate the ATR-Probe. The selected reaction was the exchange reaction of transesterification between PET and PC. The results were compared to ATR in a benchtop spectrometer.

The ATR-FTIR probe was successful in measuring differences in composition between the pure systems (PET and PC) and their blends of 50%/50%. The changes in the blend due to the exchange reaction was also evaluated by the ATR-FITR probe in different times of mixing. The use of catalyst improved the exchange reaction at 15 minute mixing time. The results show good agreement with benchtop results, despite of the noisy spectra.



## APPENDIX G: IN-LINE FTIR SYSTEM

Pictures of the prototype of the In-line FTIR system. This option was designed to interface the co-rotational twin-screw ex-truder ZSK 30 from Werner & Pfleiderer (Figure 7.42) in the laboratory of the department of Materials Engineering and Science at Universidade Federal de São Carlos.

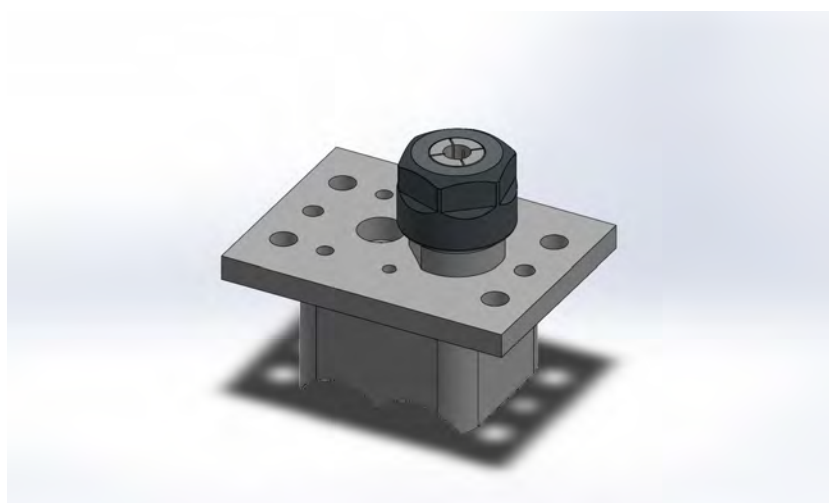


Figura 7.37: Prototype of the In-line FTIR.

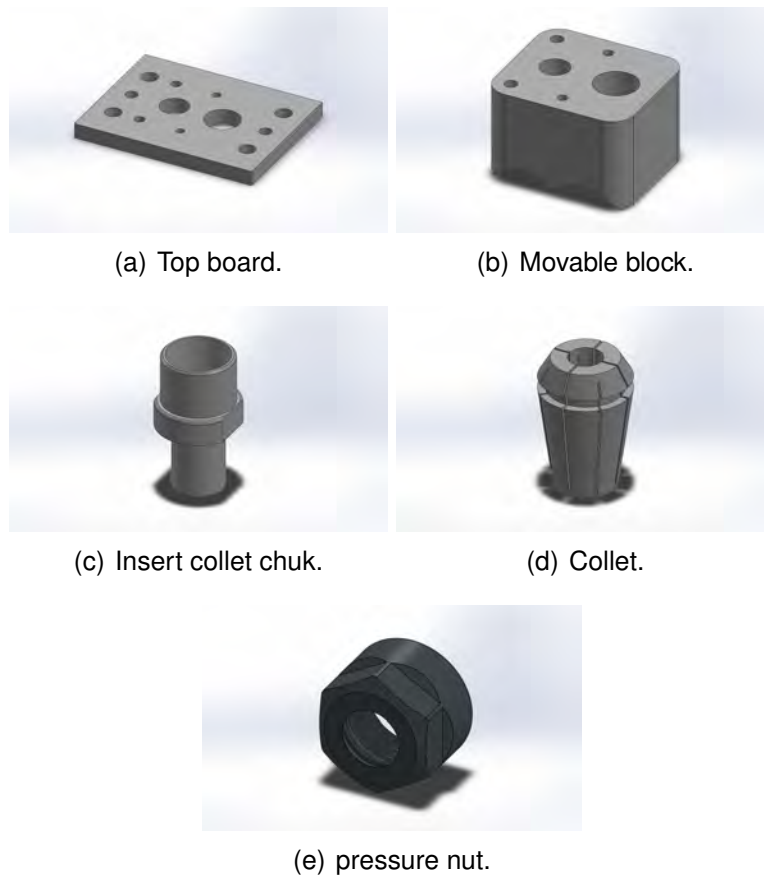


Figura 7.38: Components of the In-line FTIR.

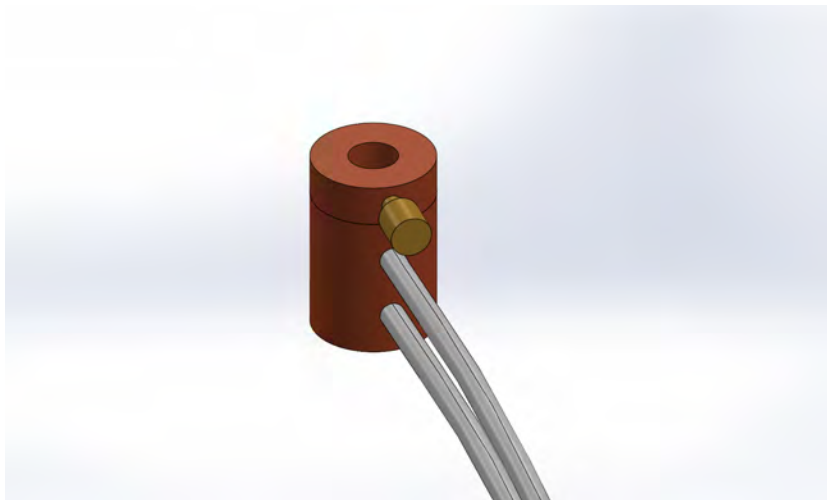


Figura 7.39: Prototype of the water cooling system for the ATR-FTIR probe. In the figure two hoses are depicted: water inlet and outlet.

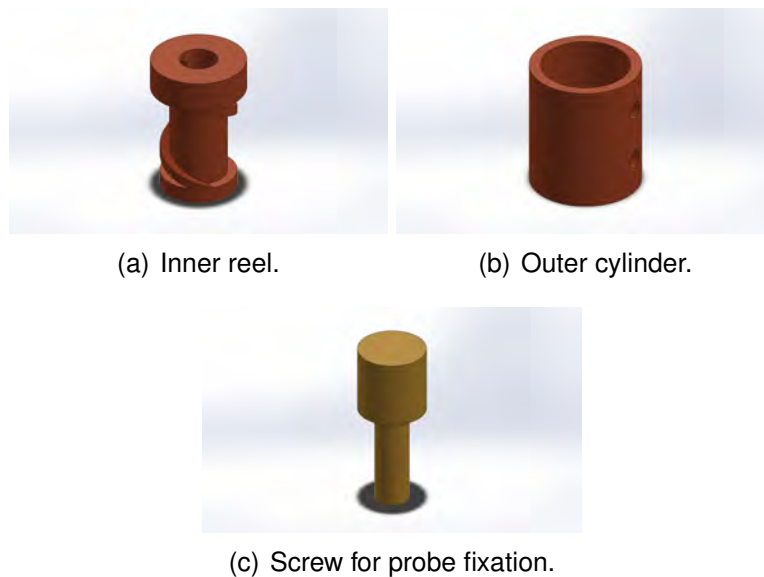


Figura 7.40: Components of the probe water cooling system.

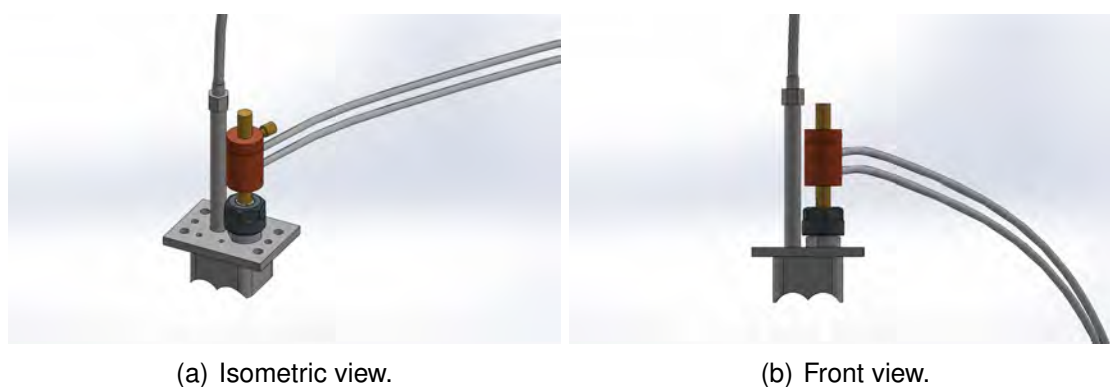
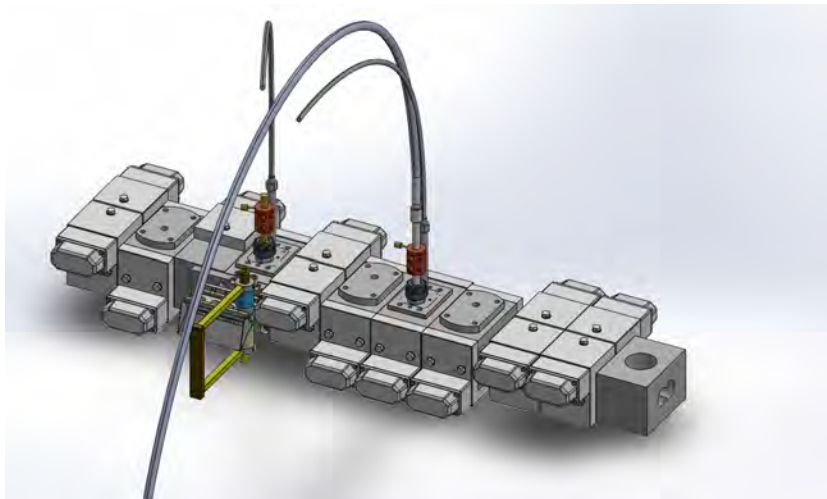


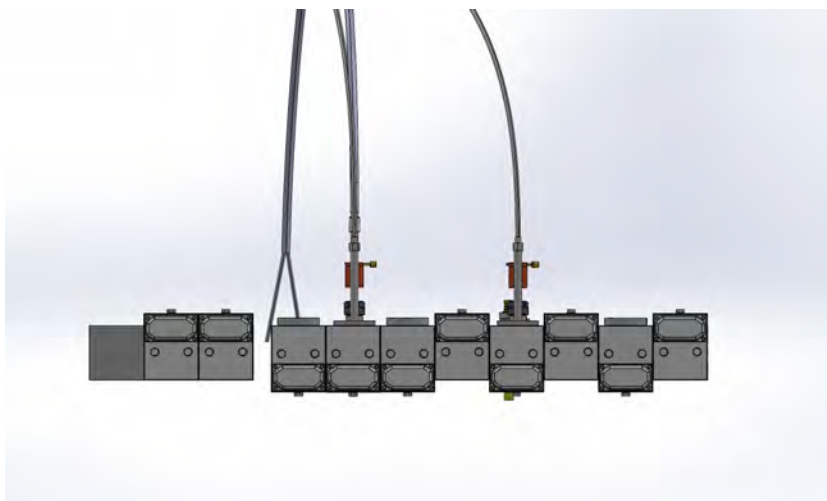
Figura 7.41: Assembly of the In-line FTIR system and probe water cooling system. The yellow rod simulates the ATR-FTIR probe with the cooling system installed. On the figure we can see a pressure transducer installed next to the probe for pressure measurement.



Figura 7.42: Digital design of the co-rotational twin-screw ex-truder ZSK 30 from Werner & Pfleiderer.



(a) Isometric view.



(b) Front view.

Figura 7.43: Assembly of whole system attached to the extruder. Direction of extrusion: right to the left.



**APPENDIX H: DATA FRAME - EXTRUSION: EXPERIMENT 1 AND 2**

Blend	PP (%)	Feed Rate	Screw Speed	Screw Geom.	L/D	Area1640	Area13
non-reactive	20	2	200	0KB30	20.25	6.696158	3.1783
non-reactive	20	2	200	0KB30	20.25	12.28285	3.4350
non-reactive	20	2	200	0KB30	20.25	11.58837	3.4049
non-reactive	20	2	200	0KB30	20.25	7.588804	3.2218
non-reactive	20	2	200	0KB30	20.25	9.430811	3.3083
non-reactive	20	2	200	0KB30	20.25	9.072091	3.2918
non-reactive	20	2	200	0KB30	20.25	10.67336	3.3645
non-reactive	20	2	200	0KB30	20.25	11.79438	3.4139
non-reactive	20	2	200	0KB30	20.25	6.401454	3.1637
non-reactive	20	2	200	0KB30	20.25	5.929973	3.1402
non-reactive	20	2	200	0KB30	20.25	12.18539	3.4308
non-reactive	20	2	200	0KB30	20.25	8.942305	3.2858
non-reactive	20	2	200	0KB30	20.25	11.57605	3.4044
non-reactive	20	2	200	0KB30	20.25	5.742878	3.1307
non-reactive	20	2	200	0KB30	20.25	9.040209	3.2903
non-reactive	20	2	200	0KB30	20.25	11.24167	3.3897
non-reactive	20	2	200	0KB30	20.25	7.39242	3.2123
non-reactive	20	2	200	0KB30	20.25	13.10823	3.4703
non-reactive	20	2	200	0KB30	20.25	12.73657	3.4545
non-reactive	20	2	200	0KB30	20.25	5.945995	3.1410
non-reactive	20	2	200	0KB30	32.75	5.578623	3.2593
non-reactive	20	2	200	0KB30	32.75	12.58415	3.2558
non-reactive	20	2	200	0KB30	32.75	10.40007	2.879
non-reactive	20	2	200	0KB30	32.75	6.001943	2.8909
non-reactive	20	2	200	0KB30	32.75	8.989909	3.2083
non-reactive	20	2	200	0KB30	32.75	8.432648	3.1663
non-reactive	20	2	200	0KB30	32.75	10.27351	3.1382
non-reactive	20	2	200	0KB30	32.75	11.00931	2.9853
non-reactive	20	2	200	0KB30	32.75	4.944665	3.1113
non-reactive	20	2	200	0KB30	32.75	4.329592	3.1116
non-reactive	20	2	200	0KB30	32.75	11.87567	3.1008
non-reactive	20	2	200	0KB30	32.75	7.634612	2.9220
non-reactive	20	2	200	0KB30	32.75	10.95785	3.0372
non-reactive	20	2	200	0KB30	32.75	3.964661	3.0215



non-reactive	20	2	200	OKB30	32.75	8.378918	3.16083
non-reactive	20	2	200	OKB30	32.75	11.4155	3.27576
non-reactive	20	2	200	OKB30	32.75	6.502211	3.25656
non-reactive	20	2	200	OKB30	32.75	12.83601	3.0852
non-reactive	20	2	200	OKB30	32.75	12.25831	3.0432
non-reactive	20	2	200	OKB30	32.75	4.150496	2.96852
non-reactive	20	2	200	OKB30	42.5	7.164478	2.9829
non-reactive	20	2	200	OKB30	42.5	10.74167	3.14598
non-reactive	20	2	200	OKB30	42.5	10.30488	3.12685
non-reactive	20	2	200	OKB30	42.5	7.746769	3.0105
non-reactive	20	2	200	OKB30	42.5	8.934556	3.06548
non-reactive	20	2	200	OKB30	42.5	8.704618	3.05497
non-reactive	20	2	200	OKB30	42.5	9.726293	3.10119
non-reactive	20	2	200	OKB30	42.5	10.43465	3.13255
non-reactive	20	2	200	OKB30	42.5	6.971193	2.97364
non-reactive	20	2	200	OKB30	42.5	6.660809	2.95865
non-reactive	20	2	200	OKB30	42.5	10.68046	3.14331
non-reactive	20	2	200	OKB30	42.5	8.62124	3.05114
non-reactive	20	2	200	OKB30	42.5	10.2971	3.1265
non-reactive	20	2	200	OKB30	42.5	6.537285	2.95265
non-reactive	20	2	200	OKB30	42.5	8.684134	3.05403
non-reactive	20	2	200	OKB30	42.5	10.0861	3.11719
non-reactive	20	2	200	OKB30	42.5	7.619056	3.00449
non-reactive	20	2	200	OKB30	42.5	11.25819	3.16835
non-reactive	20	2	200	OKB30	42.5	11.02598	3.15833
non-reactive	20	2	200	OKB30	42.5	6.671419	2.95917
non-reactive	20	2	200	OKB90	17.75	7.933677	3.17082
non-reactive	20	2	200	OKB90	17.75	10.64057	3.16894
non-reactive	20	2	200	OKB90	17.75	9.658457	2.9651
non-reactive	20	2	200	OKB90	17.75	7.865564	2.97158
non-reactive	20	2	200	OKB90	17.75	9.226602	3.14325
non-reactive	20	2	200	OKB90	17.75	8.98776	3.12049
non-reactive	20	2	200	OKB90	17.75	9.697232	3.10534
non-reactive	20	2	200	OKB90	17.75	9.936385	3.02264
non-reactive	20	2	200	OKB90	17.75	7.583093	3.09075
non-reactive	20	2	200	OKB90	17.75	7.340604	3.09095

non-reactive	20	2	200	OKB90	17.75	10.31583	3.08509
non-reactive	20	2	200	OKB90	17.75	8.547303	2.98839
non-reactive	20	2	200	OKB90	17.75	9.931698	3.05066
non-reactive	20	2	200	OKB90	17.75	7.12896	3.04217
non-reactive	20	2	200	OKB90	17.75	8.963836	3.11752
non-reactive	20	2	200	OKB90	17.75	10.19631	3.17969
non-reactive	20	2	200	OKB90	17.75	8.28886	3.1693
non-reactive	20	2	200	OKB90	17.75	10.69178	3.07662
non-reactive	20	2	200	OKB90	17.75	10.45219	3.05391
non-reactive	20	2	200	OKB90	17.75	7.164825	3.01352
non-reactive	20	2	200	OKB90	20.25	8.150385	3.48191
non-reactive	20	2	200	OKB90	20.25	11.90121	3.47516
non-reactive	20	2	200	OKB90	20.25	9.040893	2.74175
non-reactive	20	2	200	OKB90	20.25	6.979703	2.76506
non-reactive	20	2	200	OKB90	20.25	9.774742	3.38272
non-reactive	20	2	200	OKB90	20.25	9.307586	3.30082
non-reactive	20	2	200	OKB90	20.25	10.15115	3.24632
non-reactive	20	2	200	OKB90	20.25	9.835357	2.94877
non-reactive	20	2	200	OKB90	20.25	7.279441	3.19383
non-reactive	20	2	200	OKB90	20.25	6.962947	3.19454
non-reactive	20	2	200	OKB90	20.25	10.81173	3.17347
non-reactive	20	2	200	OKB90	20.25	7.895604	2.82555
non-reactive	20	2	200	OKB90	20.25	10.0491	3.0496
non-reactive	20	2	200	OKB90	20.25	6.459991	3.01904
non-reactive	20	2	200	OKB90	20.25	9.256997	3.29016
non-reactive	20	2	200	OKB90	20.25	11.3612	3.51382
non-reactive	20	2	200	OKB90	20.25	8.63644	3.47645
non-reactive	20	2	200	OKB90	20.25	11.23107	3.143
non-reactive	20	2	200	OKB90	20.25	10.73502	3.06127
non-reactive	20	2	200	OKB90	20.25	6.365643	2.91594
non-reactive	20	2	200	OKB90	32.75	9.337479	3.3907
non-reactive	20	2	200	OKB90	32.75	11.25475	3.38559
non-reactive	20	2	200	OKB90	32.75	9.219819	2.83044
non-reactive	20	2	200	OKB90	32.75	8.118224	2.84808
non-reactive	20	2	200	OKB90	32.75	10.08847	3.31562
non-reactive	20	2	200	OKB90	32.75	9.780249	3.25363

non-reactive	20	2	200	OKB90	32.75	10.1756	3.21237
non-reactive	20	2	200	OKB90	32.75	9.789906	2.98715
non-reactive	20	2	200	OKB90	32.75	8.634181	3.17264
non-reactive	20	2	200	OKB90	32.75	8.469344	3.17318
non-reactive	20	2	200	OKB90	32.75	10.46612	3.15723
non-reactive	20	2	200	OKB90	32.75	8.660109	2.89387
non-reactive	20	2	200	OKB90	32.75	9.97521	3.06347
non-reactive	20	2	200	OKB90	32.75	8.050942	3.04034
non-reactive	20	2	200	OKB90	32.75	9.745346	3.24556
non-reactive	20	2	200	OKB90	32.75	11.00811	3.41486
non-reactive	20	2	200	OKB90	32.75	9.58186	3.38657
non-reactive	20	2	200	OKB90	32.75	10.66426	3.13417
non-reactive	20	2	200	OKB90	32.75	10.34597	3.0723
non-reactive	20	2	200	OKB90	32.75	7.9118	2.9623
non-reactive	20	2	200	OKB90	42.5	8.895175	3.57312
non-reactive	20	2	200	OKB90	42.5	12.43292	3.56472
non-reactive	20	2	200	OKB90	42.5	8.94251	2.65306
non-reactive	20	2	200	OKB90	42.5	7.130069	2.68203
non-reactive	20	2	200	OKB90	42.5	10.33211	3.44982
non-reactive	20	2	200	OKB90	42.5	9.811875	3.34802
non-reactive	20	2	200	OKB90	42.5	10.54141	3.28026
non-reactive	20	2	200	OKB90	42.5	9.911571	2.9104
non-reactive	20	2	200	OKB90	42.5	7.821372	3.21502
non-reactive	20	2	200	OKB90	42.5	7.528583	3.2159
non-reactive	20	2	200	OKB90	42.5	11.07285	3.18971
non-reactive	20	2	200	OKB90	42.5	8.015873	2.75722
non-reactive	20	2	200	OKB90	42.5	10.22604	3.03574
non-reactive	20	2	200	OKB90	42.5	6.907745	2.99775
non-reactive	20	2	200	OKB90	42.5	9.75384	3.33476
non-reactive	20	2	200	OKB90	42.5	11.96383	3.61279
non-reactive	20	2	200	OKB90	42.5	9.349598	3.56633
non-reactive	20	2	200	OKB90	42.5	11.4246	3.15184
non-reactive	20	2	200	OKB90	42.5	10.86914	3.05025
non-reactive	20	2	200	OKB90	42.5	6.726864	2.86959
non-reactive	20	2	200	EMEL2	17.75	5.283098	2.83862
non-reactive	20	2	200	EMEL2	17.75	8.473257	3.15189

non-reactive	20	2	200	EMEL2	17.75	7.705478	2.97363
non-reactive	20	2	200	EMEL2	17.75	6.429659	3.21295
non-reactive	20	2	200	EMEL2	17.75	7.376338	3.23525
non-reactive	20	2	200	EMEL2	17.75	5.92801	2.66224
non-reactive	20	2	200	EMEL2	17.75	6.420351	2.60869
non-reactive	20	2	200	EMEL2	17.75	9.044546	3.45184
non-reactive	20	2	200	EMEL2	17.75	5.189433	2.8605
non-reactive	20	2	200	EMEL2	17.75	4.927556	2.83491
non-reactive	20	2	200	EMEL2	17.75	9.665665	3.61363
non-reactive	20	2	200	EMEL2	17.75	6.790185	3.07624
non-reactive	20	2	200	EMEL2	17.75	8.935976	3.45081
non-reactive	20	2	200	EMEL2	17.75	5.264009	3.08246
non-reactive	20	2	200	EMEL2	17.75	7.218861	3.2489
non-reactive	20	2	200	EMEL2	17.75	6.98944	2.74928
non-reactive	20	2	200	EMEL2	17.75	6.393971	3.2446
non-reactive	20	2	200	EMEL2	17.75	9.758978	3.48311
non-reactive	20	2	200	EMEL2	17.75	8.611464	3.13036
non-reactive	20	2	200	EMEL2	17.75	5.837533	3.35342
non-reactive	20	2	200	EMEL2	20.25	5.484815	2.60819
non-reactive	20	2	200	EMEL2	20.25	9.849841	3.19079
non-reactive	20	2	200	EMEL2	20.25	8.496349	2.85927
non-reactive	20	2	200	EMEL2	20.25	7.4992	3.30434
non-reactive	20	2	200	EMEL2	20.25	8.703121	3.34581
non-reactive	20	2	200	EMEL2	20.25	5.78659	2.28016
non-reactive	20	2	200	EMEL2	20.25	6.141983	2.18056
non-reactive	20	2	200	EMEL2	20.25	11.26813	3.74862
non-reactive	20	2	200	EMEL2	20.25	5.422316	2.64887
non-reactive	20	2	200	EMEL2	20.25	5.089697	2.60127
non-reactive	20	2	200	EMEL2	20.25	12.43548	4.04951
non-reactive	20	2	200	EMEL2	20.25	7.670097	3.05008
non-reactive	20	2	200	EMEL2	20.25	11.12564	3.7467
non-reactive	20	2	200	EMEL2	20.25	5.879662	3.06167
non-reactive	20	2	200	EMEL2	20.25	8.536317	3.3712
non-reactive	20	2	200	EMEL2	20.25	7.114166	2.44202
non-reactive	20	2	200	EMEL2	20.25	7.510665	3.3632
non-reactive	20	2	200	EMEL2	20.25	12.26533	3.80678

non-reactive	20	2	200	EMEL2	20.25	9.961002	3.15075
non-reactive	20	2	200	EMEL2	20.25	6.987503	3.56558
non-reactive	20	2	200	EMEL2	32.75	8.44281	3.28514
non-reactive	20	2	200	EMEL2	32.75	12.73097	3.89468
non-reactive	20	2	200	EMEL2	32.75	11.3063	3.54783
non-reactive	20	2	200	EMEL2	32.75	10.7894	4.01348
non-reactive	20	2	200	EMEL2	32.75	11.86165	4.05686
non-reactive	20	2	200	EMEL2	32.75	8.469373	2.94196
non-reactive	20	2	200	EMEL2	32.75	8.731385	2.83774
non-reactive	20	2	200	EMEL2	32.75	14.381	4.47829
non-reactive	20	2	200	EMEL2	32.75	8.420105	3.32771
non-reactive	20	2	200	EMEL2	32.75	8.083654	3.27791
non-reactive	20	2	200	EMEL2	32.75	15.6129	4.7931
non-reactive	20	2	200	EMEL2	32.75	10.72687	3.74747
non-reactive	20	2	200	EMEL2	32.75	14.25855	4.47629
non-reactive	20	2	200	EMEL2	32.75	9.174828	3.75959
non-reactive	20	2	200	EMEL2	32.75	11.73904	4.08343
non-reactive	20	2	200	EMEL2	32.75	9.786376	3.1113
non-reactive	20	2	200	EMEL2	32.75	10.84989	4.07506
non-reactive	20	2	200	EMEL2	32.75	15.27283	4.53915
non-reactive	20	2	200	EMEL2	32.75	12.79789	3.85279
non-reactive	20	2	200	EMEL2	32.75	10.58111	4.2868
non-reactive	20	2	200	EMEL2	42.5	8.592396	3.38996
non-reactive	20	2	200	EMEL2	42.5	12.25966	3.87699
non-reactive	20	2	200	EMEL2	42.5	11.11828	3.59985
non-reactive	20	2	200	EMEL2	42.5	10.48934	3.97191
non-reactive	20	2	200	EMEL2	42.5	11.42837	4.00658
non-reactive	20	2	200	EMEL2	42.5	8.761367	3.11574
non-reactive	20	2	200	EMEL2	42.5	9.066569	3.03248
non-reactive	20	2	200	EMEL2	42.5	13.50987	4.34331
non-reactive	20	2	200	EMEL2	42.5	8.55657	3.42397
non-reactive	20	2	200	EMEL2	42.5	8.262036	3.38418
non-reactive	20	2	200	EMEL2	42.5	14.48243	4.59484
non-reactive	20	2	200	EMEL2	42.5	10.51591	3.75936
non-reactive	20	2	200	EMEL2	42.5	13.40383	4.3417
non-reactive	20	2	200	EMEL2	42.5	9.114581	3.76905

non-reactive	20	2	200	EMEL2	42.5	11.31151	4.0278
non-reactive	20	2	200	EMEL2	42.5	9.920189	3.25105
non-reactive	20	2	200	EMEL2	42.5	10.52618	4.02111
non-reactive	20	2	200	EMEL2	42.5	14.26613	4.39193
non-reactive	20	2	200	EMEL2	42.5	12.33647	3.84352
non-reactive	20	2	200	EMEL2	42.5	10.23833	4.1903
non-reactive	20	2	200	EMES4	17.75	6.689019	2.98996
non-reactive	20	2	200	EMES4	17.75	11.64635	3.47699
non-reactive	20	2	200	EMES4	17.75	10.30045	3.19985
non-reactive	20	2	200	EMES4	17.75	8.663525	3.57191
non-reactive	20	2	200	EMES4	17.75	10.09997	3.60658
non-reactive	20	2	200	EMES4	17.75	7.410603	2.71574
non-reactive	20	2	200	EMES4	17.75	8.013374	2.63248
non-reactive	20	2	200	EMES4	17.75	12.84715	3.94331
non-reactive	20	2	200	EMES4	17.75	6.57402	3.02397
non-reactive	20	2	200	EMES4	17.75	6.182535	2.98418
non-reactive	20	2	200	EMES4	17.75	13.97444	4.19484
non-reactive	20	2	200	EMES4	17.75	9.079241	3.35936
non-reactive	20	2	200	EMES4	17.75	12.67931	3.9417
non-reactive	20	2	200	EMES4	17.75	6.842002	3.36905
non-reactive	20	2	200	EMES4	17.75	9.876141	3.6278
non-reactive	20	2	200	EMES4	17.75	8.989788	2.85105
non-reactive	20	2	200	EMES4	17.75	8.634247	3.62111
non-reactive	20	2	200	EMES4	17.75	13.98042	3.99193
non-reactive	20	2	200	EMES4	17.75	11.82429	3.44352
non-reactive	20	2	200	EMES4	17.75	7.865896	3.7903
non-reactive	20	2	200	EMES4	20.25	5.432574	2.88514
non-reactive	20	2	200	EMES4	20.25	11.41467	3.49468
non-reactive	20	2	200	EMES4	20.25	9.770864	3.14783
non-reactive	20	2	200	EMES4	20.25	7.650135	3.61348
non-reactive	20	2	200	EMES4	20.25	9.447205	3.65686
non-reactive	20	2	200	EMES4	20.25	6.340385	2.54196
non-reactive	20	2	200	EMES4	20.25	7.03622	2.43774
non-reactive	20	2	200	EMES4	20.25	12.8564	4.07829
non-reactive	20	2	200	EMES4	20.25	5.282672	2.92771
non-reactive	20	2	200	EMES4	20.25	4.827032	2.87791

non-reactive	20	2	200	EMES4	20.25	14.24972	4.3931
non-reactive	20	2	200	EMES4	20.25	8.240969	3.34747
non-reactive	20	2	200	EMES4	20.25	12.64098	4.07629
non-reactive	20	2	200	EMES4	20.25	5.463936	3.35959
non-reactive	20	2	200	EMES4	20.25	9.158223	3.68343
non-reactive	20	2	200	EMES4	20.25	8.193738	2.7113
non-reactive	20	2	200	EMES4	20.25	7.592968	3.67506
non-reactive	20	2	200	EMES4	20.25	14.30536	4.13915
non-reactive	20	2	200	EMES4	20.25	11.63953	3.45279
non-reactive	20	2	200	EMES4	20.25	7.702161	3.8868
non-reactive	20	2	200	EMES4	32.75	5.761824	2.72562
non-reactive	20	2	200	EMES4	32.75	10.30716	3.5216
non-reactive	20	2	200	EMES4	32.75	8.688819	3.06866
non-reactive	20	2	200	EMES4	32.75	8.278364	3.67674
non-reactive	20	2	200	EMES4	32.75	9.428963	3.7334
non-reactive	20	2	200	EMES4	32.75	5.632567	2.27745
non-reactive	20	2	200	EMES4	32.75	5.789359	2.14136
non-reactive	20	2	200	EMES4	32.75	12.25111	4.28374
non-reactive	20	2	200	EMES4	32.75	5.750903	2.78121
non-reactive	20	2	200	EMES4	32.75	5.413571	2.71617
non-reactive	20	2	200	EMES4	32.75	13.6786	4.69484
non-reactive	20	2	200	EMES4	32.75	8.170674	3.32937
non-reactive	20	2	200	EMES4	32.75	12.11458	4.28112
non-reactive	20	2	200	EMES4	32.75	6.567177	3.34519
non-reactive	20	2	200	EMES4	32.75	9.301568	3.76809
non-reactive	20	2	200	EMES4	32.75	6.954428	2.4986
non-reactive	20	2	200	EMES4	32.75	8.346756	3.75716
non-reactive	20	2	200	EMES4	32.75	13.25709	4.36321
non-reactive	20	2	200	EMES4	32.75	10.36048	3.4669
non-reactive	20	2	200	EMES4	32.75	8.468948	4.03367
non-reactive	20	2	200	EMES4	42.5	6.050103	2.65726
non-reactive	20	2	200	EMES4	42.5	11.31951	3.53314
non-reactive	20	2	200	EMES4	42.5	9.392702	3.03474
non-reactive	20	2	200	EMES4	42.5	9.014208	3.70385
non-reactive	20	2	200	EMES4	42.5	10.34281	3.7662
non-reactive	20	2	200	EMES4	42.5	5.81386	2.16411

non-reactive	20	2	200	EMES4	42.5	5.940791	2.01436
non-reactive	20	2	200	EMES4	42.5	13.6727	4.37178
non-reactive	20	2	200	EMES4	42.5	6.04625	2.71843
non-reactive	20	2	200	EMES4	42.5	5.661634	2.64686
non-reactive	20	2	200	EMES4	42.5	15.38248	4.82415
non-reactive	20	2	200	EMES4	42.5	8.85126	3.32161
non-reactive	20	2	200	EMES4	42.5	13.51349	4.3689
non-reactive	20	2	200	EMES4	42.5	7.02827	3.33902
non-reactive	20	2	200	EMES4	42.5	10.20009	3.80437
non-reactive	20	2	200	EMES4	42.5	7.319009	2.40745
non-reactive	20	2	200	EMES4	42.5	9.099872	3.79234
non-reactive	20	2	200	EMES4	42.5	14.8537	4.45923
non-reactive	20	2	200	EMES4	42.5	11.37047	3.47295
non-reactive	20	2	200	EMES4	42.5	9.593933	4.09661
reactive	20	2	200	OKB30	20.25	9.701893	2.35726
reactive	20	2	200	OKB30	20.25	18.83527	3.23314
reactive	20	2	200	OKB30	20.25	15.3831	2.73474
reactive	20	2	200	OKB30	20.25	14.99464	3.40385
reactive	20	2	200	OKB30	20.25	17.26719	3.4662
reactive	20	2	200	OKB30	20.25	9.080863	1.86411
reactive	20	2	200	OKB30	20.25	9.182215	1.71436
reactive	20	2	200	OKB30	20.25	23.14766	4.07178
reactive	20	2	200	OKB30	20.25	9.718751	2.41843
reactive	20	2	200	OKB30	20.25	9.062447	2.34686
reactive	20	2	200	OKB30	20.25	26.22966	4.52415
reactive	20	2	200	OKB30	20.25	14.59836	3.02161
reactive	20	2	200	OKB30	20.25	22.87328	4.0689
reactive	20	2	200	OKB30	20.25	11.54399	3.03902
reactive	20	2	200	OKB30	20.25	17.03678	3.50437
reactive	20	2	200	OKB30	20.25	11.64111	2.10745
reactive	20	2	200	OKB30	20.25	15.16412	3.49234
reactive	20	2	200	OKB30	20.25	25.20618	4.15923
reactive	20	2	200	OKB30	20.25	18.89542	3.17295
reactive	20	2	200	OKB30	20.25	14.68107	3.79661
reactive	20	2	200	OKB30	32.75	10.075	2.08839
reactive	20	2	200	OKB30	32.75	20.40337	3.27853



reactive	20	2	200	OKB30	32.75	15.7618	2.6013
reactive	20	2	200	OKB30	32.75	17.76696	3.51048
reactive	20	2	200	OKB30	32.75	19.8912	3.5952
reactive	20	2	200	OKB30	32.75	7.719197	1.4183
reactive	20	2	200	OKB30	32.75	7.093514	1.21483
reactive	20	2	200	OKB30	32.75	26.98611	4.41805
reactive	20	2	200	OKB30	32.75	10.30338	2.1715
reactive	20	2	200	OKB30	32.75	9.575386	2.07426
reactive	20	2	200	OKB30	32.75	31.20508	5.03272
reactive	20	2	200	OKB30	32.75	16.18113	2.9911
reactive	20	2	200	OKB30	32.75	26.73318	4.41414
reactive	20	2	200	OKB30	32.75	13.76178	3.01476
reactive	20	2	200	OKB30	32.75	19.82007	3.64707
reactive	20	2	200	OKB30	32.75	10.4523	1.74895
reactive	20	2	200	OKB30	32.75	18.18809	3.63072
reactive	20	2	200	OKB30	32.75	29.10534	4.53687
reactive	20	2	200	OKB30	32.75	20.23297	3.19673
reactive	20	2	200	OKB30	32.75	18.68676	4.04415
reactive	20	2	200	OKB30	42.5	10.31255	2.1924
reactive	20	2	200	OKB30	42.5	21.65604	3.38254
reactive	20	2	200	OKB30	42.5	16.78109	2.70531
reactive	20	2	200	OKB30	42.5	18.04098	3.6145
reactive	20	2	200	OKB30	42.5	20.58181	3.69921
reactive	20	2	200	OKB30	42.5	8.303288	1.52231
reactive	20	2	200	OKB30	42.5	7.82837	1.31884
reactive	20	2	200	OKB30	42.5	28.31924	4.52207
reactive	20	2	200	OKB30	42.5	10.48396	2.27552
reactive	20	2	200	OKB30	42.5	9.696025	2.17828
reactive	20	2	200	OKB30	42.5	32.74415	5.13674
reactive	20	2	200	OKB30	42.5	16.75866	3.09511
reactive	20	2	200	OKB30	42.5	28.01009	4.51815
reactive	20	2	200	OKB30	42.5	13.68744	3.11877
reactive	20	2	200	OKB30	42.5	20.42321	3.75108
reactive	20	2	200	OKB30	42.5	11.30754	1.85296
reactive	20	2	200	OKB30	42.5	18.40706	3.73473
reactive	20	2	200	OKB30	42.5	30.79388	4.64089

reactive	20	2	200	OKB30	42.5	21.5569	3.30075
reactive	20	2	200	OKB30	42.5	18.48665	4.14817
reactive	20	2	200	OKB90	17.75	5.782766	2.3924
reactive	20	2	200	OKB90	17.75	14.02418	3.58254
reactive	20	2	200	OKB90	17.75	10.86269	2.90531
reactive	20	2	200	OKB90	17.75	10.18708	3.8145
reactive	20	2	200	OKB90	17.75	12.38151	3.89921
reactive	20	2	200	OKB90	17.75	5.302837	1.72231
reactive	20	2	200	OKB90	17.75	5.320998	1.51884
reactive	20	2	200	OKB90	17.75	17.90278	4.72207
reactive	20	2	200	OKB90	17.75	5.773135	2.47552
reactive	20	2	200	OKB90	17.75	5.219159	2.37828
reactive	20	2	200	OKB90	17.75	20.7604	5.33674
reactive	20	2	200	OKB90	17.75	10.02962	3.29511
reactive	20	2	200	OKB90	17.75	17.62592	4.71815
reactive	20	2	200	OKB90	17.75	7.100177	3.31877
reactive	20	2	200	OKB90	17.75	12.13096	3.95108
reactive	20	2	200	OKB90	17.75	7.493735	2.05296
reactive	20	2	200	OKB90	17.75	10.29081	3.93473
reactive	20	2	200	OKB90	17.75	19.94471	4.84089
reactive	20	2	200	OKB90	17.75	14.10095	3.50075
reactive	20	2	200	OKB90	17.75	9.562582	4.34817
reactive	20	2	200	OKB90	20.25	5.343277	1.98981
reactive	20	2	200	OKB90	20.25	21.3798	4.76079
reactive	20	2	200	OKB90	20.25	18.98027	4.43569
reactive	20	2	200	OKB90	20.25	7.354333	2.45887
reactive	20	2	200	OKB90	20.25	12.21302	3.39293
reactive	20	2	200	OKB90	20.25	11.19643	3.21439
reactive	20	2	200	OKB90	20.25	15.97876	3.99975
reactive	20	2	200	OKB90	20.25	19.68145	4.53264
reactive	20	2	200	OKB90	20.25	4.732675	1.83241
reactive	20	2	200	OKB90	20.25	3.813442	1.57783
reactive	20	2	200	OKB90	20.25	21.0369	4.71545
reactive	20	2	200	OKB90	20.25	10.83671	3.1494
reactive	20	2	200	OKB90	20.25	18.93862	4.42988
reactive	20	2	200	OKB90	20.25	3.468897	1.47585

reactive	20	2	200	OKB90	20.25	11.10764	3.19844
reactive	20	2	200	OKB90	20.25	17.8212	4.27157
reactive	20	2	200	OKB90	20.25	6.891617	2.35664
reactive	20	2	200	OKB90	20.25	24.36074	5.14098
reactive	20	2	200	OKB90	20.25	23.0016	4.97061
reactive	20	2	200	OKB90	20.25	3.843488	1.58654
reactive	20	2	200	OKB90	32.75	14.24004	2.13606
reactive	20	2	200	OKB90	32.75	34.76616	4.62182
reactive	20	2	200	OKB90	32.75	32.13769	4.33018
reactive	20	2	200	OKB90	32.75	17.41551	2.55684
reactive	20	2	200	OKB90	32.75	24.10198	3.39475
reactive	20	2	200	OKB90	32.75	22.78655	3.23459
reactive	20	2	200	OKB90	32.75	28.70504	3.93912
reactive	20	2	200	OKB90	32.75	32.91541	4.41715
reactive	20	2	200	OKB90	32.75	13.20176	1.99486
reactive	20	2	200	OKB90	32.75	11.55157	1.76649
reactive	20	2	200	OKB90	32.75	34.39602	4.58114
reactive	20	2	200	OKB90	32.75	22.3121	3.17629
reactive	20	2	200	OKB90	32.75	32.09128	4.32497
reactive	20	2	200	OKB90	32.75	10.90061	1.67501
reactive	20	2	200	OKB90	32.75	22.66994	3.22029
reactive	20	2	200	OKB90	32.75	30.83298	4.18295
reactive	20	2	200	OKB90	32.75	16.71301	2.46513
reactive	20	2	200	OKB90	32.75	37.91424	4.96287
reactive	20	2	200	OKB90	32.75	36.49363	4.81004
reactive	20	2	200	OKB90	32.75	11.60748	1.77431
reactive	20	2	200	OKB90	42.5	16.79309	2.49721
reactive	20	2	200	OKB90	42.5	30.07347	3.56485
reactive	20	2	200	OKB90	42.5	24.35459	2.95733
reactive	20	2	200	OKB90	42.5	26.46499	3.77293
reactive	20	2	200	OKB90	42.5	29.21834	3.84892
reactive	20	2	200	OKB90	42.5	14.18482	1.8961
reactive	20	2	200	OKB90	42.5	13.65045	1.71357
reactive	20	2	200	OKB90	42.5	38.05079	4.58708
reactive	20	2	200	OKB90	42.5	17.04455	2.57178
reactive	20	2	200	OKB90	42.5	16.07578	2.48455

reactive	20	2	200	OKB90	42.5	43.20491	5.13848
reactive	20	2	200	OKB90	42.5	24.60709	3.307
reactive	20	2	200	OKB90	42.5	37.73076	4.58357
reactive	20	2	200	OKB90	42.5	21.32503	3.32823
reactive	20	2	200	OKB90	42.5	29.10376	3.89546
reactive	20	2	200	OKB90	42.5	17.83552	2.19272
reactive	20	2	200	OKB90	42.5	26.97654	3.88079
reactive	20	2	200	OKB90	42.5	40.69844	4.69367
reactive	20	2	200	OKB90	42.5	29.90688	3.49147
reactive	20	2	200	OKB90	42.5	27.5325	4.25167
reactive	20	2	200	EMEL2	17.75	5.24924	2.49053
reactive	20	2	200	EMEL2	17.75	6.875014	2.02731
reactive	20	2	200	EMEL2	17.75	9.878449	3.04833
reactive	20	2	200	EMEL2	17.75	5.133235	2.2079
reactive	20	2	200	EMEL2	17.75	5.238172	1.89954
reactive	20	2	200	EMEL2	17.75	8.20555	3.06761
reactive	20	2	200	EMEL2	17.75	14.79128	4.86765
reactive	20	2	200	EMEL2	17.75	14.64698	4.45804
reactive	20	2	200	EMEL2	17.75	8.820769	4.33502
reactive	20	2	200	EMEL2	17.75	4.679625	2.44131
reactive	20	2	200	EMEL2	17.75	11.92555	3.53853
reactive	20	2	200	EMEL2	17.75	6.96159	2.63218
reactive	20	2	200	EMEL2	17.75	7.348718	2.26958
reactive	20	2	200	EMEL2	17.75	3.809929	2.03782
reactive	20	2	200	EMEL2	17.75	6.442248	2.41507
reactive	20	2	200	EMEL2	17.75	15.50915	4.90084
reactive	20	2	200	EMEL2	17.75	10.37962	4.55728
reactive	20	2	200	EMEL2	17.75	15.9803	4.47965
reactive	20	2	200	EMEL2	17.75	15.55131	4.45802
reactive	20	2	200	EMEL2	17.75	4.498663	2.34198
reactive	20	2	200	EMEL2	20.25	7.633123	2.29053
reactive	20	2	200	EMEL2	20.25	9.216659	1.82731
reactive	20	2	200	EMEL2	20.25	13.79463	2.84833
reactive	20	2	200	EMEL2	20.25	7.272955	2.0079
reactive	20	2	200	EMEL2	20.25	7.136436	1.69954
reactive	20	2	200	EMEL2	20.25	11.72503	2.86761

reactive	20	2	200	EMEL2	20.25	21.34899	4.66765
reactive	20	2	200	EMEL2	20.25	20.87691	4.25804
reactive	20	2	200	EMEL2	20.25	13.37786	4.13502
reactive	20	2	200	EMEL2	20.25	6.898819	2.24131
reactive	20	2	200	EMEL2	20.25	16.74553	3.33853
reactive	20	2	200	EMEL2	20.25	9.847021	2.43218
reactive	20	2	200	EMEL2	20.25	10.01567	2.06958
reactive	20	2	200	EMEL2	20.25	5.541119	1.83782
reactive	20	2	200	EMEL2	20.25	9.035115	2.21507
reactive	20	2	200	EMEL2	20.25	22.28997	4.70084
reactive	20	2	200	EMEL2	20.25	15.50769	4.35728
reactive	20	2	200	EMEL2	20.25	22.59077	4.27965
reactive	20	2	200	EMEL2	20.25	22.02857	4.25802
reactive	20	2	200	EMEL2	20.25	6.604581	2.14198
reactive	20	2	200	EMEL2	32.75	16.89971	2.39053
reactive	20	2	200	EMEL2	32.75	15.27416	1.92731
reactive	20	2	200	EMEL2	32.75	23.06989	2.94833
reactive	20	2	200	EMEL2	32.75	15.20698	2.1079
reactive	20	2	200	EMEL2	32.75	13.50144	1.79954
reactive	20	2	200	EMEL2	32.75	22.10154	2.96761
reactive	20	2	200	EMEL2	32.75	36.66375	4.76765
reactive	20	2	200	EMEL2	32.75	34.23097	4.35804
reactive	20	2	200	EMEL2	32.75	29.73336	4.23502
reactive	20	2	200	EMEL2	32.75	16.25389	2.34131
reactive	20	2	200	EMEL2	32.75	27.20262	3.43853
reactive	20	2	200	EMEL2	32.75	18.80782	2.53218
reactive	20	2	200	EMEL2	32.75	16.97249	2.16958
reactive	20	2	200	EMEL2	32.75	13.39175	1.93782
reactive	20	2	200	EMEL2	32.75	17.23028	2.31507
reactive	20	2	200	EMEL2	32.75	37.32197	4.80084
reactive	20	2	200	EMEL2	32.75	32.01535	4.45728
reactive	20	2	200	EMEL2	32.75	35.22342	4.37965
reactive	20	2	200	EMEL2	32.75	34.82019	4.35802
reactive	20	2	200	EMEL2	32.75	15.57035	2.24198
reactive	20	2	200	EMEL2	42.5	17.52133	2.03606
reactive	20	2	200	EMEL2	42.5	42.13694	4.52182

reactive	20	2	200	EMEL2	42.5	39.06537	4.23018
reactive	20	2	200	EMEL2	42.5	21.43893	2.45684
reactive	20	2	200	EMEL2	42.5	29.54267	3.29475
reactive	20	2	200	EMEL2	42.5	27.96255	3.13459
reactive	20	2	200	EMEL2	42.5	35.02329	3.83912
reactive	20	2	200	EMEL2	42.5	39.97625	4.31715
reactive	20	2	200	EMEL2	42.5	16.22949	1.89486
reactive	20	2	200	EMEL2	42.5	14.16433	1.66649
reactive	20	2	200	EMEL2	42.5	41.70561	4.48114
reactive	20	2	200	EMEL2	42.5	27.39104	3.07629
reactive	20	2	200	EMEL2	42.5	39.01096	4.22497
reactive	20	2	200	EMEL2	42.5	13.34547	1.57501
reactive	20	2	200	EMEL2	42.5	27.82219	3.12029
reactive	20	2	200	EMEL2	42.5	37.53329	4.08295
reactive	20	2	200	EMEL2	42.5	20.57642	2.36513
reactive	20	2	200	EMEL2	42.5	45.79083	4.86287
reactive	20	2	200	EMEL2	42.5	44.14523	4.71004
reactive	20	2	200	EMEL2	42.5	14.23455	1.67431
reactive	20	2	200	EMES4	17.75	20.98327	4.9004
reactive	20	2	200	EMES4	17.75	30.58773	4.87179
reactive	20	2	200	EMES4	17.75	10.66704	1.76481
reactive	20	2	200	EMES4	17.75	8.60936	1.86353
reactive	20	2	200	EMES4	17.75	23.71353	4.48021
reactive	20	2	200	EMES4	17.75	21.34534	4.13325
reactive	20	2	200	EMES4	17.75	22.36115	3.90234
reactive	20	2	200	EMES4	17.75	16.15257	2.64183
reactive	20	2	200	EMES4	17.75	15.34019	3.67999
reactive	20	2	200	EMES4	17.75	14.677	3.68297
reactive	20	2	200	EMES4	17.75	22.44603	3.59374
reactive	20	2	200	EMES4	17.75	10.84798	2.11979
reactive	20	2	200	EMES4	17.75	18.53698	3.06898
reactive	20	2	200	EMES4	17.75	11.49831	2.93952
reactive	20	2	200	EMES4	17.75	21.0651	4.08808
reactive	20	2	200	EMES4	17.75	29.84117	5.0356
reactive	20	2	200	EMES4	17.75	22.17325	4.87725
reactive	20	2	200	EMES4	17.75	22.70222	3.46467

reactive	20	2	200	EMES4	17.75	20.05066	3.11843
reactive	20	2	200	EMES4	17.75	9.989426	2.50275
reactive	20	2	200	EMES4	20.25	23.80078	5.02015
reactive	20	2	200	EMES4	20.25	31.48205	4.98939
reactive	20	2	200	EMES4	20.25	10.09738	1.64835
reactive	20	2	200	EMES4	20.25	8.78418	1.75452
reactive	20	2	200	EMES4	20.25	25.28752	4.56832
reactive	20	2	200	EMES4	20.25	22.79821	4.19522
reactive	20	2	200	EMES4	20.25	23.20375	3.94692
reactive	20	2	200	EMES4	20.25	16.01682	2.59145
reactive	20	2	200	EMES4	20.25	17.24851	3.70781
reactive	20	2	200	EMES4	20.25	16.72857	3.71102
reactive	20	2	200	EMES4	20.25	22.71757	3.61507
reactive	20	2	200	EMES4	20.25	10.95744	2.03008
reactive	20	2	200	EMES4	20.25	18.67825	3.05077
reactive	20	2	200	EMES4	20.25	12.95667	2.91156
reactive	20	2	200	EMES4	20.25	22.49682	4.14665
reactive	20	2	200	EMES4	20.25	31.16294	5.16555
reactive	20	2	200	EMES4	20.25	24.72024	4.99527
reactive	20	2	200	EMES4	20.25	22.68284	3.47627
reactive	20	2	200	EMES4	20.25	19.95402	3.10395
reactive	20	2	200	EMES4	20.25	11.01964	2.44189
reactive	20	2	200	EMES4	32.75	39.30186	4.92015
reactive	20	2	200	EMES4	32.75	44.98317	4.88939
reactive	20	2	200	EMES4	32.75	14.02486	1.54835
reactive	20	2	200	EMES4	32.75	13.55571	1.65452
reactive	20	2	200	EMES4	32.75	38.43542	4.46832
reactive	20	2	200	EMES4	32.75	34.90622	4.09522
reactive	20	2	200	EMES4	32.75	34.11152	3.84692
reactive	20	2	200	EMES4	32.75	22.67307	2.49145
reactive	20	2	200	EMES4	32.75	28.57054	3.60781
reactive	20	2	200	EMES4	32.75	28.1938	3.61102
reactive	20	2	200	EMES4	32.75	32.26947	3.51507
reactive	20	2	200	EMES4	32.75	16.39645	1.93008
reactive	20	2	200	EMES4	32.75	26.7204	2.95077
reactive	20	2	200	EMES4	32.75	21.82642	2.81156

reactive	20	2	200	EMES4	32.75	34.46402	4.04665
reactive	20	2	200	EMES4	32.75	45.51974	5.06555
reactive	20	2	200	EMES4	32.75	39.88872	4.89527
reactive	20	2	200	EMES4	32.75	31.62377	3.37627
reactive	20	2	200	EMES4	32.75	27.91255	3.00395
reactive	20	2	200	EMES4	32.75	18.29372	2.34189
reactive	20	2	200	EMES4	40	38.20555	4.7096
reactive	20	2	200	EMES4	40	46.96404	4.67883
reactive	20	2	200	EMES4	40	13.12607	1.3378
reactive	20	2	200	EMES4	40	12.18439	1.44396
reactive	20	2	200	EMES4	40	38.69095	4.25776
reactive	20	2	200	EMES4	40	34.81867	3.88466
reactive	20	2	200	EMES4	40	34.57738	3.63636
reactive	20	2	200	EMES4	40	22.533	2.28089
reactive	20	2	200	EMES4	40	27.18789	3.39725
reactive	20	2	200	EMES4	40	26.6121	3.40046
reactive	20	2	200	EMES4	40	33.06513	3.30451
reactive	20	2	200	EMES4	40	15.33461	1.71952
reactive	20	2	200	EMES4	40	26.87502	2.74021
reactive	20	2	200	EMES4	40	20.17122	2.601
reactive	20	2	200	EMES4	40	34.34083	3.83609
reactive	20	2	200	EMES4	40	47.08199	4.85499
reactive	20	2	200	EMES4	40	39.19767	4.68471
reactive	20	2	200	EMES4	40	32.61226	3.16571
reactive	20	2	200	EMES4	40	28.44604	2.79339
reactive	20	2	200	EMES4	40	16.69275	2.13133
reactive	20	2	200	EMES4	42.5	43.11437	4.72015
reactive	20	2	200	EMES4	42.5	52.19619	4.68939
reactive	20	2	200	EMES4	42.5	14.69224	1.34835
reactive	20	2	200	EMES4	42.5	13.77733	1.45452
reactive	20	2	200	EMES4	42.5	43.30258	4.26832
reactive	20	2	200	EMES4	42.5	39.01632	3.89522
reactive	20	2	200	EMES4	42.5	38.59298	3.64692
reactive	20	2	200	EMES4	42.5	25.12877	2.29145
reactive	20	2	200	EMES4	42.5	30.74083	3.40781
reactive	20	2	200	EMES4	42.5	30.14407	3.41102



reactive	20	2	200	EMES4	42.5	36.79075	3.31507
reactive	20	2	200	EMES4	42.5	17.24827	1.73008
reactive	20	2	200	EMES4	42.5	29.96213	2.75077
reactive	20	2	200	EMES4	42.5	22.88716	2.61156
reactive	20	2	200	EMES4	42.5	38.48562	3.84665
reactive	20	2	200	EMES4	42.5	52.44187	4.86555
reactive	20	2	200	EMES4	42.5	44.12812	4.69527
reactive	20	2	200	EMES4	42.5	36.22425	3.17627
reactive	20	2	200	EMES4	42.5	31.63386	2.80395
reactive	20	2	200	EMES4	42.5	18.94189	2.14189
reactive	20	2	600	EMES4	17.75	22.03572	4.36236
reactive	20	2	600	EMES4	17.75	30.90771	4.34144
reactive	20	2	600	EMES4	17.75	14.23412	2.06993
reactive	20	2	600	EMES4	17.75	11.57033	2.14211
reactive	20	2	600	EMES4	17.75	24.73011	4.05516
reactive	20	2	600	EMES4	17.75	22.67667	3.8015
reactive	20	2	600	EMES4	17.75	23.79874	3.63268
reactive	20	2	600	EMES4	17.75	18.83949	2.71112
reactive	20	2	600	EMES4	17.75	17.12109	3.47012
reactive	20	2	600	EMES4	17.75	16.47217	3.4723
reactive	20	2	600	EMES4	17.75	24.14035	3.40706
reactive	20	2	600	EMES4	17.75	13.78269	2.32946
reactive	20	2	600	EMES4	17.75	20.77772	3.02341
reactive	20	2	600	EMES4	17.75	13.67081	2.92876
reactive	20	2	600	EMES4	17.75	22.43485	3.76848
reactive	20	2	600	EMES4	17.75	30.13157	4.4612
reactive	20	2	600	EMES4	17.75	23.13982	4.34544
reactive	20	2	600	EMES4	17.75	24.52379	3.3127
reactive	20	2	600	EMES4	17.75	22.26078	3.05956
reactive	20	2	600	EMES4	17.75	12.39588	2.60945
reactive	20	2	600	EMES4	20.25	17.50076	2.89431
reactive	20	2	600	EMES4	20.25	32.27341	4.19862
reactive	20	2	600	EMES4	20.25	24.47427	3.26574
reactive	20	2	600	EMES4	20.25	21.21349	3.35432
reactive	20	2	600	EMES4	20.25	17.38241	2.52759
reactive	20	2	600	EMES4	20.25	13.45213	1.98661

reactive	20	2	600	EMES4	20.25	19.93198	2.75447
reactive	20	2	600	EMES4	20.25	17.17384	2.27419
reactive	20	2	600	EMES4	20.25	19.20678	3.22616
reactive	20	2	600	EMES4	20.25	25.94447	4.47105
reactive	20	2	600	EMES4	20.25	27.91847	3.64479
reactive	20	2	600	EMES4	20.25	16.08665	2.38925
reactive	20	2	600	EMES4	20.25	31.48507	4.20316
reactive	20	2	600	EMES4	20.25	22.71944	3.95643
reactive	20	2	600	EMES4	20.25	25.67854	3.7975
reactive	20	2	600	EMES4	20.25	31.33675	4.23635
reactive	20	2	600	EMES4	20.25	24.24122	3.8701
reactive	20	2	600	EMES4	20.25	31.16067	3.93856
reactive	20	2	600	EMES4	20.25	22.08494	2.82747
reactive	20	2	600	EMES4	20.25	25.70543	4.42592
reactive	20	2	600	EMES4	30.25	23.37221	3.10175
reactive	20	2	600	EMES4	30.25	31.24006	3.27747
reactive	20	2	600	EMES4	30.25	29.51646	3.17466
reactive	20	2	600	EMES4	30.25	33.71932	4.28283
reactive	20	2	600	EMES4	30.25	27.36697	3.20225
reactive	20	2	600	EMES4	30.25	34.04912	4.04503
reactive	20	2	600	EMES4	30.25	25.40347	2.82782
reactive	20	2	600	EMES4	30.25	39.11668	4.17584
reactive	20	2	600	EMES4	30.25	31.31077	4.21878
reactive	20	2	600	EMES4	30.25	22.44415	3.10074
reactive	20	2	600	EMES4	30.25	32.0372	3.37266
reactive	20	2	600	EMES4	30.25	35.75427	4.27136
reactive	20	2	600	EMES4	30.25	35.03966	3.77041
reactive	20	2	600	EMES4	30.25	22.68377	3.16598
reactive	20	2	600	EMES4	30.25	20.94035	2.49111
reactive	20	2	600	EMES4	30.25	25.2728	2.75325
reactive	20	2	600	EMES4	30.25	28.92617	3.70873
reactive	20	2	600	EMES4	30.25	23.0341	2.34905
reactive	20	2	600	EMES4	30.25	41.05358	4.23978
reactive	20	2	600	EMES4	30.25	18.90247	2.60918
reactive	20	2	600	EMES4	32.75	32.9851	3.72564
reactive	20	2	600	EMES4	32.75	35.526	3.21094

reactive	20	2	600	EMES4	32.75	35.06496	3.24534
reactive	20	2	600	EMES4	32.75	33.0906	3.586
reactive	20	2	600	EMES4	32.75	34.14947	3.42424
reactive	20	2	600	EMES4	32.75	26.74437	2.72057
reactive	20	2	600	EMES4	32.75	25.67652	2.45545
reactive	20	2	600	EMES4	32.75	35.15348	3.23041
reactive	20	2	600	EMES4	32.75	37.58779	4.30659
reactive	20	2	600	EMES4	32.75	29.95868	3.51426
reactive	20	2	600	EMES4	32.75	23.35606	2.11791
reactive	20	2	600	EMES4	32.75	39.27747	4.01668
reactive	20	2	600	EMES4	32.75	40.78067	3.77596
reactive	20	2	600	EMES4	32.75	35.79259	4.23905
reactive	20	2	600	EMES4	32.75	23.69622	2.41362
reactive	20	2	600	EMES4	32.75	40.81611	3.82396
reactive	20	2	600	EMES4	32.75	18.98342	2.07556
reactive	20	2	600	EMES4	32.75	40.80663	3.58981
reactive	20	2	600	EMES4	32.75	29.44693	2.62183
reactive	20	2	600	EMES4	32.75	21.35827	2.50336
reactive	20	2	600	EMES4	40	49.06634	4.10217
reactive	20	2	600	EMES4	40	34.34814	2.54979
reactive	20	2	600	EMES4	40	32.73247	2.46223
reactive	20	2	600	EMES4	40	50.94416	4.17006
reactive	20	2	600	EMES4	40	38.22331	3.00365
reactive	20	2	600	EMES4	40	47.39479	3.75305
reactive	20	2	600	EMES4	40	26.20448	2.00704
reactive	20	2	600	EMES4	40	38.02874	2.84931
reactive	20	2	600	EMES4	40	28.07155	2.36386
reactive	20	2	600	EMES4	40	42.72608	3.64042
reactive	20	2	600	EMES4	40	28.73587	2.13709
reactive	20	2	600	EMES4	40	54.88754	4.3586
reactive	20	2	600	EMES4	40	26.45373	1.9904
reactive	20	2	600	EMES4	40	44.21052	3.78482
reactive	20	2	600	EMES4	40	24.98312	1.9797
reactive	20	2	600	EMES4	40	34.03381	2.57746
reactive	20	2	600	EMES4	40	48.62823	3.99872
reactive	20	2	600	EMES4	40	31.81864	2.32624

reactive	20	2	600	EMES4	40	32.5243	2.39408
reactive	20	2	600	EMES4	40	43.30379	3.68815
reactive	20	5	200	EMES4	17.75	30.11841	4.49257
reactive	20	5	200	EMES4	17.75	39.70417	4.47111
reactive	20	5	200	EMES4	17.75	18.46192	2.14055
reactive	20	5	200	EMES4	17.75	15.66263	2.21461
reactive	20	5	200	EMES4	17.75	32.6085	4.17739
reactive	20	5	200	EMES4	17.75	30.02778	3.91714
reactive	20	5	200	EMES4	17.75	31.0091	3.74393
reactive	20	5	200	EMES4	17.75	24.34894	2.79841
reactive	20	5	200	EMES4	17.75	23.53916	3.57714
reactive	20	5	200	EMES4	17.75	22.83831	3.57938
reactive	20	5	200	EMES4	17.75	31.06595	3.51244
reactive	20	5	200	EMES4	17.75	18.32729	2.40683
reactive	20	5	200	EMES4	17.75	26.88513	3.11882
reactive	20	5	200	EMES4	17.75	19.03807	3.02171
reactive	20	5	200	EMES4	17.75	29.71937	3.88325
reactive	20	5	200	EMES4	17.75	39.03036	4.59399
reactive	20	5	200	EMES4	17.75	31.29125	4.47521
reactive	20	5	200	EMES4	17.75	31.35105	3.41562
reactive	20	5	200	EMES4	17.75	28.54502	3.15591
reactive	20	5	200	EMES4	17.75	17.20812	2.69409
reactive	20	5	200	EMES4	20.25	20.53167	2.98636
reactive	20	5	200	EMES4	20.25	38.40283	4.32458
reactive	20	5	200	EMES4	20.25	29.11127	3.36745
reactive	20	5	200	EMES4	20.25	24.95029	3.45833
reactive	20	5	200	EMES4	20.25	20.59479	2.61011
reactive	20	5	200	EMES4	20.25	15.94975	2.05506
reactive	20	5	200	EMES4	20.25	23.67968	2.84288
reactive	20	5	200	EMES4	20.25	20.48141	2.35012
reactive	20	5	200	EMES4	20.25	22.49366	3.32684
reactive	20	5	200	EMES4	20.25	30.28138	4.60409
reactive	20	5	200	EMES4	20.25	33.23363	3.75635
reactive	20	5	200	EMES4	20.25	19.03993	2.46817
reactive	20	5	200	EMES4	20.25	37.40766	4.32924
reactive	20	5	200	EMES4	20.25	26.50795	4.07609

reactive	20	5	200	EMES4	20.25	30.32469	3.91303
reactive	20	5	200	EMES4	20.25	37.20202	4.36329
reactive	20	5	200	EMES4	20.25	28.47321	3.98752
reactive	20	5	200	EMES4	20.25	37.14969	4.05776
reactive	20	5	200	EMES4	20.25	26.35321	2.91778
reactive	20	5	200	EMES4	20.25	30.00562	4.55779
reactive	20	5	200	EMES4	30.25	39.27348	3.19919
reactive	20	5	200	EMES4	30.25	47.29856	3.37948
reactive	20	5	200	EMES4	30.25	45.16158	3.27399
reactive	20	5	200	EMES4	30.25	55.43358	4.41098
reactive	20	5	200	EMES4	30.25	43.41507	3.30231
reactive	20	5	200	EMES4	30.25	54.32135	4.167
reactive	20	5	200	EMES4	30.25	39.46344	2.91814
reactive	20	5	200	EMES4	30.25	59.58991	4.30121
reactive	20	5	200	EMES4	30.25	52.91835	4.34527
reactive	20	5	200	EMES4	30.25	38.4431	3.19816
reactive	20	5	200	EMES4	30.25	48.56768	3.47715
reactive	20	5	200	EMES4	30.25	57.17099	4.39921
reactive	20	5	200	EMES4	30.25	53.57917	3.88524
reactive	20	5	200	EMES4	30.25	39.04101	3.26509
reactive	20	5	200	EMES4	30.25	33.51219	2.57268
reactive	20	5	200	EMES4	30.25	38.90827	2.84164
reactive	20	5	200	EMES4	30.25	47.78876	3.82196
reactive	20	5	200	EMES4	30.25	34.53951	2.42693
reactive	20	5	200	EMES4	30.25	61.68569	4.36681
reactive	20	5	200	EMES4	30.25	32.39531	2.69382
reactive	20	5	200	EMES4	32.75	54.66674	3.83931
reactive	20	5	200	EMES4	32.75	52.93634	3.31122
reactive	20	5	200	EMES4	32.75	52.81412	3.34651
reactive	20	5	200	EMES4	32.75	53.72043	3.69603
reactive	20	5	200	EMES4	32.75	53.3886	3.53007
reactive	20	5	200	EMES4	32.75	42.15338	2.80811
reactive	20	5	200	EMES4	32.75	39.32667	2.53609
reactive	20	5	200	EMES4	32.75	52.77627	3.3312
reactive	20	5	200	EMES4	32.75	62.71328	4.43536
reactive	20	5	200	EMES4	32.75	50.63712	3.62243

reactive	20	5	200	EMES4	32.75	34.94512	2.18977
reactive	20	5	200	EMES4	32.75	61.94575	4.13791
reactive	20	5	200	EMES4	32.75	61.39179	3.89093
reactive	20	5	200	EMES4	32.75	60.75124	4.36606
reactive	20	5	200	EMES4	32.75	37.40064	2.49317
reactive	20	5	200	EMES4	32.75	61.77532	3.94018
reactive	20	5	200	EMES4	32.75	31.05753	2.14632
reactive	20	5	200	EMES4	32.75	60.0383	3.69994
reactive	20	5	200	EMES4	32.75	43.63167	2.70679
reactive	20	5	200	EMES4	32.75	36.15283	2.58525
reactive	20	5	200	EMES4	40	72.49047	4.22562
reactive	20	5	200	EMES4	40	49.89342	2.63288
reactive	20	5	200	EMES4	40	47.65554	2.54305
reactive	20	5	200	EMES4	40	74.99052	4.29527
reactive	20	5	200	EMES4	40	55.97215	3.09855
reactive	20	5	200	EMES4	40	69.41383	3.86743
reactive	20	5	200	EMES4	40	38.31731	2.07602
reactive	20	5	200	EMES4	40	55.28239	2.94019
reactive	20	5	200	EMES4	40	41.64552	2.44212
reactive	20	5	200	EMES4	40	63.36179	3.75186
reactive	20	5	200	EMES4	40	41.80464	2.20946
reactive	20	5	200	EMES4	40	80.37596	4.48872
reactive	20	5	200	EMES4	40	38.57597	2.05895
reactive	20	5	200	EMES4	40	65.60625	3.90002
reactive	20	5	200	EMES4	40	36.73644	2.04797
reactive	20	5	200	EMES4	40	49.58795	2.66127
reactive	20	5	200	EMES4	40	71.64863	4.11948
reactive	20	5	200	EMES4	40	46.139	2.40352
reactive	20	5	200	EMES4	40	47.20228	2.47313
reactive	20	5	200	EMES4	40	64.2104	3.80084
reactive	20	5	600	EMES4	17.75	23.25671	4.48902
reactive	20	5	600	EMES4	17.75	31.1139	4.46816
reactive	20	5	600	EMES4	17.75	14.87972	2.20299
reactive	20	5	600	EMES4	17.75	12.47266	2.27497
reactive	20	5	600	EMES4	17.75	25.44525	4.18268
reactive	20	5	600	EMES4	17.75	23.45507	3.92973

reactive	20	5	600	EMES4	17.75	24.35069	3.76138
reactive	20	5	600	EMES4	17.75	19.37572	2.84239
reactive	20	5	600	EMES4	17.75	18.28264	3.59927
reactive	20	5	600	EMES4	17.75	17.70386	3.60145
reactive	20	5	600	EMES4	17.75	24.52239	3.53639
reactive	20	5	600	EMES4	17.75	14.59062	2.4618
reactive	20	5	600	EMES4	17.75	21.29008	3.15381
reactive	20	5	600	EMES4	17.75	14.83868	3.05942
reactive	20	5	600	EMES4	17.75	23.21848	3.89679
reactive	20	5	600	EMES4	17.75	30.50169	4.58759
reactive	20	5	600	EMES4	17.75	24.22469	4.47214
reactive	20	5	600	EMES4	17.75	24.81227	3.44229
reactive	20	5	600	EMES4	17.75	22.64309	3.18986
reactive	20	5	600	EMES4	17.75	13.48945	2.741
reactive	20	5	600	EMES4	20.25	18.06663	3.02507
reactive	20	5	600	EMES4	20.25	32.00373	4.32574
reactive	20	5	600	EMES4	20.25	24.55298	3.39546
reactive	20	5	600	EMES4	20.25	21.64732	3.4838
reactive	20	5	600	EMES4	20.25	17.80299	2.65937
reactive	20	5	600	EMES4	20.25	13.99675	2.1199
reactive	20	5	600	EMES4	20.25	20.21878	2.88561
reactive	20	5	600	EMES4	20.25	17.52309	2.40668
reactive	20	5	600	EMES4	20.25	19.77111	3.35599
reactive	20	5	600	EMES4	20.25	26.48228	4.59741
reactive	20	5	600	EMES4	20.25	27.82957	3.77345
reactive	20	5	600	EMES4	20.25	16.56346	2.52142
reactive	20	5	600	EMES4	20.25	31.29975	4.33027
reactive	20	5	600	EMES4	20.25	23.31183	4.08422
reactive	20	5	600	EMES4	20.25	25.88766	3.92574
reactive	20	5	600	EMES4	20.25	31.18341	4.36336
reactive	20	5	600	EMES4	20.25	24.63284	3.99813
reactive	20	5	600	EMES4	20.25	30.88069	4.0664
reactive	20	5	600	EMES4	20.25	22.20707	2.95841
reactive	20	5	600	EMES4	20.25	26.24351	4.55241
reactive	20	5	600	EMES4	30.25	51.58147	3.23193
reactive	20	5	600	EMES4	30.25	61.18084	3.40716

reactive	20	5	600	EMES4	30.25	58.56568	3.30463
reactive	20	5	600	EMES4	30.25	71.86931	4.40972
reactive	20	5	600	EMES4	30.25	56.54978	3.33215
reactive	20	5	600	EMES4	30.25	70.27589	4.17258
reactive	20	5	600	EMES4	30.25	51.50669	2.95876
reactive	20	5	600	EMES4	30.25	76.56006	4.30302
reactive	20	5	600	EMES4	30.25	68.86657	4.34584
reactive	20	5	600	EMES4	30.25	50.60626	3.23092
reactive	20	5	600	EMES4	30.25	62.77086	3.50208
reactive	20	5	600	EMES4	30.25	73.8711	4.39827
reactive	20	5	600	EMES4	30.25	69.07817	3.89873
reactive	20	5	600	EMES4	30.25	51.38314	3.29598
reactive	20	5	600	EMES4	30.25	44.14724	2.623
reactive	20	5	600	EMES4	30.25	50.77712	2.8844
reactive	20	5	600	EMES4	30.25	62.25609	3.83722
reactive	20	5	600	EMES4	30.25	45.23589	2.48133
reactive	20	5	600	EMES4	30.25	79.0727	4.36679
reactive	20	5	600	EMES4	30.25	42.94572	2.74074
reactive	20	5	600	EMES4	32.75	66.28046	3.85408
reactive	20	5	600	EMES4	32.75	64.17138	3.34081
reactive	20	5	600	EMES4	32.75	64.03416	3.37512
reactive	20	5	600	EMES4	32.75	65.15017	3.71483
reactive	20	5	600	EMES4	32.75	64.72985	3.55352
reactive	20	5	600	EMES4	32.75	51.57839	2.85182
reactive	20	5	600	EMES4	32.75	48.27144	2.58744
reactive	20	5	600	EMES4	32.75	63.98809	3.36023
reactive	20	5	600	EMES4	32.75	75.73705	4.43341
reactive	20	5	600	EMES4	32.75	61.56617	3.64329
reactive	20	5	600	EMES4	32.75	43.16063	2.25083
reactive	20	5	600	EMES4	32.75	74.7589	4.1443
reactive	20	5	600	EMES4	32.75	74.05678	3.90426
reactive	20	5	600	EMES4	32.75	73.45682	4.36606
reactive	20	5	600	EMES4	32.75	46.01277	2.54572
reactive	20	5	600	EMES4	32.75	74.51054	3.95212
reactive	20	5	600	EMES4	32.75	38.57028	2.2086
reactive	20	5	600	EMES4	32.75	72.45464	3.71863



reactive	20	5	600	EMES4	32.75	53.30651	2.75335
reactive	20	5	600	EMES4	32.75	44.54778	2.63521
reactive	20	5	600	EMES4	40	75.82099	4.22955
reactive	20	5	600	EMES4	40	52.85011	2.6815
reactive	20	5	600	EMES4	40	50.58695	2.5942
reactive	20	5	600	EMES4	40	78.33135	4.29725
reactive	20	5	600	EMES4	40	59.01269	3.13411
reactive	20	5	600	EMES4	40	72.63791	3.88141
reactive	20	5	600	EMES4	40	41.13505	2.14027
reactive	20	5	600	EMES4	40	58.29964	2.98019
reactive	20	5	600	EMES4	40	44.49356	2.4961
reactive	20	5	600	EMES4	40	66.56759	3.76909
reactive	20	5	600	EMES4	40	44.67279	2.26996
reactive	20	5	600	EMES4	40	83.7512	4.48527
reactive	20	5	600	EMES4	40	41.40386	2.12368
reactive	20	5	600	EMES4	40	68.85414	3.91309
reactive	20	5	600	EMES4	40	39.52184	2.11301
reactive	20	5	600	EMES4	40	52.54145	2.7091
reactive	20	5	600	EMES4	40	74.9457	4.1264
reactive	20	5	600	EMES4	40	49.05792	2.45858
reactive	20	5	600	EMES4	40	50.13109	2.52624
reactive	20	5	600	EMES4	40	67.42965	3.81669